University of Alberta

DESIGN AND SYNTHESIS OF HETEROCYCLIC COX-2 INHIBITORS

By

AMGAD G. HABEEB

A thesis submitted to the Faculty of Graduate Studies and Research in partial fulfillment

of the requirements for degree of

Doctor of Philosophy

In

Pharmaceutical Sciences

Faculty of Pharmacy and Pharmaceutical Sciences

Edmonton, Alberta

Fall, 2001

National Library of Canada
Acquisitions and Bibliographic Services
395 Wellington Street
Ottawa ON K1A 0N4
Canada

Bibliothèque nationale du Canada
Acquisitions et services bibliographiques
395, rue Wellington
Ottawa ON K1A 0N4
Canada

Your file Votre référence

Our file Notre référence

The author has granted a non-exclusive licence allowing the National Library of Canada to reproduce, loan, distribute or sell copies of this thesis in microform, paper or electronic formats.

The author retains ownership of the copyright in this thesis. Neither the thesis nor substantial extracts from it may be printed or otherwise reproduced without the author's permission.

L'auteur a accordé une licence non exclusive permettant à la Bibliothèque nationale du Canada de reproduire, prêter, distribuer ou vendre des copies de cette thèse sous la forme de microfiche/film, de reproduction sur papier ou sur format électronique.

L'auteur conserve la propriété du droit d'auteur qui protège cette thèse. Ni la thèse ni des extraits substantiels de celle-ci ne doivent être imprimés ou autrement reproduits sans son autorisation.

0-612-68939-5

Canada

University of Alberta

Library Release Form

Name of Author: Amgad G. Habeeb

Title of Thesis: Design and synthesis of heterocyclic COX-2 inhibitors

Degree: Doctor of Philosophy

Year this Degree Granted: 2001

Permission is hereby granted to the University of Alberta Library to reproduce single copies of this thesis and to lend or sell such copies for private, scholarly, or scientific research purposes only.

The author reserves all other publications and other rights in association with the copyright in the thesis, and except as hereinbefore provided, neither the thesis nor any substantial portion thereof may be printed or otherwise reproduced in any material form whatever without the author's prior written permission.

Amgad G. Habeeb

2137 DP Bldg.
Faculty of Pharmacy and Pharmaceutical Sciences
University of Alberta
Edmonton, Alberta, Canada T6G 2N8

Date: July 10th, 2001

University of Alberta

Faculty of Graduate Studies and Research

The undersigning certify that they have read, and recommend to the Faculty of Graduate Studies and Research for acceptance, a thesis entitled **DESIGN AND SYNTHESIS OF HETEROCYCLIC COX-2 INHIBITORS** submitted by Amgad G. Habeeb in partial fulfillment of the requirements for the degree of Doctor of Philosophy in Pharmaceutical Sciences.

E. E. Knaus

Dr. Edward Knaus (supervisor)

Dr. Franco Pasutto

D. L. J. Clive

Dr. Derrick Clive

Dr. John Samuel

John R. Mercer

Dr. John Mercer

Dr. Jonathon Dimmock
College of Pharmacy and Nutrition.
University of Saskatchewan
(External Reader)

Date: June 27, 2001.

ABSTRACT

4,5-Diarylisoxazoles (**32a-p**), 3,4-diaryl-5-trifluoromethylisoxazoles (**36**, **42**), 4,5-diphenyl-3-methylsulfonamidoisoxazole (**44**), 4,5-diaryl-3-methylisoxazoles (**48a-b**) and 4,5-diaryl-4-isoxazolines (**50a-k**) possessing H, F, MeS, MeSO, and/or $MeSO_2$ substituents at the *para*-position of one of the phenyl rings were synthesized for evaluation as analgesic, and selective COX-2 inhibitory and antiinflammatory (AI) agents.

4,5-Diarylisoxazoles **32a-p** exhibited potent analgesic and AI activities, but those compounds evaluated (**32a**, **32b**, and **32m**) were non-selective inhibitors of COX-2. In contrast, 3-(4-methylsulphonylphenyl)-4-phenyl-5-trifluoromethylisoxazole (**36**), which retained good analgesic and AI activities, was a highly potent and selective COX-2 inhibitor (COX-1 $IC_{50} > 500$ μM; COX-2 $IC_{50} < 0.001$ μM; SI of > 500,000) relative to celecoxib (COX-1 $IC_{50} = 22.9$ μM; COX-2 $IC_{50} = 0.0567$ μM; SI = 404). 4,5-Diphenyl-3-methylsulfonamidoisoxazole (**44**) exhibited potent and selective COX-2 inhibition (COX-1 $IC_{50} > 200$ μM; COX-2 $IC_{50} = 0.226$ μM; SI = 752).

4,5-Diaryl-4-isoxazolines (**50a-i**), having two C-3 hydrogen atoms, exhibited potent analgesic and AI activities, but those compounds evaluated (**50a**, **50b**, **50h**, and **50i**) were non-selective inhibitors of COX-2. However, 2,3-dimethyl-5-(4-methylsulphonylphenyl)-4-phenyl-4-isoxazoline (**50k**) exhibited excellent analgesic and AI activities, and selective COX-2 inhibition (COX-1 $IC_{50} = 258$ μM; COX-2 $IC_{50} = 0.004$ μM; SI = 61,454).

Docking isoxazoles **32e**, **32m**, **36**, **44**, and **48a-b**, and isoxazolines **50h**, and **50k** in the binding site of the COX-1 and COX-2 isozymes and comparative molecular volume analysis for compounds **32m** and **50h** showed that the size and nature of the central ring

substituents are crucial to selective inhibition of COX-2. The intermolecular energy between the docked ligands and both COX-1 and COX–2 was a determinant of enzyme inhibition in quantitative structure activity relationship (QSAR) regression equations.

Finally, celecoxib (**54**, **57**) and rofecoxib (**61**) analogues, in which the respective SO_2NH_2 and SO_2Me pharamacophores were replaced by an azido substituent, were synthesized. Docking compounds **54**, **57** and **61** analogues in COX-2 showed that the azido substituent was inserted into the secondary pocket of the COX-2 binding site where it underwent electrostatic interaction with Arg^{513}. The 1,5-diarylisoxazole (**57**) was a more selective COX-2 inhibitor than the 1,3-regioisomer (**54**). The rofecoxib analogue **61**, the most potent and selective inhibitor of COX-2 in this group (COX-1 IC_{50} = 159.7 μM; COX-2 IC_{50} = 0.196 μM; SI = 812), exhibited good AI and analgesic activities.

ACKNOWLEDGMENTS

I wish to express my deepest appreciation to Dr. Edward E. Knaus for his inspiring supervision, guidance and mentoring. Dr. Knaus' support was the driving force that made this investigation possible.

I am also indebted to my family for their boundless patience and constant encouragement during my Ph. D. program.

My gratitude is extended to Dr. Nabih I. Abdou for his continuous support and mentoring.

I also like to thank Dr. V. Somayajii for providing the NMR spectra, Mr. Don Whyte for his expert technical assistance, Mr. P. N. Praveen Rao and Miss Carol-Anne McEwen for technical assistance in performing the *in vitro* enzyme inhibition and antiinflammatory-analgesic assays, respectively.

Finally, I wish to thank my friends and colleagues in the medicinal chemistry laboratory for their discussions and suggestions.

Table of Contents

1.0	**INTRODUCTION.**	1
1.1	Arthritis.	1
1.2	Joints.	1
1.3	Inflammation.	2
1.4	Antiinflammatory drugs for treatment of arthritis.	4
1.4.1	Nonsteroidal antiinflammmatory drugs (NSAIDs).	4
1.4.2	Disease modifying antirheumatic drugs (DMARDS).	5
1.4.3	Pharmacological and biochemical basis of NSAIDs activity.	6
1.4.4	Gastrointestinal-safe NSAIDs.	7
1.5	Inflammatory laboratory models for testing NSAIDs.	7
1.6	Cyclooxygenase (COX) isozymes.	8
1.6.1	Biochemical activity of the COX enzyme.	8
1.6.2	Structural analysis of the COX enzyme.	11
1.6.3	COX-1 and COX-2 isozymes.	12
1.6.3.1	Structural differences between COX-1 and COX-2.	13
1.6.3.2	Biochemical similarities and differences between COX-1 and COX-2.	14
1.6.3.3	Expression of COX-1 and COX-2.	14
1.6.3.4	Molecular biology of COX-1 and COX-2.	15
1.6.3.5	Tissue expression of COX-1 and COX-2 under basal conditions.	16
1.6.3.6	Regulation of COX-1 and COX-2 during inflammation.	16
1.6.3.7	Regulation of COX-2 during carcinogenesis.	17
1.6.3.8	COX-2 role in Alzheimer's disease (AD).	18
1.6.4	Selective COX-2 isozyme inhibitors.	18
1.6.4.1	The sulfonanilide class of selective COX-2 inhibitors	21
1.6.4.2	The tricyclic class of selective COX-2 inhibitors.	21
1.6.4.2.1	Four-membered ring selective COX-2 inhibitors.	22
1.6.4.2.2	Five-membered ring selective COX-2 inhibitors.	22
1.6.4.2.3	Six-membered ring selective COX-2 inhibitors.	28
1.6.4.2.4	Fused ring system selective COX-2 inhibitors.	29
1.6.4.2	Di-tert-butylphenol derivatives as selective COX-2 inhibitors.	29

1.6.4.3	Modification of non-selective NSAIDs to selective COX-2 inhibitors.	30
1.6.4.4	Covalent modifiers of COX-2.	31
1.6.4.5	Other clinical applications of selective COX-2 inhibitors.	32
1.6.5	COX-1 and COX–2 inhibition assays.	32
1.7	Other molecular targets for anti-arthritic drugs.	34
1.8	Molecular modeling and drug design.	36
1.8.1	Principles of computational chemistry.	36
1.8.2	Molecular mechanics.	36
1.8.3	Quantum mechanical methods.	37
1.8.4	Geometry optimization.	38
1.8.5	Molecular dynamics.	40
1.8.6	Intermolecular forces and molecular binding.	41
1.8.7	Drug-receptor interactions.	41
1.8.8	Calculation of drug-receptor interactions.	41
1.8.9	Docking experiments.	42
1.9	Quantitative structure-activity relationships (QSARs).	43
1.9.1	QSARs : models and parameters.	44
1.9.2	Three dimensional QSARs.	45
2.0	**OBJECTIVES OF RESEARCH.**	47
3.0	**RESULTS AND DISCUSSION.**	49
3.1	Synthesis.	49
3.1.1	Synthesis of 3-dimethylamino-1,2-diarylprop-2-ene-1-ones **31a-h**.	49
3.1.2	Synthesis of 4,5-diarylisoxazoles **32a-p**.	57
3.1.3	Synthesis of trisubstituted-isoxazoles **36, 42, 44**, and **48a-b**.	67
3.1.4	Synthesis of 4,5-diaryl-2-methyl-4-isoxazolines **50a-k**.	87
3.1.5	Synthesis of 1-(4-azidophenyl)-3-(4-methylphenyl)-5-trifluoromethyl-pyrazole (**54**), 1-(4-azidophenyl)-5-(4-methylphenyl)-3-trifluoromethyl-pyrazole (**57**) and 4-(4-azidophenyl)-3-phenyl-2(5*H*)-furanone (**61**).	104
3.2	Molecular modeling.	117
3.2.1	Docking experiments.	117
3.2.1.1	Docking of **SC-588** in the binding site of COX-1 and COX-2.	118

3.2.1.2	Docking of 5-(4-methylthiophenyl)-4-phenylisoxazole (**32e**) and 5-(4-methylsulphonylphenyl)-4-phenylisoxazole (**32m**) in the binding site of COX-1 and COX-2.	122
3.2.1.3	Docking of 3-(4-methylsulphonylphenyl)-4-phenyl-5-trifluoromethyl-isoxazole (**36**) in the binding site of COX-1 and COX-2.	125
3.2.1.4	Docking of 4-(4-fluorophenyl)-5-(4-methylsulphonylphenyl)-3-methyl-isoxazole (**48a**) and 4-(4-methylphenyl)-5-(4-methylsulphonylphenyl)-3-methylisoxazole (**48b**) in the binding site of COX-2.	128
3.2.1.5	Docking of 4,5-diphenyl-3-methylsulfonamidoisoxazole (**44**) in the binding site of COX-2.	133
3.2.1.6	Docking of 5-(4-methylsulphonylphenyl)-2-methyl-4-phenyl-4-isoxazoline (**50h**) and 2,3- dimeth[illegible]-5-(4-methylsulphonylphenyl)-4-phenyl-4-isoxazoline (**50k**) in the b[illegible]site of COX-2.	134
3.2.1.7	Docking of 1-(4-azidophenyl)-3-(4-[illegible])-5-[illegible]oromethyl-pyrazole (**54**), 1-(4-azidophenyl)-5-(4-methylphenyl)-3-trifluoromethyl-pyrazole(**57**) and 4-(4- azidophenyl)-3-phenyl-2(5*H*)-furanone (**61**) in the binding site of COX-2.	136
3.2.2	Comparative molecular volume study.	142
3.3	Structure-activity relationships (SARs).	147
3.3.1	Antiinflammatory and analgesic activity, and COX-2 selective inhibition by isoxazoles **32a-p**, **36**, **42**, **44** and **48**.	147
3.3.2	Antiinflammatory and analgesic activity, and COX-2 selective inhibition by isoxazolines **50a-k**.	154
3.3.3	Antiinflammatory and analgesic Activity, and COX-2 selective inhibition by celecoxib (**53**, **57**) and rofecoxib (**61**) azido analogues.	159
3.4	Quantitative structure-activity relationships (QSARs).	161
3.4.1	QSARs of the isoxazole series as COX-1 and COX-2 inhibitors.	165
3.4.2	QSARs for the isoxazoline series as COX-1 and COX-2 inhibitors.	167
3.4.3	QSARs of the combined isoxazole and isoxazoline series as COX-1 and COX-2 inhibitors.	169
4.0	**EXPERIMENTAL**.	173

4.1	Synthesis	174
4.1.1	General method for the preparation of 3-dimethylamino-1,2-diarylprop-2-ene-1-ones (**31a-h**)	174
4.1.2	General method for the preparation of 4,5-diarylisoxazoles (**32a-h**)	174
4.1.3	General method for the preparation of 4- or 5-(4-methylsulfphinyl-phenyl)-4- or 5-(phenyl or 4-fluorophenyl)isoxazoles (**32i-l**)	175
4.1.4	General method for the preparation of 4- or 5-(4-methylsulfphonyl-phenyl)-4- or 5-(phenyl or 4- fluorophenyl)isoxazoles (**32m-p**)	175
4.1.5	Preparation of 3-(4-methylsulphonylphenyl)-4-phenyl-5-phenyl-5-trifluoromethylisoxazole (**36**)	175
4.1.5.1	Preparation of 4-(4-methylthiophenyl)-3-phenyl-1,1,1-trifluorobut-3-en-2-one (**33**)	176
4.1.5.2	Preparation of 4-hydroxylamino-4-(4-methylthiophenyl)-3-phenyl-1,1,1-trifluorobutan-2-one (**34**)	176
4.1.5.3	Preparation of 3-(4-methylthiophenyl)-4-phenyl-5-trifluoromethyl-isoxazole (**35**)	177
4.1.5.4	Preparation of 3-(4-methylsulphonylphenyl)-4-phenyl-5-trifluoromethyl-isoxazole (**36**)	177
4.1.6	Preparation of 4-(4-methylsulphonylphenyl)-3-phenyl-5-trifluoromethyl-isoxazole (**42**)	178
4.1.6.1	Preparation of 2-(4-methylthiophenyl)-3-phenyl-2-propenoic acid (**37**)	178
4.1.6.2	Preparation of methyl 2-(4-methylthiophenyl)-3-phenyl-2-propenoate (**38**)	178
4.1.6.3	Preparation of 3-(4-methylthiophenyl)-4-phenyl-1,1,1-trifluorobut-3-en-2-one (**39**)	178
4.1.6.4	Preparation of 4-hydroxylamino-3-(4-methylthiophenyl)-4-phenyl-1,1,1-trifluorobutan-2-one (**40**)	179
4.1.6.5	Preparation of 4-(4-methylthiophenyl)-3-phenyl-5-trifluoromethyl-isoxazole (**41**)	179
4.1.6.6	Preparation of 4-(4-methylsulphonylphenyl)-3-phenyl-5-trifluoromethyl-isoxazole (**42**)	180

4.1.7 Preparation of 4,5-diphenyl-3-methylsulphonamidoisoxazole (**44**). 180

4.1.8 General method for the preparation of 4-aryl-3-methyl-5-(4-methyl-sulphonylphenyl)isoxazoles (**48**). 181

4.1.8.1 General method for the preparation of 3-aryl-4-(4-methylthio-phenyl)-3-buten-2-ones (**45**). 181

4.1.8.2 General method for the preparation of 3-aryl-4-(4- methylthiophenyl)-3-buten-2-one oximes (**46**). 181

4.1.8.3 General method for the preparation of 4-aryl-3-methyl-5-(4-methylthio-phenyl)isoxazoles (**47**). 181

4.1.8.4 General method for the preparation of 4-aryl-3-methyl-5-(4-methyl-sulphonylphenyl)isoxazoles (**48**). 182

4.1.9 General method for the preparation of 4,5-diaryl-2-methylisoxazolium tetrafluoroborate (**49**). 182

4.1.10 General method for the preparation of 4,5-diaryl-2-methyl-4-isoxazolines (**50a-k**). 183

4.1.11 Preparation of 1-(4-azidophenyl)-3-(4-methylphenyl)-5-trifluoromethyl-pyrazole (**54**). 184

4.1.11.1 Preparation of 4,5-dihydro-5-hydroxy-3-(4-methylphenyl)-1-(4-nitrophenyl)-5-trifluoromethylpyrazole (**51**). 184

4.1.11.2 Preparation of 3-(4-methylphenyl)-1-(4-nitrophenyl)-5-trifluoromethyl-pyrazole (**52**). 184

4.1.11.3 Preparation of 1-(4-aminophenyl)-3-(4-methylphenyl)-5-trifluoromethyl-pyrazole (**53**). 185

4.1.11.4 Preparation of 1-(4-azidophenyl)-3-(4-methylphenyl)-5-trifluoromethyl-pyrazole (**54**). 185

4.1.12 Preparation of 1-(4-azidophenyl)-5-(4-methylphenyl)-5-trifluoromethyl-3-trifluoromethylpyrazole (**57**). 186

4.1.12.1 Preparation of 5-(4-methylphenyl)-1-(4-nitrophenyl)-5-trifluoromethyl-3-trifluoromethylpyrazole (**55**). 186

4.1.12.2 Preparation of 1-(4-aminophenyl)-5-(4-methylphenyl)-5-trifluoromethyl-3-trifluoromethylpyrazole (**56**). 186

4.1.12.3	Preparation of 1-(4-azidophenyl)-5-(4-methylphenyl)-5-trifluoromethyl-pyrazole (**57**).	187
4.1.13	Preparation of 4-(4-azidophenyl)-3-phenyl-2(5*H*)-furanone (**61**).	187
4.1.13.1	Preparation of 4-azidophenacyl bromide (**59**).	187
4.1.13.2	Preparation of 4-azidophenacylphenyl acetate (**60**).	188
4.1.13.3	Preparation of 4-(4-azidophenyl)-3-phenyl-2(5*H*)- furanone (**61**).	188
4.2	Antiinflammatory activity assay.	188
4.3	Analgesic activity assay.	189
4.4	*In vitro* enzyme inhibition assay.	190
4.5	Molecular modeling study.	191
4.5.1	Docking study.	191
4.5.2	Comparative molecular volume study.	192
4.5.3	Conformational analysis.	192
4.5.4	Quantitative structure-activity relationships (QSARs).	192
5.0	Conclusions.	193
6.0	References.	195

List Of Figures

1	Arachidonic acid cascade.	8
2	Oxidation of arachidonic acid to prostaglandin H_2.	9
3	Branched chain mechanism for the COX enzyme activity.	10
4	Cyclooxygenase enzyme domains.	12
5	SC-588 bound to the active site of COX-2 (1CX2 PDB file).	25
6	Possible geometrical isomers of propenones **31a-h**.	49
7	Propenone **31a-h** resonance structures.	50
8	Docking of SC-588 (**19**) (ball and stick) in (a) COX-1 (line and stick) ($E_{intermolecular}$ = -10.12 Kcal/mol) and (b) COX-2 (line and stick) ($E_{intermolecular}$ = -42.44 Kcal/mol).	120
9	Docking of (a) isoxazole **32e** (ball and stick) ($E_{intermolecular}$ = −15.71 Kcal/mol), and (b) isoxazole **32m** (ball and stick) ($E_{intermolecular}$ = -39.06 Kcal/mol) in the binding site of COX-2 (line and stick).	122
10	Docking of isoxazole **36** (ball and stick) in the binding site of (a) ovine COX-1 (line and stick) ($E_{intermolecular}$ = 16.51 Kcal/mol), and (b) human COX-2 (line and stick) ($E_{intermolecular}$ = -53.06 Kcal/mol).	127
11	Docking of (a) isoxazole **48a** (ball and stick) ($E_{intermolecular}$ = −19.68 Kcal/mol), and (b) isoxaozle **48b** (ball and stick) ($E_{intermolecular}$ = -18.12 Kcal/mol) in the binding site of COX-2 (line and stick).	130
12	Conformation analysis of isoxazoles **48a**, **48b** and **36**.	131
13	Docking isoxazole **44** (ball and stick) in the binding site of COX-2 (line and stick) ($E_{intermolecular}$ = -45.6 Kcal/mol).	134
14	Docking of (a) isoxazoline **50h** (ball and stick) ($E_{intermolecular}$ = -35.46 Kcal/mol), and (b) isoxazoline **50k** (ball and stick) ($E_{intermolecular}$ = -49.26 Kcal/mol) in the binding site of COX-2 isozyme (line and stick).	136
15	Azide resonance hybrid structures.	137

16 Docking of (a) pyrazole **54** (ball and stick) ($E_{intermolecular}$ = -34.12 Kcal/mol), and (b) pyrazole **57** (ball and stick) ($E_{intermolecular}$ = -46.9 Kcal/mol) in the binding site of COX-2 (line and stick). 138

17 Docking of celecoxib **17** (ball and stick) in the binding site of human COX-2 (line and stick) ($E_{intermolecular}$= -43.62 Kcal/mol). 139

18 Docking of (a) furanone **61** (ball and stick) in the binding site of human COX-2 (line and stick)($E_{intermolecular}$= -49.6 Kcal/mol) and (b) rofecoxib (**18**) (ball and stick) in the binding site of human COX-2 (line and stick) ($E_{intermolecular}$= -42.16 Kcal/mol)..... 141

19 Comparative molecular volume study for isoxazole **32m**. 145

20 Comparative molecular volume study for isoxazole **50h**. 146

List of Schemes

1	Synthesis of 4,5-diarylisoxazoles **32a-p**.	51
2	Synthesis of 3-(4-methylsulphonylphenyl)-4-phenyl-5-trifluoro-methylisoxazole (**36**).	68
3	Synthesis of 4-(4-methylsulphonylphenyl)-3-phenyl-5-trifluoro-methylisoxazole (**42**).	69
4	Synthesis of 4,5-diphenyl-3-methylsulfonamidoisoxazole (**44**).	78
5	Synthesis of 4,5-diaryl-3-methylisoxazole (**48**).	79
6	Synthesis of 4,5-diaryl-2-methyl-4-isoxazolines (**50**).	88
7	Synthesis of 1-(4-azidophenyl)-3-(4-methylphenyl)-5-trifluoromethyl-pyrazole (**54**) and 1-(4-azidophenyl)-5-(4-methylphenyl)-3-trifluoromethylpyrazole (**57**).	105
8	Synthesis of 4-(4-azidophenyl)-3-phenyl-2(5*H*)-furanone (**61**).	113

List of Tables

1	Some inflammatory mediators released and/or activated during the inflammatory process and their putative roles.	3
2	Other molecular targets for arthritis.	35
3	IR and ^{1}H NMR spectral data for 3-dimethylamino-1,2-diarylprop-2-ene-1-one (**31**).	52
4	^{13}C NMR spectral data for 3-dimethylamino-1,2-diarylprop-2-ene-1-one (**31**).	54
5	Physical data for 3-dimethylamino-1,2-diarylprop-2-ene-1-one (**31**).	56
6	IR and ^{1}H NMR spectral data for 4,5-diarylisoxazoles (**32**).	58
7	^{13}C and ^{19}F NMR spectral data for 4,5-diarylisoxazoles (**32**).	61
8	Physical data for 4,5-diarylisoxazoles (**32**).	65
9	IR and ^{1}H NMR spectral data for 2-(4-methylthiophenyl)-3-phenyl-2-propenoic acid (**37**), methyl 2-(4-methylthiophenyl)-3-phenyl-2-propenoate (**38**), and 3,4-diaryl-1,1,1-trifluorobut-3-ene-2-ones (**33**, **39**).	70
10	^{13}C and ^{19}F NMR spectral data for 3,4-diaryl-1,1,1-trifluorobut-3-ene-2-ones (**33**, **39**).	71
11	Physical data for 2-(4-methylthiophenyl)-3-phenyl-2-propenoic acid (**37**), methyl 2-(4-methylthiophenyl)- 3-phenyl-2-propenoate (**38**), and 3,4-diaryl-1,1,1-trifluorobut-3-ene-2-ones (**33**, **39**).	72
12	IR and ^{1}H NMR spectral data for 3,4-diaryl-4-hydroxylamino-1,1,1-trifluorobutan-2-ones (**34**, **40**), and 3,4-diaryl-5-trifluoromethyl-isoxazoles (**35**, **41**, **36**, **42**).	73
13	^{13}C and ^{19}F NMR spectral data for 3,4-diaryl-4-hydroxylamino-1,1,1-trifluorobutan-2-ones (**34**, **40**), and 3,4-diaryl-5-trifluoromethyl-isoxazoles (**35**, **41**, **36**, **42**).	75
14	Physical data for 3,4-diaryl-4-hydroxylamino-1,1,1-trifluorobutan-2-ones (**34**, **40**), and 3,4-diaryl-5-trifluoromethylisoxazoles (**35**, **41**, **36**, **42**).	77

15 IR and ^{1}H NMR spectral data for 4,5-diphenyl-3-methylsulfonamido-isoxazole (**44**), 3,4-diaryl-3-butene-2-ones (**45**), 3,4- diaryl-3-butene-2-one oximes (**46**), and 4,5-diaryl-3-methylisoxazoles (**47, 48**). 80

16 ^{13}C and ^{19}F NMR spectral data for 4,5-diphenyl-3-methylsulfonamido-isoxazole (**44**), 3-(4-flourphenyl)-4-(4-methylthiophenyl)-3-butene-2-one (**45a**), 3-(4-flourphenyl)-4-(4-methylthiophenyl)-3,4-diaryl-3-butene-2-one oxime (**46a**), and 4,5-diaryl-3-methylisoxazoles (**47, 48**). 83

17 Physical data for 4,5-diphenyl-3-methylsulfonamidoisoxazole (**44**), 3,4-diaryl-3-butene-2-one (**45**), 3,4-diaryl-3-butene-2-one oxime (**46**), and 4,5-diaryl-3-methylisoxazole (**47, 48**). 86

18 IR and ^{1}H NMR spectral data for 4,5-diaryl-2-methylisoxazolium tetrafluoroborates (**49**). 90

19 ^{13}C and ^{19}F NMR spectral data for 4,5-diaryl-2-methylisoxazolium tetrafluoroborate (**49**). 93

20 Physical data for 4,5-diaryl-2-methylisoxazolium tetrafluoroborate (**49**). 95

21 IR and ^{1}H NMR spectral data for 4,5-diaryl-2-methyl-4-isoxazolines (**50**). 97

22 ^{13}C and ^{19}F NMR spectral data for 4,5-diaryl-2-methyl-4-isoxazolines (**50**). 100

23 Physical data for 4,5-diaryl-2-methyl-4-isoxazolines (**50**). 102

24 IR and ^{1}H NMR spectral data for 4,5-dihydro-5-hydroxy-3-(4-methyl-phenyl)-1-(4-nitrophenyl)-5-trifluoromethylpyrazole (**51**), and 1-aryl-3-(4-methylphenyl)-5-trifluoromethyl-1*H*-pyrazoles (**52-54**). 106

25 ^{13}C and ^{19}F NMR spectral data for 4,5-dihydro-5-hydroxy-3-(4-methyl-phenyl)-1-(4-nitrophenyl)-5-trifluoromethylpyrazole (**51**), and 1-aryl-3-(4-methylphenyl)-5-trifluoromethyl-1*H*-pyrazoles (**52-54**). 107

26 Physical data for 4,5-dihydro-5-hydroxy-3-(4-methylphenyl)-1-(4-nitrophenyl)-5-trifluoromethylpyrazole (**51**), and 1-aryl-3-(4-methylphenyl)-5-trifluoromethyl-1*H*-pyrazoles (**52-54**). 109

27 IR and ^{1}H NMR spectral data for 1-aryl-5-(4-methylphenyl)-3-trifluoro-methyl-1*H*-pyrazoles (**55-57**). 110

28 ^{13}C NMR spectral data for 1-aryl-5-(4-methylphenyl)-3-trifluoro-methyl-1*H*-pyrazoles (**55-57**). 111

29 Physical data for 1-aryl-5-(4-methylphenyl)-3-trifluoromethyl-1*H*-pyrazoles (**55-57**). 112

30 IR and ^{1}H NMR spectral data for 2-substituted-1-(4-azidophenyl)-ethanones (**59**, **60**), and 4-(4-azidophenyl)-3-phenyl-2(5*H*)-furanone (**61**). 114

31 ^{13}C NMR spectral data for 2-substituted-1-(4-azidophenyl)ethanones (**59**, **60**), and 4-(4-azidophenyl)-3-phenyl-2(5*H*)-furanone (**61**). 115

32 Physical data for 2-substituted-1-(4-azidophenyl)ethanones (**59**, **60**), and 4-(4-azidophenyl)-3-phenyl-2(5*H*)-furanone (**61**). 116

33 Distances between selected COX-1 and COX-2 residues and SC-588 (**19**). 119

34 Distances between selected COX-1 and COX-2 residues and 5-(4-methylthiophenyl)-4-phenylisoxazole (**32e**). 123

35 Distances between selected COX-1 and COX-2 residues and 5-(4-methylsulphonylphenyl)-4-phenylisoxazole (**32m**). 124

36 Distances between selected COX-1 and COX-2 residues and 3-(4-methylsulphonylphenyl)-4-phenyl-5-trifluoromethylisoxazole (**36**). 126

37 Distances between selected COX-2 residues and 4-(4-fluorophenyl)-3-methyl-5-(4-methylsulfonylphenyl)isoxazole (**48a**) and 4-(4-methylphenyl)-3-methyl-5-(4-methylsulfonylphenyl)isoxazole (**48b**). 129

38 RMSD of selected residues in COX-2 active site in assemblies of COX-2 and isoxazoles **48a-b** and **36**. 132

39 Distances between selected COX-2 residues and 5-(4-methylsulphonyl-phenyl)-2-methyl-4-phenyl-4-isoxazoline (**50h**) and 2,3-dimethyl-5-(4-methylsulphonylphenyl)-4-phenyl-4-isoxazoline (**50k**). 135

40 Distances between selected COX-2 residues and 1-(4-azidophenyl)-3-(4-methylphenyl)-5-trifluoromethylpyrazole (**54**), 1-(4-azidophenyl)-5-(4-methylphenyl)-3-trifluoromethylpyrazole (**57**) and 4-(4-azidophenyl)-3-phenyl-2(5*H*)-furanone (**61**). 140

41 Structures of azole derivatives used as selective COX-2 inhibitors training set. 144

42 Antiinflammatory and analgesic activities, *in vitro* COX-1 and COX-2 inhibition data, and molecular volumes of the diarylisoxazoles **(32a-p, 36, 42, 44)**. 151

43 Antiinflammatory and analgesic activities and *in vitro* COX-1 and COX-2 inhibition data, and molecular volumes of 4,5-diarylisoxazolines **(50a-k)**. 157

44 Antiinflammatory and analgesic activities, *in vitro* COX-1 and COX-2 inhibition data, and molecular volumes of 1-(4-azido phenyl)-3-(4-methylphenyl)-5-trifluoromethylpyrazole (**53**), 1-(4-azidophenyl)-5-(4-methylphenyl)-3-trifluoromethylpyrazole (**57**), and 4-(4-azidophenyl)-3-phenyl-2(5*H*)-furanone (**61**). 160

45 Parameters used in QSAR studies. 162

46 Enzyme inhibition (IC_{50}) and intermolecular energy ($E_{intermolecular}$) of isoxazoles **32b-c**, **32m-n**, **36**, **42**, **44** and **48a-b**, and isoxazolines **50a-b** and **50h-k**. 164

47 Experimental *vs.* calculated IC_{50} (COX-1) for the isoxazole series. 165

48 Experimental *vs.* calculated IC_{50} (COX-2) for the isoxazole series. 166

49 Experimental *vs.* calculated IC_{50} (COX-1) for the isoxazoline series. 168

50 Experimental *vs.* calculated IC_{50} (COX-2) for the isoxazoline series. 169

51 Experimental *vs.* calculated IC_{50} (COX-1) for both the isoxazole and isoxazoline series. 170

52 Experimental *vs.* calculated IC_{50} (COX-2) for both the isoxazole and isoxazoline series. 171

LIST OF ABBREVIATIONS

AA	Arachidonic acid.
AD	Alzheimer's disease.
AI	Antiinflammatory.
AMBER	Assisted model building with energy refinement.
Arg	Arginine.
Asn	Aspargine.
ASA	Aspirin.
ATP	Adenosine triphosphate.
CG	Conjugate gradient.
CHARM	Chemistry at Harvard using molecular mechanics.
COX	Cyclooxygenase.
COX-1	Cyclooxygenase-1.
COX-2	Cyclooxygenase-2.
CVFF	Consistent volume force field.
DMARDs	Disease modifying anti-rheumatic drugs.
EGF	Epidermal growth factor.
EIA	Enzyme immunoassay.
ER	Endoplasmic reticulum.
FAP	Familial adenomatous polyposis.

FLAP	5-Lipoxygenase activating protein.
GC/MS	Gas chromatography coupled to mass spectrometry.
GI	Gastrointestinal.
GMP	Guanine monophosphate.
Gln	Glutamide.
Glu	Glutamic acid.
Gly	Glycine.
His	Histidine.
IC_{50}	Concentration required to produce 50% inhibition.
IL-1	Interleukin-1.
Ile	Isoleucine.
IR	Infrared.
Kb	Kilobases
K_{cat}	Catalysis constant
K_m	Michaelis-Menton constant
Leu	Leucine.
LO	Lipoxygenase.
LT	Leukotriene.
MAPK	Mitogen activated protein kinase.
MBD	Membrane binding domain.

MD	Molecular dynamics.
Met	Methionine.
MM	Molecular mechanics.
MMP	Matrix metalloproteinase.
MR	Molecular or fragment size.
mRNA	Messenger ribonucleic acid
MSK	Musculoskeletal.
NF	Nuclear factor.
NMR	Nuclear magnetic resonance.
NOS	Nitric oxide synthase.
NSAIDs	Nonsteroidal antiinflammatory drugs.
OA	Osteoarthritis.
PG	Prostaglandin.
Phe	Phenylalanine.
PLA	Phospholipase A.
PMN	Polymorphonuclear leukocytes.
POD	Peroxidase.
PPAR	Peroxisome proliferator activated receptor.
QSAR	Quantitative structure activity relationship.
RA	Rheumatoid arthritis.

RIA	Radioimmunoassay.
RH-IL-1RA	Recombinant human interleukin-1 receptor antagonist.
Ser	Serine
SI	Selectivity index.
TGF-β	Transforming growth factor-beta.
TNF-α	Tissue necrosis factor-alpha.
Trp	Tryptophan.
Tx	Thromboxane.
Tyr	Tyrosine.
UV	Ultraviolet.
Val	Valine.

1.0 Introduction.

1.1 Arthritis.

Arthritis ('arth' meaning joint, 'itis' meaning inflammation) is not a one-note story, or even a few variations on a single theme. Arthritis consists of more than 100 different conditions, that can be anything from relatively mild forms of tendonitis such as tennis elbow to systemic forms such as rheumatoid arthritis (RA). Arthritis is classified by researchers and clinicians under the category of musculoskeletal (MSK) disorders. Population studies indicate that arthritis affects 20% of the adult population and is the most frequent cause of long-term physical disability [Arthritis Society of Canada]. The 1990 Ontario Health Survey (which is considered representative of Canada as a whole) showed 21% of women of all ages, compared to 15% of men of all ages have some form of arthritis. Health Canada's economic burden of arthritis in Canada in 1993 was $17.8 billion which constituted about 12% of all health costs. The 1990 Ontario Health Survey suggested that more than half of all arthritis morbidity is related to osteoarthritis (OA) with an associated cost of $9 billion.

1.2 Joints.

There are more than 100 joints connecting the body's 206 bones. The bones of joints are capped with cartilage, which acts as a shock absorber and allows bone ends to glide smoothly across each other. If the cartilage is destroyed as in OA, the bones of a joint can grind against each other causing pain, loss of mobility, deformity and dysfunction [Mankin, 1985].

The joint cavity between the bones is enclosed by a capsule that is flexible to prevent joint dislocation. The inner lining of this capsule, the synovium, produces a thick fluid

that lubricates and nourishes the joint. In many forms of arthritis, the synovium becomes inflamed, and thickened producing extra fluid that contains inflammatory cells, causing damage of the cartilage and underlying bone.

Cartilage tissue is comprised of a small number of cells called chondrocytes, which are embedded in a large volume of extracellular matrix, composed mainly of collagen and proteoglycan in water. Maintenance of the extracellular matrix homeostasis is the function of chondrocytes. In normal tissue, the rate of new matrix formation is equal to the rate of matrix degradation, so that there is neither net tissue gain nor loss. Both processes are controlled by a variety of extracellular proteins such as growth factors and cytokines. Transforming growth factor-β (TGF-β) is among the most commonly associated with the stimulation of connective tissue formation, whereas cytokines such as interleukin-1 (IL-1) and tissue necrosis factor-α (TNF-α) are major players associated with matrix degradation through activation of matrix metalloproteinases (MMP) [Bottomley *et al.*, 1998]. In an arthritic cartilage, proteoglycan is progressively depleted with a qualitative change in proteoglycan structure. This was mainly attributed to the imbalance between activities of MMP in the chondrocytes and tissue inhibitor metalloproteinases-1 (TIMP-1). Once cartilage degradation begins, breakdown products such as fragments of extracellular matrix components, are released into the synovial fluid and phagocytosed by cells from the synovial membrane. This process will result in an inflammatory response.

1.3 Inflammation.

Inflammation is a complex stereotypical reaction of the body expressing its response to cell damage. Elucidation of the detailed inflammation process has revealed a close

relationship between inflammation and the immune response. The five basic symptoms of inflammation, redness, swelling, heat, pain and deranged function, have been known since the ancient Greek and Roman era. These symptoms are caused by extravasation of plasma and infiltration of leukocytes into the site of inflammation.

There are a number of triggers that cause inflammation such as mechanical, chemical, biological, or nutritive stimulation that activate and/or release inflammatory mediators (Table 1) [Dawson & Willoughby, 1985].

Table 1. Some Inflammatory Mediators Released and/or Activated during the Inflammatory Process and Their Putative Roles.

Substance	Proposed Pathophysiologic Role	Types of Inflammation
Histamine	• Increased vascular permeability. • Triple response. • Elevation of cyclic AMP.	Acute, transient.
5-Hydroxytryptamine	• Increased vascular permeability. • Gastrointestinal inflammation.	Acute, transient.
Kinins	• Increased vascular permeability. • Pain.	Acute, experimental.
PGE_2	• Vasodilation. • Pain and change of vascular tone. • Amplification of inflammation. • Elevation of cyclic AMP. • Increased enzyme secretion.	Acute.
$PGF_{2\alpha}$	• Vasoconstriction. • Reduction of permeability. • Elevation of cyclic GMP	Acute.
PGI_2 and TxA_2	• Vasodilation. • Reduction in adherence of platelets.	Acute.
LTB_4	• Chemo-attractant. • Increased vascular permeability.	Acute.
Inflammatory Cytokines	• Cell growth and differentiation. • Chondrocyte activation.	Acute/Chronic.

Inflammatory mediators produce a microvascular response that consists of an initial brief vasoconstriction of the arteriolar vessels followed by vasodilation. The endothelial cells of the vessel wall contract, notably in the post capillary venules, which leads to extravasation of plasma proteins. The initial movement of solute and proteins is followed by a wave of polymorphonuclear leukocytes (PMNs) migration, presumably in response to chemoattractants. Monocytes migrating with PMNs act to clear up certain debris, which the PMNs are unable to handle. A typical acute inflammatory process can bud to a more chronic lesion.

1.4 Antiinflammatory Drugs for Treatment of Arthritis.

The management of arthritic disorders involves a stepwise approach to the use of therapeutic agents currently available. Relief of pain and reduction of inflammation are immediate goals. Longer-term goals would be to halt the progression of the disease and preserve the functions of muscles and joints in order to permit the patient to lead a more productive life.

1.4.1 Nonsteroidal Antiinflammatory Drugs (NSAIDs).

Felix Hoffman, a chemist at Farben Fabriken Friedrich Bayer in Germany, began tinkering with salicylic acid in hopes of preserving its inflammation-fighting properties while easing its harsh effects on the stomach. These studies led to the discovery of acetyl salicylic acid in 1897, which Bayer began marketing in 1899 under the trade name Aspirin®. In the following century, a multitude of NSAIDs emerged, that belongs to three major families: carboxylic acids, pyrazoles and oxicams.

The carboxylic acid family is subdivided into salicylic acid derivatives such as acetylsalicylic acid, acetic acid derivatives such as indomethacin, propionic acid derivatives such as ibuprofen, and fenamates such as mefenamic acid. Phenylbutazone and piroxicam are typical parent compounds from the pyrazole and oxicam families, respectively. Aside from the NSAIDs mentioned above, acetaminophen and pyrazole drugs such as phenazone, and 4-methylaminophenazone have been used as antipyretic over the counter (OTC) analgesics. This latter group of compounds, unlike NSAIDs, are non-acidic and do not exhibit antiinflammatory (AI) activity at therapeutic doses [Stern *et al.*, 1989]

1.4.2 Disease-Modifying Antirheumatic Drugs (DMARDs).

The previously mentioned NSAIDs were proven to be beneficial in the symptomatic treatment of arthritic disorders thereby providing a popular therapeutic regimen. DMARDs differ from NSAIDs in that they retard or halt the underlying progression of arthritis, in spite of the fact that they are devoid of the AI and analgesic effects exhibited by NSAIDs. Unfortunately, DMARDs showed dangerous side effects, which in many cases, limit their long-term use. DMARDs include: gold compounds such as auranofen, sulfhydryl compounds such as penicillamine, the antimalarial agent hydroxyquine sulfate, and the immunosupressive agents azathioprine, methotrexate, cyclophosphamide, and cyclosporine [Borne, 1995].

1.4.3 Pharmacological and Biochemical Basis of NSAIDs Activity.

As indicated in section **1.3**, several chemical mediators have been postulated to play important roles in the inflammatory process. Prior to 1971, the proposal that NSAIDs

exert their AI activity by interacting with a hypothetical AI receptor was widely accepted. In 1971, Vane published a classic paper in which he reported that indomethacin, aspirin, and salicylate in this descending order of potency, inhibited the biosynthesis of prostaglandins (PGs) from the substrate arachidonic acid (AA) [Vane, 1971]. Vane further suggested that the clinical actions of these agents are due to this inhibition of PG biosynthesis.

The role of NSAIDs in the treatment of arthritis is not completely understood. While indomethacin decreased proteoglycan synthesis, benoxaprofen augmented the same pathway [Dingle, 1991; Palmoski *et al.*, 1983]. This difference could be attributed to the broad spectrum of NSAIDs' biochemical effects on inflammation pathways. In addition to their ability to inhibit PG biosynthesis, NSAIDs also inhibit platelet aggregation [Vane 1971], leukocyte adhesion [Kurose et *al.*, 1996], induced nitric oxide synthase (NOS) expression [Amin *et al.*, 1995], and nuclear factor NF-κB [Diaz-Gonzalez *et al.*, 1998].

The introduction of NSAIDs for the treatment of arthritic diseases has resulted in a vast increase in the number and severity of adverse drug reactions. The main side effects associated with NSAIDs use include: gastrointestinal (GI) perforation, ulceration, and/or bleeding, impaired renal clearance and other nephrotoxic syndromes, pulmonary and other hypersensitivity reactions, elevated hepatic serum/plasma levels of liver enzymes reflecting hepatotoxic reactions, and hematological side effects such as aplastic anemia, agranulocytosis, and leucopenia [Zimmerman, 1994]. The most frequently reported adverse effects are GI side effects. NSAIDs-induced gastroenteropathy can be further divided into two categories: gastroduodenal injuries and lower bowel NSAIDs-induced enteropathy. The main biochemical effect, responsible for this damage was found to be

NSAID-induced uncoupling of oxidative phosphorylation which leads to a heightened activity of the tricarboxylic acid cycle, with an increased flow of electrons down the respiratory chain, forming oxygen-reactive species. Consequently, the cell becomes depleted of ATP and loses control over its intercellular junction [Somasundaram *et al.*, 1995].

1.4.4 Gastrointestinal-Safe NSAIDs.

Over the past 30 years a number of strategies have been used to reduce the GI injury caused by NSAIDs. These include enteric coating of the NSAID tablet to prevent absorption in the stomach [Hoftiezer *et al.*, 1980], parenteral administration and formulation of prodrugs of NSAIDs [Graham *et. al.*, 1985] that require hepatic metabolism to produce the active drug. These modifications had little impact on decreasing the incidence of the severe adverse GI reactions.

Etodolac and nabumatone, two newly marketed NSAIDs, were claimed to have markedly reduced capacities for causing gastric ulceration and bleeding compared to previously marketed NSAIDs [Benhamou, 1990; Jenner, 1990]. The improved safety profile of etodolac and nabumetone was attributed to their non-acidic nature, and the fact that they by-pass the enterohepatic circulation. Unfortunately, these drugs quickly lose this latter advantage at the upper limit of their recommended dose.

1.5 Inflammatory Laboratory Models for Testing NSAIDs.

Pharmacological models used to determine the AI activity of NSAIDs can be divided into two main classes: acute and chronic inflammatory models [Otterness *et al.*, 1985]. Acute inflammatory models are based on the four cardinal signs of inflammation, edema

model as the carrageenan foot edema method; erythema model as UV light-induced erythema method; pain model as the abdominal constriction method; and exudative model as the carrageenan pleurisy method. The most popular chronic inflammatory model is the induced adjuvant arthritis model.

1.6 Cyclooxygenase (COX) Isozymes.

COX enzyme was first isolated from bovine vesicular gland microsomes [Miyamoto *et al.*, 1976]. COX enzyme was latter classified as an epidermal growth factor (EGF) type family member according to the Structural Classification of Proteins (SCOP) [Murzin *et al.*, 1995].

1.6.1 Biochemical Activity of the COX Enzyme.

COX enzyme catalyzes a key reaction in the AA cascade, the oxidation of AA to PGH_2 (Figure 1).

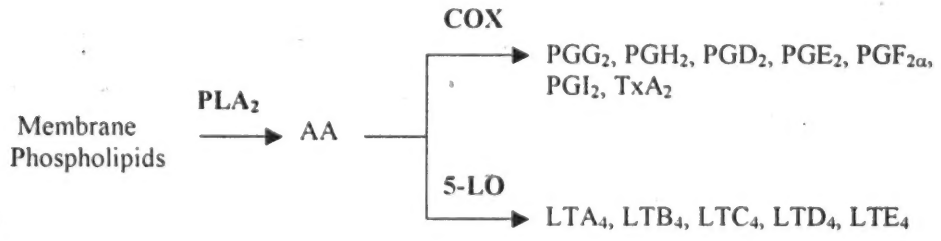

PLA_2: Phospholipase A_2 enzyme; 5-LO: 5-Lipoxygenase enzyme; TxA_2: Thromboxane, LT: Leukotriene

Figure 1. Arachidonic acid cascade.

Formation of PGH_2 from AA involves two distinct reactions, both of which are catalyzed by COX enzyme. The initial COX reaction introduces two molecules of O_2 into AA to produce PGG_2. A second peroxidase (POD) reaction involves the reduction of

PGG_2 to PGH_2 (Figure 2). All the remaining PGs are produced from PGH_2 via the action of individual PG synthases.

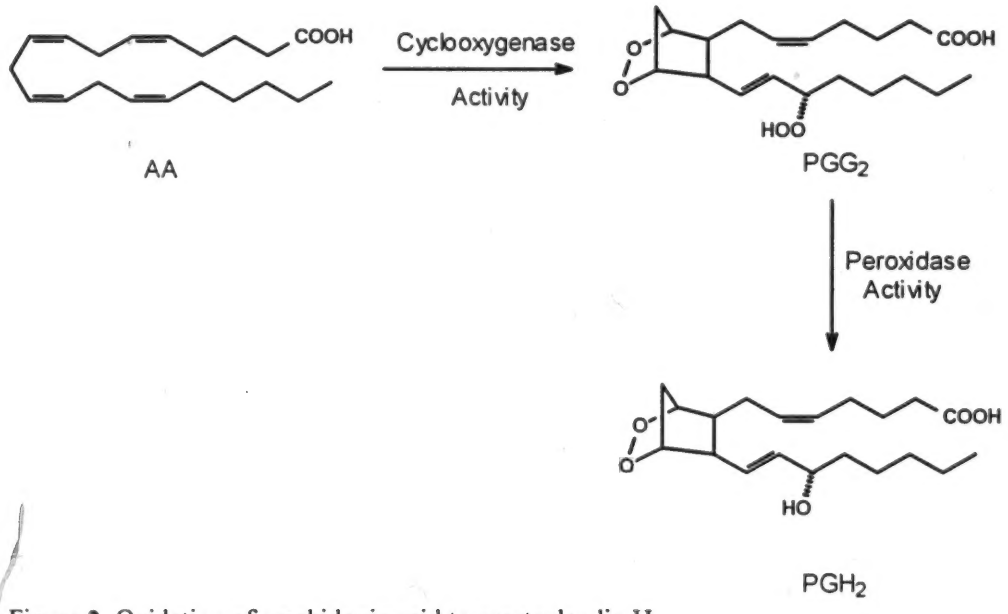

Figure 2. Oxidation of arachidonic acid to prostaglandin H_2.

The heme group attached to the apoenzyme was found to be essential for both COX and POD reactions [Smith *et al.*, 1991]. The heme moiety in the resting state of COX enzyme is predominantly in the ferric oxidation state, or high-spin state. The high spin state implies a five or six coordination complex with His^{207} and His^{388} [Shimokawa *et al.*, 1991].

Despite the dependence of COX and POD reactions on heme, it is possible to resolve the COX and POD reactions functionally, suggesting that they are independent but interactive active sites [Smith *et al.*, 1992]. Dietz and coworkers proposed a very plausible model to describe the COX enzyme activity that has became known as the

branched-chain mechanism (Figure 3) [Dietz *et al.*, 1988]. According to this mechanism, reaction of a hydroperoxide with the heme group (PPIX-Fe^{3+}) at the peroxidase active site leads to the formation of intermediate **I**; this occurs with concomitant reduction of the hydroperoxide to its corresponding alcohol. Intermediate **I** then abstracts a hydrogen atom from a neighboring tyrosine (Tyr^{385}), to produce a second oxidized heme species intermediate **II**, containing a tyrosyl radical. Finally, the tyrosyl radical, that is envisioned to be the active species, abstracts a hydrogen atom from the AA molecule to initiate the COX reaction [Garavito *et al.*, 1999].

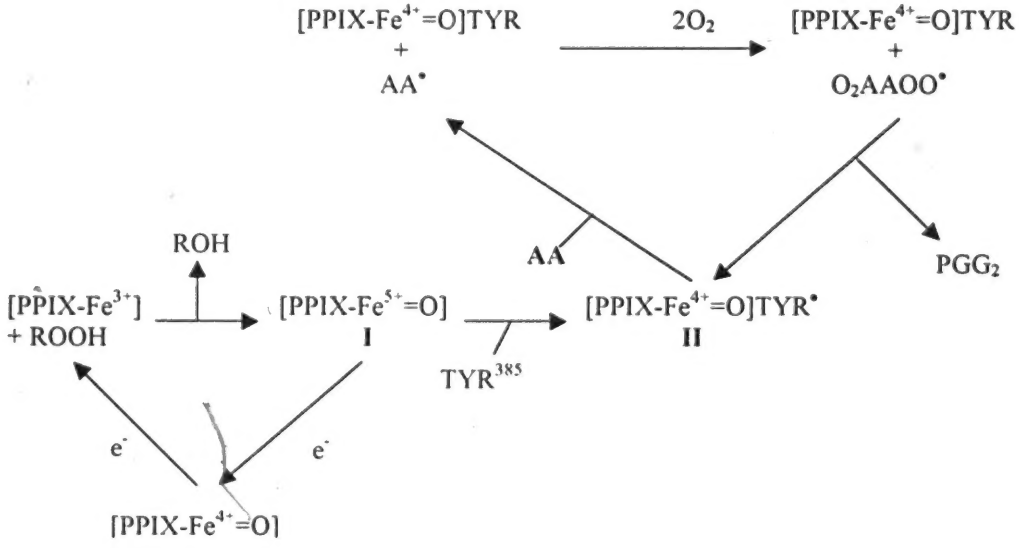

Figure 3: Branched chain mechanism for the COX enzyme activity.

Based on the branched chain mechanism, Hawkey suggested that AA binds to the COX enzyme active site in a bent conformation [Hawkey, 1999]. A rotation about the C-9/C-10 single bond produces the conformation of AA that leads to the formation of the

trans-aliphatic side chains of the cyclopentane ring. This conformation facilitates the stereospecific abstraction of the pro-*S* hydrogen form the allylic C-13 position.

1.6.2 Structural Analysis of COX Enzyme.

The x-ray crystal structure established by Picot and co-workers suggested that COX is a homodimeric enzyme in a monotopic arrangement with respect to the cell membrane (Picot *et al.*, 1994). The dimer binds 1 mole of high spin ferric heme per mole of monomer. It extends over residues 25-600 (residues 1-24 form the cleaved signal sequence). Each monomer consists of 3 independent folding domains. The *N*-terminal EGF domain in green extends from residues 34-72. The second is the membrane binding domain (MBD) in copper color which consists of 43 residues in 4 right handed amphipathic α-helices A, B, C and D comprised of amino acids 73-116 which are essential for anchoring the enzyme onto the endoplasmic reticulum (ER) lipid bilayer. The catalytic domain in blue, that extends from residues 117-587, is a globular structure containing the COX and POD reaction active sites (Figure **4**).

The POD reaction active site is located at the interface between the two lobes composing the catalytic domain. The COX active site, at which NSAIDs bind, consists of a long, narrow channel (~8 x 25Å) extending from the outer surface of the MBD through helices A, B, and C to the center of the COX enzyme monomer. Among the important residues in COX reaction active site are Ser^{530}, that is positioned in the COX reaction active site such that its acetylation by aspirin could easily block access to the upper part of the COX enzyme channel and Arg^{120} which is located near the channel's mouth of the COX enzyme, and is favorably positioned such that its guanidinuim group can bind to the carboxylic group of classical NSAIDs.

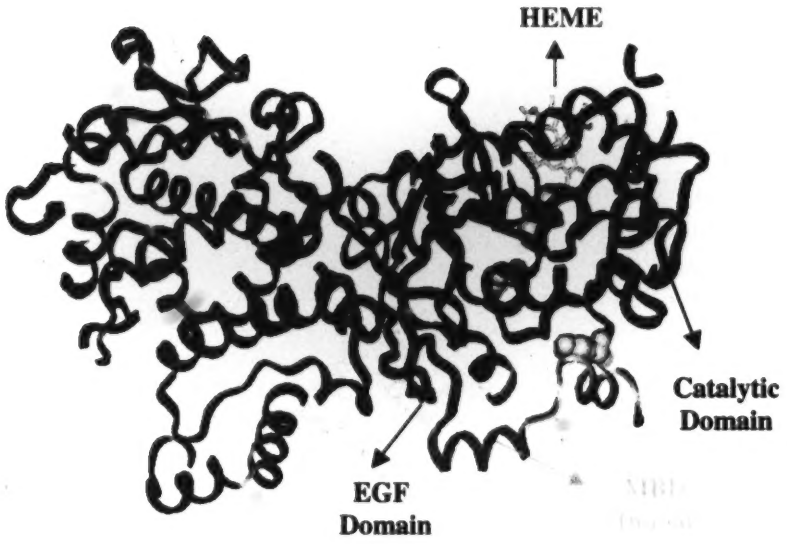

Figure 4. Cyclooxygenase enzyme domains.

1.6.3 COX-1 and COX-2 Isozymes.

Investigators studying growth pathways identified a unique inducible gene enzyme product different from the known COX isozyme sequence isolated and characterized by the end of the 1970's [Herschman, 1996]. Concurrently, investigators looking at PG production in response to cytokines and other inflammatory mediators noted increases in COX enzyme activity that could only be accounted for by increased expression of another COX gene, to produce a second COX isozyme. The new COX isozyme was designated as COX-2 isozyme, while the previously isolated COX isozyme became known as COX-1 isozyme.

1.6.3.1 Structural Differences Between COX-1 and COX-2.

Comparison of the amino acid sequence of COX-1 with the corresponding amino acid sequence of COX-2 leads to a sequence identity not less than 60%. However, there are two main differences between COX-1 and COX-2. The signal peptide for COX-1 is seven residues longer than that of COX-2, and the *N*-terminus of COX-1 has an insertion of eight residues, whereas the *C*-terminus of COX-2 has 18 residues inserted. This latter 18 amino acid peptide provide a unique epitope to distinguish the two isozymes immunologically [Habib *et al.*, 1993]. The other difference is that COX-2 has a proline after Ile^{106} at the junction of the membrane-anchoring helices. This additional proline residue causes only minor perturbation in the local structure, and does not affect the overall topology of the enzyme [Kurumbail *et al.*, 1996]. The secondary and tertiary structures of COX-1 and COX-2 are virtually identical.

The COX reaction active site, AA binding channel, is almost conserved in both isozymes. The only amino acid residue lining the channel that is not identical between COX-1 and COX-2 is at position 523, where COX-2 has Val versus Ile in COX-1 [Luong *et al.*, 1996]. This difference at position 523 changes the size and shape of COX-1 and COX-2 binding sites. The volume of the inhibitor-binding site of COX-2 is 394 $Å^3$ compared to 316 $Å^3$ for COX-1. The 25% increase in the size of COX-2 active site, relative to COX-1 active site could be attributed to the formation of a secondary pocket, extending off the main channel, that is absent in COX-1. In COX-2, the smaller size of the valine side chain (Val^{523}) coupled with the conformational changes of Tyr^{355} opens up the hydrophobic segment of the new secondary pocket that comprises Leu^{352}, Ser^{353}, Tyr^{355}, Phe^{518}, and Val^{523}.

1.6.3.2 Biochemical Similarities and Differences between COX-1 and COX-2.

In spite of their structural similarity, COX-1 and COX-2 have clear biochemical differences. *In vitro*, COX-2 effectively oxygenates a wider array of fatty acid substrates than does COX-1 [Laneuville *et al.*, 1995]. Comparison of K_{cat}/K_m values indicate that the oxygenation efficiency order is arachidonate > dihomogamalinolenate > linolenate > α-linolenate for both isozymes. While oxygenation efficiency order was the same for COX-1 and COX-2, α-linolenate was a particularly poor substrate for COX-1. Similarly, α-linolenate and eicosapentaenoate were poor substitutes for both enzymes. These studies are consistent with other investigations which showed that the cyclooxygenase reaction active site of COX-2 is larger and more flexible than that of COX-1. On the other hand, aspirin acetylation of the Ser^{530} hydroxyl group of COX-2 will oxidize AA to 15-hydroxyeicosatetraenoic acid (HETE) compared to the conversion of AA to PGG_2 by the natural COX-2. In contrast, similarly acetylated COX-1 does not oxidize AA at all [LeComte *et al.*, 1994; Schneider *et al.*, 2000].

1.6.3.3 Expression of COX-1 and COX-2.

The 1990s saw a new dawn in AI research, when biological studies demonstrated increased COX activity in a variety of cells after exposure to endotoxin, pro-inflammatory cytokines, growth factors, hormones and tumor promoters [Jouzeau *et al.*, 1997]. This induced activity required a new protein synthesis which was inhibitable by corticosteroids.These results gave rise to the concept that there must be a constitutive COX isozyme (COX-1) and an inducible COX isozyme (COX-2).

1.6.3.4 Molecular Biology of COX-1 and COX-2.

The genes for COX-1 and COX-2 are located on human chromosomes 9 and 1, respectively [Kraemer *et al.*, 1992; Fletcher *et al.*, 1992]. The intron/exon arrangements are identical, except that exons 1 and 2 for COX-1, containing the translational start site and signal peptide, are condensed into a single exon in COX-2. The introns of COX-2 are smaller, such that the COX-2 gene is 8 Kb compared to 22 Kb for COX-1. These features are consistent with rapid transcription and mRNA processing. While COX-1 isozyme has the common characteristics of "housekeeping" genes, and the promoter has not shown any significant inducible transcription, COX-2 promoter contains a number of transcriptional elements that are common in highly regulated genes, particularly those involved in inflammation such as cyclic adenosine monophosphate (cAMP) response element binding protein [Smith *et al.*, 1995; Appleby *et al.*, 1994].

COX-2 mRNA, in contrast to COX-1 mRNA, has a long 3'-untranslated region containing several polyadenylation signals and multiple Adenine-Uridine-Uridine-Uridine-Adenine (AUUUA) instability nucleotide sequences that mediate rapid degradation of the transcript. These differing gene structures afford a molecular basis for COX-1 as a continuously transcribed stable message, providing relatively constant levels of enzyme in most cell types. COX-1 is then poised to catalyze PG production responsible for homeostatic functions. The gene structure of COX-2 is consistent with the notion that it is an "immediate early" gene product that is rapidly up regulated during inflammation and other pathological processes.

1.6.3.5 Tissue Expression of COX-1 and COX-2 under Basal Conditions.

Tissue localization studies in rodents under basal conditions showed that the COX-1 isozyme is expressed in virtually all tissues, while the COX-2 isozyme is expressed in the brain and renal cortex [Smith *et al.*, 1995]. The highest levels of basal expression of COX-2 is observed in the hippocampus of the adult rat brain, associated with the granular and pyramidal cell layers [Yamagata *et al.*, 1993]. In the renal cortex, COX-2 was found to be scattered in the renal cortex and in medullar interstitial cells, particularly at the papillary tip. In site hybridization, showed that cells expressing COX-2 are present in the macula densa of the juxtaglomerular apparatus and in the adjacent thick ascending limb of Henle's loop [Harris *et al.*, 1994].

1.6.3.6 Regulation of COX-1 and COX-2 during Inflammation.

Glucocorticoids was found to inhibit synthesis of both COX-2 isozyme and m-RNA [O'Sullivan *et al.*, 1992]. Animal models of inflammatory arthritis provided information regarding the expression of COX isozymes during acute and chronic inflammation. Intraparitoneal injection of streptococcal cell walls, or intradermal injection of Freund's complete adjuvant, increased expression of COX isozymes in rat joint tissues. [Sano *et al.*, 1992]. COX-2 isozyme immune staining was detected in multiple cell types within the joints and surrounding tissues, including synovial lining cells, sublining synovial fibroblast-like cells, vascular endothelial cells, infiltrating mononuclear inflammatory cells, chondrocytes, subchondral osteoblasts, and adjacent bone marrow [Siegle *et al.*, 1998]. Anderson and coworkers performed specific COX isoform analysis in rats with adjuvant- induced arthritis [Anderson *et al.*, 1996]. These studies confirmed that COX-2, but not COX-1, mRNA increased concomitant with, or just prior to, the onset of

clinically detectable paw swelling. Furthermore, treatment of arthritic animals with the specific COX-2 inhibitor SC-58125 (**1**) suppressed paw swelling by 80-85%. While there are abundant data indicating that COX-2 is important in inflammation and pain, COX-1 has also been suggested to play a role in inflammatory processes. [Langenbach *et al.*, 1995; Wallace *et al.*, 1998]. To address the latter question pharmacologically, Smith *et al.* used a highly selective COX-1 inhibitor, SC-560 (**2**) (COX-1 IC_{50} = 0.009 μM; COX-2 IC_{50} = 6.3 μM) [Smith *et al.*, 1998]. SC-560 inhibited COX-1 derived platelet TxB_2, gastric PGE_2 and dermal PGE_2 production, indicating that SC-560 was orally active, but did not inhibit COX-2 derived PGs in a lipopolysacharide induced rat air pouch model. Therapeutic or prophylactic administration of SC-560 in the rat carrageenan foot paw model did not affect acute inflammation or hyperalgesia at doses that markedly inhibited *in vivo* COX-1 activity. In contrast, SC-58125 (**1**) was an antiinflammatory and analgesic agent in the carrageenan foot paw model.

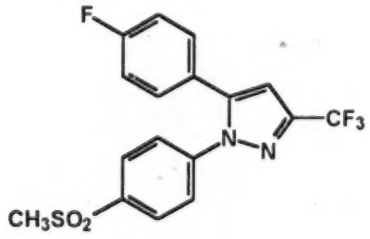

SC-58125 (1)

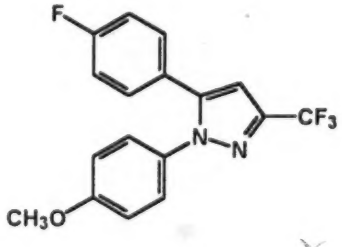

SC-560 (2)

1.6.3.7 Regulation of COX-2 during Carcinogenesis.

Several lines of evidence suggested a role for the COX enzyme in the pathogenesis of malignancy, particularly colon cancer [DuBois, 1995]. Epidemiological studies showed a

decreased relative risk of colon cancer in individuals using NSAIDs. A reduction in size and number of adenomas had been observed in patients with familial adenomas polyposis (FAP) who were treated with NSAIDs. It had been shown that COX-2 expression was up regulated in individuals with colorectal adenomas and carcinomas with a marked increase of COX-2 mRNA in 80% of carcinomas compared with normal mucosa [Eberhart *et al.*, 1994]. Further evidence that COX-2 might be involved in the pathogenesis of colorectal carcinomas was provided by Tsuji and Dubois, who observed that stably transfected rat intestinal epithelial cells over-expressing COX-2 isozyme were resistant to apoptosis [Tsujii & Dubois, 1995].

1.6.3.8 COX-2 Role in Alzheimer's Disease (AD).

COX-2 isozyme was shown to be expressed constitutively in neurons in the brains of AD patients and age matched controls [O'Banion *et al.*, 1997]. The enzymatic generation of oxygen radicals as a by-product of COX-2 in neurons may also add to free-radical overload and neurodegeneration. Neural COX-2 synthesis was found to be induced by IL-1 [Bauer *et al.*, 1997], hypoxia, NF-κB, PGE_2, and adenosine A_{2A} receptors [Hüll *et al.*, 1999].

1.6.4 Selective COX-2 Isozyme Inhibitors.

It had been proposed that a selective COX-2 isozyme inhibitor could have useful AI activity without the ulcerogenic side effects associated with currently available NSAIDs, all of which inhibit both COX-1 and COX-2 isozymes [Cryer & Feldman, 1998]. The design of selective inhibitors logically followed after the extensive structural and biochemical analysis of the two isoforms of COX. However, the first generation of

selective COX-2 isozyme inhibitors originated from animal studies in which compounds showed potent AI activity with minimal side effects on the stomach. Meloxicam (**3**) and nimesulide (**4**) were discovered in this way.

Meloxicam is an enolcarboxamide related to piroxicam. In various assays, meloxicam has been estimated to be 3-77 fold selective for COX-2 [Pairet *et al.*, 1997; Noble *et al.*, 1996]. The limited selectivity of meloxicam for COX-2 led to its classification as a preferential COX-2 inhibitor [Lipsky *et al.*, 1998].

In 1985, nimesulide was introduced for clinical use [Davis *et al.*, 1994]. Nimesulide has a structure potentially capable of accessing the COX-2 side pocket, and it was shown to be 5-16 fold more selective for COX-2 [Tavares *et al.*, 1995]. Clinical studies showed nimesulide to exhibit analgesic, AI, and antipyretic effects for a wide range of arthritic conditions. However, symptomatic GI tolerability was found to be similar to other NSAIDs and one epidemiological study suggested that ulcer complications were as common for nimesulide as for other NSAIDs. [Garcia *et al.*, 1998].

Novel NSAID-like compounds, arising from the two distinct chemical classes of compounds DuP-697 (**5**) and NS-398 (**6**) were shown, in animal models, to possess potent AI and analgesic activity, without accompanying GI toxicity [Gans *et al.*, 1990; Futaki *et al.*, 1993]. A pharmacological profile of this type would be expected for selective COX-2 inhibitors. Cloned human COX-1 and COX-2 cDNAs have been used to develop *in vitro* assays permitting the evaluation of novel compounds such as DuP-697 and NS-398.

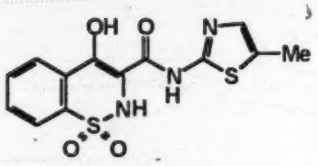

Meloxicam (3)

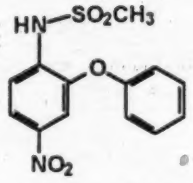

Nimesulide (4)

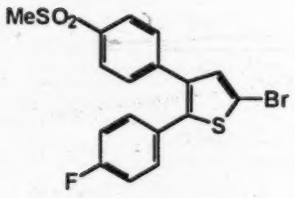

DuP-697 (5)

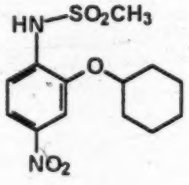

NS-398 (6)

Currently available commercial NSAIDs such as indomethacin and naproxen inhibit non-selectively both COX-1 and COX-2 isozymes, whereas both DuP-697 (COX-1 IC_{50} = 0.8 μM, COX-2 IC_{50} = 0.01 μM), and NS-398 (COX-1 IC_{50} > 100 μM, COX-2 IC_{50} = 3.8 μM) are *in vitro* selective inhibitors of COX-2 [Gierse *et al.*, 1995].

The commercially available NSAIDs belong to two mechanistic categories that include reversible inhibitors of COX-1 such as mefenamic acid and time-dependent irreversible inhibitors such as indomethacin [Kulmacz & Lands, 1985; Rome & Lands, 1975]. It was suggested that DuP-697 and NS-398 inhibit COX-2 isozyme in an irreversible, time dependent manner, while weakly inhibiting COX-1 by a competitive mechanism that is time independent. [Gierse *et al.*, 1995; Copeland *et al.*, 1994].

Early studies undertaken by several laboratories to develop selective COX-2 inhibitors had focused mainly on modifying the two original lead compounds: DuP-697 and NS-398. These studies had resulted in an impressive array of highly selective COX-2 inhibitors. Since some of these new selective COX-2 inhibitors were recently marketed, it

would be interesting to see the long-term clinical experience with these compounds, particularly with respect to the potential side effects of COX-2 inhibition and to the level of selectivity required to prevent the attendant toxicity thought to be caused by concomitant inhibition of COX-1 isozyme in the GI tract. Selective COX-2 inhibitors can now be classified in five different classes that include sulfonanilides, tricycles, di-tertiary-butyl phenols, modified NSAIDs, and covalent modifiers of COX-2 that are discussed in the Sections **1.6.4.1–1.6.4.5**.

1.6.4.1 The Sulfonanilide Class of Selective COX-2 Inhibitors.

The sulfonanilide class of compounds was developed from the lead compound NS-398. Flusolide (7) was among the earliest, in this class of selective COX-2 isozyme inhibitors, to be prepared and tested for selectivity [Rufer *et al.*, 1982; Klein *et al.*, 1994]. Flusolide showed good AI and analgesic activities in various animal models with GI toxicity lower than that of traditional NSAIDs such as indomethacin [Wiesenberg-Boettcher *et al.*, 1989].

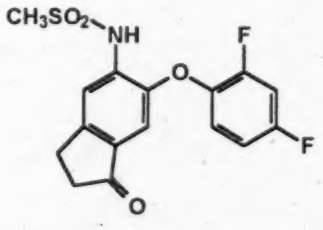

Flusolide (7)

1.6.4.2 The Tricyclic Class of Selective COX-2 Inhibitors.

The tricyclic class of selective COX-2 inhibitors had been extensively investigated world-wide. Structure-activity studies showed that a cis-stilbene moiety containing a 4-

methylsulfonyl, or 4-sulfonamide substituent in one of the pendent phenyl rings is required for COX-2 selectivity [Talley, 1999]. Unlike the sulfonanilides class, which contains an acidic proton capable of salt formation, the main challenge for this class of compounds has been obtaining acceptable bioavailability. Due to the amount of research data reported for this class of compounds, the subject is subdivided based on the central ring size.

1.6.4.2.1. Four-Membered Ring Selective COX-2 Inhibitors.

2,3-Diarylcyclobutenone regioisomers **8** and **9**, had been reported to be selective COX-2 inhibitors [Friesen *et al.*, 1998]. While both cyclobutenones **8** and **9** showed equal efficacy to indomethacin in the rat carrageenan foot paw edema model (ED_{50} = 2.4 mg/kg), only compound **8** was found to be a highly potent selective inhibitor of COX-2 (COX-1 IC_{50} = 2 μM, COX-2 IC_{50} ≈ 0.003 μM; SI ≈ 700).

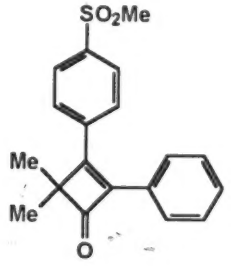

8

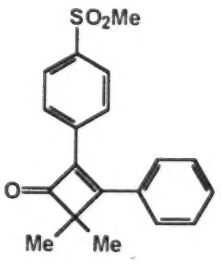

9

1.6.4.2.2. Five-Membered Ring Selective COX-2 Inhibitors.

Systematic studies have been reported for the replacement of the substituted-thiophene ring of DuP-697 (**5**) by a variety of other 5-membered ring systems that include the unsubstituted thiophene **10** [Leblanc *et al.*, 1995], spirocyclopentene **11**

[Reitz *et al.*, 1995], imidazole **12** [Barta *et al.*, 1998], pyrrole **13** [Khanna *et al.*, 1997], cyclopentene **14** [Li *et al.*, 1995], thiazole **15** [Carter *et al.*, 1999], and oxazole **16** [Haruta *et al.*, 1996]. From this group of compounds, two drugs celecoxib **17** (Celebrex)® having a pyrazole [Penning *et al.*, 1997], and rofecoxib **18** (Vioxx)® having a furanone [Prasit *et al.*, 1999] central rings are now marketed as antiinflammatory selective COX-2 isozyme inhibitors.

Recent X-ray crystal structure for SC-588 (**19**) bound to the COX-2 isozyme has been reported. This important data has provided a plausible explanation for the selective COX-2 inhibition displayed by this class of compounds, despite structural similarity between COX-1 and COX-2 isozymes (Figure 5) [Kurumbail *et al.*, 1996].

The bromophenyl ring of SC-588 is bound in a hydrophobic cavity formed by Phe^{381}, Leu^{384}, Tyr^{385}, Trp^{387}, Phe^{513} and Ser^{530}, with contributions from the backbone atoms of Gly^{526} and Ala^{527}. The 3-trifluoromethyl group is bound in an adjacent pocket formed by Met^{113}, Val^{116}, Val^{349}, Tyr^{355}, Leu^{359}, and Leu^{531}. The phenyl ring is surrounded by hydrophobic residues Leu^{352}, Tyr^{355}, Phe^{518}, Val^{523}, and the backbone of Ser^{353}. Beyond this hydrophobic pocket, the sulphonamide group extends into a region near the surface of COX-2 isozyme that is relatively polar where it interacts with His^{90}, Gln^{192} and Arg^{513}. The oxygen atoms of the sulfonamide group of SC-588 are hydrogen bonded to His^{90} and Arg^{513}, while the amide hydrogen formed a hydrogen bond to Phe^{518} backbone.

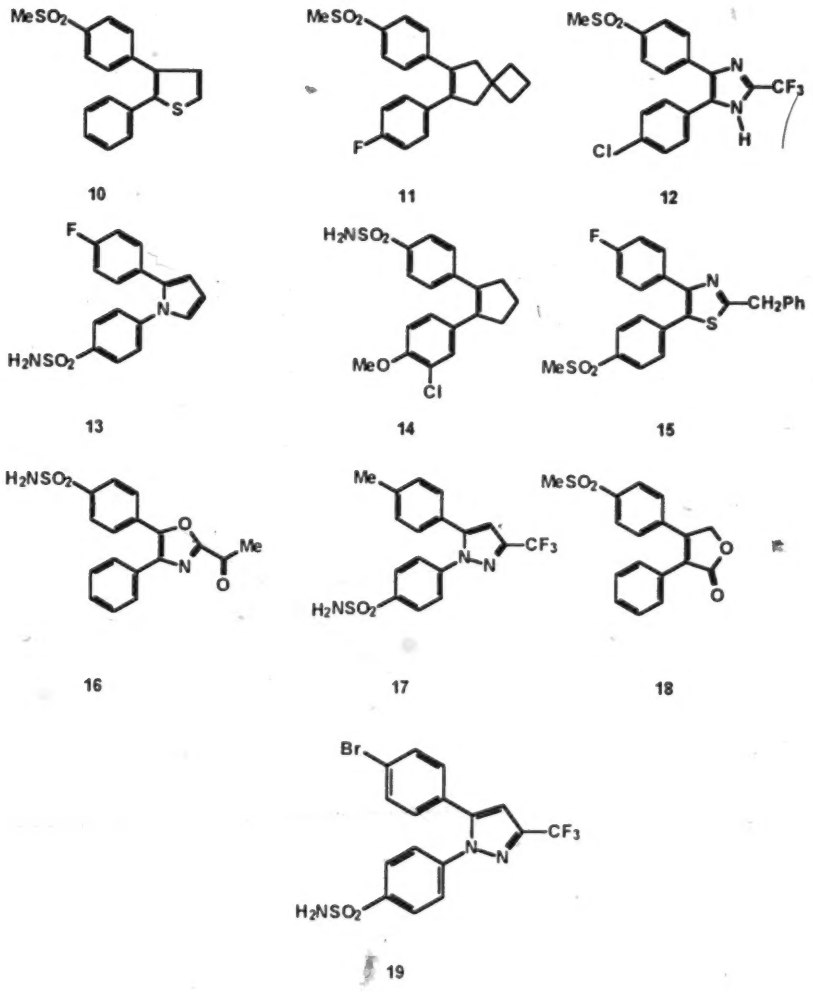

The COX-2 selectivity of SC-588 seems to result from binding of the sulfonamide moiety in the secondary pocket that is more restricted in COX-1 and which is unoccupied in complexes of the COX-2 with non-selective COX-2 inhibitors [Luong *et al.*, 1996]. This observation was attributed to the presence of isoleucine versus valine substitution at position 523 as mentioned earlier (see section **1.6.3.1**).

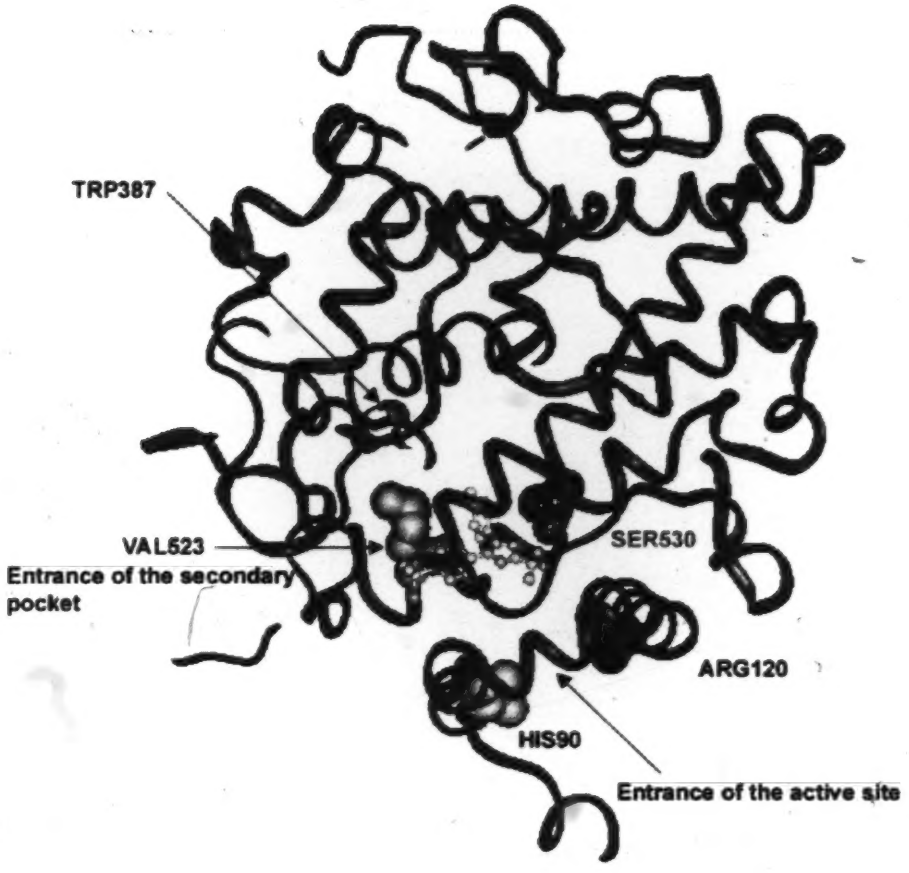

Figure 5. SC-588 (ball and stick) bound to the active site of COX-2 (1CX2 PDB file).

Two other differences in the COX-2 active site affect selectivity. Isoleucine to valine substitution at residue 434 in COX-2 facilitates the access of the sulfonamide group into the COX-2 secondary pocket and the presence of Arg^{513}, in place of His, in COX-2 isozyme also furnishes a hydrogen bond with selective COX-2 inhibitors.

Llorens *et al.* proposed that differences between the MBD of COX-1 and COX-2, could contribute to a dynamic mechanism for ligand binding to COX isozymes [Llorens

et al., 1999]. It was proposed that inhibitors bind rapidly to a cavity in the MBD, where they remain until the gate to the COX isozymes binding site opens. This initial binding is indicative of the competitive reversible binding observed. If the residence time of the ligand is larger than the period required for the gate to open, ligands will enter to the COX isozyme binding site. However, this process may be accelerated by inhibitors capable of enhancing the process of gate opening when bound to this cavity, by perturbing the network of hydrogen bonds at the entrance. Accordingly, inhibitors that bind only to the first site and are not capable of perturbing the hydrogen bonds network, will likely exhibit a time-independent inhibition mechanism which is observed for classical NSAIDs. In contrast, those inhibitors that bind first to the cavity and remain until the gate to the COX reaction binding site opens, will bind in a time-dependent manner as observed for selective COX-2 inhibitors.

In vitro testing showed that celecoxib is a potent and selective COX-2 inhibitor (COX-1 IC_{50} = 15 μM, COX-2 IC_{50} = 0.04 μM; SI ≈ 375). Celecoxib reduced inflammation in the rat carrageenan foot paw edema model with an ED_{50} = 7.1 mg/kg and reduced chronic inflammation in the adjuvant arthritis Hargreaves hyperalgesic model [Hargreaves *et al.*, 1988] with an ED_{50} = 34.5 mg/kg. These data suggested that celecoxib is equipotent to standard NSAIDs, yet showed no acute GI toxicity in rats at doses up to 600 mg/kg over 10 days. All standard NSAIDs showed severe toxicity at these doses. Celecoxib showed good bioavailability and an excellent safety profile.

In a comparative phase I clinical study, 7-day treatment with celecoxib (100 and 200 mg, po, bid) did not produce gastric erosions or ulcers. Naproxen (500mg, po, bid) given over the same period caused ulcers and gastric erosions in 72% of subjects tested. At a

dose of 400 mg, po, bid for 6 days, celecoxib did not affect platelet aggregation [Parnham, 1996]. Four phase II trials have been reported that include: a 2 week OA efficacy trial, a 4 week RA efficacy trial, a 1-week endoscopic study of GI mucosal effects, and a 1 week study of effects on platelet function. [Simon *et al.*, 1998]. In the OA study, 293 patients were randomized to receive celecoxib (40 mg, po, bid; 100 mg, po, bid or 200 mg, po, bid) or placebo for 2 weeks. Rates of withdrawal due to lack of efficacy were 14% from the placebo group, 8% from 40 mg group, 1% from the 100 mg group and 4% from the 200 mg group. Significant reductions in the signs and symptoms of OA, as evaluated by patients and physicians, were observed for all doses of celecoxib adminstered. In the RA study, 330 patients were randomized to receive treatment with celecoxib (40 mg, po, bid, 200 mg, po, bid or 400 mg, po, bid) or placebo for 4 weeks. The difference between the rates of withdrawal from placebo and celecoxib studies were statistically significant. In the upper GI endoscopy study, 19% of subjects receiving naproxen (6 of 32) developed gastric ulcers, whereas no ulceration occurred in subjects receiving celecoxib or placebo. In the platelet effect study, 6 healthy male subjects received celecoxib 400 mg twice daily. The results of pre-treatment and post-treatment studies of collagen-induced platelet aggregation, as a representative measure, were recorded. Mean values after celecoxib administration remained essentially unchanged from the pretreatment values and for 12 hours after the last dose. A comparative study showed that aspirin caused significant decreases in thromboxane levels and aggregation values in the post treatment group compared to the pretreatment group. Phase III and post marketing clinical studies, showed celecoxib to be equipotent to classical NSAIDs, while

maintaining a better safety profile for both OA and RA patients [Silverstein *et al.*, 2000; Goldstein *et al.*, 2000].

The second selective COX-2 isozyme inhibitor to be marketed was rofecoxib (Vioxx)®. Rofecoxib selectively inhibits COX-2 activity in a dose-dependent manner (COX-1 IC_{50} = 19 μM, COX-2 IC_{50} = 0.5 μM; SI ≈ 38) [Prasit *et al.*, 1999]. Rofecoxib was a potent AI agent in the rat paw edema model (ED_{50} = 2.0 mg/kg). The absence of the GI side effects for rofecoxib, is consistent with its low COX-1 isozyme inhibitory activity. Utilization of the ^{51}Cr salts assay to probe the intestinal permeability, showed that rofecoxib did not induce any ^{51}Cr leakage at a daily oral dose of 200 mg/kg (100 mg/kg, bid) for 5 days in either rats or squirrel monkeys. Phase III and post marketing clinical studies showed rofecoxib to be equipotent to classical NSAIDs, while less toxic towards the GI tract [Langman *et al.*, 1999; Day *et al.*, 2000].

1.6.4.2.3. Six-Membered ring Selective COX-2 Inhibitors.

Benzene and pyridine rings have been used as central ring templates in place of five membered ring templates [Batt *et al.*, 1996]. The nature and position of substituents on the central phenyl or pyridyl ring were determinants of selective COX-2 isozyme inhibition [Li *et al.*, 1996]. While both compounds **20** and **21** displayed high selectivity

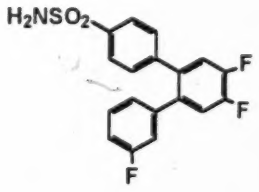

20

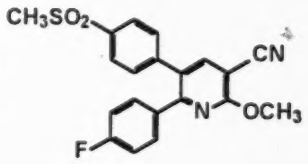

21

towards COX-2, only the benzene based-inhibitor exhibited a high potency in the adjuvant arthritis model.

1.6.4.2.4. Fused Ring System Selective COX-2 Inhibitors.

Several series of compounds bearing a fused-ring system as the central ring template such as imidazopyridines, imidazothiazoles and thiazolotriazoles, had been reported [Beswick *et al.*, 1996]. The imidazopyridine **22** exhibited *in vitro* COX-2 isozyme selective inhibition (COX-1 IC_{50} > 100 μM, COX-2 IC_{50} ≈ 0.14 μM; SI ≈ 714), but it was not evaluated in *in vivo* models of inflammation. The orally active imidazothiazole **23** and the thiazolotriazole **24** are reported to be potent and selective COX-2 isozyme inhibitors (COX-1 IC_{50} > 50 μM, COX-2 IC_{50} ≈ 0.016 μM; and COX-1 IC_{50} = 43 μM, COX-2 IC_{50} ~ 0.01 μM, respectively). No chromium leakage was observed for either of these compounds after administration for 5 days at 100 mg/kg bid oral dose [Therien *et al.*, 1997].

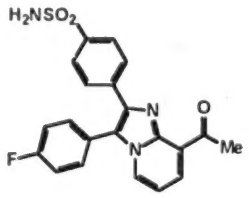

22

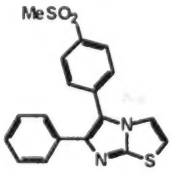

23

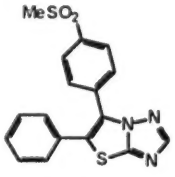

24

1.6.4.3 Di-tert-butyl Phenol Derivatives as Selective COX-2 Inhibitors.

The Park-Davis group had disclosed a new class of potent selective orally active COX-2 inhibitors, illustrated by compound **25** (COX-2 IC_{50} = 1.7 μM, COX-1 IC_{50} > 100 μM) [Song *et al.*, 1999]. Compound **25** was also orally active *in vivo* (ED_{50} = 16 mg/kg

in the carrageenan foot edema AI model) and caused no GI side effects in rats after a 100 mg/kg oral dose.

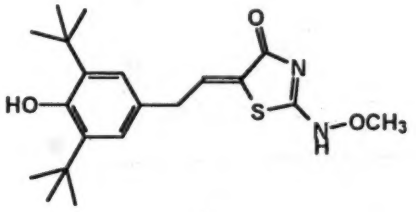

25

1.6.4.4 Modification of Non-Selective NSAIDs to Selective COX-2 Inhibitors.

The Merck-Frosst and Roche groups had reported the transformation of non-selective COX-2 inhibitors such as indomethacin (**26**) into selective inhibitors [Lau *et al.*, 1996; Leblanc *et al.*, 1996]. In this regard, replacement of the chlorobenzoyl group in indomethacin by a trichlorobenzyl **27** or bromobenzyl group **28** confers selectivity towards COX-2.

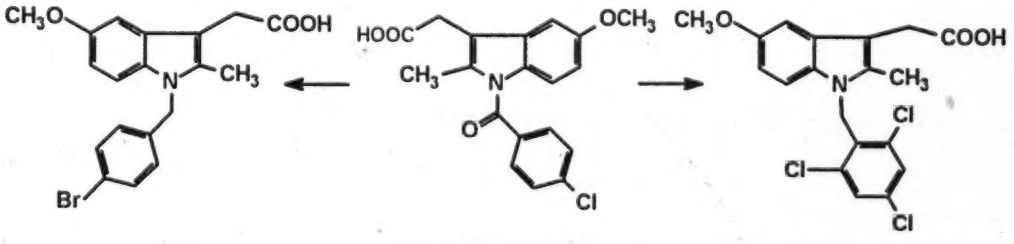

(28) Indomethacin (26) (27)

Recently a more general way to convert classical non-selective into selective COX-2 inhibitors was reported [Kalgutkar *et al.*, 2000]. Their strategy entailed the elaboration of arylacetic acid NSAIDs to the corresponding ester or amides derivatives. Primary and

secondary amide analogues of indomethacin were found to be selective COX-2 inhibitors which act as potent AI agents.

1.6.4.5 Covalent Modifiers of COX-2.

This unique class of COX-2 isozyme inhibitors was inspired by the aspirin mechanism of COX isozymes modulation that involves acetylation of Ser^{530}. The only series of COX-2 isozyme selective inhibitors investigated with respect to this acetylation mechanism involved replacement of the carboxylic group of aspirin by a thioalkyl chain [Kalgutkar *et al.*, 1998]. Extension of the S-alkyl chain in compound **29** by higher alkyl homologues led to significant increases in the COX inhibitory potency. The heptyl chain provided optimum COX-2 inhibitory potency, and the subsequent introduction of a triple bond in the heptyl chain [R= CH_2-C≡C-$(CH_2)_3$-CH_3] led to further enhancement in COX-2 isozyme potency and selectivity. A structure-activity relationship study showed that sulfides were more potent and selective COX-2 isozyme inhibitors than the corresponding sulfoxides, sulfones, or other heteroatom analogs. Tryptic digestion of the product from the reaction of COX-2 isozyme with the [1-^{14}C-acetyl] analogue of compound **29** indicated that selective COX-2 inhibition resulted from acetylation of Ser^{530}.

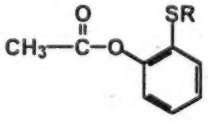

29

1.6.4.6 Other Clinical Applications of Selective COX-2 Inhibitors.

Recent studies during the last two years revealed that other diseases such as cancer and neurodegenerative diseases like AD could potentially be treated with COX-2 selective inhibitors. In rats, it has been shown that celecoxib reduced azoxymethane-induced colon cancer by more than 90% within an observation period of about one year [Kawamori *et al.*, 1998]. The effect of celecoxib on colorectal polyps in patients with FAP who are known to have a nearly 100% risk developing colorectal cancer has been investigated [Steinbach *et al.*, 2000]. It was shown that 6 months of twice daily treatment with 400 mg of celecoxib resulted in a significant reduction in the number of colorectal polyps. These trials were culminated with the FDA approval of celecoxib for the treatment of FAP.

The rationale for the prescription of selective COX-2 inhibitors as neuroprotective drugs in AD was based on epidemiological data collected from testing the effect of classical NSAIDs in AD patients and the safety profile of selective COX-2 inhibitors [Blain *et al.*, 2000]. Currently, clinical studies focusing on both the prevention and the slowing down of early AD symptoms are underway for both celecoxib and rofecoxib.

1.6.5 COX-1 and COX–2 Inhibition Assays.

Numerous *in vitro* assays have been developed for characterization and comparison of the relative inhibitory activities of NSAIDs against COX-1 and COX-2 isozymes. Inhibitory activities are expressed as IC_{50} values (concentrations that inhibit enzyme activity by 50%) and the indices of selectivity (SI) are expressed as the ratios of the IC_{50} values for COX-1 and COX-2 inhibition. The great diversity of systems developed, has resulted in a multitude of IC_{50} values and ratios, which sometimes results in confusing

comparisons. These test systems can be classified into three groups: systems using animal enzymes, animal cells, and cell lines targeted by NSAIDs. Recently, models using human cells that are target cells for the AI and adverse effects of NSAIDs were developed.

There are also other differences in experimental conditions that must be taken into consideration. The first one of these factors is the source of AA, since PG synthesis can be quantitated from either endogenously released AA or exogenously added AA. Secondly, there are various expression systems used for gene replication of recombinant COX-1 and COX-2 isozymes. Thirdly, the absence or presence of a COX-2 inducing agent can vary. Cells that are stably transfected with the enzyme gene express this enzyme constitutively. This contrasts with other cells in which the COX-2 gene has to be induced. A fourth factor involves the duration of the incubation of the enzyme with the drug, which varies between different laboratories. Fifth, the protein concentrations present in the medium can vary making this a critical issue for NSAIDs which are known to bind avidly to plasma proteins.

COX-1 and COX-2 activities have been assessed using O_2 consumption, or peroxidase activity assays, yet the most relevant marker is PG production [Gierse *et al.*, 1995]. Two analytical techniques providing complementary quantitative information and proven to be useful are gas chromatography coupled to mass spectrometry (GC/MS) and radioimmunoassay (RIA).

GC/MS has provided structural information for all of the various oxygenated metabolites of arachidonic acid [Murphy & Harper, 1985]. However, the cost of equipment and the high degree of expertise required to use this technique limited its widespread use, but it is good as a reference for all quantitative assays.

The second technique RIA is a reliable quantitative technique, but it entails certain disadvantages, such as the limited half life of reagents susceptible to radiolysis, increasing expenses in developed countries inherent upon the rigid rules imposed for radioactive isotopes, cost of tubes, scintillation cocktails associated with radioactive disposal, and the high personal time requirement per sample due to limited automation.

All these factors show why a number of more applicable enzyme immunoassays (EIA) have been developed. The first EIA for $PGF_{2\alpha}$ was developed in 1981 using alkaline phosphatase [Hayashi *et al.*, 1981]. Other enzymes had been used in EIA for measurement of eicosanoids such as β-galactosidase [Hayashi *et al.*, 1983], alkaline phosphatase [Miller *et al.*, 1985] and horseradish peroxidase [Hiroshima *et al.*, 1986]. However, in most cases the sensitivity achieved using EIA was much lower than that obtained using RIA. Maclouf *et al.* developed an EIA technique using for the first time acetylcholine esterase (Ache) from electric eels as the label coupled to different eicosanoids [Maclouf *et al.*, 1987]. This method, which uses 96-well microtiter plates coated with a second antibody, allowed sensitivity equal or superior to that obtained with RIA using (^{125}I)-radioiodinated tracers. In addition, the partial automation of the assay and the long shelf life of the label promoted the use of EIA as a substitute for RIA.

1.7 Other Molecular Targets for Antiarthritic Drugs.

The application of molecular biology techniques to study arthritis continues to yield important advances in the development of drugs to treat arthritis (Table **2**).

Table 2. Other Molecular Targets for Arthritis.

Anti-arthritic Agents	Proposed Target(s)	Reference
I. Cytokines Inhibitors.		
Rh-IL-1RA (Antril)®	IL-1	Bersnihan *et al.*, 1998
TNF-R (Enbrel)®	TNF	Moreland *et al.*, 1997
II. Immunosuppressive Agents.		
Leflunamide	Pyrimidine biosynthesis	Schuna *et al.*, 2000
Anti-TNF-α antibody	TNF	Lewis *et al.*, 1999
III. Inhibitors of Leukocyte Migration.		
Zileuton	5-LO	Cohn, 1994
NSAIDs	Selectin E	Diaz-Gonzalez *et al.*, 1998
IV. Proteinase Inhibitors.		
R031-9790	MMP-1,2	Bottomley, 1998
IV. Proteinase Inhibitors.		
LY311727	PLA_2	Balsinde *et al.*, 1999
MK-886	FLAP	Steinhilber, 1999

Current approaches to the discovery of new drugs to treat arthritis are largely mechanism-based. Over the past decade, many discrete immunological and biochemical mechanisms have been defined which may contribute to the pathology of arthritis.

Recently, other molecular targets for arthritis have emerged, that requires the development of proven modulators that can be used clinically, such as mitogen activated protein (MAP) kinases responsible for the synthesis of several cytokines [Newton, 1999], caspases responsible for apoptosis [Talanian, 2000], peroxisome proliferator activated receptor (PPAR)-γ which is the nuclear site of action for prostaglandins [Willson, 2000], and NOS.

1.8 Molecular Modeling and Drug Design.

Random (or serendipitous) drug discovery has played a key role in identifying most lead pharmaceutical compounds to date. In these cases, synthesis of large number of compounds was required. One-estimate suggests that only one compound in every 20,000 screened randomly will make it into the clinic [Tute, 1990]. Commonly used pharmaceutical industry statistics indicate that in the late 1980s and early 1990s, bringing a drug to market cost approximately $120 to 130 million and required about 8 to 10 years. Rational drug design has changed the way in which potential new drugs are discovered. The standard philosophy behind rational drug design is to build biologically active molecules that resemble available lead molecules. Rational drug design can be broadly classified into two categories: structure-aided drug design, the basis of ligand-receptor simulation, will be discussed in sections **1.8.1** to **1.8.9**, and activity-based drug design, the basis of QSAR, will be discussed in section **1.9**.

1.8.1 Principles of Computational Chemistry.

The computational aspects of molecular modeling simulate particular behaviors and properties of molecules. The molecular properties can then be calculated and validated. Some of these properties include a compound's potential energy for a particular conformation, the electronic density at each atom, and the compound's molecular volume and shape.

1.8.2 Molecular Mechanics.

The most computationally expedient approach to modeling is that based on the so-called molecular mechanics approach [Burkert & Allinger, 1982]. In this approach, each

atom is treated as a mass proportional to its atomic mass and each of its bonds is treated as an analog of a mechanical spring. Each bond has a restoring force including one for stretching, bending, and torsional movement of the bond. Nonbonded interactions such as van der Waals (vdw) and electrostatic (columbic) interactions are also considered (equation **1**).

$$E_{total} = \sum E_{stretch} + \sum E_{bend} + \sum E_{torsion} + \sum E_{vdw} + \sum E_{colomb.} \quad \text{.....(1)}$$

The first three terms in equation **1** represent the stretching, bending and torsional movement of bonds. The last two terms represent vdw and electrostatic interactions. Because molecular mechanics algorithm is based on classic models, it could not be used for computing some electronic properties such as electronic density for all elements in the periodic table. To overcome this disadvantage, different force fields have been developed like AMBER [Weiner et al., 1986], CVFF [Dinur, 1991], CHARM [Brooks, 1983], and MM_3 [Lii et al., 1989] force fields.

1.8.3 Quantum Mechanical Methods.

A more rigorous approach to molecular modeling lies in the realm of quantum chemical calculations [Clark, 1985] that require 100 to 100,000 times more computer time than molecular mechanics. Quantum mechanical calculations are based on the Schrödinger wave function (equation **2**):

$$H\Psi = E\Psi \quad \text{.....(2)}$$

where H is the Hamiltonian operator, Ψ is the wave function, E is the eigen value or energy composed of potential and kinetic energy types. Since the electrons are faster than the nuclei, the Schrödinger equation for an atom can be expressed by equation **3**:

$$(-1/2\nabla^2 + 1/R)\Psi = E\Psi \quad \text{.....(3)}$$

in which $1/2\nabla^2$ is an operator giving the kinetic energy of the system and 1/R represents the attractive columbic potential in atomic units. This is called the Born-Oppenheimer approximation. In a hydrogen molecule, there are 4 particles 2 electrons and 2 protons. The inter-particle interaction can be described by the following equation;

$$H = -1/2\nabla_1^2 - 1/2\nabla_2^2 + 1/R_1R_2 - 1/R_1r_1 - 1/R_1r_2 - 1/R_2r_1 - 1/R_2r_2 \quad \text{.....(4)}$$

The first two and the last four terms in the equation represent the kinetic energy of the two electrons and electron-proton interactions, respectively, while the third term represents the interaction between the two nuclei.

Hartree & Fock developed the second approximation where they grouped electron-interactions together. Further approximations were applied to save computer resources and time. The end result is a broad band of methods ranging from *ab initio*, which treat electrons explicitly, expressed by the Gaussian programs up to the semi-empirical methods which are approximate approaches of the *ab initio* method. Semi-empirical methods are roughly 1000 times faster than *ab initio* calculations. There are many different types of the semi-empirical methods. The most commonly used methods in drug design include the modified neglect differential overlap (MNDO) approach which is the basis for many semi-empirical methods such as the Austin Model (AM) and parameterized model (PM3). These methods neglect to various degrees, the interactions among non-valance orbital electrons.

1.8.4 Geometry Optimization.

One of the more powerful features of modern molecular modeling is the ability to determine a minimum energy conformation of a molecule. In the simplest terms, a minimization calculation begins with an assigned starting geometry and computes the

steric or potential energy of the molecule for that geometry. The positions of the atoms of the molecule are then adjusted in a systematic way to lower the energy of each atom, and then the energy of the entire molecule is recomputed. If the energy of the new geometry is less than the starting energy, the new geometry is adopted as the revised starting geometry.

There are a number of energy minimization techniques that fall under two main categories, described as either first or second derivative methods. [Seibel & Kollman, 1990]. The simplest among the first derivative methods is the steepest descent (SD) method, which moves atoms directly down the energy gradient. This SD method is robust and has the advantage of quickly improving bad starting geometries, but suffers from poor convergence near the minimum. A better first derivative method is the conjugate gradient (CG) minimizer that stores information on the direction of previous moves in order to predict better movement directions. This results in a somewhat better convergence properties than SD, although it is less tolerant of poor starting geometry. Using both methods successively will allow one to compute a greater variety of molecules with better convergence. Second derivative methods are much more efficient in locating a global minimum, although they have the least tolerance for poor starting geometry. The full Newton-Raphson method requires the storage and inversion of a 3N x 3N second derivative matrix, because of the large storage requirement; an approximate version of Newton-Raphson is used instead.

In some cases, energy functions are too complex or too ill behaved to afford good derivatives. In these situations, it is possible to use other, non-derivative approaches to seek a global minimum. One approach is called the Downhill Simplex Method. This is a

numerical method, which keeps track of the direction that is being followed on the hyper surface. This approach updated the directions so as to allow the minimizer to track along narrow valleys or non-interfering directions.

1.8.5 Molecular Dynamics.

An alternative approach to determining conformational energies, as well as evaluating interactions between macromolecules and potential drug molecules, is molecular dynamics [Henkel & Billings, 1995]. The result is a series of predicted coordinates that, when plotted, trace the movement of atoms within the molecule. The motion of the nuclei of molecules follows the laws of classic physics. Because the nuclei are more massive than electrons, their quantum behavior can be neglected. For each atom, the force exerted by the atom, as it moves, is expressed by Newton's classic equation, Force = atom mass (m) x acceleration ($\delta^2 r_i / \delta t_i^2$). To relate this fundamental property to the motion of the molecule over time, the expression must be recast into one equation that is based on the coordinates of the atom (r_i) and the potential energy of the atom (V). This provides the differential equation **5**.

$$- \delta V / \delta r_i = m_i \, \delta^2 r_i / \delta t_i^2 \quad \text{.....(5)}$$

By using the Taylor series, equation **5** could be expanded to equation **6**:

$$r(t + \Delta t) = r_i + \delta r / \delta t \, \Delta t + \delta^2 r / \delta t^2 \, \Delta t^{/2} + \quad \text{.....(6)}$$

in which r_t is the coordinates of the atom at time "t", and $\delta r_i / \delta t_i$ is the atom velocity.

One can compute the position of the atom after a short time interval, Δt, if one knows r(t), $\delta r / \delta t$ and $\delta^2 r / \delta t^2$. The most important assumption the equation **6** makes is that the atom interval Δt must be small enough to simulate the motions of all atoms. The fastest moving atoms in any molecule are the hydrogen atoms, which have a C-H stretching periodicity

of about 10^{-14} sec. To capture the motion of those atoms accurately, one needs to take about 10 samples for each vibration, which requires a time interval (Δt) of 10^{-15} sec or 1 femtosecond (fs). Because the motion of the heavy atoms (C, N, O, etc.) occurs on a picosecond (ps) time scale, a molecular dynamics run must cover at least a 10,000-fs (10-ps) time interval, although a 100,000-fs (100-fs) interval would be better yet.

1.8.6 Intermolecular Forces and Molecular Binding.

Intermolecular forces, which are of fundamental importance in biological processes, account for recognition, binding, and catalysis. Enzyme-substrate, antibody-antigen, hormone-receptor, drug-receptor, drug-serum protein, receptor-transmitter and protein-protein recognition are all examples of highly specific intermolecular interactions. Most of the available knowledge pertaining to molecular interactions was derived from enzyme-inhibitor binding studies [Andrews & Tintelnat, 1990].

1.8.7 Drug-Receptor Interactions.

The strongest intermolecular interactions are covalent bonds. Their use in drug binding is limited to irreversibly covalent binding as observed for the suicide inhibition of COX-1 with aspirin. Other kinds of intermolecular forces include electrostatic, van der Waals, and entropy-based interaction.

1.8.8 Calculation of Drug-Receptor Interactions.

In this section, approaches to quantifying intermolecular interactions by means of interaction energy calculations will be discussed. Among the numerous approaches available, molecular orbital and classical potential energy calculations are the most frequently used. *Ab initio* methods are used in intermolecular calculations involving

relatively small biological targets. When limited computer resources are available for complex calculations, semi-empirical approaches will provide acceptable approximation. Classical potential energy calculations use molecular mechanics force fields. In most applications, this takes the form of a single equation accounting for electrostatic, dispersion and repulsion terms.

1.8.9 Docking Experiments.

Docking is a modeling technique used to bring two molecules, a ligand and a receptor, into close juxtaposition thereby permitting the evaluation of how these two molecules might recognize and interact with one another. Besides identifying potential lead compounds, docking calculations are used for studying conformational variations of an active compound, and identifying the binding site of a receptor.

A considerable number of docking procedures have been described in the literature [Morris *et al.*, 1996; Rarey *et al.*, 1997; Jones, 1997]. These range from the use of interactive graphics systems where one manually manipulates the position of the ligand and evaluates the interaction by intuition, to the fully automated procedures in which the positioning and evaluation are done completely by the computer. In principle, docking programs follow a very similar pattern. Atomic coordinates of both the ligand and the receptor are brought in a common interface and both structures are worked on by force fields. The ligand molecule is oriented to the active site of the receptor where the intermolecular interaction is scored. If the resulting orientation provided a score lower than the starting orientation, it is accepted and worked upon, till no lower scores can be attained.

Scoring functions associated with docking programs are used to rank drug-receptor associates to distinguish active from inactive compounds independent of the docking method used. Scoring function can vary extensively. For example, the DOCK program, which is considered to be the predecessor of all docking programs, used energy scores, chemical scores [Meng *et al.*, 1992], and contact scores [Shoichet *et al.*, 1992]. However, it does not necessarily follow that these same scoring functions are able to predict binding affinity in statistically rigorous terms since the functional forms used to describe the chemistry and physics of ligand binding are notoriously incomplete. [Ajay *et al.*, 1995]. Recently, it was reported that combining scoring functions in an intersection-based consensus approach results in an enhancement in the ability to discriminate between active and inactive enzyme inhibitors [Charifson *et al.*, 1999].

1.9 Quantitative Structure-Activity Relationships (QSARs).

An early correlation of properties with structure was reported by the Russian chemist Mendelev in 1870. When he arranged the elements in an 8-member raw table he noticed that every eighth element shared similar properties. In the late 1930s, Hammett showed that the chemical reactivity of *meta*- and *para*-substituted-benzene derivatives could be correlated by the following equation:

$$\text{Log}(K_x/K_H) = \rho\sigma_x \quad \text{.....(7)}$$

in which K_H and K_X is the rate constant for the unsubstituted and substituted molecules, respectively, and σ_x refers to the electronic effect of the substitutent relative to hydrogen. Between 1952 and 1956, Taft devised a procedure for separating polar, steric and resonance effects derived from the rates of base- and acid-catalyzed hydrolysis of esters.

This latter development paved the evolution of QSAR from an art to science by the Hansch research group.

The objective of QSAR studies is to identify parameters from experimental data or theoretical calculations, which when substituted into an equation along with the biological activity for a series of molecules, gives a statistically significant correlation. This main objective could be manipulated to determine the mechanism of action [Hansch, 1971], predict activity [Hansch, 1977], categorize bioactive derivatives [Martin *et al.*, 1974], or optimize the biological activity of a lead compound [Cramer *et al.*, 1979].

1.9.1 QSARs : Models and Parameters.

During the late 1930s and 1940s, some medicinal chemists were correlating the influence of ionization with drug activity. The first model of this type was Hammett's biologist equation **(8)** [Hansch & Fujita, 1964].

$$\text{Log } K + \log [I] = \log (dE/dt) - \log E \quad \text{.....(8)}$$

In which K is rate of inhibition, [I] refers to inhibitor concentration, and E represents the enzyme activity.

This crude model subsequently paved the way for Hansch's widely accepted linear regression equation **(9)**:

$$\text{Log } (1/C) = K_1\pi + K_2\sigma + K_3 \quad \text{..... (9)}$$

In which C is the drug conc., π is the partition coefficient ratio of derivative to parent compound, σ is the Hammett constant, and $K_1 \ldots K_n$ is the linear regression constants.

Applications using this equation produced a degree of scientific euphoria in the 1960's and early 1970's prior to the recognition of its limitations. These limitations were

attributed interalia to the failure to apply the Hansch approach to non-congeneric (do not have a common basic skeleton) compounds.

In many cases, the use of non-empirical molecular descriptors, or de novo constants, were found to possess advantages over the Hansch approach. This latter method can be used when physicochemical constants are unavailable. Two other improvements helped instill life back into the Hansch analysis to elevate it into the current information age. Thus including inactive compounds side by side with active compounds, and the use of the discriminate analysis (DA) where qualitative biological data can be related to physicochemical or non-empirical descriptors constituted useful improvements.

Molecular descriptors, which included physicochemical and non empirical descriptors were divided into two basic sets: topological indices *vs.* electronic, geometrical, and combined descriptors [Katritzky & Gordeeva, 1993]. Topological molecular descriptors have been developed from a theoretical point of view during the past 50 years since Wiener's pioneering paper in 1947 [Kier & Hall, 1986]. The most popular and widely used topological indices are; W: Wiener index; $^1\chi$: Randić index; $^1\chi^v$: Kier and Hall valence connectivity index, and ^{1}K: Kier shape index. Electronic descriptors reflect the electronic structure of the molecule such as q^- max: most negative charge, and q^+ max: most positive charge. Geometrical descriptors represent those descriptors that require access to the 3D coordinates of all the atoms in the given molecule such as molecular volume. Combined descriptors such as electronic topological, or topographic electronic, are descriptors that fall on the dividing line between the previous groups of molecular descriptors.

1.9.2 Three Dimensional QSAR.

Many attempts have been made to combine the qualitative three dimensional aspects of pharmacophore models with QSARs. These included comparative molecular field analysis (CoMFA). [Cramer *et al.*, 1988], shape-based machine learning tool (Compass) [Jain *et al.*, 1994], comparative molecular similarity indices analysis (CMSIA) [Klebe *et al.*, 1994], molecular similarity matrix analysis (MSMA) [Good *et al.*, 1993], receptor surface models (RSM) [Hahn *et al.*, 1995] and auto-correlation of molecular surface properties using neural networks [Wagener *et al.*, 1995].

CoMFA since its conception in 1988 has become the method of choice for elucidating 3D-QSARs [Clark et al., 2000]. In CoMFA procedures, steric, electrostatic, hydrophobic and indicator fields are used as descriptors in regression models. In this process, the ligand/receptor interaction is represented as the interaction between the ligand and a probe atom. As the interaction is sampled, huge numbers of descriptors become available linear regression analysis, that is why an alternative regression technique known as partial least squares (PLS) will be used. In this process, each molecule in the test set is removed from the training set and the QSAR equation re-derived from the remaining molecules. The activity of the "left out" molecule is then predicted and compared with the real experimental value.

2.0 Objectives of Research.

The severity of adverse effects associated with AI drugs has stimulated an ongoing search for safer drugs and approaches to the management of patients with arthritis. The discovery that COX inhibition was responsible for both the therapeutic effect as well as GI mucosal injury resulted in the hypothesis that there are two COX isozymes. Thus, existing NSAIDs, which possess higher COX-2 selectivity, induce less GI damage. According to this hypothesis, the high incidence of adverse GI effects observed with nonspecific NSAIDs results from the undesirable inhibition of COX-1 in addition to COX-2. This postulate is in agreement with data collected for the selective COX-2 inhibitors, celecoxib and rofecoxib, which illicit a lower incidence of adverse events than classical NSAIDs [Silverman *et al.*, 2000]. These studies raise interesting and potential clinically significant issues pertaining to the degree of COX-2 selective inhibition.

The primary objectives of this thesis research were to:

1. Design selective COX-2 inhibitors based on the structural differences between COX-1 and COX-2 isozymes previously reported. It was anticipated that molecular modeling programs such as Insight II (MSI Inc.), Alchemy 2000 (Tripos Inc.) and Cache (Fujitsu Inc.) would be useful tools for the structure-based design of novel selective COX-2 inhibitors.
2. Synthesize novel classes of 4,5-diarylisoxazoles, 3,4-diaryl-5-trifluoromethylisoxazoles, 4,5-diaryl-3-methylisoxazoles, 4,5-diaryl-2-methyl-4-isoxazolines and 4,5-diaryl-2,3-dimethyl-4-isoxazolines, which were predicted from a drug design strategy to be potential COX-2 inhibitors.

3. Synthesize celecoxib and rofecoxib analogues where the SO_2NH_2 and SO_2CH_3 groups are replaced by a dipolar azido substituent.
4. Determine *in vitro* COX-1 and COX-2 isozyme inhibition properties, IC_{50} values, and COX-2 selectivity indices (SI) for the classes of compounds prepared.
5. Determine *in vivo* AI and analgesic activities of the compounds to be investigated using the acute carrageenan-induced rat paw edema and NaCl-induced writhing assays, respectively. ED_{50} values for compounds that exhibit significant AI and analgesic activity would be determined graphically from the dose response curve.
6. Acquire QSAR correlations between *in vitro* enzyme inhibition data and compound physicochemical properties using the SciQSAR (SciVision Inc.) and Cache (Fujitsu Inc.) programs.

3.0 Results and Discussion.

3.1 Synthesis.

3.1.1 Synthesis of 3-Dimethylamino-1,2-diarylprop-2-ene-1-ones 31a-h.

Propenones **31a-h** can be classified as α-unsubstituted-β-ketoenamines, a name given and defined by Greenhill [Greenhill, 1977]. Preparation of α-unsubstituted-β-keto-enamines is mainly attained using either 1,3-dicarbonyl or ketone compounds [Kuckländer, 1994]. Propenones **31a-h** were prepared by reacting ethanones **30a-h** with dimethylformamide dimethylacetal (DMFDMA) under a nitrogen atmosphere as shown in Scheme **1** [SanMartin *et al.*, 1997].

Propenones **31a-h** could exist in any of four geometrical isomers (Figure **6**). Intramolecular hydrogen bonding, restriction of rotation around the C(1)-C(2) and C(3)-N single bonds and the push-pull system efficiency are among the factors reported to affect stereochemistry of α-unsubstituted-β-keto enamines [Chiara & Gomez-Sanchez, 1994].

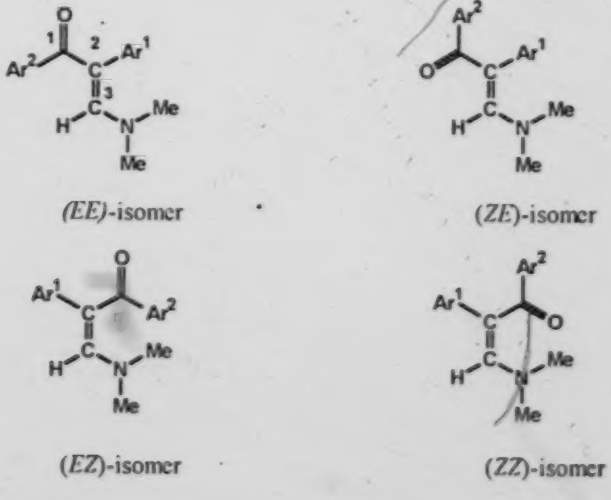

Figure **6**. Possible geometrical isomers of propenones **31a-h.**

Primary and secondary amine groups stabilize the *cis*-configuration about the ethylenic double bond *via* hydrogen bond formation. Propenones **31a-h** with a tertiary amino group, showed an IR absorption band for the CO group around 1635 cm^{-1} as shown in Table **3**. This indicated that the propenone push-pull system is in full conjugation between the "*N*" and "*O*" ends, indicating the possibility of (*EE*) conformation [Gawronski, 1989]. ^{1}H NMR spectra for propenones **31a-h** showed a resonance at lower field than δ 7.1 for the vinylic proton as shown in Table **3**, while the corresponding (*ZE*)-isomers showed a chemical shift at higher field than δ 7.0 [Chiara & Gomez-Sanchez, 1994]. Further support for the (*EE*)-isomer was derived from the observation that the ^{13}C NMR spectrum for the (*EE*)-isomer showed that the C-2 resonance was at a lower field than that of (*ZE*)-isomer. This observation was attributed to a steric compression shift often called the γ-effect [Dabrawski *et al.*, 1974]. This effect is most probably due to rotation of the phenyl ring that will push the carbonyl π orbitals out of the plane of the rest of the conjugated chain. Consequently, an increased contribution of resonance species **C** will result in an increased localization of the negative charge on C-2 (Figure 7). This conclusion is in agreement with that reported earlier [Abdulla & Fuhr, 1978]. Spectral and physical data are presented in Tables **3-5**.

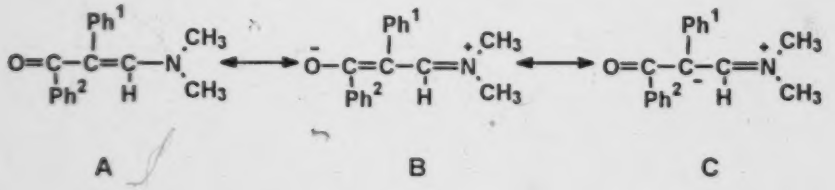

Figure 7. Propenones **31a-h** resonance structures.

Scheme 1[a]. Synthesis of 4,5-diarylisoxazoles **32a-p**.

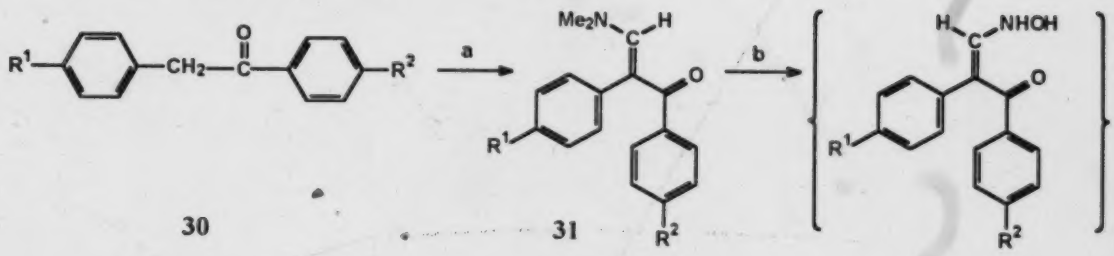

30

30a, $R^1 = R^2 = H$
30b, $R^1 = H$, $R^2 = F$
30c, $R^1 = F$, $R^2 = H$
30d, $R^1 = R^2 = F$
30e, $R^1 = H$, $R^2 = SMe$
30f, $R^1 = SMe$, $R^2 = H$
30g, $R^1 = F$, $R^2 = SMe$
30h, $R^1 = SMe$, $R^2 = F$

31

31a, $R^1 = R^2 = H$
31b, $R^1 = H$, $R^2 = F$
31c, $R^1 = F$, $R^2 = H$
31d, $R^1 = R^2 = F$
31e, $R^1 = H$, $R^2 = SMe$
31f, $R^1 = SMe$, $R^2 = H$
31g, $R^1 = F$, $R^2 = SMe$
31h, $R^1 = SMe$, $R^2 = F$

32a, $R^1 = R^2 = H$
32b, $R^1 = H$, $R^2 = F$
32c, $R^1 = F$, $R^2 = H$
32d, $R^1 = R^2 = F$
32e, $R^1 = H$, $R^2 = SMe$ —c→ **32i**, $R^1 = H$, $R^2 = SOMe$
32f, $R^1 = SMe$, $R^2 = H$ —c→ **32j**, $R^1 = SOMe$, $R^2 = H$
32g, $R^1 = F$, $R^2 = SMe$ —c→ **32k**, $R^1 = F$, $R^2 = SOMe$
32h, $R^1 = SMe$, $R^2 = F$ —c→ **32l**, $R^1 = SOMe$, $R^2 = F$
32e —d→ **32m**, $R^1 = H$, $R^2 = SO_2Me$
32f —d→ **32n**, $R^1 = SO_2Me$, $R^2 = H$
32g —d→ **32o**, $R^1 = F$, $R^2 = SO_2Me$
32h —d→ **32p**, $R^1 = SO_2Me$, $R^2 = F$

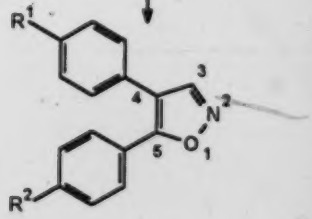

32

[a] Reagents and conditions: (**a**) dimethylformamide dimethylacetal (DMFDMA), toluene, heat (12 h at 25°C and then 24 h at 50°C followed by increasing the reaction temperature about 15°C each day for 3 days); (**b**) $HONH_2.HCl$, MeOH-H_2O, Na_2CO_3, 25°C, 1 h, and then HOAc (pH = 4-5), reflux, 2h; (**c**) 1.1 equiv. *m*-chloroperbenzoic acid, CH_2Cl_2, 25°C, 2-3 h; (**d**) 2.1 equiv. *m*-chloroperbenzoic acid, CH_2Cl_2, 25°C, 2-3 h.

Table 3. IR and ^{1}H NMR spectral data for 3-Dimethylamino-1,2-diarylprop-2-ene-1-ones (**31**).

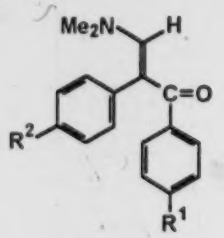

31

Entry	R^1	R^2	IR, KBr (cm^{-1})	^{1}H NMR, $CDCl_3$ (δ)
31b	H	F	1629 (C=O)	2.70 (s, 6H, NC*H*$_3$), 6.87-6.95 (m, 2H, H_{arom}), 7.13-7.27 (m, 5H, H_{arom}), 7.41 (s, 1H, =C*H*), 7.39-7.45 (m, 2H, H_{arom}).
31c	F	H	1635 (C=O)	2.70 (s, 6H, NC*H*$_3$), 6.94-7.01 (m, 2H, H_{arom}), 7.10-7.17 (m, 2H, H_{arom}), 7.26-7.34 (m, 3H, H_{arom}), 7.32 (s, 1H, =C*H*), 7.42-7.46 (m, 2H, H_{arom}).
31d	F	F	1635 (C=O)	2.74 (s, 6H, NC*H*$_3$), 6.92-7.0 (m, 4H, H_{arom}), 7.07-7.14 (m, 2H, H_{arom}), 7.35 (s, 1H, =C*H*), 7.38-7.44 (m, 2H, H_{arom}).
31e	H	SMe	1635 (C=O)	2.44 (s, 3H, SC*H*$_3$), 2.72 (s, 6H, NC*H*$_3$), 7.07-7.27 (m, 7H, H_{arom}), 7.36-7.51 (m, 2H, H_{arom}), 7.37 (s, 1H, =C*H*).

(continued)

Entry	R^1	R^2	IR, KBr (cm^{-1})	^1H NMR, $CDCl_3$ (δ)
31f	SMe	H	1632 (C=O)	2.46 (s, 3H, SCH_3), 2.73 (s, 6H, NCH_3), 7.06-7.10 (m, 2H, H_{arom}), 7.15-7.18 (m, 2H, H_{arom}), 7.24-7.32 (m, 3H, H_{arom}), 7.31 (s, 1H, =C*H*), 7.41-7.44 (m, 2H, H_{arom}).
31g	F	SMe	1629 (C=O)	2.47 (s, 3H, SCH_3), 2.74 (s, 6H, NCH_3), 6.94-7.01 (m, 2H, H_{arom}), 7.09-7.14 (m, 4H, H_{arom}), 7.35 (s, 1H, =C*H*), 7.34-7.38 (m, 2H, H_{arom}).
31h	SMe	F	1634 (C=O)	2.46 (s, 3H, SCH_3), 2.75 (s, 6H, NCH_3), 6.90-6.97 (m, 2H, H_{arom}), 7.03-7.07 (m, 2H, H_{arom}), 7.14-7.18 (m, 2H, H_{arom}), 7.35 (s, 1H, =C*H*), 7.40-7.46 (m, 2H, H_{arom}).

Table 4. ^{13}C NMR spectral data for 3-Dimethylamino-1,2-diarylprop-2-ene-1-ones (**31**).

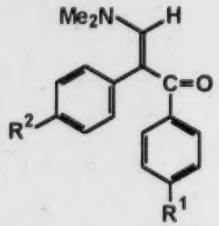

31

Entry	R^1	R^2	^{13}C, $CDCl_3$ (δ)
31b	H	F	43.45 (NCH_3), 111.68 (=*C*-Ph), 114.32 (d, J_{CCF} = 22 Hz, *C*CF), 126.25, 127.57, 130.92, 132.05 (C_{arom}-H), 137.35, 137.63 (C_{arom}-C), 153.06 (=*C*H-N), 163.18 (d, $J_{C,F}$ = 250 Hz, *C*-F), 192.96 (*C*=O).
31c	F	H	43.43 (NCH_3), 111.05 (=*C*-Ph), 114.43 (d, J_{CCF} = 22 Hz, *C*CF), 128.49, 129.16, 133.36, 133.46 (C_{arom}-H), 132.50, 141.68 (C_{arom}-C), 153.8 (=*C*H-N), 161.49 (d, $J_{C,F}$ = 250 Hz, *C*-F), 194.65 (*C*=O).
31d	F	F	43.44 (NCH_3), 110.07 (=*C*-Ph), 114.46 (d, J_{CCF} = 21 Hz, *C*CF), 114.49 (d, J_{CCF} = 22 Hz, *C*CF), 133.30 and 137.70 (C_{arom}-H), 133.13, 141.68 (C_{arom}-C), 153.48 (=*C*H-N), 161.48 (d, J_{CF} = 250 Hz, *C*-F), 163.18 (d, J_{CF} = 250 Hz, *C*-F), 193.07 (*C*=O).

(continued)

Entry	R^1	R^2	^{13}C, $CDCl_3$ (δ)
31e	H	SMe	15.35 (SCH_3), 43.45 (NCH_3), 111.89 (=*C*-Ph), 125.05, 126.18, 127.55, 129.39, 132.04 (C_{arom}-H), 137.44, 138.24 (C_{arom}-C), 140.32 (C_{arom}-*C*S), 153.02 (=*C*H-N), 193.50 (*C*=O).
31f	SMe	H	15.96 (SCH_3), 43.63 (NCH_3), 111.39 (=*C*-Ph), 125.98, 127.61, 128.64, 129.24, 132.40 (C_{arom}-H), 134.04, 137.0 (C_{arom}-C), 141.67 (C_{arom}-*C*S), 153.93 (=*C*H-N), 193.65 (*C*=O).
31h	SMe	F	15.84 (SCH_3), 43.62 (NCH_3), 110.91 (=*C*-Ph), 114.48 (d, J_{CCF} = 22 Hz, *C*CF), 125.86, 130.85, 132.29 (C_{arom}-H), 134.00, 136.70 (C_{arom}-C), 141.67 (C_{arom}-*C*S), 153.51 (=*C*H-N), 163.18 (d, $J_{C.F}$ = 250 Hz, *C*-F), 193.50 (*C*=O).

Table 5. Physical data for 3-Dimethylamino-1,2-diarylprop-2-ene-1-ones (**31**).

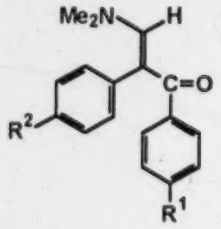

31

Entry	R^1	R^2	% Yield	mp (°C)	Elemental Analysis					
					Calculated			Found		
					C	H	N	C	H	N
31b	H	F	74	111-113	75.82	5.99	5.20	75.89	6.04	5.20
31c	F	H	82	114-116	75.82	5.99	5.20	75.83	5.92	5.18
31d	F	F	80	122-123	71.05	5.27	4.88	70.99	5.20	4.86
31e	H	SMe	81	110-111	72.69	6.44	4.71	72.60	6.40	4.75
31f	SMe	H	92	84-85	72.69	6.44	4.71	72.62	6.56	4.70
31g	F	SMe	82	139.141	68.55	5.76	4.44	68.78	5.74	4.74
31h	SMe	F	81	114-115	68.55	5.76	4.44	68.50	5.70	4.50

3.1.2 Synthesis of 4,5-Diarylisoxazoles 32a-p.

Isoxazoles have been described as having a variety of pharmacological applications including the treatment of inflammation. Isoxicam, an isoxazolyl NSAID that belongs to the oxicam NSAID family was the first isoxazolyl derivative to be clinically approved for the treatment of arthritis [Lombardino, 1985]. The isoxazole ring was also used as a scaffold for the steroidal pharmacophore in the treatment of inflammation [Pathak & Jindal, 1998]. On the other side, the isoxazole ring has been used as a pro-drug as in the case of leflunamide, which is marketed as a DMARD [Mangold *et al.*, 1999]. After identification and characterization of COX-2 isozyme, several companies prepared selective COX-2 isozyme inhibitors with isoxazole as the central ring [Suzuki *et al.*, 1994; Talley *et al.*, 1995; Ducharme *et al.*, 1995].

Enaminoketones, β-diketones, and β-chlorovinyl ketones have been used *inter alia* as starting materials for the preparation of isoxazoles [Grünanger *et al.*, 1991]. In every case, the cyclization reaction can be typified as a C-C-C + N-O ring closure process. However, only the use of an enaminoketone provides a single regioisomer, which is the result of an unusual amine exchange reaction [Dominguez *et al.*, 1995; Cecchetti *et al.*, 1991].

Enaminoketones **31a-h** were submitted to reaction with hydroxylamine hydrochloride under standard oximation conditions [Goda *et al.*, 1992] to yield 4,5-diarylisoxazoles **32a-h** in a one pot reaction (Scheme **1**). Spectral and physical data are presented in Tables **6-8**. The mechanism proposed for the formation of the isoxazoles involves an initial amine exchange reaction of dimethylamino by hydroxylamine.

Table 6. IR and ^{1}H NMR spectral data for 4,5-diarylisoxazoles (**32**).

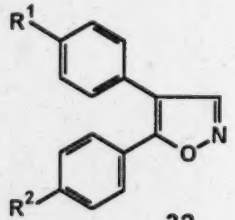

32

Entry	R^1	R^2	IR, KBr (cm^{-1})	^{1}H NMR, $CDCl_3$ (δ)
32b	H	F	1630 (C=N)[a]	7.04-7.10 (m, 2H, H_{arom}), 7.37-7.45 (m, 5H, H_{arom}), 7.61-7.67 (m, 2H, H_{arom}), 8.34 (s, 1H, H-3).
32c	F	H	1630 (C=N)	7.06-7.12 (m, 2H, H_{arom}), 7.33-7.43 (m, 5H, H_{arom}), 7.60-7.62 (m, 2H, H_{arom}), 8.32 (s, 1H, H-3).
32d	F	F	1629 (C=N)	7.05-7.14 (m, 4H, H_{arom}), 7.31-7.38 (m, 2H, H_{arom}), 7.56-7.63 (m, 2H, H_{arom}), 8.32 (s, 1H, H-3).
32e	H	SMe	1630 (C=N)	2.49 (s, 3H, SCH_3), 7.19-7.25 (m, 2H, H_{arom}), 7.35-7.43 (m, 5H, H_{arom}), 7.53-7.55 (m, 2H, H_{arom}), 8.33 (s, 1H, H-3).
32f	SMe	H	1631 (C=N)	2.47 (s, 3H, SCH_3), 7.24-7.32 (m, 5H, H_{arom}), 7.34-7.41 (m, 2H, H_{arom}), 7.62-7.65 (m, 2H, H_{arom}), 8.33 (s, 1H, H-3).

(continued)

Entry	R^1	R^2	IR, KBr (cm^{-1})	^1H NMR, $CDCl_3$ (δ)
32g	F	SMe	1630 (C=N)	2.50 (s, 3H, SCH_3), 7.08-7.13 (m, 2H, H_{arom}), 7.20-7.23 (m, 2H, H_{arom}), 7.33-7.37 (m, 2H, H_{arom}), 7.50-7.53 (m, 2H, H_{arom}), 8.31 (s, 1H, H-3).
32h	SMe	F	1630 (C=N)	2.53 (s, 3H, SCH_3), 7.04-7.13 (m, 2H, H_{arom}), 7.26-7.28 (m, 4H, H_{arom}), 7.61-7.66 (m, 2H, H_{arom}), 8.34 (s, 1H, H-3).
32i	H	SOMe	1045 (S=O) 1630 (C=N)	2.73 (s, 3H, SOCH_3), 7.35-7.46 (m, 5H, H_{arom}), 7.64-7.67 (m, 2H, H_{arom}), 7.79-7.81 (m, 2H, H_{arom}), 8.35 (s, 1H, H-3).
32j	SOMe	H	1044 (S=O) 1630 (C=N)	2.73 (s, 3H, SOCH_3), 7.22-7.29 (m, 5H, H_{arom}), 7.33-7.40 (m, 2H, H_{arom}), 7.58-7.67 (m, 2H, H_{arom}), 8.35 (s, 1H, H-3).
32k	F	SOMe	1045 (S=O) 1630 (C=N)	2.77 (s, 3H, SOCH_3), 7.09-7.17 (m, 2H, H_{arom}), 7.32-7.38 (m, 2H, H_{arom}), 7.66-7.69 (m, 2H, H_{arom}), 7.74-7.79 (m, 2H, H_{arom}), 8.37 (s, 1H, H-3).
32l	SOMe	F	1046 (S=O) 1630 (C=N)	2.80 (s, 3H, SOCH_3), 7.08-7.15 (m, 2H, H_{arom}), 7.54-7.64 (m, 4H, H_{arom}), 7.69-7.77 (m, 2H, H_{arom}), 8.41 (s, 1H, H-3).

(continued)

Entry	R^1	R^2	IR, KBr (cm^{-1})	^1H NMR, $CDCl_3$ (δ)
32m	H	SO_2Me	1152, 1313 (SO_2), 1630 (C=N)	3.08 (s, 3H, SO_2CH_3), 7.35-7.47 (m, 5H, H_{arom}), 7.82-7.86 (m, 2H, H_{arom}), 7.94-7.97 (m, 2H, H_{arom}), 8.41 (s, 1H, H-3).
32n	SO_2Me	H	1145, 1306 (SO_2), 1630 (C=N)	3.08 (s, 3H, SO_2CH_3), 7.39-7.51 (m, 3H, H_{arom}), 7.58-7.62 (m, 4H, H_{arom}), 7.96-8.09 (m, 2H, H_{arom}), 8.41 (s, 1H, H-3).
32o	F	SO_2Me	1145, 1320 (SO_2), 1630 (C=N)	3.01 (s, 3H, SO_2CH_3), 7.03-7.19 (m, 2H, H_{arom}), 7.24-7.30 (m, 2H, H_{arom}), 7.72-7.75 (m, 2H, H_{arom}), 7.87-7.90 (m, 2H, H_{arom}), 8.30 (s, 1H, H-3).
32p	SO_2Me	F	1145, 1306 (SO_2), 1630 (C=N)	3.12 (s, 3H, SO_2CH_3), 7.09-7.16 (m, 2H, H_{arom}), 7.57-7.62 (m, 4H, H_{arom}), 7.97-8.00 (m, 2H, H_{arom}), 8.41 (s, 1H, H-3).

[a] IR is measured neat.

Table 7. ^{13}C and ^{19}F NMR spectral data for 4,5-diarylisoxazoles (**32**).

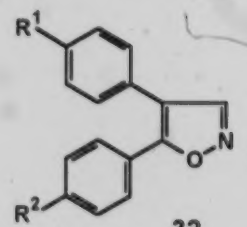

32

Entry	R^1	R^2	^{13}C, $CDCl_3$ (δ)	^{19}F, $CDCl_3$ (δ)
32b	H	F	115.80 (C-4), 115.95 (d, J_{CCF} = 22 Hz, *C*CF), 123.88, 129.92 (C_{arom}-*C*), 128.56, 129.04, 129.25, 129.36 (C_{arom}-H), 151.78 (C-3), 162.48 (d, $J_{C,F}$ = 250 Hz, *C*F), 165.2 (C-5).	45.60 (dddd, J_{FCCH} = 9.1 Hz, dddd, J_{FCCCH} = 5.5 Hz).
32c	F	H	115.22 (C-4), 116.04 (d, J_{CCF} = 21 Hz, *C*-F), 126.17, 127.53 (C_{arom}-*C*), 127.23, 128.79, 130.07, 130.46 (C_{arom}-H), 151.58 (C-3), 164.11 (d, $J_{C,F}$ = 250 Hz, *C*-F), 164.17 (C-5).	48.42 (dddd, J_{FCCH} = 9.1 Hz, dddd, J_{FCCCH} = 5.2 Hz).
32d	F	F	115.03 (C-4), 116.02 (d, J_{CCF} = 22 Hz, *C*CF), 116.12 (d, J_{CCF} = 21 Hz, *C*CF), 123.69, 125.87 (C_{arom}-*C*), 129.30, 130.41 (C_{arom}-H), 151.59 (C-3), 161.38 (d, $J_{C,F}$ = 250 Hz, *C*-F), 163.02 (d, $J_{C,F}$ = 250 Hz, *C*-F), 165.23 (C-5).	48.82 (dddd, J_{FCCH} = 9.1 Hz, dddd, J_{FCCCH} = 5.2 Hz), 52.58 (dddd, J_{FCCH} = 9.1 Hz, dddd, J_{FCCCH} = 5.5 Hz).

(continued)

Entry	R^1	R^2	^{13}C, $CDCl_3$ (δ)	^{19}F, $CDCl_3$ (δ)
32e	H	SMe	15.40 (SCH_3), 115.55 (C-4), 126.73, 127.14 (C_{arom}-*C*), 126.61, 127.15, 128.67, 128.82, 129.91 (C_{arom}-H), 138.65 (C_{arom}-*C*S), 151.57 (C-3), 163.23 (C-5).	———
32f	SMe	H	15.24 (SCH_3), 115.86 (C-4), 126.73, 127.07 (C_{arom}-*C*), 125.99, 127.46, 128.05, 128.67, 129.09 (C_{arom}-H), 141.62 (C_{arom}-*C*S), 151.79 (C-3), 163.7 (C-5).	———
32h	SMe	F	15.45 (SCH_3), 114.86 (C-4), 115.92 (d, J_{CCF} = 22 Hz, *C*CF), 123.71, 126.02 (C_{arom}-*C*), 126.64, 128.80, 129.37 (C_{arom}-H), 141.85 (C_{arom}-*C*S), 151.61 (C-3), 162.34 (d, $J_{C,F}$ = 250 Hz, *C*-F), 164.23 (C-5).	48.57 (dddd, J_{FCCH} = 8.9 Hz, dddd, J_{FCCCH} = 4.9 Hz).
32i	H	SOMe	43.75 ($SOCH_3$), 117.35 (C-4), 123.96, 127.90, 128.39, 128.50, 129.09 (C_{arom}-H), 129.43, 130.07 (C_{arom}-*C*), 147.51 (C_{arom}-*C*S), 151.87 (C-3), 162.36 (C-5).	———
32k	F	SOMe	43.76 ($SOCH_3$), 116.39 (C-4), 116.32 (d, J_{CCF} = 21 Hz, *C*CF), 124.10, 127.85, 130.34 (C_{arom}-H), 124.2, 129.89 (C_{arom}-*C*), 147.64 (C_{arom}-*C*S), 151.83 (C-3), 161.60 (d, $J_{C,F}$ = 250 Hz, *C*-F), 164.29 (C-5).	49.38 (dddd, J_{FCCH} = 9.5 Hz, dddd, J_{FCCCH} = 5.1 Hz).

(continued)

Entry	R^1	R^2	^{13}C, $CDCl_3$ (δ)	^{19}F, $CDCl_3$ (δ)
32l	SOMe	F	43.69 ($SOCH_3$), 114.72 (C-4), 116.16 (d, J_{CCF} = 22 Hz, *C*CF), 123.27, 132.84 (C_{arom}-*C*), 124.38, 129.31, 129.43 (C_{arom}-H), 147.39 (C_{arom}-*C*S), 151.31 (C-3), 163.02 (d, $J_{C,F}$ = 250 Hz, *C*-F), 165.30 (C-5).	53.13 (dddd, J_{FCCH} = 9.1 Hz, dddd, J_{FCCCH} = 5.1 Hz).
32m	H	SO_2Me	44.29 (SO_2CH_3), 118.29 (C-4), 127.65, 127.77, 128.53, 128.62, 129.19 (C_{arom}-H), 129.50, 132.01 (C_{arom}-*C*), 139.75 (C_{arom}-*C*S), 151.95 (C-3), 162.36 (C-5).	
32n	SO_2Me	H	44.75 (SO_2CH_3), 114.41 (C-4), 128.02, 128.95, 129.13, 129.68, 130.59 (C_{arom}-H), 126.83, 135.87 (C_{arom}-*C*), 139.92 (C_{arom}-*C*S), 150.96 (C-3), 165.35 (C-5).	
32o	F	SO_2Me	44.27 (SO_2CH_3), 117.27 (C-4), 116.38(d, J_{CCF} = 21 Hz, *C*CF), 127.74, 130.34, 130.44 (C_{arom}-H), 125.04, 132.24 (C_{arom}-*C*), 147.64 (C_{arom}-*C*S), 151.83 (C-3), 161.30 (d, $J_{C,F}$ = 250 Hz, *C*-F),164.29 (C-5).	49.70 (dddd, J_{FCCH} = 9.1 Hz, dddd, J_{FCCCH} = 5.1 Hz).

(continued)

Entry	R^1	R^2	^{13}C, $CDCl_3$ (δ)	^{19}F, $CDCl_3$ (δ)
32p	SO_2Me	F	44.36 (SO_2CH_3), 114.39 (C-4), 116.30 (d, J_{CCF} = 22 Hz, *C*CF), 128.13, 129.12, 129.47 (C_{arom}-H), 123.23, 132.84 (C_{arom}-*C*), 145.39 (C_{arom}-*C*S), 151.32 (C-3), 162.80 (d, $J_{C,F}$ = 250 Hz, *C*-F), 165.40 (C-5).	53.73 (dddd, J_{FCCH} = 9.1 Hz, dddd, J_{FCCCH} = 5.1 Hz).

Table 8. Physical data for 4,5-diarylisoxazoles (32).

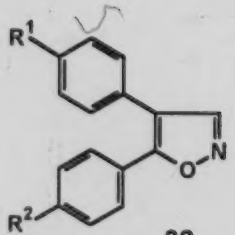

32

Entry	R^1	R^2	% Yield	mp (°C)	Elemental Analysis					
					Calculated			Found		
					C	H	N	C	H	N
32b	H	F	72	Oil	75.30	4.21	5.85	75.38	4.05	5.97
32c	F	H	50	72-73	75.30	4.21	5.85	75.37	4.01	5.86
32d	F	F	31	76-78	70.04	3.53	5.45	70.06	3.52	5.32
32e	H	SMe	67	110-111	71.88	4.90	5.24	71.81	4.97	5.24
32f	SMe	H	67	94-96	71.88	4.90	5.24	71.85	4.82	5.26
32g	F	SMe	28	90-91	67.35	4.24	4.91	67.24	4.33	4.68
32h	SMe	F	46	105-107	67.35	4.24	4.91	67.40	4.32	4.96
32i	H	SOMe	75	94-96	67.84	4.59	4.95	67.44	4.58	4.85
32j	SOMe	H	35	175-180	67.84	4.59	4.95	67.43	4.54	4.83

(continued)

Entry	R^1	R^2	% Yield	mp (°C)	Elemental Analysis					
					Calculated			Found		
					C	H	N	C	H	N
32k	F	SOMe	85	94-96	63.78	3.98	4.65	63.84	3.82	4.62
32l	SOMe	F	88	130-132	63.78	3.98	4.65	63.44	3.90	4.62
32m	H	SO_2Me	58	135-137	64.20	4.38	4.68	63.93	4.30	4.59
32n	SO_2Me	H	68	181-182	64.20	4.38	4.68	63.84	4.42	4.72
32o	F	SO_2Me	52	141-144	60.55	3.81	4.42	60.50	3.56	4.33
32p	SO_2Me	F	72	199-201	60.55	3.81	4.42	60.68	3.61	4.10

Subsequent nucleophilic attack by the hydroxyl group of the hydroxylamino moiety at the carbonyl group (cyclization reaction), and then elimination of water, leads to the formation of the target isoxazole product [Dominguez *et al.*, 1996].

Structure activity relationship (SAR) studies for the tricyclic class of selective COX-2 inhibitors, have indicated that the oxidation state of the sulfur is a key determinant of selectivity; sulfones and sulfonamides are selective for COX-2 isozyme, whereas sulfoxides and sulfides are not [Kalgutkar *et al.*, 1998]. Accordingly, the methylsulphinyl **32i-l** and the methylsulphonylisoxazoles **32m-p** were prepared by oxidation of the methylthioisoxazoles **32a-h** with 1.1 and 2.1 equivalents of *m*-chloroperbenzoic acid, respectively (Scheme **1**). Spectral and physical data are presented in Tables **6-8**.

3.1.3 Synthesis of Trisubstituted Isoxazoles 36, 42, 44, and 48a-b.

As a first step in the chemical modification of isoxazoles **32**, 3,4-diaryl-5-trifluoromethylisoxazoles (**36, 42**), 4,5-diphenyl-3-methylsulfonamidoisoxazole (**44**), and 4,5-diaryl-3-methylisoxazoles (**48a-b**) were designed based on the molecular modeling studies described in Section **3.2.1**. The Perkin condensation of 3-phenyl-1,1,1-trifluoropropan-2-one with 4-methylthiobenzaldehyde in the presence of piperidine afforded the α,β-unsaturated-ketone **33**. Reaction of the ketone **33** with hydroxylamine hydrochloride and then cyclization of 4-hydroxylamino-4-(4-methylthiophenyl)-3-phenyl-1,1,1-trifluorobutan-2-one (**34**) yielded the isoxazole **35**. Subsequent oxidation of the 3-(4-methylthiophenyl)isoxazole **35** using Oxone® afforded 3-(4-methylsulphonyl-phenyl)-4-phenyl-5-trifluoromethylisoxazole (**36**) as shown in Scheme **2**. Spectral and physical data are presented in Tables **9-14**. The high resolution mass spectrum for isoxazole **35** showed M^+ = 335.059 (100%) and M^+-$COCF_3$ = 238.064 (57.6%).

Scheme 2[a]. Synthesis of 3-(4-methylsulphonylphenyl)-4-phenyl-5-trifluoromethyl-isoxazole (**36**).

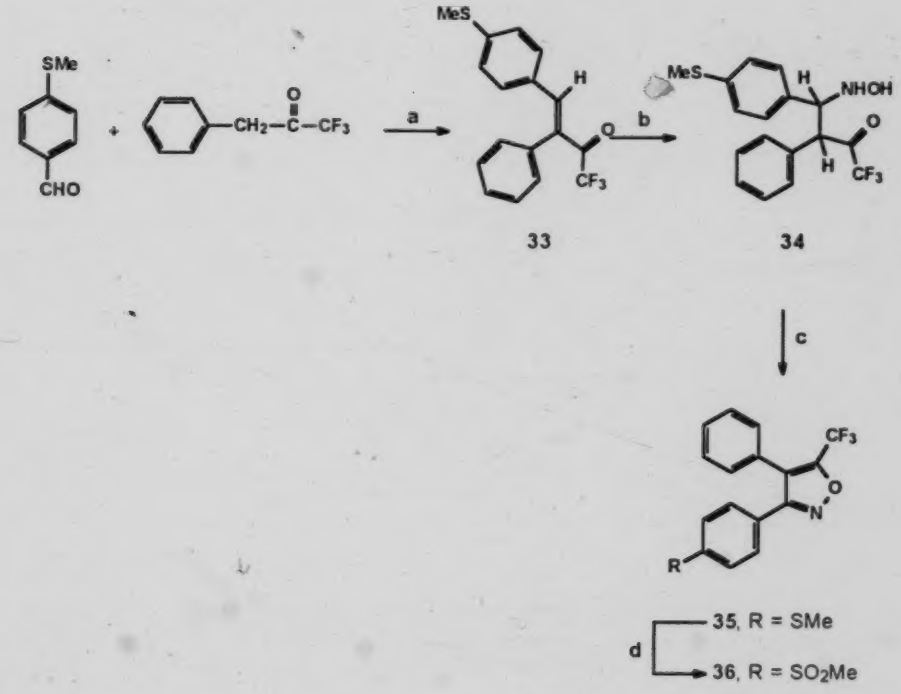

[a] Reagents and conditions: (**a**) piperidine, benzene, reflux, 24 h; (**b**) $HONH_2.HCl$, Na-OAc in ethanol, water, reflux, 90 min.; (**c**) $NaHCO_3$, KI, I_2, THF, water, reflux, 7 h; (**d**) Oxone®, MeOH, THF, 25°C, 2 h.

In order to prepare isoxazole **42**, the trifluoromethyl ketone **39** was prepared by treating methyl 2-(4-methylthiophenyl)-3-phenyl-2-propenoate (**38**) with trifluoromethyl trimethylsilane in the presence of cesium fluoride [Singh *et al.*, 1999]. Subsequent reaction of this ketone **39** with hydroxylamine hydrochloride afforded 4-hydroxylamino-3-(4-methylthiophenyl)-4-phenyl-1,1,1-trifluorobutan-2-one (**40**), which was cyclized to

the isoxazole product **41**, using potassium iodide, sodium bicarbonate, and iodine. Oxidation of the 4-(4-methylthiophenyl)isoxazole derivative **41** with Oxone® afforded the target product 4-(4-methylsulphonylphenyl)-3-phenyl-5-trifluoromethylisoxazole **(42)** as illustrated in Scheme **3**. Spectral and physical data are presented in Tables **9-14**.

Scheme 3[a]. Synthesis of 4-(4-methylsulphonylphenyl)-3-phenyl-5-trifluoro-methylisoxazole (**42**).

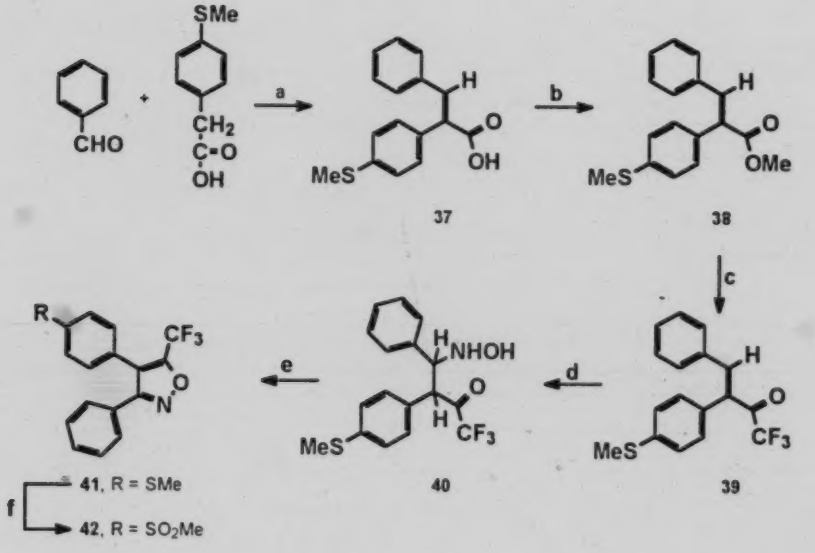

[a] Reagents and conditions: (**a**) TEA, $(Ac)_2O$, reflux, 24 h; (**b**) MeOH, H_2SO_4, reflux,15 h; (**c**) $(CH_3)_3SiCF_3$, CsF, 25°C, 3 h; (**d**) $HONH_2.HCl$, NaOAc, EtOH, H_2O, reflux, 90 min.; (**e**) $NaHCO_3$, KI, I_2, THF, water, reflux, 7h; (**f**) Oxone®, MeOH, THF, 25°C, 2h.

Table 9. IR and ^{1}H NMR spectral data for 2-(4-methylthiophenyl)-3-phenyl-2-propenoic acid (**37**); methyl 2-(4-methylthiophenyl)-3-phenyl-2-propenoate (**38**), and 3,4-diaryl-1,1,1-trifluorobut-3-ene-2-ones (**33**, **39**).

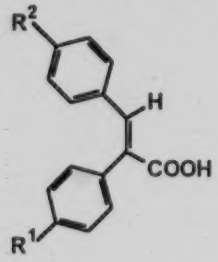

37

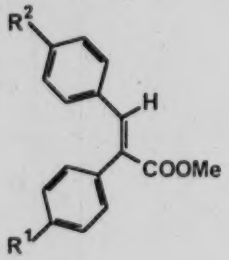

38

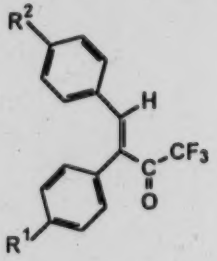

33, 39

Entry	R^1	R^2	IR, KBr (cm^{-1})	^{1}H NMR, $CDCl_3$ (δ)
37	SMe	H	1676 (C=O)	2.51 (s, 3H, SC*H*$_3$), 7.08-7.26 (m, 9H, H_{arom}), 7.86 (s, 1H, =C-*H*)[a].
38	SMe	H	1710 (C=O)	2.52 (s, 3H, SC*H*$_3$), 3.82 (s, 3H, OC*H*$_3$), 7.10-7.34 (m, 9H, H_{arom}), 7.90 (s, 1H, =C*H*).
33	H	SMe	1710 (C=O)	2.50 (s, 3H, SC*H*$_3$), 7.00-7.10 (m, 4H, H_{arom}), 7.17-7.21(m, 2H, H_{arom}), 7.43-7.50 (m, 3H, H_{arom}), 7.80 (s, 1H, =C*H*).
39	SMe	H	1710 (C=O)	2.53 (s, 3H, SC*H*$_3$), 7.10-7.45 (m, 9H, H_{arom}), 7.80 (s, 1H, =C*H*).

[a] ^{1}H NMR is measured in DMSO-d_6.

Table **10**. ^{13}C and ^{19}F NMR spectral data for 3,4-diaryl-1,1,1-trifluorobut-3-ene-2-ones (**33**, **39**).

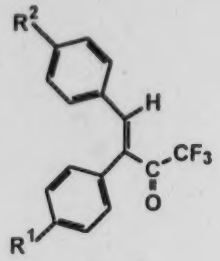

33, 39

Entry	R^1	R^2	^{13}C, $CDCl_3$ (δ)	^{19}F, $CDCl_3$ (δ)
33	H	SMe	14.67 (SCH_3), 111.1 (=*C*-Ph), 117 (q, $J_{C,F}$ = 274 Hz, *C*F_3), 125.86, 127.61, 128.64, 129.24, 132.40 (C_{arom}-H), 128.3, 134.04 (C_{arom}-C), 141.1 (C_{arom}-*C*S), 147.8 (=*C*H), 180.6 (q, J_{CCF} = 32 Hz, *C*O).	92.27 (s, C*F*$_3$).
39	SMe	H	14.62 (SCH_3), 111.10 (=*C*-Ph), 117.02 (q, J_{CF} = 274 Hz, *C*F_3), 126.52, 128.44, 130.32, 130.58, 131.32 (C_{arom}-H), 134.04, 137.0 (C_{arom}-C), 141.67 (C_{arom}-*C*S), 148.8 (=*C*H), 180.6 (q, J_{CCF} = 32 Hz, *C*O).	———

Table **11**. Physical data for 2-(4-methylthiophenyl)-3-phenyl-2-propenoic acid **(37)**; methyl 2-(4-methylthiophenyl)- 3-phenyl-2-propenoate **(38)**, and 3,4-diaryl-1,1,1-trifluorobut-3-ene-2-ones **(33, 39)**.

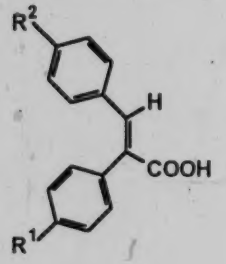

37

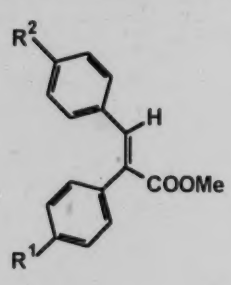

38

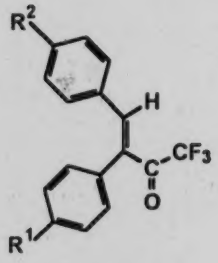

33, 39

Entry	R^1	R^2	% Yield	mp (°C)	Elemental Analysis			
					Calculated		Found	
					C	H	C	H
37	SMe	H	72	158-160	71.10	5.19	71.50	5.10
38	SMe	H	52	82-84	71.83	5.63	71.92	5.73
33	H	SMe	81	110-111	63.35	4.04	63.07	4.02
39	SMe	H	68	71-73	63.35	4.04	63.03	4.09

Table 12. IR and ^{1}H NMR spectral data for 3,4-diaryl-4-hydroxylamino-1,1,1-trifluorobutan-2-ones (**34**, **40**), and 3,4-diaryl-5-trifluoromethylisoxazoles (**35**, **41**, **36**, **42**) .

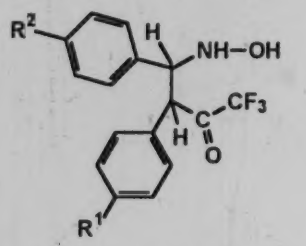

34, 40

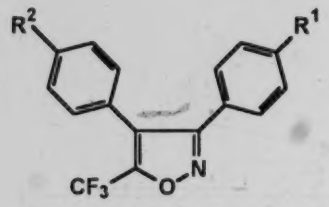

35, 41, 36, 42

Entry	R^1	R^2	IR, KBr (cm^{-1})	^{1}H NMR, $CDCl_3$ (δ)
34	H	SMe	1682 (C=O)	2.45 (s, 3H, SCH_3), 3.73 (d, *J* = 10 Hz, 1H, C*H*), 4.84 (d, *J* = 10 Hz, 1H, C*H*), 7.11-7.40 (m, 9H, H_{arom})[a].
40	SMe	H	1720 (C=O)	2.49 (s, 3H, SCH_3), 4.0 (d, 1H, *J* = 10 Hz, C*H*), 5.21 (d, 1H, *J* = 10 Hz, C*H*), 7.20-7.45 (m, 9H, H_{arom})[a].
35	SMe	H	1610 (C=O)	2.45 (s, 3H, SCH_3), 7.14-7.16 (m, 2H, H_{arom}), 7.23-7.37 (m, 4H, H_{arom}), 7.40-7.45 (m, 3H, H_{arom}).
41	H	SMe	1612 (C=N)	2.52 (s, 3H, SCH_3), 7.23-7.50 (m, 9H, H_{arom}).

(continued)

Entry	R^1	R^2	IR, KBr (cm^{-1})	^1H NMR, $CDCl_3$ (δ)
36	SO_2Me	H	1610 (C=N)	3.06 (s, 3H, SO_2CH_3), 7.22-7.24 (m, 2H, H_{arom}), 7.40-7.44 (m, 3H, H_{arom}), 7.60 (d, J = 9Hz, 2H, H_{arom}), 7.91 (d, J = 9Hz, 2H, H_{arom}).
42	H	SO_2Me	1610 (C=N)	3.11 (s, 3H, SO_2CH_3), 7.27-7.38 (m, 5H, H_{arom}), 7.45 (d, J = 9Hz, 2H, H_{arom}), 7.90 (d, J = 9Hz, 2H, H_{arom}).

[a] ^1H NMR is measured in $CDCl_3 + D_2O$.

Table **13**. ^{13}C and ^{19}F NMR spectral data for 3,4-diaryl-4-hydroxylamino-1,1,1-trifluorobutan-2-ones (**34**, **40**), and 3,4-diaryl-5-trifluoromethylisoxazoles (**35**, **41**, **36**, **42**).

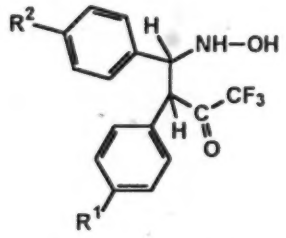

34, 40

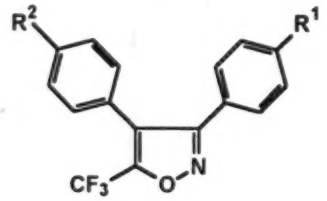

35, 41, 36, 42

Entry	R^1	R^2	^{13}C, $CDCl_3$ (δ)	^{19}F, $CDCl_3$ (δ)
34	H	SMe	15.46 (SCH_3), 60.33 (*C*H), 68.57 (*C*H), 123.5 (q, $J_{C,F}$ = 279 Hz, *C*F_3), 126.56, 127.38, 127.57, 128.02, 129.78 (C_{arom}-H), 124.95, 133.25 (C_{arom}-C), 138.7 (C_{arom}-*C*S).	80.89 (s, CF_3).
40	SMe	H	15.43 (SCH_3), 58.89 (*C*H), 67.59 (*C*H), 121.5 (q, J_{CF} = 292 Hz, *C*F_3), 126.43, 127.22, 128.83, 128.92, 130.01 (C_{arom}-H), 124.73, 133.61 (C_{arom}-C), 138.81 (C_{arom}-*C*S).	80.63 (s, C*F*$_3$).

(continued)

Entry	R^1	R^2	^{13}C, $CDCl_3$ (δ)	^{19}F, $CDCl_3$ (δ)
35	SMe	H	15.14 (SCH_3), 118.01 (q, J_{CF} = 290 Hz, CF_3), 121.14 (C-4), 125.89, 128.67, 128.75, 129.15, 129.82 (C_{arom}-H), 123.56, 126.72(C_{arom}-C), 141.87 (C_{arom}-CS), 151.04 (q, J_{CCF} = 37 Hz, C-5), 161.63 (C-3).	100.05 (s, CF_3).
41	H	SMe	15.10 (SCH_3), 118.50 (q, J_{CF} = 290 Hz, CF_3), 122.61 (C-4), 123.73, 127.09 (C_{arom}-C), 125.86, 128.44, 128.62, 130.01, 130.10 (C_{arom}-H), 140.35 (C_{arom}-CS), 154.50 (q, J_{CCF} = 37 Hz, C-5), 162.09 (C-3).	100.10 (s, CF_3).
36	SO_2Me	H	44.34 (SO_2CH_3), 117.52 (q, J_{CF} = 279 Hz, CF_3), 120.59 (C-4), 125.83, 132.63 (C_{arom}-C), 127.72, 129.06, 129.37, 129.63, 129.69 (C_{arom}-H), 142.18 (C_{arom}-CS), 155.60 (q, J_{CCF} = 39 Hz, C-5), 160.68 (C-3).	100.01 (s, CF_3).
42	H	SO_2Me	44.34 (SO_2CH_3), 117.50 (q, J_{CF} = 285 Hz, CF_3), 118.75 (C-4), 126.38, 132.41 (C_{arom}-C), 127.78, 128.48, 128.94, 130.57, 130.88 (C_{arom}-H), 141.41 (C_{arom}-CS), 155.43 (q, J_{CCF} = 34 Hz, C-5), 162.07 (C-3).	100.46 (s, CF_3).

Table **14**. Physical data for 3,4-diaryl-4-hydroxylamino-1,1,1-trifluorobutan-2-one (**34**, **40**), and 3,4-diaryl-5-trifluoromethyl isoxazoles (**35**, **41**, **36**, **42**) .

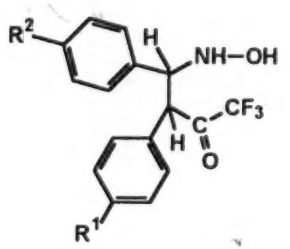

34, 40

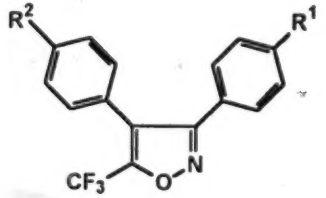

35, 41, 36, 42

Entry	R^1	R^2	% Yield	mp (°C)	Elemental Analysis					
					Calculated			Found		
					C	H	N	C	H	N
34	H	SMe	86	130-131	57.46	4.51	3.94	57.47	4.51	3.81
40	SMe	H	47	148-150	57.46	4.51	3.94	57.34	4.53	3.95
35	SMe	H	66	69-70	60.89	3.58	4.18	60.78	3.48	4.01
41	H	SMe	85	81-83	60.89	3.58	4.18	60.78	3.48	4.01
36	SO_2Me	H	73	140-141	55.58	3.26	3.81	55.34	3.18	3.65
42	H	SO_2Me	86	129-131	55.58	3.26	3.81	55.34	3.18	3.65

In a trial to include the sulfonamido group on the central ring rather than on one of the pendant phenyl rings, 4,5-diphenyl-3-methylsulfonamidoisoxazole (**44**) was prepared as shown in Scheme **4**. Spectral and physical data for 4,5-diphenyl-3-methylsulfonamidoisoxazole (**44**) are presented in Tables **15-17.**

Scheme **4**[a]. Synthesis of 4,5-diphenyl-3-methylsulfonamidoisoxazole (**44**).

43 **44**

[a] Reagents and conditions: (a) CH_3SO_2Cl, pyridine, 25°C, 24 h.

The volume and position of substituents, on the central ring of diarylheterocyclic COX-2 inhibitors, were found to be of great importance in determining potency and selectivity towards COX-2 [Almansa *et al.*, 2001]. Consequently, introducing a C-3 Me central ring substituent in **32m** in conjunction with a 4-(4-fluorophenyl)- or 4-(4-methylphenyl) group as in isoxazoles **48a-b**, is expected to affect both potency and selectivity towards COX-2. The α,β-unsaturated ketones **45a-b**, prepared by the condensation of the 4-substituted-phenylacetone with 4-methylthiobenzaldehyde in the presence of piperidine in benzene, was oximated using hydroxylamine hydrochloride in the presence of sodium acetate in ethanol and water (see Scheme **5**).

Scheme 5[a]. Synthesis of 4,5-diaryl-3-methylisoxazole (**48a-b**).

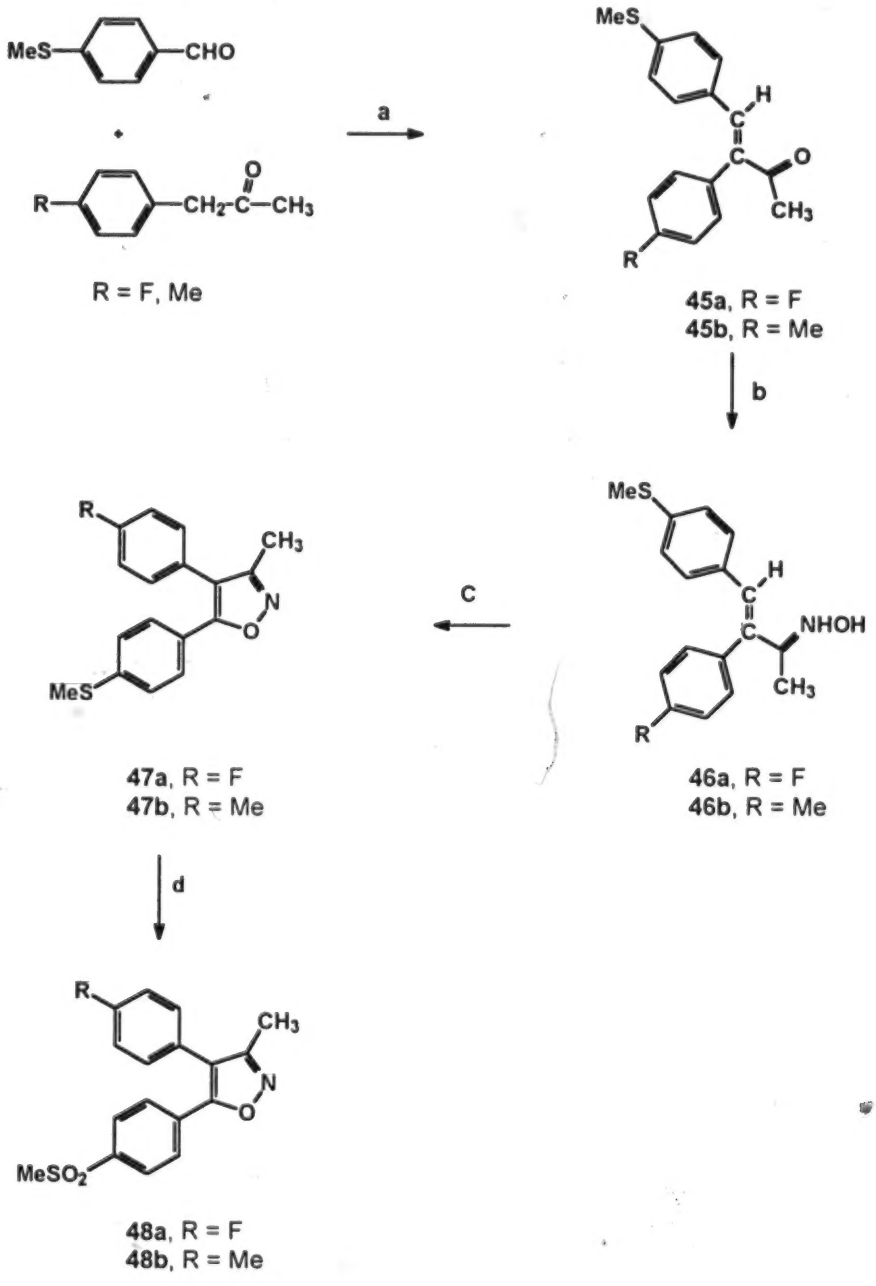

[a]Reagents and conditions: (a) Piperidine, C_6H_6, reflux, 24 h; (b) $NH_2OH.HCl$, NaOAc, EtOH, H_2O, reflux, 5 h; (c) KI, I_2, $NaHCO_3$, THF, H_2O, reflux, 7 h; (d) Oxone®, THF, MeOH, 25°C, 3 h.

Table 15. IR and ^{1}H NMR spectral data for 4,5-diphenyl-3-methylsulfonamidoisoxazole (**44**), 3,4-diaryl-3-butene-2-ones (**45**), 3,4-diaryl-3-butene-2-one oximes (**46**), and 4,5-diaryl-3-methylisoxazoles (**47, 48**).

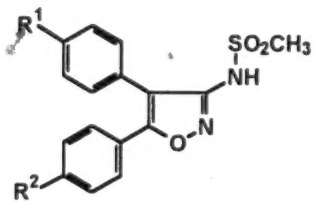

44

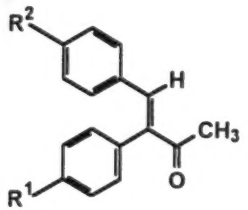

45

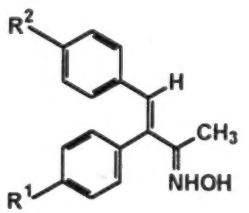

46

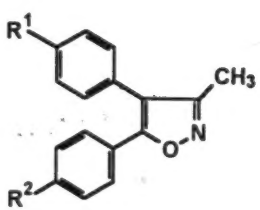

47, 48

Entry	R^1	R^2	IR, KBr (cm^{-1})	^{1}H NMR, $CDCl_3$ (δ)
44	H	H	3250 (NH), 1620 (C=N), 1330, 1150 (SO_2).	3.29 (s, 3H, SO_2CH_3), 7.20-7.50 (m, 10H, H_{arom}).
45a	F	SMe	1662 (C=O)	2.34 (s, 3H, C-CH_3), 2.44 (s, 3H, S-CH_3), 6.93 (d, J = 8 Hz, 2H, H_{arom}), 7.03 (d, J = 8 Hz, 2H, H_{arom}), 7.06-7.18 (m, 4H, H_{arom}), 7.60 (s, 1H, =CH).
45b	CH_3	SMe	1660 (C=O)[a]	2.28 (s, 3H, C-CH_3), 2.33 (s, 3H, Ph-CH_3), 2.53 (s, 3H, S-CH_3), 6.94-7.01 (m, 4H, H_{arom}), 7.20-7.30 (m, 4H, H_{arom}), 7.57 (s, 1H, =C*H*).

(continued)

Entry	R^1	R^2	IR, KBr (cm^{-1})	^1H NMR, $CDCl_3$ (δ)
46a	F	SMe	1630 (C=N)	2.08 (s, 3H, C-CH_3), 2.38 (s, 3H, S-CH_3), 6.83 (d, J = 8 Hz, 2H, H_{arom}), 6.97 (d, J = 8 Hz, 2H, H_{arom}), 7.01 (s, 1H, =CH), 7.11-7.20 (m, 4H, H_{arom})[b].
46b	CH_3	SMe	1620 (C=N)	2.31 (s, 3H, C-CH_3), 2.38 (s, 3H, Ph-CH_3), 2.48 (s, 3H, S-CH_3), 6.89-6.96 (m, 4H, H_{arom}), 7.25 (d, J = 8 Hz, 2H, H_{arom}), 7.31 (s, 1H, =CH), 7.53 (d, J = 8 Hz, 2H, H_{arom})[b].
47a	F	SMe	1630 (C=N)	2.29 (s, 3H, C-CH_3), 2.47 (s, 3H, S-CH_3), 7.08-7.19 (m, 4H, H_{arom}), 7.22-7.31 (m, 2H, H_{arom}), 7.42 (d, J = 8 Hz, 2H, H_{arom}).
47b	CH_3	SMe	1628 (C=N)[a]	2.23 (s, 3H, C-CH_3), 2.36 (s, 3H, Ph-CH_3), 2.49 (s, 3H, S-CH_3), 7.20-7.27 (m, 4H, H_{arom}), 7.30 (d, J = 8 Hz, 2H, H_{arom}), 7.47 (d, J = 8 Hz, 2H, H_{arom}).
48a	F	SO_2Me	1610 (C=N), 1150, 1310 (SO_2).	2.25 (s, 3H, C-CH_3), 3.05 (s, 3H, $SO_2C$$H_3$), 7.12-7.28 (m, 4H, H_{arom}), 7.75 (d, J = 8.5 Hz, 2H, H_{arom}), 7.90 (d, J = 8.5 Hz, 2H, H_{arom}).

(continued)

Entry	R^1	R^2	IR, KBr (cm^{-1})	^1H NMR, $CDCl_3$ (δ)
48b	CH_3	SO_2Me	1615 (C=N), 1150, 1310 (SO_2).	2.25 (s, 3H, C-C*H*$_3$), 2.43 (s, 3H, Ph-C*H*$_3$), 3.08 (s, 3H, SO_2C*H*$_3$), 7.17 (d, *J* = 7 Hz, 2H, H_{arom}), 7.28 (d, *J* = 7 Hz, 2H, H_{arom}), 7.74 (d, *J* = 8 Hz, 2H, H_{arom}), 7.87 (d, *J* = 8 Hz, 2H, H_{arom}).

[a] IR is measured as neat. [b] ^1H NMR is measured in $CDCl_3 + D_2O$.

Table **16**. ^{13}C and ^{19}F NMR spectral data for 4,5-diphenyl-3-methylsulfonamidoisoxazole (**44**), 3-(4-fluorphenyl)-4-(4-methylthiophenyl)-3-butene-2-one (**45a**), 3-(4-fluorphenyl)-4-(4-methylthiophenyl)-3,4-diaryl-3-butene-2-one oxime (**46a**), and 4,5-diaryl-3-methylisoxazoles (**47, 48**).

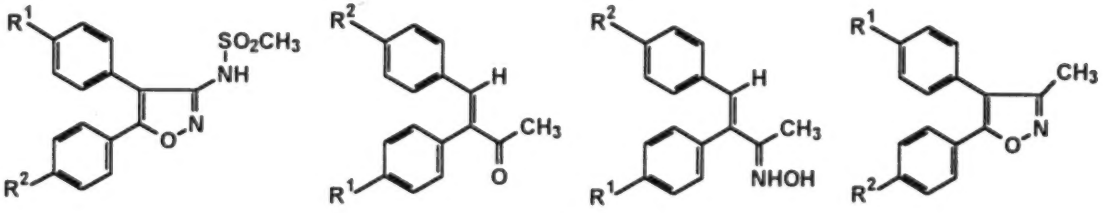

44 **45** **46** **47, 48**

Entry	R^1	R^2	^{13}C, $CDCl_3$ (δ)	^{19}F, $CDCl_3$ (δ)
44	H	H	41.73 (SO_2CH_3), 116.50 (C-4), 126.86, 127.97 (C_{arom}-C), 128.77, 129.18, 129.29, 129.64, 130.38, 130.57 (C_{arom}-H), 155.94 (C-3), 161.50 (C-5).	———
45a	F	SMe	14.96 (S-CH_3), 25.52 (CO-CH_3), 116.07 (d, J_{CCF} = 22 Hz, *C*-F), 125.32, 131.04, 131.26 (C_{arom}-H), 130.72, 131.02 (C_{arom}-C), 132.69 (=*C*-Ar), 139.11 (=*C*H-Ar), 141.10 (C_{arom}-*C*S), 162.38 (d, J_{CF} = 247 Hz, *C*-F), 198.46 (*C*O).	47.88 (dddd, J_{FCCH} = 9.6 Hz, J_{FCCCH} = 5.6 Hz, 1F).

(continued)

Entry	R^1	R^2	^{13}C, $CDCl_3$ (δ)	^{19}F, $CDCl_3$ (δ)
46a	F	SMe	10.78 (C-CH_3), 14.32 (S-CH_3), 115.26 (d, J_{CCF} = 22 Hz, *C*-F), 125.12, 129.50, 129.88 (C_{arom}-H), 131.61 (=*C*H-Ar), 132.52, 134.77 (C_{arom}-C), 137.55 (=*C*-Ar), 138.32 (C_{arom}-*C*S), 156.52 (N=*C*), 161.23 (d, J_{CF} = 242 Hz, *C*-F).	50.97 (dddd, J_{FCCH} = 9.1 Hz, J_{FCCCH} = 5.4 Hz, 1F).
47a	F	SMe	10.55 (C-CH_3), 15.10 (S-CH_3), 114.78 (C-4), 116.15 (d, J_{CCF} = 20 Hz, *C*-F), 124.05, 126.57 (C_{arom}-C), 125.78, 126.95, 131.49 (C_{arom}-H), 141.28 (C_{arom}-*C*S), 162.45 (C-3), 161.23 (d, J_{CF} = 242 Hz, *C*-F), 164.13 (C-5).	48.40 (dddd, J_{FCCH} = 9.1 Hz, J_{FCCCH} = 5.5 Hz, 1F).
47b	CH_3	SMe	10.55 (C-CH_3), 15.10 (S-CH_3), 21.26 (Ph-CH_3), 115.64 (C-4), 124.37, 127.47 (C_{arom}-C), 125.73, 128.69, 129.57, 129.66 (C_{arom}-H), 137.67 (C_{arom}-CH_3), 14[illegible] (C_{arom}-CS), 160.03 (C-3), 163.62 (C-5).	52.40 (dddd, J_{FCCH} = 9.1 Hz, J_{FCCCH} = 5.5 Hz, 1F).
48a	F	SO_2Me	10.50 (C-CH_3), 44.34 (SO_2-CH_3), 116.55 (d, J_{CCF} = 20 Hz, *C*-F), 117.40 (C-4), 125.52, 132.51 (C_{arom}-C), 127.36, 127.79, 133.46 (C_{arom}-H), 141.19 (C_{arom}-*C*S) 160.35 (C-3), 161.22 (d, J_{CF} = 242 Hz, *C*-F), 164.44 (C-5).	

(continued)

Entry	R^1	R^2	^{13}C, $CDCl_3$ (δ)	^{19}F, $CDCl_3$ (δ)
48b	CH_3	SO_2Me	10.47 (C-CH_3), 21.29 (Ph-CH_3), 44.32 (SO_2-CH_3), 118.39 (C-4), 126.83, 132.79 (C_{arom}-C), 127.28, 127.63, 129.37, 129.99 (C_{arom}-H), 138.79 (C_{arom}-CH_3), 140.60 (C_{arom}-CS), 160.48 (C-3), 161.69 (C-5).	———

Table 17. Physical data for 4,5-diphenyl-3-methylsulfonamidoisoxazole (**44**), 3,4-diaryl-3-butene-2-ones (**45**), 3,4-diaryl-3-butene-2-one oximes (**46**), and 4,5-diaryl-3-methylisoxazoles (**47, 48**).

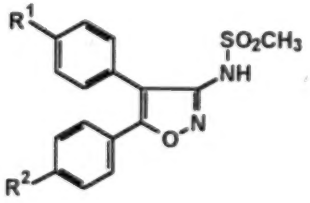

44

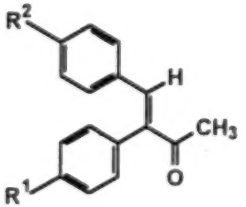

45

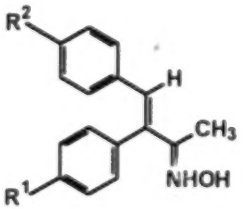

46

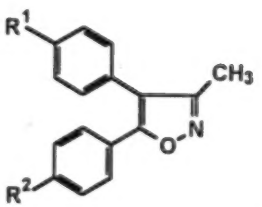

47, 48

Entry	R^1	R^2	% Yield	mp (°C)	Elemental Analysis					
					Calculated			Found		
					C	H	N	C	H	N
44	H	H	52	220-224	61.15	4.45	8.92	61.06	4.32	8.88
45a	F	SMe	62	95-96	71.32	5.24	____	71.30	5.31	____
45b	CH_3	SMe	55	oil	76.59	6.38	____	76.51	6.45	____
46a	F	SMe	71	197-198	67.77	5.31	4.65	67.56	5.28	4.66
46b	CH_3	SMe	42	107-109	72.72	6.39	4.71	73.08	6.14	4.82
47a	F	SMe	60	112-114	68.22	4.68	4.68	68.16	4.59	5.01
47b	CH_3	SMe	32	oil	73.22	5.76	4.74	73.29	5.71	4.84
48a	F	SO_2Me	81	152-153	61.63	4.22	4.22	61.71	4.18	4.20
48b	CH_3	SO_2Me	86	112-113	66.05	5.19	4.28	66.00	5.18	4.15

Reaction of the oxime **46** with iodine, potassium iodide and sodium bicarbonate afforded the 5-(4-methylthiophenyl)isoxazoles derivatives **47**, which was oxidized using Oxone® to afford the 5-(4-methylsulphonylphenyl)isoxazoles **48**, as shown in Scheme **5**. Spectral and physical data are presented in table **15-17**.

3.1.4 Synthesis of 4,5-Diaryl-2-methyl-4-isoxazolines 50a-k.

Among the first series of tricyclic COX-2 selective inhibitors to be disclosed in the literature, were derivatives of cyclopentene [Reitz *et al.*, 1994]. When the central cyclopentene ring was dehydrogenated to the diarylcyclopentadiene analogues, they appeared to be less active as COX-2 selective inhibitors.

Accordingly, we hypothesized that replacement of the central aromatic ring, isoxazole in the class of compounds **32** and **48** by the less planar non-aromatic isoxazoline ring system will result in retention of selectivity for COX-2 isozyme and *in vivo* AI activity. Similar to isoxazoles, isoxazolines also have pharmacological applications [Burton *et al.*, 1996; Hall *et al.*, 1997; Wang *et al.*, 2000]. Among these compounds 4-isoxazolines are the least studied, undoubtedly because of their more difficult preparation. Reduction of the isoxazole's C=N bond was always proceeded by hydrogenolysis of the weak N-O bond, but formation of the isoxazolium salts offers an interesting way to circumvent this difficulty [Grünanger & Vita-Finzi, 1991a].

Consequently, we first carried out N-methylation reaction of isoxazoles **32b-h, 32m-n, 48a** and **48c** with trimethyloxonium tetrafluoroborate (Meerwein salt) under mild conditions [Grünanger & Vita-Finzi, 1991b]. Subsequent reduction of the isoxazolium salts **49a-k** with sodium borohydride afforded isoxazolines **50a-k** as shown in Scheme **6**.

Scheme 6[a]. Synthesis of 4,5-diaryl-2-methyl-4-isoxazolines (**50a-k**).

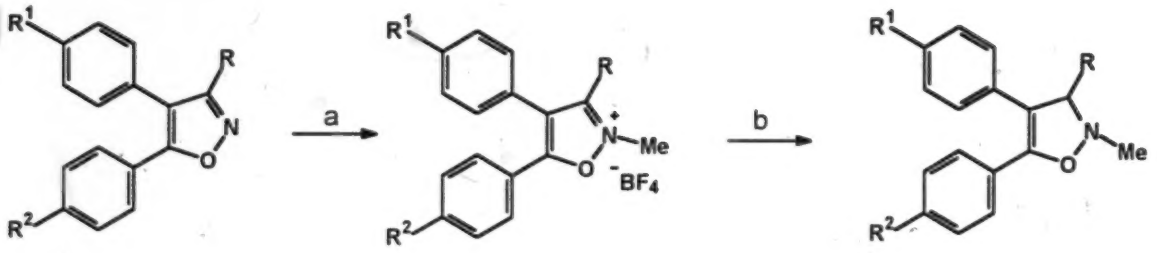

32 **49** **50**

	R	R^1	R^2		R	R^1	R^2		R	R^1	R^2
32b	H	H	F	**49a**	H	H	F	**50a**	H	H	F
32c	H	F	H	**49b**	H	F	H	**50b**	H	F	H
32d	H	F	F	**49c**	H	F	F	**50c**	H	F	F
32e	H	H	SMe	**49d**	H	H	SMe	**50d**	H	H	SMe
32f	H	SMe	H	**49e**	H	SMe	H	**50e**	H	SMe	H
32g	H	F	SMe	**49f**	H	F	SMe	**50f**	H	F	SMe
32h	H	SMe	F	**49g**	H	SMe	F	**50g**	H	SMe	F
32m	H	H	SO_2Me	**49h**	H	H	SO_2Me	**50h**	H	H	SO_2Me
32n	Me	SO_2Me	H	**49i**	Me	SO_2Me	H	**50i**	Me	SO_2Me	H
48a	Me	F	SO_2Me	**49j**	Me	F	SO_2Me	**50j**	Me	F	SO_2Me
48c	Me	H	SO_2Me	**49k**	Me	H	SO_2Me	**50k**	Me	H	SO_2Me

[a]Reagents and conditions: (a) $Me_3O^+BF_4^-$, CH_2Cl_2, N_2 atmosphere, 25°C, 15 h; (b) $NaBH_4$, EtOH, argon atmosphere, 25°C, 8-12 h.

Isoxazolines **50a-i,** having two C-3 hydrogen atoms showed two broad ^{1}H NMR resonances in the δ 3.85-3.95 and 4.55-4.65 ranges of equal intensity for the C-3 protons that coalesced to a single broad resonance upon heating to 61°C. Irradiation of either one of these two resonances resulted in complete saturation (disappearance) of the other resonance. In contrast, the isoxazolines **50j** and **50k** possessing a C-3 Me substituent showed a broad multiplet resembling a quartet in the δ 4.20-4.30 range which appeared as a sharp quartet ($J_{CH, Me}$ = 7 Hz) upon heating to 61°C. These ^{1}H NMR spectral data suggest that the 4-isoxazoline ring of compound **50** exists as a mixture of two conformers at 25°C. Spectral and physical data for are presented in tables **18-23**.

Table 18. IR and ^{1}H NMR spectral data for 4,5-diaryl-2-methylisoxazolium tetrafluoroborates (**49**).

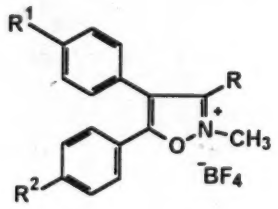

49

Entry	R	R^1	R^2	IR, KBr (cm^{-1})	^{1}H NMR, DMSO-d_6 (δ)
49a	H	H	F	1645 (C=N)	4.47 (s, 3H, 2-CH_3), 7.49-7.55 (m, 7H, H_{arom}), 7.73-8.10 (m, 2H, H_{arom}), 10.0 (s, 1H, H-3).
49b	H	F	H	1640 (C=N)[a]	4.43 (s, 3H, 2-CH_3), 7.01-7.07 (m, 2H, H_{arom}), 7.26-7.46 (m, 4H, H_{arom}), 7.53-7.60 (m, 3H, H_{arom}), 9.28 (s, 1H, H-3)[b].
49c	H	F	F	1635 (C=N)	4.48 (s, 3H, 2-CH_3), 7.40-7.59 (m, 6H, H_{arom}), 7.70 -7.76 (m, 2H, H_{arom}), 9.90 (s, 1H, H-3).
49d	H	H	SCH_3	1650 (C=N)[a]	2.69 (s, 3H, SCH_3), 4.42 (s, 3H, 2-CH_3), 7.16-7.20 (m, 2H, H_{arom}), 7.30-7.46 (m, 7H, H_{arom}), 9.28 (s, 1H, H-3)[b].

(continued)

Entry	R	R^1	R^2	IR, KBr (cm^{-1})	^1H NMR, DMSO-d_6 (δ)
49e	H	SCH_3	H	1651 (C=N)	2.50 (s, 3H, SCH_3), 4.49 (s, 3H, 2-CH_3), 7.50-7.70 (m, 5H, H_{arom}), 7.72 (d, J = 8 Hz, 2H, H_{arom}), 8.19 (d, J = 8 Hz, 2H, H_{arom}), 10.03 (s, 1H, H-3).
49f	H	F	SCH_3	1650 (C=N)	2.50 (s, 3H, SCH_3), 4.50 (s, 4H, 2-CH_3), 7.07-7.13 (m, 2H, H_{arom}), 7.20-7.30 (m, 2H, H_{arom}), 7.45-7.53 (m, 4H, H_{arom}), 9.43 (s, 1H, C-3)[b].
49g	H	SCH_3	F	1648 (C=N)	2.50 (s, 3H, SCH_3), 4.50 (s, 3H, 2-CH_3), 7.45-7.55 (m, 2H, H_{arom}), 7.67-7.85 (m, 4H, H_{arom}), 8.20-8.27 (m, 2H, H_{arom}), 10.10 (s, 1H, C-3)[b].
49h	H	H	SO_2Me	1650 (C=N)	3.28 (s, 3H, SO_2CH_3), 4.45 (s, 3H, 2-CH_3), 7.51-7.59 (m, 5H, H_{arom}), 7.90 (d, J = 8 Hz, 2H, H_{arom}), 8.14 (d, J = 8 Hz, 2H, H_{arom}), 10.11 (s, 1H, H-3).
49i	H	SO_2Me	H	1650 (C=N)	3.28 (s, 3H, SO_2CH_3), 4.45 (s, 3H, 2-CH_3), 7.50-7.75 (m, 5H, H_{arom}), 7.80 (d, J = 8 Hz, 2H, H_{arom}), 8.17 (d, J = 8 Hz, 2H, H_{arom}), 9.94 (s, 1H, H-3)[c].

(continued)

Entry	R	R^1	R^2	IR, KBr (cm^{-1})	^{1}H NMR, DMSO-d_6 (δ)
49j	CH_3	F	SO_2Me	1650 (C=N)	2.57 (s, 3H, 3-CH_3), 3.29 (s, 3H, SO_2CH_3), 4.46 (s, 3H, 2-CH_3), 7.44-7.57 (m, 4H, H_{arom}), 7.78 (d, *J*=8 Hz, 2H, H_{arom}), 8.00 (d, *J* = 8 Hz, 2H, H_{arom}).
49k	CH_3	H	SO_2Me	1650 (C=N)	2.50 (s, 3H, 3-CH_3), 3.28 (s, 3H, SO_2CH_3), 4.45 (s, 3H, 2-CH_3), 7.46-7.49 (m, 2H, H_{arom}), 7.61-7.63 (m, 3H, H_{arom}), 7.78 (d, *J* = 8 Hz, 2H, H_{arom}), 8.10 (d, *J* = 8 Hz, 2H, H_{arom}).

[a] IR was measured neat. [b] ^{1}HNMR was measured in $CDCl_3$. [c] ^{1}HNMR was measured in $CDCl_3$ + CD_3OD.

Table **19**. ^{13}C and ^{19}F NMR spectral data for 4,5-diaryl-2-methylisoxazolium tetrafluoroborates (**49**).

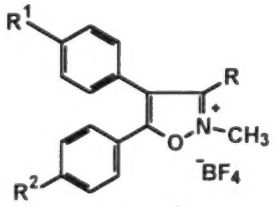

49

Entry	R	R^1	R^2	^{13}C, DMSO-d_6 (δ)	^{19}F, DMSO-d_6 (δ)
49b	H	F	H	41.09 (2-*C*H$_3$), 116.50 (d, J_{CCF} = 22 Hz, *C*CF), 119.09 (C-4), 121.34, 122.93 (C$_{arom}$-*C*), 128.29, 129.37, 131.17, 133.31 (*C*$_{arom}$-H), 149.50 (C-3), 163.34 (d, $J_{C,F}$ = 249 Hz, *C*-F), 167.29 (*C*-5)[a].	10.37 (s, 4F, B*F*$_4$), 51.57 (dddd, J_{FCCH} = 9.1, J_{FCCCH} = 5.1 Hz, 1F, C$_{arom}$-*F*)[a].
49c	H	F	F	41.10 (2-*C*H$_3$), 116.50 (d, J_{CCF} = 22 Hz, *C*CF), 116.97 (d, J_{CCF} = 22 Hz, *C*CF), 118.20 (C-4), 119.48, 121.65 (C$_{arom}$-*C*), 130.90, 131.716 (*C*$_{arom}$-H), 149.0 (C-3), 161.08 (d, J_{CF} = 252 Hz, *C*-F), 163.0 (d, J_{CF} = 250 Hz, *C*-F), 166.10 (*C*-5).	18.11 (s, 4F, B*F*$_4$), 55.57 (dddd, J_{FCCH} = 9.1, J_{FCCCH} = 5.1 Hz, 1F, C$_{arom}$-*F*).

(continued)

Entry	R	R^1	R^2	^{13}C, DMSO-d_6 (δ)	^{19}F, DMSO-d_6 (δ)
49f	H	F	SCH_3	14.62 (S-*C*H_3), 41.30 (2-*C*H_3), 116.70 (d, J_{CCF} = 22 Hz, *C*CF), 118.58 (C-4), 121.30, 121.40 (C_{arom}-*C*), 125.74, 128.30, 131.16 (C_{arom}-H), 147.43 (C_{arom}-*C*S), 150.01 (C-3), 163.57 (d, $J_{C,F}$ = 252 Hz, *C*-F), 167.28 (*C*-5)[a].	10.06 (s, 4F, B*F*$_4$), 52.06 (dddd, J_{FCCH} = 9.1, J_{FCCCH} = 5.1 Hz, 1F, C_{arom}-*F*)[a].
49j	CH_3	F	SO_2CH_3	11.28 (3-*C*H_3), 38.88 (2-*C*H_3), 42.92 (SO_2-*C*H_3), 116.66 (d, J_{CCF} = 22 Hz, *C*CF), 120.01 (C-4), 121.38, 127.27 (C_{arom}-C), 128.00, 128.69, 132.15 (C_{arom}-H), 144.09 (*C*-SO_2), 160.15 (C-3), 161.86 (d, J_{CF} = 250 Hz, *C*F), 164.60 (C-5).	18.09 (m, 4F, B*F*$_4$), 56.20 (dddd, J_{FCCH} = 9.1, J_{FCCCH} = 5.1 Hz, 1F).

[a] NMR is measured in $CDCl_3$.

Table **20**. Physical data for 4,5-diaryl-2-methylisoxazolium tetrafluoroborates (**49**).

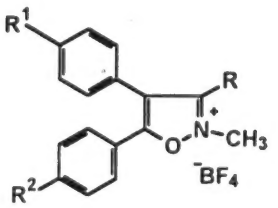

49

Entry	R	R^1	R^2	% Yield	mp (°C)	Elemental Analysis					
						Calculated			Found		
						C	H	N	C	H	N
49a	H	F	H	98	131-132	56.30	3.81	4.11	56.38	3.80	4.08
49b	H	H	F	80	oil	56.30	3.81	4.11	56.46	3.49	4.06
49c	H	F	F	88	152-153	53.48	3.34	3.90	53.39	3.08	3.85
49d	H	H	SCH_3	55	150-153	55.28	4.33	3.79	54.98	4.34	3.74
49e	H	SCH_3	H	65	233-235	55.28	4.33	3.79	55.12	4.22	3.70
49f	H	F	SCH_3	72	144-146	52.71	3.87	3.62	52.62	3.91	3.63
49g	H	SCH_3	F	75	235-237	52.71	3.87	3.62	52.79	3.89	3.57

(continued)

Entry	R	R^1	R^2	% Yield	mp (°C)	Elemental Analysis					
						Calculated			Found		
						C	H	N	C	H	N
49h	H	H	SO_2CH_3	71	148-151	50.87	3.99	3.49	50.93	4.00	3.45
49i	H	SO_2CH_3	H	68	220-221	50.87	3.99	3.49	50.84	3.92	3.44
49j	CH_3	F	SO_2CH_3	91	233-235	49.88	3.92	3.23	50.12	4.08	3.21
49k	CH_3	H	SO_2CH_3	69	179-181	52.05	4.33	3.37	52.12	4.51	3.25

Table **21**. IR and ^{1}H NMR spectral data for 4,5-diaryl-2-methyl-4-isoxazolines (**50**).

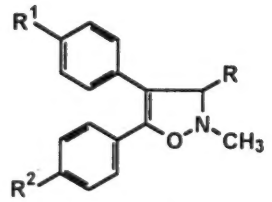

50

Entry	R	R^1	R^2	IR, neat (cm^{-1})	^{1}H NMR, $CDCl_3$ (δ)
50a	H	H	F	1660 (C=C)	2.90 (s, 3H, 2-CH_3), 3.90-4.0 (br m, 1H, H-3), 4.70-4.80 (br m, 1H, H-3), 6.90-7.03 (m, 2H, H_{arom}), 7.16-7.27 (m, 5H, H_{arom}), 7.43-7.49 (m, 2H, H_{arom}).
50b	H	F	H	1660 (C=C)	2.92 (s, 3H, 2-CH_3), 3.85-3.95 (br m, 1H, H-3), 4.65-4.75 (br m, 1H, H-3), 6.91-6.98 (m, 2H, H_{arom}), 7.12-7.19 (m, 2 H, H_{arom}), 7.31-7.38 (m, 3H, H_{arom}), 7.43-7.50 (m, 2H, H_{arom}).
50c	H	F	F	1660 (C=C)	2.92 (s, 3H, 2-CH_3), 3.85-3.95 (br m, 1H, H-3), 4.65-4.75 (br m, 1H, H-3), 6.91-6.97 (m, 2H, H_{arom}), 7.13-7.18 (m, 2H, H_{arom}), 7.31-7.34 (m, 2H, H_{arom}), 7.45-7.49 (m, 2H, H_{arom}).

(continued)

Entry	R	R^1	R^2	IR, KBr (cm^{-1})	^1H NMR, $CDCl_3$ (δ)
50d	H	H	SCH_3	1659 (C=C)	2.47 (s, 3H, S-CH_3), 2.91 (s, 3H, 2-CH_3), 3.85- 3.95 (br m, 1H, H-3), 4.65-4.75 (br m, 1H, H-3), 7.16-7.29 (m, 7H, H_{arom}), 7.42 (d, J = 8.5 Hz, 2H, H_{arom}).
50e	H	SCH_3	H	1660 (C=C)	2.47 (s, 3H, S-CH_3), 2.91 (s, 3H, 2-CH_3), 3.85- 3.95 (br m, 1H, H-3), 4.55-4.65 (br m, 1H, H-3), 7.13-7.35 (m, 7H, H_{arom}), 7.48-7.50 (m, 2H, H_{arom}).
50f	H	F	SCH_3	1661 (C=C)	2.47 (s, 3H, S-CH_3), 2.89 (s, 3H, 2-CH_3), 3.60- 3.70 (br m, 1H, H-3), 4.40-4.50 (br m, 1H, H-3), 6.91-6.98 (m, 2H, H_{arom}), 7.13-7.18 (m, 4H, H_{arom}), 7.35 (d, J = 8.5 Hz, 2H, H_{arom}).
50g	H	SCH_3	F	1660 (C=C)	2.48 (s, 3H, S-CH_3), 2.91 (s, 3H, 2-CH_3), 3.85- 3.95 (br m, 1H, H-3), 4.55-4.65 (br m, 1H, H-3), 6.90-6.98 (m, 2H, H_{arom}), 7.13-7.18 (m, 4H, H_{arom}), 7.31-7.38 (m, 2H, H_{arom}).

(continued)

Entry	R	R^1	R^2	IR, KBr (cm^{-1})	^1H NMR, $CDCl_3$ (δ)
50h	H	H	SO_2CH_3	1655 (C=C)	2.94 (s, 3H, 2-CH_3), 3.06 (s, 3H, SO_2CH_3), 3.95-4.10 (br m, 1H, H-3), 4.50-4.57 (br m, 1H, H-3), 7.19-7.33 (m, 5H, H_{arom}), 7.66 (d, J = 8 Hz, 2H, H_{arom}), 7.85 (d, J = 8 Hz, 2H, H_{arom}).
50i	H	SO_2CH_3	H	1658 (C=C)	2.82 (s, 3H, 2-CH_3), 2.95 (s, 3H, SO_2CH_3), 3.90-4.0 (br m, 1H, H-3), 4.60-4.70 (br m, 1H, H-3), 7.10-7.30 (m, 5H, H_{arom}), 7.57 (d, J = 8 Hz, 2H, H_{arom}), 7.76 (d, J = 8 Hz, 2H, H_{arom}).
50j	CH_3	F	SO_2CH_3	1660 (C=C)[a]	1.33 (d, $J_{CH,Me}$ = 6 Hz, 3H, CH_3), 2.92 (s, 3H, 2-CH_3), 3.01 (s, 3H, SO_2CH_3), 4.20-4.30 (br q, $J_{CH,Me}$ = 7 Hz, 1H, H-3), 7.04-7.10 (m, 2H, H_{arom}), 7.15-7.20 (m, 2H, H_{arom}), 7.54 (d, J = 8 Hz, 2H, H_{arom}), 7.82 (d, J = 8 Hz, 2H, H_{arom}).
50k	CH_3	H	SO_2CH_3	1660 (C=C)	1.35 (d, $J_{CH,Me}$= 7 Hz, 3H, CH_3), 2.92 (s, 3H, 2-CH_3), 3.02 (s, 3H, SO_2CH_3), 4.22-4.30 (br q, $J_{CH,Me}$ = 7 Hz, 1H, H-3), 7.20-7.34 (m, 5H, H_{arom}), 7.57 (d, J = 8 Hz, 2H, H_{arom}), 7.80 (d, J = 8 Hz, 2H, H_{arom}).

[a] IR is measured as KBr disc.

Table **22**. ^{13}C and ^{19}F NMR Spectral data for 4,5-Diaryl-2-methyl-4-isoxazolines (**50**).

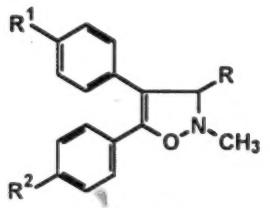

50

Entry	R	R^1	R^2	^{13}C, $CDCl_3$ (δ)	^{19}F, $CDCl_3$ (δ)
50a	H	H	F	47.43 (2-*C*H$_3$), 65.65 (*C*H$_2$), 105.80 (C-4), 115.35 (d, J_{CCF} = 22 Hz, *C*CF), 126.45, 126.83, 128.41, 130.06 (*C*$_{arom}$-H), 128.80, 133.60 (C$_{arom}$-*C*), 148.10 (C-5), 164.58 (d, $J_{C,F}$ = 251 Hz, *C*F).	50.81 (dddd, J_{FCCH} = 9.1, J_{FCCH} = 5.1 Hz, 1F).
50d	H	H	SCH_3	15.27 (S-*C*H$_3$), 47.42 (2-*C*H$_3$), 65.72 (*C*H$_2$), 105.61 (C-4), 125.10, 133.53 (C$_{arom}$-*C*), 125.72, 126.38, 126.85, 128.38, 128.51 (*C*$_{arom}$-H), 140.03 (*C*$_{arom}$-CS) 147.10 (C-5).	————
50f	H	F	SCH_3	15.30 (S-*C*H$_3$), 47.50 (2-*C*H$_3$), 65.86 (*C*H$_2$), 104.67 (C-4), 115.35 (d, J_{CCF} = 22 Hz, *C*CF), 125.83, 128.36, 128.61 (*C*$_{arom}$-H), 125.59, 129.58 (C$_{arom}$-*C*), 140.26 (*C*$_{arom}$-CS) 146.70 (C-5), 161.30 (d, $J_{C,F}$ = 251 Hz, *C*-F).	46.53 (dddd, J_{FCCH}= 9.1, J_{FCCCH}= 5.1 Hz, 1F).

(continued)

Entry	R	R^1	R^2	^{13}C, $CDCl_3$ (δ)	^{19}F, $CDCl_3$ (δ)
50h	H	H	SO_2CH_3	44.33 (SO_2CH_3), 47.49 (2-CH_3), 66.17 (CH_2), 109.50 (C-4), 127.22, 127.26, 127.30, 128.53, 128.72 (C_{arom}-H), 132.54, 134.74 (C_{arom}-C), 140.42 (C_{arom}-CS), 144.77 (C-5).	————
50j	CH_3	F	SO_2CH_3	19.79 (CH-CH_3), 44.40 (SO_2CH_3), 46.26 (2-CH_3), 72.74 (CH_3-CH), 114.62 (C-4), 116.10 (d, J_{CCF} = 22 Hz, CCF), 126.70, 127.95, 130.12 (C_{arom}-H), 128.70, 134.70 (C_{arom}-C), 140.07 (C_{arom}-CS), 148.68 (C-5), 161.30 (d, $J_{C,F}$ = 251 Hz, C-F).	18.17 (dddd, J_{FCCH}= 9.1, J_{FCCH}= 5.1 Hz, 1F).

Table 23. Physical data for 4,5-diaryl-2-methyl-4-isoxazolines (50).

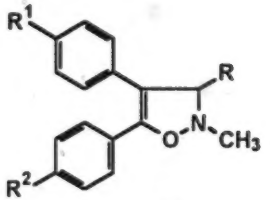

50

Entry	R	R^1	R^2	% Yield	mp (°C)	Elemental Analysis					
						Calculated			Found		
						C	H	N	C	H	N
50a	H	H	F	50	oil	75.29	5.48	5.48	75.28	5.58	5.21
50b	H	F	H	25	oil	75.29	5.48	5.48	74.98	5.38	5.40
50c	H	F	F	60	oil	70.30	4.79	5.13	70.44	4.81	5.12
50d	H	H	SCH_3	50	oil	72.08	6.00	4.94	72.08	5.83	4.80
50e	H	SCH_3	H	52	oil	72.08	6.00	4.94	71.70	5.79	4.84
50f	H	F	SCH_3	50	oil	67.77	5.35	4.65	67.40	5.44	4.43
50g	H	SCH_3	F	52	oil	67.77	5.35	4.65	67.97	5.42	4.45
50h	H	H	SO_2CH_3	55	Oil	61.26	5.10	4.20	61.59	5.40	4.01

(continued)

Entry	R	R^1	R^2	% Yield	mp (°C)	Elemental Analysis					
						Calculated			Found		
						C	H	N	C	H	N
50i	H	SO_2CH_3	H	50	oil	61.26	5.10	4.20	61.27	5.31	4.01
50j	CH_3	F	SO_2CH_3	71	116-120	62.24	5.18	4.03	62.31	5.28	4.10
50k	CH_3	H	SO_2CH_3	76	oil	65.65	5.77	4.26	65.82	5.95	4.41

3.1.5 Synthesis of 1-(4-Azidophenyl)-3-(4-methylphenyl)-5-trifluoromethyl-pyrazole (54), 1-(4-Azidophenyl)-5-(4-methylphenyl)-3-trifluoromethyl-pyrazole (57) and 4-(4-Azidophenyl)-3-phenyl-2(5*H*)-furanone (61).

The SO_2Me and SO_2NH_2 pharmacophores are believed to induce COX-2 isozyme selectivity by insertion into the secondary pocket of COX-2 isozyme that is absent in COX-1, with subsequent hydrogen bond formation between the *O* and/or *N* in the pharmacophore to His^{90}, Arg^{120}, Gln^{192}, Arg^{513}, and Phe^{518} [Kurumbail *et al.*, 1996]. The design of compounds **57** and **61** by replacement of the SO_2Me and SO_2NH_2 pharmacophores with an azido group in celecoxib and rofecoxib, respectively is discussed in Section **3.2.1.7**.

Reaction of 4-nitrophenylhydrazine with 1-(4-methylphenyl)-4,4,4-trifluorobutane-1,3-dione in EtOH afforded the cyclic pyrazoline-5-ol **51** which eliminated a molecule of water upon treatment with HOAc at reflux temperature to yield the pyrazole **52** (see Scheme 7). Reduction of the nitro group in the pyrazole **52** with hydrazine hydrate and 10% Pd/C yielded the corresponding amino product **53**. Diazotization of **53**, and treatment of the diazonium salt with NaN_3, afforded the 1,3-regioisomer of celecoxib **54**, having an azido substituent in place of the SO_2NH_2 pharmacophore. Spectral and physical data are presented in tables **24-26**. In contrast, the 1,5-regioisomer was prepared by condensation of 4-nitrophenylhydrazine with 1-(4-methylphenyl)-4,4,4-trifluorobutane-1,3-dione in EtOH under acidic reaction conditions to yield the pyrazole **55**. The azido analogue of celecoxib **57** was prepared starting from the pyrazole **55** using the same reaction sequence used for the elaboration of the nitro compound **52** to the azido product **57** as shown in Scheme 7. Spectral and physical data are presented in tables **27-29.**

Scheme 7[a]. Synthesis of 1-(4-azidophenyl)-3-(4-methylphenyl)-5-trifluoromethylpyrazole (**54**) and 1-(4-azidophenyl)-5-(4-methylphenyl)-3-trifluoromethylpyrazole (**57**).

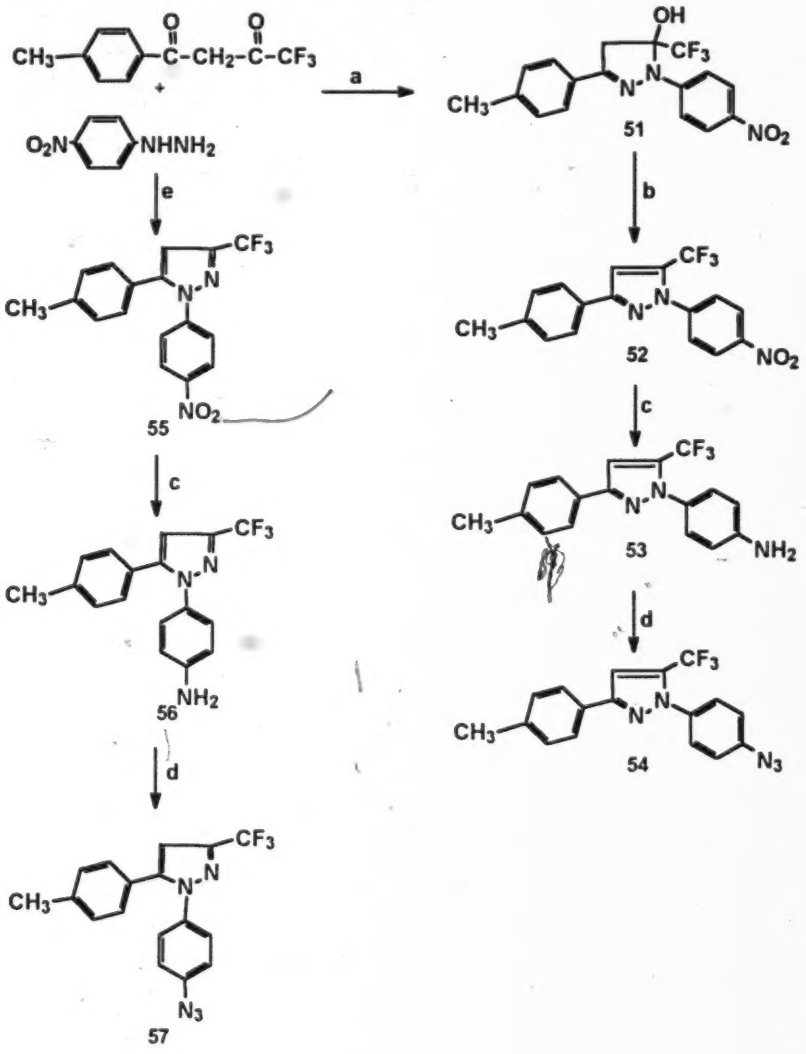

[a]Reagents and conditions: (a) EtOH, reflux, 20 h; (b) HOAc, reflux, 2 h; (c) $NH_2NH_2.xH_2O$, Pd/C, reflux, 45 min; (d)$NaNO_2$/HCl, and then NaN_3, 0-5°C, 45 min; (e) EtOH, HCl, reflux, 20 h.

Table **24**. IR and ^{1}H NMR spectral data for 4,5-dihydro-5-hydroxy-3-(4-methylphenyl)-1-(4-nitrophenyl)-5-trifluoromethylpyrazole (**51**), and 1-aryl-3-(4-methylphenyl)-5-trifluoromethyl-1*H*-pyrazoles (**52-54**).

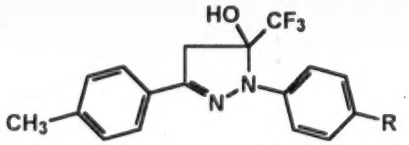

51

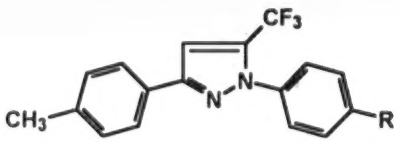

52-54

Entry	R	IR, KBr (cm^{-1})	^{1}H NMR, $CDCl_3$ (δ)
51	NO_2	1616 (C=N)	2.30 (s, 3H, C*H*$_3$), 3.53 (d, J_{gem} = 19 Hz, 1H, C*H*$_a$H$_b$), 3.67 (d, J_{gem} = 19 Hz, 1H, CH$_a$*H*$_b$), 7.15 (d, *J* = 8 Hz, 2H, H$_{arom}$), 7.50 (d, *J* = 8 Hz, 2H, H$_{arom}$), 7.60 (d, *J* = 9.5 Hz, 2H, H$_{arom}$), 8.03 (d, *J* = 9.5 Hz, 2H, H$_{arom}$)[a].
52	NO_2	1606 (C=N)	2.35 (s, 3H, C*H*$_3$), 7.10 (s, 1H, H-4), 7.21 (d, *J* = 8.2 Hz, 2H, H$_{arom}$), 7.69 (d, *J* = 8.2 Hz, 2H, H$_{arom}$), 7.75 (d, *J* = 9.15 Hz, 2H, H$_{arom}$), 8.21 (d, *J* = 9.15 Hz, 2H, H$_{arom}$).
53	NH_2	1609 (C=N)	2.40 (s, 3H, C*H*$_3$), 6.71 (d, *J* = 8.5 Hz, 2H, H$_{arom}$), 7.04 (s, 1H, H-4), 7.24 (d, *J* = 8.5 Hz, 2H, H$_{arom}$), 7.30 (d, *J* = 8.5 Hz, 2H, H$_{arom}$), 7.76 (d, *J* = 8.5 Hz, 2H, H$_{arom}$)[a].
54	N_3	2092, 2132 (N_3)	2.41 (s, 3H, C*H*$_3$), 7.10 (s, 1H, H-4), 7.15 (d, *J* = 8.8 Hz, 2H, H$_{arom}$), 7.27 (d, *J* = 8.2 Hz, 2H, H$_{arom}$), 7.55 (d, *J* = 8.8 Hz, 2H, H$_{arom}$), 7.77 (d, *J* = 8.2 Hz, 2H, H$_{arom}$).

[a] ^{1}H NMR is measured in $CDCl_3$ + D_2O.

Table **25**: ^{13}C and ^{19}F NMR spectral data for 4,5-dihydro-5-hydroxy-3-(4-methylphenyl)-1-(4-nitrophenyl)-5-trifluoromethylpyrazole (**51**), and 1-aryl-3-(4-methylphenyl)-5-trifluoromethyl-1*H*-pyrazoles (**52-54**).

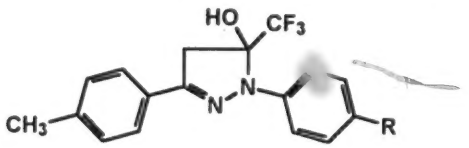

51

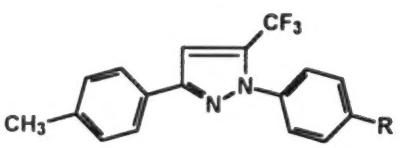

52-54

Entry	R	^{13}C, $CDCl_3$ (δ)	^{19}F, $CDCl_3$ (δ)
51	NO_2	21.15 (CH_3), 44.44 (C-4), 93.15 (q, J_{CCF} = 33 Hz, C-5), 115.13, 125.41, 126.16, 129.16 (C_{arom}-H), 123.0 (q, J_{CF} = 288 Hz, CF_3), 127.91, 140.0 (C_{arom}-C), 140.10, 147.67 (C_{arom}-N), 149.34 (C-3).	81.54 (s, CF_3).
52	NO_2	21.35 (CH_3), 107.88 (C-4), 119.20 (q, J_{CF} = 269 Hz, CF_3), 124.62, 125.48,125.83, 129.58 (C_{arom}-H), 128.20, 139.22 (C_{arom}-C), 133.75 (q, J_{CCF} = 40 Hz, C-5), 143.98, 147.42 (C_{arom}-N), 152.97 (C-3).	104.58 (s, CF_3).
53	NH_2	21.29 (CH_3), 105.11 (C-4), 114.72, 125.67, 127.11, 129.38 (C_{arom}-H), 118.75 (q, J_{CF} = 269 Hz, CF_3), 129.18, 138.25 (C_{arom}-C), 130.14, 147.30 (C_{arom}-N), 133.75 (q, $J_{C\text{-}CF}$ = 34 Hz, C-5), 152.97 (C-3).	101.20 (s, CF_3).

(continued)

Entry	R	^{13}C, $CDCl_3$ (δ)	^{19}F, $CDCl_3$ (δ)
54	N_3	21.23 (CH_3), 105.97 (C-4), 118.76 (q, J_{CF} = 268 Hz, CF_3), 119.44, 125.68, 127.09, 129.42 (C_{arom}-H), 128.77, 138.57 (C_{arom}-C), 133.44 (q, $J_{C\text{-}CF}$ = 31 Hz, C-5), 135.86, 141.04 (C_{arom}-N), 151.79 (C-3).	_____

Table **26**. Physical data for 4,5-dihydro-5-hydroxy-3-(4-methylphenyl)-1-(4-nitrophenyl)-5-trifluoromethylpyrazole (**51**), and 1-aryl-3-(4-methylphenyl)-5-trifluoromethyl-1*H*-pyrazoles (**52-54**).

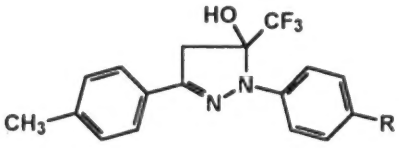

51

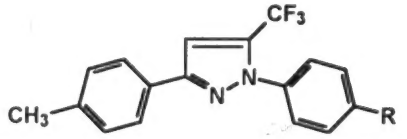

52-54

Entry	R	% Yield	mp (°C)	Elemental Analysis					
				Calculated			Found		
				C	H	N	C	H	N
51	NO_2	53	177-179	55.89	3.83	11.50	55.59	3.81	11.18
52	NO_2	52	95-97	58.79	3.46	12.10	58.70	3.53	12.18
53	NH_2	51	118-120	64.35	4.42	13.25	64.38	4.43	13.18
54	N_3	72	71-72	59.48	3.49	20.41	59.67	3.61	20.14

Table **27**: IR and ^{1}H NMR spectral data for 1-aryl-5-(4-methylphenyl)-3-trifluoromethyl-1*H*-pyrazoles (**55-57**).

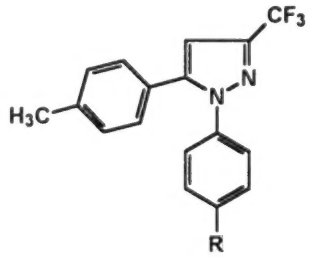

55-57

Entry	R	IR, KBr (cm^{-1})	^{1}H NMR, $CDCl_3$ (δ)
55	NO_2	1610 (C=N)	2.40 (s, 3H, C*H*$_3$), 6.67 (s, ~~1H~~, H-4), 7.13 (d, *J* = 8.2 Hz, 2H, H_{arom}), 7.22 (d, *J* = 8.2 Hz, 2H, H_{arom}), 7.53 (d, *J* = 8.8 Hz, 2H, H_{arom}), 8.22 (d, *J* = 8.8 Hz, 2H, H_{arom}).
56	NH_2	1610 (C=N)	2.35 (s, 3H, C*H*$_3$), 6.60 (d, *J* = 8.5 Hz, 2H, H_{arom}), 6.69 (s, 1H, H-4), 7.05 (d, *J* = 8.5 Hz, 2H, H_{arom}), 7.12-7.20 (m, 4H, H_{arom})[a].
57	N_3	2099, 2126 (N_3)[b]	2.25 (s, 3H, C*H*$_3$), 6.64 (s, 1H, H-4), 6.92 (d, *J* = 8.8 Hz, 2H, H_{arom}), 7.04-7.07 (m, 4H, H_{arom}), 7.19-7.25 (m, 2H, H_{arom}).

[a] ^{1}H NMR is measured in $CDCl_3$ + D_2O. [b] IR is measured neat.

Table **28**: ^{13}C and ^{19}F NMR NMR spectral data for 1-aryl-5-(4-methylphenyl)-3-trifluoromethyl-1*H*-pyrazoles (**55-57**).

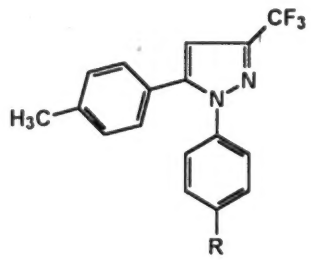

55-57

Entry	R	^{13}C, $CDCl_3$ (δ)	^{19}F, $CDCl_3$ (δ)
55	NO_2	21.25 (CH_3), 106.61 (C-4), 121.25 (q, J_{CF} = 270 Hz, CF_3), 124.39, 125.30, 128.68, 129.73 (C_{arom}-H), 125.64, 139.92 (C_{arom}-C), 143.95, 145.38 (C_{arom}-N), 144.30 (q, J_{CCF} = 40 Hz, C-3), 146.71 (C-5).	99.60 (s, CF_3).
57	N_3	21.28 (CH_3), 105.36 (C-4), 120.9 (q, J_{CF} = 270 Hz, CF_3), 119.45, 126.82, 128.64, 129.44 (C_{arom}-H), 126.12, 136.11 (C_{arom}-C), 139.22, 140.18 (C_{arom}-N), 142.99 (q, J_{CCF} = 40 Hz, C-3), 144.78 (C-5).	99.41 (s, CF_3).

Table **29**. Physical data for 1-aryl-5-(4-methylphenyl)-3-trifluoromethyl-1*H*-pyrazoles (**55-57**).

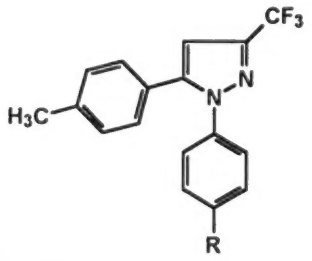

55-57

Entry	R	% Yield	mp (°C)	Elemental Analysis					
				Calculated			Found		
				C	H	N	C	H	N
55	NO_2	76	123-125	58.79	3.46	12.10	58.46	3.38	11.84
56	NH_2	92	125-127	64.35	4.42	13.20	64.35	4.46	13.03
57	N_3	56	oil	59.48	3.49	20.41	59.42	3.68	20.31

The azido analogue **61** of rofecoxib, where $MeSO_2$ was replaced by N_3, was prepared starting with the bromination of 4-azidoacetophenone **58** using Br_2. The subsequent reaction of the bromo compound **59** with phenylacetic acid in the presence of $(Et)_3N$ gave 4-(4-azidophenyl)-3-phenyl-2(5*H*)-furanone (**61**) that was formed via the intermediate ester **60** as illustrated in Scheme **8**. Spectral and physical data are presented in tables **30-32.**

Scheme **8**[a]: Synthesis of 4-(4-azidophenyl)-3-phenyl-2(5*H*)-furanone (**61**).

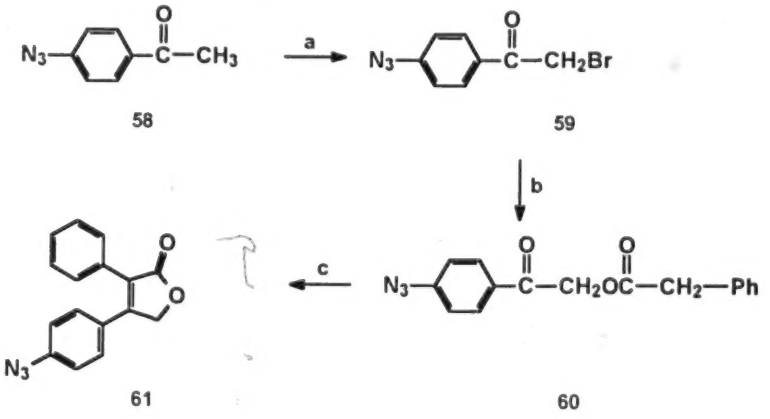

58 59 60 61

[a] Reagents and conditions: (a) Br_2, $CHCl_3$, 25°C, 2 h; (b) $PhCH_2COOH$, Et_3N, CH_3CN, 25°C, 1 h; (c) Et_3N, CH_3CN, reflux, 8 h.

Table **30**. IR and ^{1}H NMR spectral data for 2-substituted-1-(4-azidophenyl)ethanones (**59**, **60**), and 4-(4-azidophenyl)-3-phenyl-2(5*H*)-furanone (**61**).

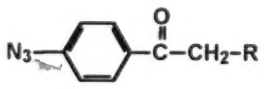

59, 60

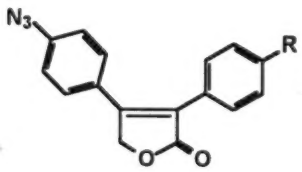

61

Entry	R	IR, KBr (cm^{-1})	^{1}H NMR, $CDCl_3$ (δ)
59	Br	2106 (N_3), 1703, 1743 (CO).	4.41 (s, 2H, CH_2), 7.12 (d, J = 8.5 Hz, 2H, H_{arom}), 8.01 (d, J = 8.5 Hz, 2H, H_{arom}).
60	Ph-CH_2OCO	2105 (N_3), 1710, 1750 (CO)	3.82 (s, 2H, CH_2), 5.30 (s, 2H, CH_2), 7.09 (d, J = 8.8 Hz, 2H, H_{arom}), 7.27-7.36 (m, 5H, H_{arom}), 7.88 (d, J = 8.8 Hz, 2H, H_{arom}).
61	H	2108 (N_3), 1748 (CO),	5.14 (s, 2H, CH_2), 6.70 (d, J = 8.5 Hz, 2H, H_{arom}), 7.30 (d, J = 8.5 Hz, 2H, H_{arom}), 7.38-7.42 (m, 5H, H_{arom}).

Table **31**. ^{13}C NMR spectral data for 2-substituted-1-(4-azidophenyl)ethanones (**59**, **60**), and 4-(4-azidophenyl)-3-phenyl-2(5*H*)-furanone (**61**).

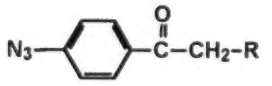

59, 60

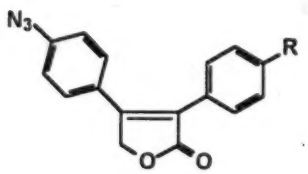

61

Entry	R	^{13}C, $CDCl_3$ (δ)
59	Br	30.38 (CH_2), 119.20, 130.92 (C_{arom}-H), 130.49 (C_{arom}-C), 145.77 (C_{arom}-N), 189.74 (CO).
60	Ph-CH_2OCO	40.97 (CH_2), 66.18 (CH_2), 119.20, 127.18, 128.56, 129.35, 129.70 (C_{arom}-H), 130.76, 133.46 (C_{arom}-C), 145.66 (C_{arom}-N), 170.92, 190.47 (CO).
61	H	70.30 (CH_2), 119.51, 128.75, 128.89, 129.03, 129.18 (C_{arom}-H), 125.99, 127.25, 130.11 (C_{arom}-C and C-3), 142.40 (C_{arom}-N), 154.64 (C-4), 173.17 (CO).

Table **32**: Physical data for 2-substituted-1-(4-azidophenyl)ethanones (**59**, **60**), and 4-(4-azidophenyl)-3-phenyl-2(5*H*)-furanone (**61**).

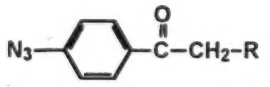

59, 60

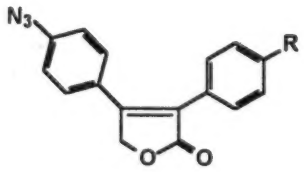

61

Entry	R	% Yield	mp (°C)	Elemental Analysis					
				Calculated			Found		
				C	H	N	C	H	N
59	Br	66	66-67	40.00	2.50	17.50	40.12	2.31	17.46
60	Ph-CH_2OCO	54	Oil	65.08	4.40	14.23	65.12	4.36	13.98
61	H	42	79-81	69.31	3.97	15.16	69.52	3.98	15.21

3.2 Molecular Modeling.

The kinetic mechanism of COX isozymes inhibition has been studied and it is now well accepted that the different activity of a selective compound for each enzyme, *viz.* the selectivity, may arise from the difference in kinetics of enzyme inhibition for both COX-1 and COX-2 [Gravito, 1996; Copeland *et al.*, 1994].

On the other hand, studies of the static 3D structure of the enzyme have been of great value to the understanding of the enzyme inhibition mechanism and design of selective compounds. However, it has been shown that static 3D structures alone are insufficient, and some authors have suggested the importance of dynamic factors related to selective inhibitors including enzyme flexibility and rearrangement of the hydrogen bonding network at the entrance of the active site [Luong *et al.*, 1996; So *et al.*, 1998].

Moreover, dynamic models of COX isozymes inhibitor complexes with SC-588 [Filizola *et al.*, 1997], NS-398, indoprofen [Kothekar *et al.*, 1999] and flurbiprofen [Bayly *et al.*, 1999] have not only added a more comprehensive understanding of the mode of action of inhibitors but have also been used for the design of selective COX-2 inhibitors.

3.2.1 Docking Experiments.

Most docking methods described in the literature are based on descriptors or empirical rules (for a review see Kuntz *et al.*, 1994). In docking experiments reported here, the Molecular Simulation Inc. Affinity algorithm (module) was used. Affinity uses a Monte Carlo-type procedure to dock a guest molecule in a host. It has the feature where the "bulk" of the receptor, defined as atoms not in the specified binding (active) site, is held

rigid during the docking process, while the binding site atoms and ligand atoms are movable. Affinity distinguishes itself from other methods in the literature in three aspects. First, it uses full molecular mechanics in searching for and evaluating docked structures. In contrast, descriptor-based methods use empirical rules, which usually take into account only hydrogen bonding, hydrophobic interactions, or steric effects. Meng *et al.* studied three scoring methods for evaluating docked structures generated by the DOCK program [Meng *et al.*, 1992]. These studies showed that only the force field scores from molecular mechanics correctly identify structures closest to the experimental binding energy, while scoring functions that consider only steric factors or only electrostatic factors are less successful. Second, in Affinity the bulk of the protein is fixed, while the defined binding site is free to move, thereby allowing the protein to adjust to the binding of different ligands. In comparison, nearly all of the descriptor-based methods fix the entire receptor with few exceptions [Leach, 1994; Jones *et al.*, 1995]. Third, the ligand itself is flexible in Affinity compared to most docking methods with a few exceptions in DOCK [Oshiro *et al.*, 1995] and FLOG [Miller *et al.*, 1995].

3.2.1.1 Docking of SC-588 in the Binding Site of COX-1 and COX-2.

The selective COX-2 isozyme inhibitor SC-588 (**19**) was docked in the active site of ovine COX-1 (1CQE PDB file) and human COX-2 (1CX2 PDB file) isozymes, which were subsequently used as a reference for other docking experiments in this study (Figure **8**). The distances between specified groups in the ligand and COX-1 and COX-2 active site residues are illustrated in Table **33**

Table 33. Distances between Selected COX-1 and COX-2 Residues and SC-588 (19).

SC-588	COX-1[a]	Distance (Å)[b]	COX-2[a]	Distance (Å)[b]
*C*F$_3$	Tyr^{355} (*O*H)	6.05	Tyr^{355} (*O*H)	3.57
	Arg^{120} (*CZ*)[c]	6.84	Arg^{120} (*CZ*)[c]	5.01
	Ser^{530} (*O*H)	8.49	Ser^{530} (*O*H)	15.51
B (Center)[d]	Ile^{523} (*CB*)[e]	5.51	Val^{523} (*CB*)[f]	5.51
	Phe^{518}(*CZ*)[g]	10.49	Phe^{518}(*CZ*)[g]	7.78
	His^{513} (*CZ*)[h]	8.89	Arg^{513} (*CZ*)[c]	7.60
A (Center)[i]	Tyr^{385} (*O*H)	8.51	Tyr^{385} (*O*H)	10.01
	Trp ^{387} (*CA*)[j]	6.16	Trp ^{387} (*CA*)[j]	10.51
S[k]	His^{90} (*CE1*)[h]	12.01	His^{90} (*CE1*)[h]	2.61
	Ile^{523} (*CB*)[e]	7.61	Val^{523} (*CB*)[f]	5.48

[a] COX active site residues with atoms involved in distance measurements in parenthesis. [b] Distance after minimization. [c] NH*C*(=NH)-NH group of arginine residue. [d] Center of the 1-(4-sulphonamidophenyl) ring. [e] *C*H$_2$ group of isoleucine residue. [f] *C*H group of valine group. [g] *C*H$_2$ group of phenylalanine. [h] N=*C*H-N group of histidine residue. [i] Center of the 5-(4-bromophenyl) ring. [j] *C*H$_2$ group of tryptophane residue. [k] *S* atom of the SO_2NH_2 group.

Inspection of the data in table **33** shows that distances between the *C*F$_3$ group of SC-588 and the phenolic *O*H of Tyr^{355} (3.57 Å) and the *CZ* (C-atom of NH*C*(=NH)-NH group) of Arg^{120} (5.01 Å) are shorter in COX-2 than in COX-1 (6.05 Å and 6.84 Å, respectively), whereas the distance from the same group to the Ser^{530} *O*H group is longer in COX-2 (15.51 Å) than in COX-1 (8.49 Å).

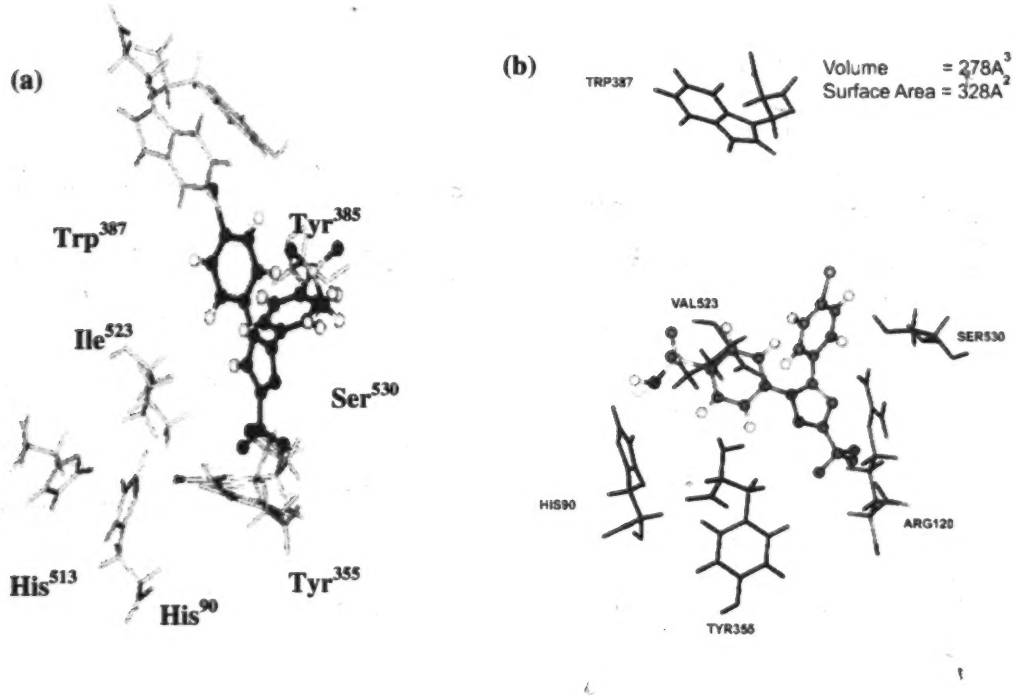

Figure **8**. Docking of SC-588 (**19**) (ball and stick) in (a) COX-1 (line and stick) ($E_{intermolecular}$ = -10.12 Kcal/mol) and (b) COX-2 (line and stick) ($E_{intermolecular}$ = -42.44 Kcal/mol)

Clearly, the CF_3 group in SC-588 interacts with residues Tyr^{355} and Arg^{120} in COX-2, whereas the CF_3 group interacts with Ser^{530} in COX-1, forcing the ligand to be docked in an alternative position, at the top of the binding pocket. This differential binding mode can be directly attributed to two structural differences between COX-1 and COX-2; the difference in the enzyme conformation in the vicinity of Tyr^{355}, and the steric hindrance caused by the replacement of Ile^{523} in COX-1 by Val^{523} in COX-2. First, the interaction of the CF_3 group of SC-588 with Tyr^{355} and Arg^{120} residues in COX-2 disrupts the hydrogen bond network, between Tyr^{355}, Arg^{120}, His^{90}, and Arg^{513} that facilitates the

entry of the inhibitor to the active site [Llorens *et al.*, 1999]. Also the interaction of the CF_3 group with Tyr^{355} and Arg^{120} residues in COX-2 isozyme anchors SC-588 at the mouth of the primary channel, allowing the SO_2NH_2 pharmacophore to be inserted in the secondary pocket. Second, the smaller size of Val^{523} in COX-2, than Ile^{523} in COX-1, allows the ligand to relax in the secondary pocket behind the primary channel. In addition to the absence of the secondary pocket in COX-1, the size of the main channel is smaller than that of its counterpart in COX-2. These differences in the size and shape of the active site of COX-1 and COX-2 leads to high energy ligand-enzyme complex, which leaves that complex vulnerable to competition with a more stable complex between the enzyme and the substrate, hence the competitive nature of inhibition of COX-1 isozymes. In COX-2 isozyme the SO_2NH_2 group is nearer to His^{90} (2.61 Å) than that in COX-1 (12.01 Å). The difference in position of the SO_2NH_2 of SC-588 docked in COX-2 from that in COX-1, tends to enhance the stability of the enzyme-inhibitor complex by hydrogen-bonding and/or electrostatic interaction in COX-2, more than in COX-1, hence the tight binding inhibition of COX-2 characteristic for COX-2 selective inhibitors.

Accordingly, the CF_3 and the SO_2NH_2 groups could be considered as determinants of the different affinities of the selective COX-2 inhibitor, SC-588, towards COX-1 and COX-2, and consequently correlated to the selectivity and potency of inhibition of COX-2 (COX-1 IC_{50} = 17.7 μM, COX-2 IC_{50} = 0.0093 μM, SI ≈ 1903) [Kurumbail *et al.*, 1996].

3.2.1.2 Docking of 5-(4-Methylthiophenyl)-4-phenylisoxazole (32e) and 5-(4-Methylsulphonylphenyl)-4-phenylisoxazole (32m) in the Binding Site of COX-1 and COX-2.

The SO_2Me and SO_2NH_2 pharmacophores are believed to induce COX-2 selectivity by insertion into the secondary pocket of COX-2 (Luong *et al.*, 1996]. Accordingly, isoxazoles **32a-p** were designed to incorporate H, F, MeS, MeSO or $MeSO_2$ substituents at the *para*-position of the C-4 or C-5 phenyl ring.

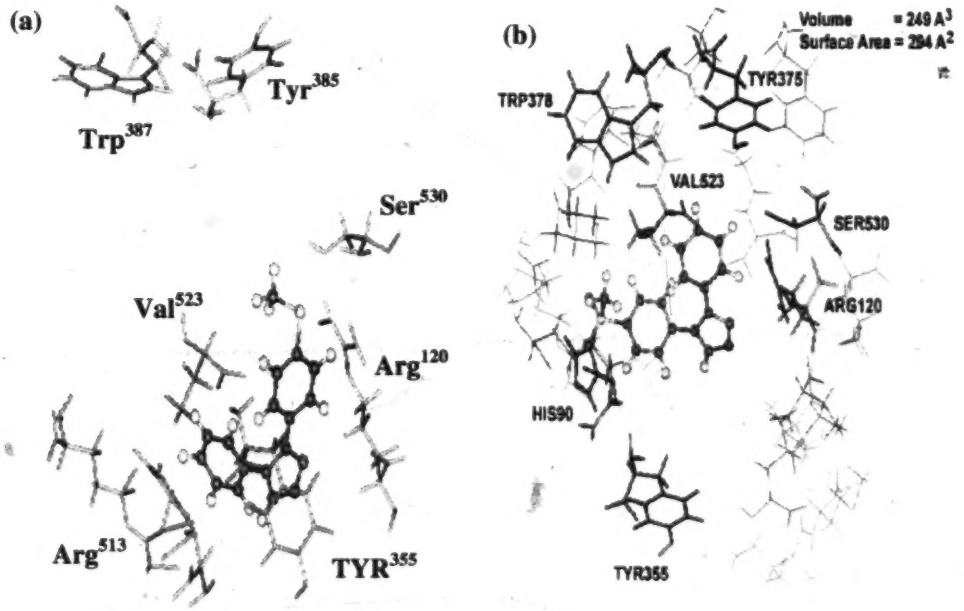

Figure **9**. Docking of (a) isoxazole **32e** (ball and stick) ($E_{intermolecular}$ = –15.71 Kcal/mol), and (b) isoxazole **32m** (ball and stick) ($E_{intermolecular}$ = -39.06 Kcal/mol) in the binding site of COX-2 (line and stick).

Docking of isoxazoles **32e** (with a MeS substituent) and **32m** (with a $MeSO_2$ substituent) in the COX-1 and COX-2 active site helped to interpret the role of the $MeSO_2$ pharmacophore in stabilizing the bound ligand in the COX reaction active site of

COX-2 (Figure 9). Docking of both **32e** and **32m** in the COX-1 active site did not show any significant differences in binding (Table **35**).

Table **34.** Distances between Selected COX-1 and COX-2 Residues and 5-(4-Methylthiophenyl)-4-phenylisoxazole (**32e**).

32e	COX-1[a]	Distance (Å)[b]	COX-2[a]	Distance (Å)[b]
N[c]	Tyr^{355} (*OH*)	3.62	Tyr^{355} (*OH*)	8.51
	Arg^{120} (*CZ*)[d]	4.86	Arg^{120} (*CZ*)[d]	6.84
	Ser^{530} (*OH*)	5.21	Ser^{530} (*OH*)	2.42
B (Center)[e]	Ile^{523} (*CB*)[f]	6.32	Val^{523} (*CB*)[g]	5.51
	Phe^{518}(*CZ*)[h]	10.01	Phe^{518}(*CZ*)[h]	8.99
	His^{513} (*CZ*)[i]	9.79	Arg^{513} (*CZ*)[d]	10.00
A (Center)[j]	Tyr^{385} (*OH*)	8.37	Tyr^{385} (*OH*)	9.62
	Trp^{387} (*CA*)[k]	7.17	Trp^{387} (*CA*)[k]	10.11
S[l]	His^{90} (*CE1*)[i]	11.99	His^{90} (*CE1*)[i]	10.15
	Ile^{523} (*CB*)[f]	4.98	Val^{523} (*CB*)[g]	5.56

[a] COX active site residues with atoms involved in distance measurements in parentheses. [b] Distance after minimization. [c] *N* of the isoxazole ring. [d] NH*C*(=NH)-NH group of arginine residue. [e] Center of the 5-(4-methylthiophenyl) ring. [f] CH_2 group of isoleucine residue. [g] *C*H group of valine group. [h] CH_2 group of phenylalanine. [i] N=*C*H-N group of histidine residue. [j] Center of the 4-phenyl ring. [k] CH_2 group of tryptophan residue. [l] *S* atom of the SMe group.

While isoxazole **32e** docks in the main channel of COX-2 with an intermolecular energy of –15.71 Kcal/mol between the ligand and COX-2 enzyme, the isoxazole **32m** was found to bind in a similar manner to SC-588 (**19**) with the SO_2CH_3 group residing in the secondary COX-2 pocket with an intermolecular energy of –39.06 Kcal/mol. These

results confirm the reported role of the oxidation level of S in the selective inhibitors of COX-2 isozyme [Kalgutkar *et al.*, 2000].

The most prominent difference between docking of **32m** and SC-558 in the active site of COX-2 isozyme was the interactions of the ligand with Tyr^{355}, Arg^{120} and Ser^{530} (Table **35**).

Table **35.** Distances between Selected COX-1 and COX-2 Residues and 5-(4-Methyl-sulphonylphenyl)-4-phenylisoxazole (**32m**).

32m	COX-1[a]	Distance (Å)[b]	COX-2[a]	Distance (Å)[b]
N[c]	Tyr^{355} (*OH*)	3.75	Tyr^{355} (*OH*)	10.75
	Arg^{120} (*CZ*)[d]	4.71	Arg^{120} (*CZ*)[d]	6.68
	Ser^{530} (*OH*)	5.19	Ser^{530} (*OH*)	7.83
B (Center)[e]	Ile^{523} (*CB*)[f]	6.10	Val^{523} (*CB*)[g]	4.72
	Phe^{518}(*CZ*)[h]	10.51	Phe^{518}(*CZ*)[h]	9.41
	His^{513} (*CZ*)[i]	9.91	Arg^{513} (*CZ*)[d]	6.92
A (Center)[j]	Tyr^{385} (*OH*)	8.51	Tyr^{385} (*OH*)	11.79
	Trp^{387} (*CA*)[k]	7.01	Trp^{387} (*CA*)[k]	12.77
S[l]	His^{90} (*CE1*)[i]	12.44	His^{90} (*CE1*)[i]	3.39
	Ile^{523} (*CB*)[f]	4.86	Val^{523} (*CB*)[g]	5.60

[a] COX active site residues with atoms involved in distance measurements in parentheses. [b] Distance after minimization. [c] *N* of the isoxazole ring. [d] NH*C*(=NH)-NH group of arginine residue. [e] Center of the 5-(4-methylsulphonylphenyl) ring. [f] CH_2 group of isoleucine residue. [g] *C*H group of valine group. [h] CH_2 group of phenylalanine. [i] N=*C*H-N group of histidine residue. [j] Center of the 4-phenyl ring. [k] CH_2 group of tryptophan residue. [l] *S* atom of the SO_2Me group.

The distance between the N-atom of the isoxazole ring of compound **32e** to either the phenolic *O*H of Tyr^{355} (10.75 Å) or the *CZ*-atom of Arg^{120} (6.68 Å) was longer than that

observed for SC-588, when docked in the COX-2 isozyme active site. In contrast, the distance between the *C*-atom of the CF_3 group in SC-588 and the *OH* group of Ser^{530} was about double that between the *N*-atom of the isoxazole ring of compound **32m** and the *OH* group of Ser^{530}. These data would indicate that **32m** is oriented more towards the apex of the COX-2 active site compared to SC-588. This orientation of **32m** is similar to that observed by flurbiprofen, a non-selective COX-2 inhibitor, in the COX-2 active site [Filizola *et al.*, 1997]. An enzyme inhibition study showed that the isoxazole **32m** was non-selective inhibitor of COX-2 (COX-1 IC_{50} = 2.7 μM, COX-2 IC_{50} = 227.3 μM, SI = 0.012) as will be shown in Section **3.3.1**.

3.2.1.3 Docking of 3-(4-Methylsulphonylphenyl)-4-phenyl-5-trifluoromethyl-isoxazole (36) in the Binding Site of COX-1 and COX-2.

It was anticipated that incorporation of a small lipophilic central ring substituent (CF_3) would reorient the isoxazole ring such that the isoxazole ring is positioned similar to that of the pyrazole ring of SC-588, and the $MeSO_2$ moiety on the aryl ring would be suitably positioned to facilitate its insertion into the COX-2 secondary pocket.

Docking of isoxazole **36** (with a 5-CF_3 substituent) in the human COX-2 active site showed that the CF_3 central ring substituent is about 3.35Å from the phenolic *O*H of Tyr^{355} and 4.89 Å from the *CZ* atom of Arg^{120} (as illustrated in Table **36**).

Table **36.** Distances between Selected COX-1 and COX-2 Residues and 3-(4-Methyl-sulphonylphenyl)-4-phenyl-5-trifluoromethylisoxazole (**36**).

36	COX-1[a]	Distance (Å)[b]	COX-2[a]	Distance (Å)[b]
CF_3	Tyr^{355} (*OH*)	8.44	Tyr^{355} (*OH*)	3.55
	Arg^{120} (*CZ*)[c]	6.86	Arg^{120} (*CZ*)[c]	4.89
	Ser^{530} (*OH*)	8.19	Ser^{530} (*OH*)	6.91
B (Center)[d]	Ile^{523} (*CB*)[e]	5.61	Val^{523} (*CB*)[f]	3.91
	Phe^{518}(*CZ*)[g]	10.31	Phe^{518}(*CZ*)[g]	6.03
	His^{513} (*CZ*)[h]	7.95	Arg^{513} (*CZ*)[c]	6.59
A (Center)[i]	Tyr^{385} (*OH*)	6.42	Tyr^{385} (*OH*)	11.27
	Trp^{387} (*CA*)[j]	4.60	Trp^{387} (*CA*)[j]	11.98
S[k]	His^{90} (*CE1*)[h]	12.66	His^{90} (*CE1*)[h]	2.61
	Ile^{523} (*CB*)[e]	7.74	Val^{523} (*CB*)[f]	7.40

[a] COX active site residues with atoms involved in distance measurements in parentheses. [b] Distance after minimization. [c] NH*C*(=NH)-NH group of arginine residue. [d] Center of the 3-(4-methylsulphonylphenyl) ring. [e] CH_2 group of isoleucine residue. [f] *C*H group of valine group. [g] CH_2 group of phenylalanine. [h] N=*C*H-N group of histidine residue. [i] Center of the 4-phenyl ring. [j] CH_2 group of tryptophan residue. [k] *S* atom of the SO_2CH_3 group.

This orientation is similar to that observed for SC-588 in the COX-2 active site. The *S*-atom of the $MeSO_2$ substituent in isoxazole **36** inserts deeper (7.40Å from *CB* atom of Val^{523}) than does the *S*-atom of the SO_2NH_2 group of SC-588, while the *O*-atom of the same moiety is engaged in hydrogen bonding to the Ala^{516} and Phe^{518} back bone in the COX-2 secondary pocket which was not detected for the corresponding $MeSO_2$ substituent of the isoxazole **32m** (Figure **10**).

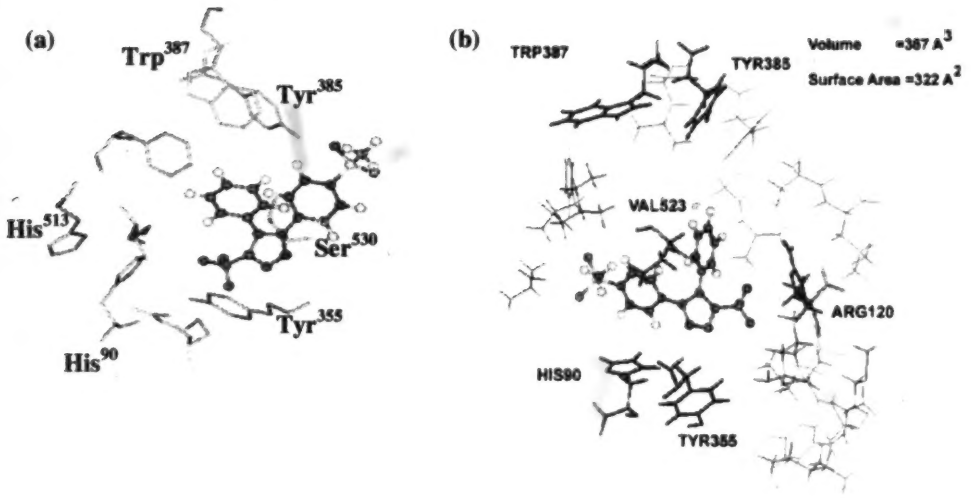

Figure **10**. Docking of isoxazole **36** (ball and stick) in the binding site of (a) ovine COX-1 (line and stick) ($E_{intermolecular}$ = 16.51 Kcal/mol), and (b) human COX-2 (line and stick) ($E_{intermolecular}$ = -53.06 Kcal/mol) isozymes.

The intermolecular energy between isoxazole **36** and COX-2 was lower (-53.06 Kcal/mol) than that for either SC-588 (-42.44 Kcal/mol) or the isoxazole **32m** (-39.06 Kcal/mol). Docking isoxazole **36** in the ovine COX-1 active site showed longer distances between the *C*-atom of the CF_3 group and the phenolic *O*H of Tyr^{355} (8.44 Å) and *CZ* atom of Arg^{120} (6.86 Å) than those shown by the same residues in COX-2 isozyme. The intermolecular energy between isoxazole **36** and COX-1 was higher (+16.51 Kcal/mol) than that for either SC-588 (-10.12 Kcal/mol) or **32m** (-12.43 Kcal/mol) (Figure **10**).

Accordingly, isoxazole **36** with a CF_3 substituent would be expected to be a more potent and selective inhibitor of COX-2 than either SC-588 or isoxazole **32m**. An enzyme inhibition assay showed that isoxazole **36** was a more potent and selective COX-2 inhibitor (COX-1 IC_{50} > 500 μM, COX-2 IC_{50} < 0.001 μM, SI = 500,000) than celecoxib (**17**), an analogue of SC-588 (COX-1 IC_{50} = 22.9 μM, COX-2 IC_{50} = 0.0567 μM, SI =

404) and isoxazole **32m** (COX-1 IC_{50} = 2.7 μM, COX-2 IC_{50} = 227.3 μM, SI = 0.012) as will be shown in Section **3.3.1**.

3.2.1.4 Docking of 4-(4-Fluorophenyl)-5-(4-methylsulphonylphenyl)-3-methyl-isoxazole (48a) and 4-(4-Methylphenyl)-5-(4-methylsulphonylphenyl-3-methylisoxazole (48b) in the Binding Site of COX-2.

Following the same hypothesis, that a small lipophilic central ring substituent would modulate the selective inhibition of COX-2 isozyme, a C-3 methyl central ring substituent was incorporated into isoxazole **32m** in conjunction with 4-(4-fluorophenyl) (**48a**), or 4-(4-methylphenyl) groups (**48b**). A methyl group has a similar size [(molar refractivity (MR) = 5.65)] and a slightly lower lipophilicity (π = -0.04) than the CF_3 moiety (5.02 and 0.38, respectively) [Hansch *et al.*, 1973].

When the designed compounds **48a** and **48b** having a C-3 Me substituent were docked in the COX-2 active site, they were orientated in the active site like non-selective COX-2 inhibitors [Sahi *et al.*, 2000] as illustrated in Table **37**. For example, the SO_2CH_3 group was positioned outside the secondary pocket and the CH_3 group was directed towards the apex of the COX-2 active site (Figure **11**). The intermolecular energy between isoxazole **48a** and **48b** was higher (-19.68 and –18.12 Kcal/mol, respectively) than that expected for selective COX-2 inhibitors such as SC-588 (-42.44 Kcal/mol). An enzyme inhibition assay showed that isoxazoles **48a-b** did not inhibit either COX-1 or COX-2 (COX-1 IC_{50}> 100, COX-2 IC_{50} > 100) as will be shown in Section **3.3.1**.

Table 37. Distances between Selected COX-2 Residues and 4-(4-Fluorophenyl)-3-methyl-5-(4-methylsulfonylphenyl)isoxazole (**48a**) and 4-(4-Methyl-phenyl)-3-methyl-5-(4-methylsulfonylphenyl)isoxazole (**48b**).

48a	COX-2[a]	Distance (Å)[b]	**48b**	COX-2[a]	Distance (Å)[b]
3-*C*H$_3$	Tyr^{355} (*OH*)	17.22	3-*CH$_3$*	Tyr^{355} (*OH*)	16.24
	Arg^{120} (*CZ*)[c]	7.08		Arg^{120} (*CZ*)[c]	4.60
	Ser^{530} (*OH*)	5.20		Ser^{530} (*OH*)	2.83
B (Center)[d]	Val^{523} (*CB*)[e]	6.03	B (Center)[d]	Val^{523} (*CB*)[e]	5.81
	Phe^{518}(*CZ*)[f]	10.69		Phe^{518}(*CZ*)[f]	10.48
	Arg^{513} (*CZ*)[c]	10.88		Arg^{513} (*CZ*)[c]	7.62
A (Center)[g]	Tyr^{385} (*OH*)	12.48	A (Center)[i]	Tyr^{385} (*OH*)	10.91
	Trp^{387} (*CA*)[h]	11.25		Trp^{387} (*CA*)[i]	11.07
S[j]	His^{90} (*CE1*)[k]	8.08	*S*[j]	His^{90} (*CE1*)[k]	7.37
	Val^{523} (*CB*)[e]	7.82		Val^{523} (*CB*)[e]	9.23

[a] COX active site residues with atoms involved in distance measurements in parentheses. [b] Distance after minimization. [c] NH*C*(=NH)-NH group of arginine residue. [d] Center of the 5-(4-methylsulphonylphenyl) ring. [e] *C*H group of valine group. [f] *C*H$_2$ group of phenylalanine. [g] Center of the 4-(4-fluorophenyl) ring. [h] *C*H$_2$ group of tryptophan residue. [i] Center of the 4-(4-methylphenyl) ring. [j] *S* atom of the SO_2CH_3 group. [k] N=*C*H-N group of histidine residue.

To better understand these unexpected results, we studied both the ligand and receptor for isoxazoles **36**, **48a** and **48b** before and after docking. Conformational analysis (stepwise changing angles ϕ and θ, 3.6° per step, and calculating the energy for each conformer as shown by the 3D map in Figure **12**) for isoxazoles **36**, **48a** and **48b** showed a similar conformation distribution with global energy minima of 17.48, 16.15, and 15.99 Kcal/mol, respectively. This study showed that the conformation of any of

isoxazoles **36**, **48a** and **48b** docked in COX-2 active site was of similar energy and conformation attributes for the three compounds. After docking isoxazoles **36**, **48a** and **48b** in COX-2 active site, it was found that isoxazoles **48a-b** had a larger root mean square deviation (rmsd) (1.15 and 1.22 Å) compared to isoxazole **36** (rmsd = 0.88 Å).

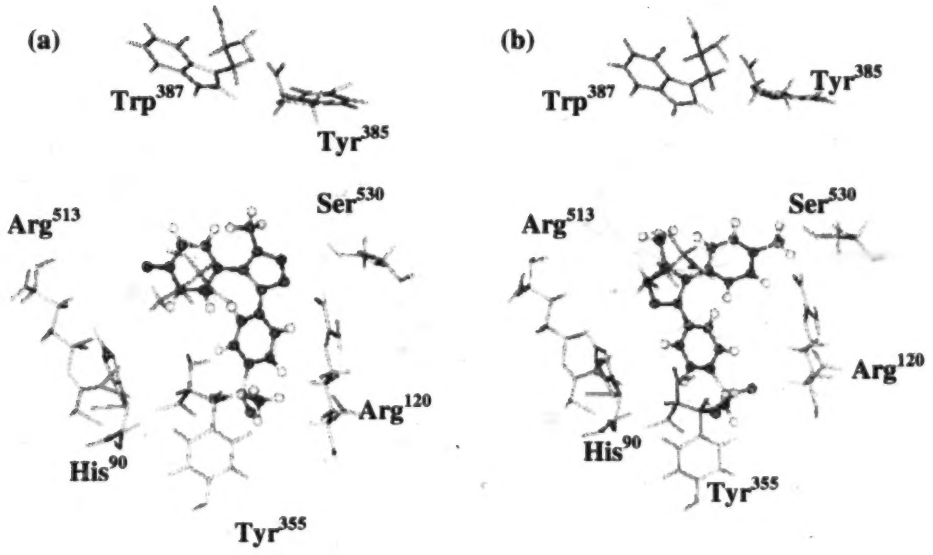

Figure **11**. Docking of (a) isoxazole **48a** (ball and stick) ($E_{intermolecular}$ = –19.68 Kcal/mol), and (b) isoxaozle **48b** (ball and stick) ($E_{intermolecular}$ = -18.12 Kcal/mol) in the binding site of COX-2 (line and stick).

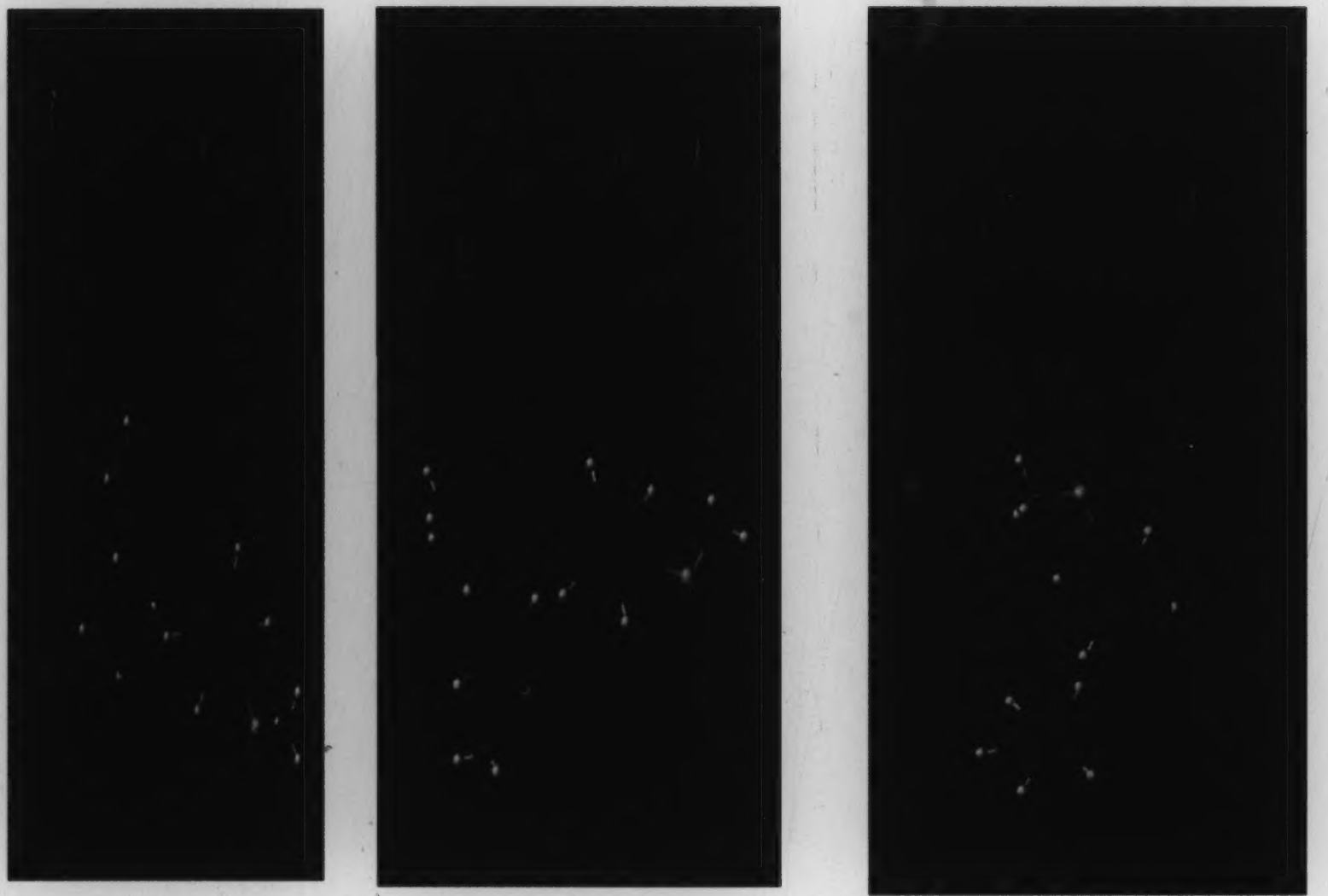

Figure 12. Conformational analysis of isoxazoles **48a**, **48b** and **36** (ball and stick), represented in the conformational maps by a gray sphere.

This data indicate that isoxazoles **48a-b** underwent a greater perturbation to achieve energetically stable binding in the COX-2 active site than isoxazole **36**. On the other hand monitoring the rmsd of selected residues side chains such as His^{90}, Arg^{120}, Tyr^{355}, Tyr^{385}, Arg^{513}, and Val^{523} showed that isoxazoles **48a-b** caused a lower rmsd than isoxazole **36** (Table **38**).

Table **38**. RMSD of Selected Residues in the COX-2 Isozyme Active Site in Assemblies of COX-2 and Isoxazoles **48a-b** and **36.**

	RMSD[a]		
COX-2 active site residues	Isoxazole **48a**	Isoxazole **48b**	Isoxazole **36**
His^{90}	0.15	0.16	0.72
Arg^{120}	0.19	0.21	0.86
Tyr^{355}	0.22	0.18	0.81
Tyr^{385}	0.31	0.38	0.12
Arg^{513}	0.09	0.16	0.65
Val^{523}	0.55	0.61	0.82
Ser^{530}	0.49	0.52	0.31

[a] RMSD is calculated by comparing the specified residues in the structures before and after docking of isoxazoles **48a-b** and **36** in the binding site of COX-2 isozyme.

From these data it can be concluded that the isoxazole **36** affects the dynamic flexibility in COX-2, while isoxazoles **48a** and **48b** did not. This difference between the way isoxazole **36** interacts with the COX-2 active site and that for **48a** and **48b** could be attributed to the electronic nature of the C-5 CF_3 group in isoxazole **36** relative to the C-3 Me group in **48a-b**. The weak hydrogen bond accepting character of the CF_3 group in isoxazole **36** disrupts the hydrogen bond network, between Tyr^{355}-Arg^{120}-Gln^{524} on one side of the mouth of the primary channel, and Tyr^{355}-His^{90}-Arg^{513} on the other side. The

CF_3 group present in isoxazole **36** does not interact extensively with Arg^{120} whereas, the CO_2H group of non-selective COX-2 inhibitor, flurbiprofen, strongly binds to with Arg^{120} at the mouth of the binding site. These results are consistent with the comparative molecular volume study described in Section **3.2.2** and *in vitro* enzyme inhibition assay data in Section **3.3.1**.

3.2.1.5 Docking of 4,5-Diphenyl-3-methylsulfonamidoisoxazole (44) in the Binding Site of COX-2.

In an attempt to understand the effect of size and nature of the central ring substituent, the SO_2NH_2 pharmacophore was moved from the phenyl rings in the *cis*-stilbene structure to the central isoxazole ring. In addition to, the larger size of isoxazole **44** (C-3 $MeSO_2NH$) when compared to isoxazole **43** (C-3 NH_2), the greater flexibility of the $MeSO_2NH$ central ring substituent may result in a superior interaction of the ligand with the COX-2 active site.

When isoxazole **44** was docked in COX-2 (1CX2 PDB file), the C-3 $MeSO_2NH$ central ring substituent was found to interact in a manner similar to the selective COX-2 inhibitor NS-398 (**6**) as reported in the literature (Figure **13**) [Sahi *et al.*, 2000]. The isoxazole **44** was located near the apex of the COX-2 active site where the $MeSO_2NH$ pharmacophore was 3.61 Å from Ser^{530} and 2.09 Å from Arg^{120} with an intermolecular energy of –45.6 Kcal/mol. Enzyme inhibition study showed that isoxazole **44** is a more potent and selective inhibitor of COX-2 (COX-1 IC_{50} > 200 μM, COX-2 IC_{50} = 0.266 μM; SI = 752) than celecoxib as described in Section **3.3.1**.

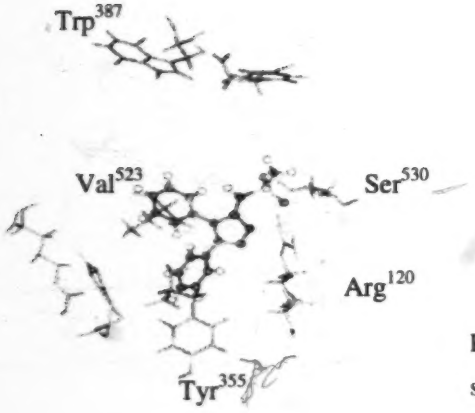

Figure **13**. Docking of isoxazole 44 (ball and stick) in the binding site of COX-2 (line and stick) ($E_{intermolecular}$ = - 45.6 Kcal/mol)

3.2.1.6 Docking of 5-(4-Methylsulphonylphenyl)-2-methyl-4-phenyl-4-isoxazoline (50h) and 2,3-Dimethyl-5-(4-methylsulphonylphenyl)-4-phenyl-4-isoxazoline (50k) in the Binding Site of COX-2.

Replacement of a planar with a non-planar central ring was reported to provide a more active COX-2 inhibitor *in vivo* [Reitz & Seibert, 1995]. It was therefore of interest to design selective COX-2 inhibitors with the less planar (more puckered) isoxazoline ring in place of the planar isoxazole central ring compounds described previously.

Docking of isoxazoline **50h** (C-3 hydrogen substituent) and **50k** (C-3 methyl substituent) in the active site of COX-2 showed similar interactions to the COX-2 active site residues in spite of the fact that intermolecular energy between isoxazoline **50h** and COX-2 was higher (-35.46 Kcal/mol) than that for the isoxazoline **50k** (-49.26 Kcal/mol). The interspacial distance between the N*C*H$_3$ substituent for isoxazoline **50h** and **50k** and the *OH* group of either Tyr^{355} or Ser^{530} was similar. However the, isoxazoline **50h** was positioned deeper in the COX-2 primary channel than **50k**, and the MeSO$_2$ group in **50k**

was inserted deeper into the secondary COX-2 pocket than that of **50h**, allowing the formation of a hydrogen bond with the backbone of Phe^{518} in the secondary pocket of COX-2 (Table **39**). An enzyme inhibition assay showed isoxazoline **50k** to be more potent selective COX-2 inhibitor (COX-1 IC_{50} = 258 μM, COX-2 IC_{50} = 0.004 μM; SI = 61, 454) than isoxazoline **50h** (COX-1 IC_{50} >100 μM, COX-2 IC_{50} = >100 μM) as shown in Section **3.3.2**.

Table **39.** Distances between Selected COX-2 Residues and 5-(4-Methylsulphonyl-phenyl)-2-methyl-4-phenyl-4-isoxazoline (**50h**) and 2,3-Dimethyl-5-(4-methylsulphonyl- phenyl)-4-phenyl-4-isoxazoline (**50k**).

50h	COX-2[a]	Distance (Å)[b]	**50k**	COX-2[a]	Distance (Å)[b]
N-*CH*$_3$	Tyr^{355} (*OH*)	11.24	N-*CH*$_3$	Tyr^{355} (*OH*)	9.55
	Arg^{120} (*CZ*)[c]	4.16		Arg^{120} (*CZ*)[c]	3.70
	Ser^{530} (*OH*)	6.20		Ser^{530} (*OH*)	8.31
B (Center)[d]	Val^{523} (*CB*)[e]	4.61	B (Center)[d]	Val^{523} (*CB*)[e]	4.20
	Phe^{518}(*CZ*)[f]	7.19		Phe^{518}(*CZ*)[f]	7.58
	Arg^{513} (*CZ*)[c]	7.16		Arg^{513} (*CZ*)[c]	7.98
A (Center)[g]	Tyr^{385} (*OH*)	10.86	A (Center)[g]	Tyr^{385} (*OH*)	10.52
	Trp^{387} (*CA*)[h]	11.83		Trp^{387} (*CA*)[h]	11.51
S[i]	His^{90} (*CE1*)[j]	4.51	*S*[i]	His^{90} (*CE1*)[j]	4.64
	Val^{523} (*CB*)[e]	4.69		Val^{523} (*CB*)[e]	6.46

[a] COX-2 active site residues with atoms involved in distance measurements in parenthesis. [b] Distance after minimization. [c] NH*C*(=NH)-NH group of arginine residue. [d] Center of the 5-(4-methylsulphonyl phenyl) ring. [e] *C*H group of valine group. [f] *C*H_2 group of phenylalanine. [g] Center of the 4-phenyl ring. [h] *C*H_2 group of tryptophane residue. [i] *S* atom of the *S*O_2CH_3 group. [k] N=*C*H-N group of histidine residue.

This latter observation could be due to a steric interaction between C-3 Me substituent and Arg^{120} that is located near the mouth of the COX-2 channel which is possible for **50k**, but not for **50h** having a C-3 H-substituent (Figure **14**).

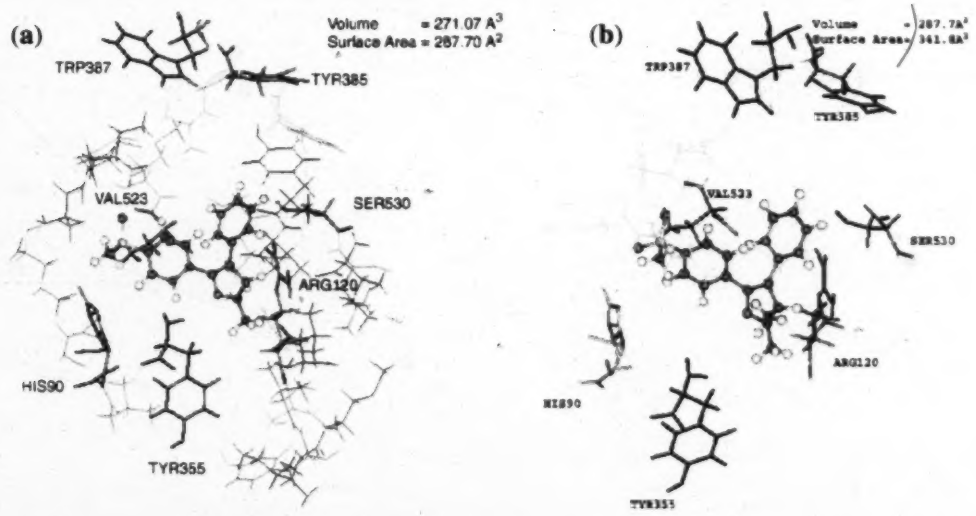

Figure **14**. Docking of (a) isoxazoline **50h** (ball and stick) ($E_{intermolecular}$ = -35.46 Kcal/mol), and (b) isoxazoline **50k** (ball and stick) ($E_{intermolecular}$ = -49.26 Kcal/mol) in the binding site of COX-2 isozyme (line and stick).

3.2.1.7 Docking of 1-(4-Azidophenyl)-3-(4-methylphenyl)-5-trifluoromethyl-pyrazole (54), 1-(4-Azidophenyl)-5-(4-methylphenyl)-3-trifluoromethyl-pyrazole (57) and 4-(4-Azidophenyl)-3-phenyl-2(5*H*)-furanone (61) in the Binding Site of COX-2.

Many selective COX-2 inhibitors that belong to the tricyclic group of compounds, have a central ring possessing a diaryl stilbene-like structure with a sulphonyl (SO_2) group at the *para*-position of one of the pendant aryl rings. The COX-2 selectivity of this group of compounds is attributed to insertion of the SO_2 moiety in the secondary pocket in COX-2, which is not present in COX-1. The secondary COX-2 pocket is attributed to

the presence of Ile^{523} in COX-1 relative to the smaller Val^{523} in COX-2 isozyme [Luong *et al.*, 1996]. Replacement of His^{513} in COX-1 by arginine Arg^{513} in COX-2 isozyme has been reported to play a key role in the hydrogen bond network of the COX-2 active site [Llorens *et al.*, 1999]. In this regard the presence of Arg^{513} residue has not been exploited for the design of selective COX-2 inhibitors.

It was therefore of interest to determine whether replacement of the SO_2Me or SO_2NH_2 pharmacophore by a dipolar azido (N_3) group would retain *in vitro* COX-2 selectivity and *in vivo* AI activity. The azido substituent is particularly attractive since it has the potential to undergo electrostatic (ion-ion) binding interactions with amino acid residues, particularly Ar^{513}, lining the secondary pocket of COX-2. Covalent azides can be viewed as resonant hybrids between structures **A**, **B** and **C** (see Figure **15**) [Lieber, 1966].

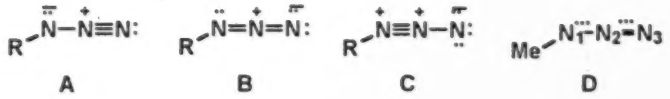

Figure 15. Azide resonance hybrid structures.

Pauling rejected **C** as a major contributor based on the *adjacent charge rule* [Pauling, 1960]. The remaining hybrids **A** and **B** predict a 2.5 bond order for the N_2-N_3 bond and a 1.5 bond order for the N_1-N_2 bond (see **D**, Figure **15**). This prediction was in very good agreement with a structure determination of methyl azide (**D**) where the bond lengths from electron diffraction studies were: N_2-N_3 = 1.12 Å, N_1-N_2 = 1.24 Å, C-N_1 = 1.47 Å and the C-N_1-N_2 bond angle was 120° [Livingston *et al.*, 1960]. The azido group is

slightly smaller in size [MR (molar refractivity) = 10.20] than a SO_2Me (MR = 13.49) or SO_2NH_2 (MR = 12.28) substituent, but more lipophilic (π = 0.46) relative to the more polar SO_2Me (π = -1.63) and SO_2NH_2 (π = -1.82) subsituents [Hansch *et al.*, 1973], which has the potential to improve absorption and provide a more rapid onset of action.

Docking of 1-(4-azidophenyl)-5-(4-methylphenyl)-3-trifluoromethylpyrazole **(57)** in the active site of human COX-2 (1CX2 PDB file) showed that the terminal *N*-atom of the azido group was inserted into the secondary COX-2 pocket about 4.52 Å from Val^{523}, and about 3.15 Å from the center of the guanidino group of Arg^{513} as illustrated in Table **40**. This orientation of the pyrazole **57**, within the COX-2 active site provides an intermolecular energy between the enzyme and pyrazole **57** of about –46.49 Kcal/mol, where the electrostatic component accounts for about 12 % of this total energy (Figure **16**).

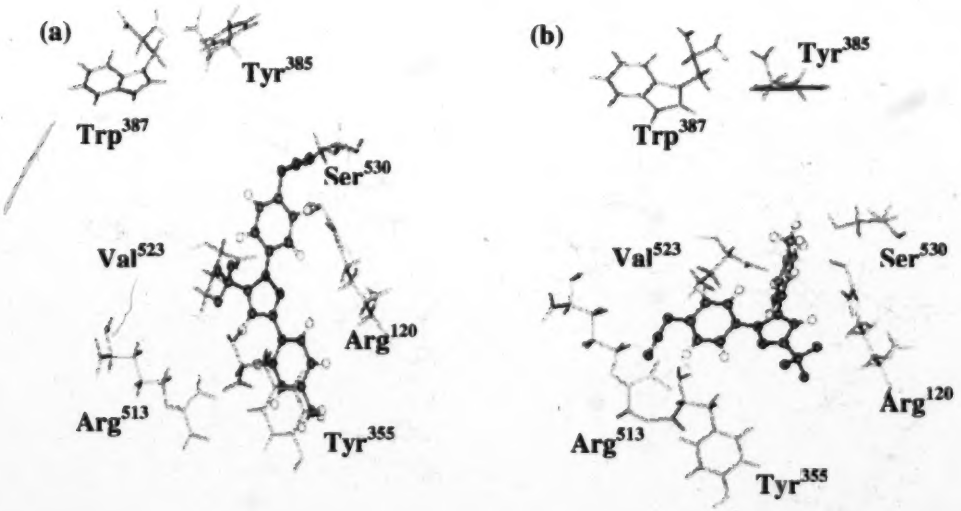

Figure **16**. Docking of (a) pyrazole **54** (ball and stick) ($E_{intermolecular}$ = -34.12 Kcal/mol), and (b) pyrazole **57** (ball and stick) ($E_{intermolecular}$ = -46.9 Kcal/mol) in the binding site of COX-2 (line and stick).

Levitt's criterion for distinguishing between hydrogen bonds and electrostatic contacts was used [Levitt, 1983]. The donor-acceptor pair with H-X distance between 1.8-2.4 Å and angle X-Y-Z between 145-210° is defined as hydrogen bond, whereas a donor acceptor distance between 2.4-3.5 Å was categorized as an electrostatic interaction.

In comparison, when celecoxib (**17**) was docked in the active site of COX-2, it showed an intermolecular energy of about –45.16 Kcal/mol where less than 3% was due to an electrostatic component (Figure **17**).

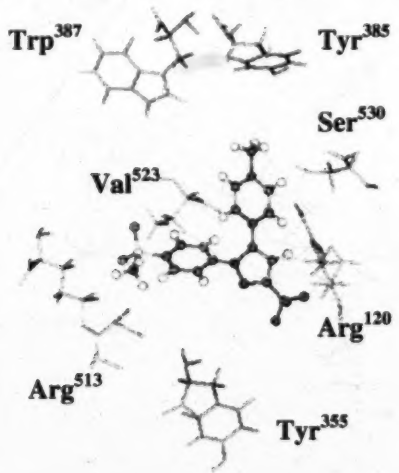

Figure **17**. Docking of celecoxib **17** (ball and stick) in the binding site of human COX-2 (line and stick) ($E_{intermolecular}$= -45.16 Kcal/mol).

This difference is likely due to a greater electrostatic interaction between the dipolar azido group in pyrazole **57** and the charged guanidino moiety of Arg^{513} in the secondary COX-2 pocket. Similar docking of the 1-(4-azidophenyl)-3-(4-methylphenyl)-5-trifluoromethylpyrazole regioisomer (**54**) in the active site of human COX-2 showed that the azido substituent did not insert into the secondary pocket since the ligand **54** extended parallel to the longitudinal axis of the hydrophobic primary COX-2 channel (cavity), in a manner characteristically observed for non-selective COX-2 inhibitors (Figure **16a**).

Table **40.** Distances between Selected COX-2 Residues and 1-(4-Azidophenyl)-3-(4-methylphenyl)-5-trifluoromethylpyrazole (**54**), 1-(4-Azidophenyl)-5-(4-methylphenyl)-3-trifluoromethylpyrazole (**57**) and 4-(4-Azidophenyl)-3-phenyl-2(5*H*)-furanone (**61**).

54	COX-2[a]	Distance (Å)[b]	**57**	COX-2[a]	Distance (Å)[b]	**61**	COX-2[a]	Distance (Å)[b]
CF_3	Tyr^{355} (*OH*)	12.25	CF_3	Tyr^{355} (*OH*)	10.26	*CO*[d]	Tyr^{355} (*OH*)	13.51
	Arg^{120} (*CZ*)[c]	7.97		Arg^{120} (*CZ*)[c]	4.23		Arg^{120} (*CZ*)[c]	3.43
	Ser^{530} (*OH*)	8.56		Ser^{530} (*OH*)	7.18		Ser^{530} (*OH*)	4.03
B (Center)[e]	Val^{523} (*CB*)[f]	6.46	B (Center)[e]	Val^{523} (*CB*)[f]	3.95	B (Center)[g]	Val^{523} (*CB*)[f]	4.11
	Phe^{518}(*CZ*)[h]	13.03		Phe^{518}(*CZ*)[h]	5.03		Phe^{518}(*CZ*)[h]	7.16
	Arg^{513} (*CZ*)[c]	8.80		Arg^{513} (*CZ*)[c]	9.61		Arg^{513} (*CZ*)[c]	7.92
A (Center)[i]	Tyr^{385} (*OH*)	10.08	A (Center)[i]	Tyr^{385} (*OH*)	6.95	A (Center)[j]	Tyr^{385} (*OH*)	8.92
	Trp^{387} (*CA*)[k]	12.06		Trp^{387} (*CA*)[k]	9.57		Trp^{387} (*CA*)[k]	13.34
N[l]	His^{90} (*CE1*)[m]	11.29	*N*[l]	His^{90} (*CE1*)[m]	4.51	*N*[l]	His^{90} (*CE1*)[m]	3.17
	Val^{523} (*CB*)[f]	10.30		Val^{523} (*CB*)[f]	4.52		Val^{523} (*CB*)[f]	4.52
	Arg^{513}(*CZ*)[c]	11.72		Arg^{513}(*CZ*)[c]	3.15		Arg^{513}(*CZ*)[c]	3.31

[a] COX-2 active site residues with atoms involved in distance measurements in parentheses. [b] Distance after minimization. [c] NHC(=NH)-NH group of arginine residue. [d] O-atom of the carbonyl moiety in the furanone structure. [e]Center of the 1-(4-sulphonamidophenyl) ring. [f] *C*H group of valine group. [g] Center of the 5-(4-methylsulphonyl phenyl) ring. [h] CH_2 group of phenylalanine. [i]Center of the 1-(4-methylphenyl) ring. [j] Center of the 4-phenyl ring. [k] CH_2 group of tryptophan residue. [l] The terminal nitrogen of the azido group. [m] N=CH-N group of histidine residue.

These results are similar to those described for other studies utilizing compounds not having a 1,2-diarylstilbene-like structure [Penning *et al.*, 1997; Talley, 1999]. These results were found to correlate with the enzyme inhibition assay observations, where pyrazole **57** was found to be more potent as selective COX-2 inhibitor (COX-1 IC_{50} > 100 μM, COX-2 IC_{50} = 1.55 μM; SI = 64.55) than pyrazole **54** (COX-1 IC_{50} = 9.88 μM, COX-2 IC_{50} = 2.63 μM; SI = 3.74).

Docking the rofecoxib analogue **61**, in which the SO_2Me moiety was replaced by an azido substituent, in the active site of human COX-2 showed a similar interaction between the azido group and the COX-2 secondary pocket amino acid residues similar to that observed for the pyrazole **57** as illustrated in Table **40**. The intermolecular energy between the ligand and the enzyme was –49.6 Kcal/mol with the electrostatic component comprising 5.8 % of the total energy (Figure **18**).

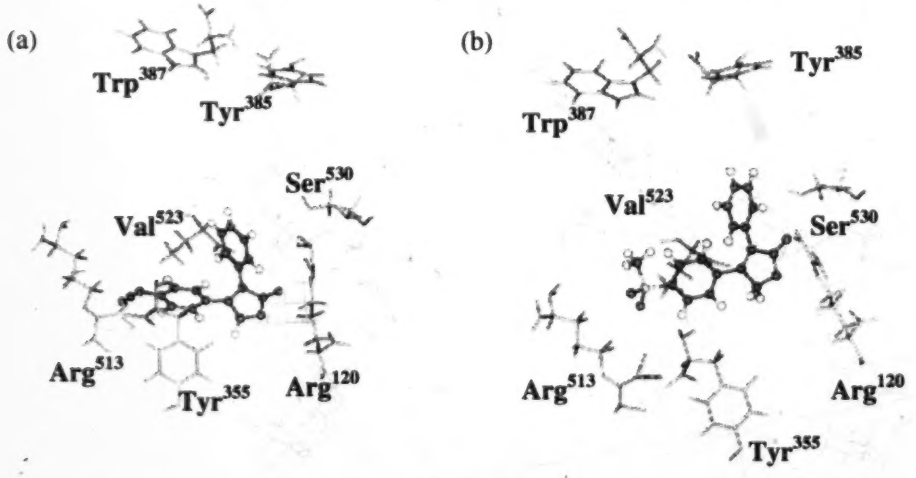

Figure **18**. Docking of (a) furanone **61** (ball and stick) in the binding site of human COX-2 (line and stick)($E_{intermolecular}$= -49.6 Kcal/mol) and (b) rofecoxib (**18**) (ball and stick) in the binding site of human COX-2 (line and stick)($E_{intermolecular}$= -42.16 Kcal/mol).

In comparison when rofecoxib (**18**) was docked in the active site of COX-2, it showed an intermolecular energy of -42.16 Kcal/mol, where only 1.2% was due to an electrostatic component (Figure **18**). The higher electrostatic component for the azido compound **61** (5.8%), relative to that for rofecoxib (**18**) (1.2%), is attributed to the fact that the $MeSO_2$ moiety present in rofecoxib undergoes hydrogen-bonding to the imidazole N*H* of His^{90} in the secondary pocket. In contrast, the azido moiety in **61** undergoes an electrostatic interaction with Arg^{513} in the secondary COX-2 pocket. The lower contribution of the electrostatic energy to the total intermolecular energy in the case of the furanone **61** relative to the pyrazole **57**, can be attributed to the observed hydrogen bonding interaction between the *O*-atom of the C=*O* in the furanone structure and residues lining the primary COX-2 channel, particularly Arg^{120}.

3.2.2 Comparative Molecular Volume Study.

Both COX-1 and COX-2 active sites consist of a long narrow channel (≅ 8 x 25 Å) extending from the outer membrane-binding motif surface through helices A, B and C to the center of both isozymes [Kurumbail *et al.*, 1996; Picot *et al.*, 1994]. The only amino acid residue lining the channel that is not conserved between COX-1 and COX-2 is at position 523 where COX-2 has valine and COX-1 has isoleucine. This difference, in addition to the Tyr^{355} conformational variability between COX-1 and COX-2, changes the size and shape of the NSAIDs binding site for COX-1 and COX-2. The COX-2 isozyme structure showed a second internal pocket extending off the NSAID binding site. In COX-2, the volume of the primary inhibitor binding site and the secondary pocket (394 Å) is about 25% larger than the COX-1 binding site (316 Å).

Accordingly, a study of the shape and size of potential COX-2 ligands is crucial to the design of selective COX-2 inhibitors. Observations from the docking study as described previously indicate that, a potential selective COX-2 inhibitor in the tricyclic group of compounds should have a central ring possessing a diaryl stilbene-like structure with a sulphonyl (SO_2) group at the *para*-position of one of the pendant aryl rings. The presence of a suitably positioned central ring substituent was found to enhance selectivity and inhibition of COX-2. Unfortunately, the position and nature of the central ring substituents could not be predicted from the docking experiments.

Consequently, a model representing the mean molecular volume of a training set of reported selective COX-2 inhibitors was developed [Penning *et al.*, 1997; Talley *et al.*, 1997; Tsuji *et al.*, 1997] (Table **41**). The training set was designed on the following basis: (a) all members of the training set should be selective COX-2 isozyme inhibitors, with IC_{50} (COX-2) lower than or equal to celecoxib with SI values higher than or equal to celecoxib; (b) All selective COX-2 inhibitors in the training set should be from the tricyclic class with a 1,2-dihetero-5-membered ring, where one of the heteroatoms, at least, is a nitrogen; (c) central ring substituents should cover a wide range of volumes; and (d) both SO_2NH_2 and SO_2CH_3 pharmacophores should be represented in the training set.

Table **41.** Structures of Azole Derivatives used as Selective COX-2 Isozyme Inhibitors Training Set.

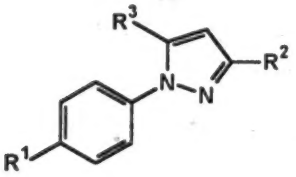

62-69

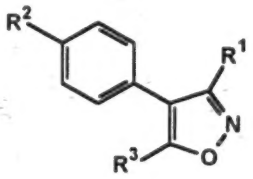

70-74

Entry	R^1	R^2	R^3
62[a]	H_2NSO_2-	-CF_3	Ph-
63[a]	H_2NSO_2-	-CF_3	2-F-Ph-
64[a]	H_2NSO_2-	-CF_3	4-F-Ph-
65[a]	H_2NSO_2-	-CF_3	2-Cl-Ph-
66[a]	H_2NSO_2-	-CF_3	4- Cl-Ph-
67[a]	H_2NSO_2-	-CF_3	2-CH_3-Ph-
68[b]	F	-CN	4- CH_3SO_2-Ph-
69[b]	CH_3SO_2-	-CF_3	4-F-Ph-
70[c]	Ph-	H_2NSO_2-	-CH_3
71[c]	Ph-	H_2NSO_2-	-$C(CH_3)_3$
72[c]	Ph-	H_2NSO_2-	-CHF_2
73[c]	CH_3-	CH_3SO_2-	-Ph
74[c]	C_2H_5	CH_3SO_2-	-Ph

[a] [Penning et al., 1997], [b] [Tsuji et al., 1997], [a] [Talley et al., 1997].

The difference, between the molecular volume of the non-selective COX isozyme inhibitor **32m** and the mean molecular volume of the selective COX-2 training set, overlaid on the molecular structure of isoxaozle **32m**, is expected to indicate the size, shape and position of central ring substituents needed to enhance COX-2 inhibition (Figure **19**).

Figure **19**. Comparative molecular volume study for isoxazole **32m.**

Upon inspection of Figure **19,** it could be observed that **32m** (molecular volume = 249.7 $Å^3$) differed from the structures of selective COX-2 in the training set in three areas. The first difference was localized around the 3-position of the isoxazole ring, with a volume of 95-123 $Å^3$ that is planar in shape. The best candidate to provide these properties is a 4-methylsulphonylphenyl moiety. The second difference in volume between the model and isoxazole **32m** was in the area above and below the phenyl ring at 4-position of the isoxazole ring. This difference can be attributed to a difference in the dihedral angle between the various central ring heterocycles included in the training set such as pyrazoles and isoxazoles. The last, but not the least important, difference is the substituent at the 5-position of the isoxazole ring, where it was supposed to occupy a volume of 25-38 $Å^3$. One suitable substituent choice that could be in agreement with this observation is a methyl group. It was shown in Section **3.2.1.1** and **3.2.1.3** that a central ring substituent in COX-2 selective inhibitors is expected to play a role in disrupting the hydrogen bond network at the entrance of the COX-2 isozyme. Consequently, a CF_3 group may be a better substituent choice at the 5-position in the isoxazole ring. These

results were found to correlate closely with docking study observations and enzyme inhibition studies data described in Sections **3.2.1.3-3.2.1.4** and **3.3.1**, respectively.

In a similar study, the volume of isoxazoline **50h** was compared to the mean molecular volume of the selective COX-2 inhibitor training set shown in Table **41**. The molecular volume of isoxazoline **50h** differed from that of the training set in three areas, the first two were at C-4 and C-5 of the isoxazoles, where the difference in volume was in the area above and below the phenyl rings at these positions. These differences were attributed to the differences in the dihedral angles between the various central ring heterocycles included in the training set. The molecular volume of isoxazoline **50h** was also found to lack one moiety with a volume of 22-30 $Å^3$ at the 3-position of the isoxazoline ring (Figure **20**). This model was used to design isoxazoline **50k** with a central ring 3-Me substituent. These results confirmed the observations from the docking experiments for both isoxazolines **50h** and **50k** and enzyme inhibition assay results in Sections **3.2.1.6** and **3.3.2**, respectively.

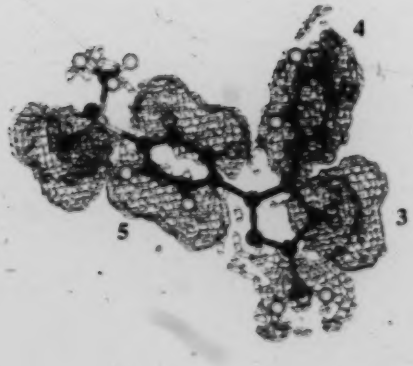

Figure **20**. Comparative molecular volume study for isoxazoline **50h**.

These models can be considered as a local template, in the sense that it describes the structure-property relationship of a series of congeners and, consequently, it has no general applicability to other classes of COX-2 inhibitors, which differ in size of the central ring or which have different pharmacophoric requirements [Marshall, 1993].

3.3 Structure-Activity Relationships (SARs).

3.3.1 Antiinflammatory and Analgesic Activity, and COX-2 Selective Inhibition by Isoxazoles 32a-p, 36, 42, 44 and 48.

A group of 4,5-diarylisoxazoles **32a-p** was prepared to determine the effect of H, F, MeS, MeSO, or $MeSO_2$ substituents at the *para*-position of one of the aryl rings upon AI and analgesic activity and COX-2 selective inhibition.

Comparison of the AI activities for regioisomeric compounds at 3 hours post drug administration (Table **42**) showed that the *para*-phenyl substituents (R^1, R^2) are determinants of AI activity for compounds **32a-p**. Accordingly, **32c** (R^1 = F) > **32b** (R^2 = F) and **32n** (R^1 = $MeSO_2$) > **32m** (R^2 = $MeSO_2$), but **32e** (R^2 = MeS) > **32f** (R^1 = MeS). These data are consistent with the observations that the relative activity profiles are **32g** (R^1 = F, R^2 = MeS) > **32h** (R^1 = MeS, R^2 = F) and **32p** (R^1 = $MeSO_2$, R^2 = F) > **32o** (R^1 = F, R^2 = $MeSO_2$). It is well documented that *para*-phenyl substituents in isomeric compounds can dramatically alter COX-2 isozyme selectivity and potency [Khanna *et al.*, 1997; Carter *et al.*, 1999]. Compounds having R^1 or R^2 = F, $MeSO_2$ and MeS as *para*-phenyl substituents exhibited the most potent AI activity, where the AI potency order for the C-4 phenyl *para*-R^1-substituents was F (**32c**) > $MeSO_2$ (**32n**) > MeS (**32f**) > MeSO (**32j**) > H (**32a**), and for the C-5 phenyl *para*-R^2-substituents was MeS (**32e**) > F (**32b**) > $MeSO_2$ (**32m**) > MeSO (**32i**) > H (**32a**). One of the most potent compounds, among the

group of compounds **32a-p**, 5-(4-methylthiophenyl)-4-phenylisoxazole (**32e**, $ID_{50} \approx 5$ mg/kg) exhibited more potent AI activity than celecoxib (ID_{50} = 10.8 mg/kg) at 3 hours post-drug administration. Although the 4,5-diarylisoxazole group of compounds **32a-p** exhibited potent AI activity, the *para*-fluorophenyl regioisomers (**32b-c**), and 4-phenyl-5-(4-methylsulphonylphenyl)isoxazole (**32m**), were more selective for COX-1 than COX-2 (Table **41**). In contrast, 4-(4-methylsulphonylphenyl)-5-phenylisoxazole (**32n**) showed a modest COX-2 selectivity of 2.1.

Docking of the selective COX-2 inhibitor SC-588 (**19**), and isoxazole **36** showed that a small lipophilic central ring substituent is a requirement for COX-2 selectivity as shown in Sections **3.2.1.1** and **3.2.1.3**. This latter observation is consistent with the high COX-2 selectivity index (SI) for isoxazole **36** (SI = 500,000) relative to **32n** (SI = 2.1). A comparison of the COX-2 selectivity for the regioisomers **36** (SI = 500,000) and **42** (SI = 1122) shows that the specific C-4 or C-5 aryl ring to which the $MeSO_2$ substituent is attached is an important determinant of COX-2 selectivity. Similarly, the 3-(4-methylsulphonylphenyl) compound **36** was a more potent AI agent than the 4-(4-methylsulphonylphenyl) regioisomer **42**.

The C-3 $NHSO_2Me$ central ring substituent present in 4,5-diphenyl-3-methylsulfonamidoisoxazole (**44**, SI = 752), like the C-5 CF_3 substituent present in **36**, confers COX-2 selectivity. In contrast, 3-amino-4,5-diphenylisoxazole (**43**), having a C-3 NH_2 substituent, was an inactive COX-1/COX-2 inhibitor (IC_{50} > 200 μM for both COX-1 and COX-2). The 3-methylsulfonamido compound **44** exhibited good AI activity (35 and 30% inhibition at 3 and 5 hours, respectively for a 10 mg/kg ip dose).

Incorporating a C-3 CH_3 group in 4,5-diarylisoxazoles **48a-b** showed more potent AI activity when compared to the isoxazole **32o** which lacks a C-3 CH_3 substituent. Unfortunately, isoxazoles **48a-b** were inactive as COX-1/COX-2 inhibitors (IC_{50} > 100 μM for both COX-1 and COX-2). This enzyme inhibition profile was expected as shown from the docking and comparative molecular volume studies shown in sections **3.2.1.4** and **3.2.2**, respectively.

Analgesic activity was determined using the 4% NaCl-induced writhing assay [Fukawa *et al.*, 1980; Buolamwuini & Knaus, 1990] and the results are listed in Table **42.** Compounds **32a-p** are effective analgesic agents that inhibited writhing 24-89% at 30 minutes, and 34-90% at 60 minutes, post-drug administration relative to the reference drug celecoxib that inhibited writhing by 32% and 62% at 30 and 60 minutes, respectively for a 50 mg/kg intraperitoneal (ip) dose. 3,4-Diarylisoxazole regioisomers possessing a C-5 CF_3 substituent (**36**, **42**) exhibited potent analgesic activity at a 10 mg/kg ip dose that was superior to related compounds not having a central ring CF_3 substituent (**32m**, **32n**) at a 50 mg/kg ip dose. Similarly, the 4,5-diarylisoxazole with a C-3 methysulfonamido substituent (**44**) showed more potent analgesic activity at a 10 mg/kg ip dose than 4,5-diphenylisoxazole (**32a**) at a 50 mg/kg ip dose. 4,5-Diarylisoxazole regioisomers possessing a C-3 CH_3 substituent (**48a**, **48b**) exhibited potent analgesic activity relative to isoxazole **32o** that does not have a C-3 CH_3 substituent.

In summary, the results of AI and analgesic activity, and COX-2 selectivity of isoxazoles **32a-p**, **36**, **42**, **44** and **48** showed that (1) incorporating a central isoxazole ring substituent such as C-5 CF_3 substituent provided a useful drug design concept to orient

the central isoxazole ring in the primary COX-2 binding site such that the *para*-SO_2Me substituent on a phenyl ring is suitably positioned for insertion into the COX-2 secondary pocket; (2) introduction of C-3 CH_3 group caused the loss of selectivity and inhibition of COX-2 enzyme; (3) a larger drug molecular volume ($Å^3$) closer to the molecular volume of the larger COX-2 binding site (394 $Å^3$) enhanced COX-2 selectivity; and (4) molecular modeling provided a complementary drug design technique for optimization of COX-2 selectivity.

Table 42. Antiinflammatory and Analgesic Activities, *In Vitro* COX-1 and COX-2 Inhibition Data, and Molecular Volumes of, the Diarylisoxazoles (**32a-p**, **36**, **42**, **44** and **48**).

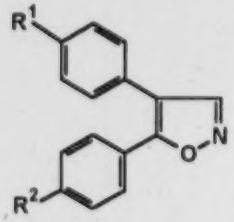

32

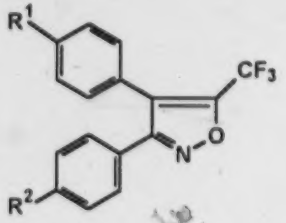

36, 42

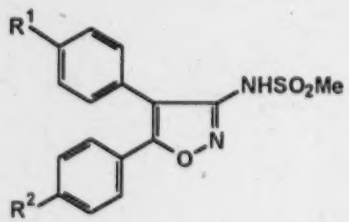

44

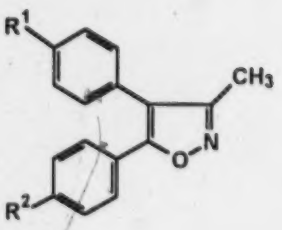

48

Cmpd	R^1	R^2	Antiinflammatory Activity.[a] % Inhibit. at 3 hours	Antiinflammatory Activity.[a] % Inhibit. at 5 hours	Analgesic Activity.[b] % Inhibit. at 30 min	Analgesic Activity.[b] % Inhibit. at 60 min	Volume ($Å^3$)[c]	IC_{50} (μM)[d] COX-1	IC_{50} (μM)[d] COX-2	Selectivity Index[e] (COX-1 /COX-2)
32a	H	H	9.2 ± 3.6	12.3 ± 2.5	54.8 ± 9.9	65.6 ± 0.6	203.2	—	—	—
32b	H	F	45.4 ± 6.7	39.7 ± 7.9	62.5 ± 6.5	63.7 ± 12.6	208.4	2.1	2.4	0.87
32c	F	H	80.7 ± 1.4[f]	61.4 ± 3.9	51.3 ± 15.4	82.4 ± 3.3	207.3	1.7	2.3	0.74
32d	F	F	59.1 ±11.4[g]	30.3 ± 11.9	62.5 ± 21.2	71.3 ± 9.3	211.5	—	—	—
32e	H	SMe	75.8 ± 3.4[h]	46.6 ± 2.1	62.5 ± 4.4	68.7 ± 5.4	238.2	—	—	—
32f	SMe	H	54.2 ± 1.1[i]	33.2 ± 1.8	47.5 ± 7.7	50.4 ± 18.6	238.4	—	—	—
32g	F	SMe	52.4 ± 5.4	6.1 ± 4.8	57.8 ± 7.2	50.4 ± 4.2	242.5	—	—	—
32h	SMe	F	26.5 ± 2.7	30.5 ± 4.2	76.5 ± 7.1	51.8 ± 10.3	242.4	—	—	—

(continued)

Cmpd	R^1	R^2	Antiinflammatory Activiyt.[a]		Analgesic Activity.[b]		Volume ($Å^3$)[c]	IC_{50} (μM)[d]		Selectivity Index[e]
			% Inhibit. at 3 hours	% Inhibit. at 5 hours	% Inhibit. at 30 min	% Inhibit. at 60 min		COX-1	COX-2	(COX-1/COX-2)
32i	H	SOMe	18.8 ± 0.4	18.5 ± 4.1	58.8 ± 15.8	90.2 ± 3.7	242.1	—	—	—
32j	SOMe	H	19.1 ± 5.0	Inactive	88.9 ± 7.8	65.2 ± 8.7	242.0	—	—	—
32k	F	SOMe	-0.4 ± 4.1	8.0 ± 3.1	58.5 ± 9.4	83.9 ± 2.5	246.6	—	—	—
32l	SOMe	F	15.8 ± 4.3	7.8 ± 7.8	71.3 ± 6.1	86.2 ± 2.1	246.2	—	—	—
32m	H	SO_2Me	39.7 ± 4.8	14.9 ± 1.7	36.7 ± 11.4	50.7 ± 15.8	253.8	2.7	227.3	0.012
32n	SO_2Me	H	61.7 ± 6.3	47.9 ± 2.5	57.8 ± 4.1	64.6 ± 8.2	249.7	55.7	26.3	2.1
32o	F	SO_2Me	17.1 ± 2.8	13.2 ± 1.7	32.8 ± 4.8	59.1 ± 5.6	253.8	—	—	—
32p	SO_2Me	F	39.5 ± 4.9	15.5 ± 5.3	24.1 ± 13.7	33.9 ± 12.5	253.8	—	—	—
36	SO_2Me	H	39.9 ± 12.0[j]	34.0 ± 6.3[j]	76.9 ± 7.3[k]	74.8 ± 8.7[k]	277.4	> 500	< 0.001	500,000
42	H	SO_2Me	16.5 ± 7.3[j]	25.0 ± 9.3[j]	74.3 ± 9.3[k]	73.8 ± 8.7[k]	278.2	251.6	0.2336	1,122
44	H	H	35.0 ± 11.2[j]	29.6 ±11.0[j]	70.6 ± 3.6[k]	70.4 ± 7.3[k]	259.3	> 200	0.266	752
48a	F	SO_2Me	56.4 ± 5.5[l]	16.9 ± 2.4	59.7 ± 9.91	63.8 ± 13.6	270.1	>100	>100	
48b	Me	SO_2Me	36.8 ± 2.9	1.90 ± 4.3	45.4 ± 5.28	64.2 ± 5.2	283.5	>100	>100	
Ibuprofen			43.8 ± 2.8[m]	51.7 ± 3.6[m]	—	—	212.0	—	—	—
Celecoxib			79.9 ± 1.9[n]	58.2 ± 1.8[o]	31.7 ± 9.6	62.0 ± 7.3	298.4	22.9	0.0567	404

[a] Inhibitory activity on carrageenan-induced rat paw edema; the result is the mean value ± SEM using four animals following a 50 mg/kg (**32a-p, 48a-b**), or 10 mg/kg (**36**, **42**, **44**), oral dose of the test compound. [b] Inhibitory activity in the rat 4% NaCl-induced abdominal constriction assay; the result is the mean value ± SEM using four animals following a 50 mg/kg (**32a-p, 48a-b**), or 10 mg/kg (**36**, **42**, **44**), intraperitoneal dose of the test compound. [c] The volume of the molecule, after minimization using the MM3 force field, was calculated using the Alchemy 2000 program. [d] The *in vitro* test compound concentration (μM) required to produce 50% inhibition of COX-1 or COX-2. The result is the mean of two determinations. Standard error was less than 10%. [e] Selectivity Index = IC_{50} for COX-1/ IC_{50} for COX-2. [f] ID_{50} = 17.6 mg/kg po dose. [g] ID_{50} = 17.3 mg/kg po dose. [h] ID_{50} is close to 5 mg/kg po since a 5 mg/kg po dose gave a 53% inhibition at 3 hours. [i] ID_{50} = 42.85 mg/kg po dose. [j] 10 mg/kg po dose. ED_{50} values could not be determined for compounds **36** and **42** since they were toxic to rats at a dose 10 and 50 mg/kg po, respectively. Compound **44** inhibited inflammation by 41.3% at 3 hours for a 100 mg/kg po dose. [k] 10 mg/kg ip dose. [l] ID_{50} = 49.07 mg/kg po dose. [m] 100 mg/kg po dose. [n] ID_{50} = 10.8 mg/kg po dose. [o] ID_{50} = 40.8 mg/kg po dose.

3.3.2 Antiinflammatory and Analgesic Activity, and COX-2 Selective Inhibition by Isoxazolines 50a-k.

A group of 4,5-diphenyl-4-isoxazolines **50a-k** were prepared to investigate the effect of a H, F, MeS or $MeSO_2$ substituent (R^1, R^2) at the *para*-position of one of the pendant phenyl rings, in conjunction with a C-3 substituent (R^1= H or Me), upon AI and analgesic activity and COX-2 selectivity (Table **43**).

Comparison of the AI activities for **50a-i** at three hours post drug administration, determined using the carrageenan-induced rat paw edema assay, shows that the nature (H, F, MeS, $MeSO_2$) and regioisomeric location of these substituents on either the C-4 or C-5 phenyl ring (R^1 or R^2) were determinants of activity. In this regard, the relative AI activity profile for compounds having a C-4 phenyl ring (R^1= H) with respect to the C-5 *para*-phenyl ring substituent (R^2) was F (**50a**) > SMe (**50d**) > $MeSO_2$ (**50h**). A similar comparison for compounds having a C-5 phenyl substituent (R^2= H) with respect to the C-4 *para*-phenyl substituent (R^1) showed the relative AI potency order is F (**50b**) > $MeSO_2$ (**50j**) > inactive SMe (**50e**). The location of specific substituents at the *para*-position of the phenyl ring for C-4 and C-5 regioisomers was also a determinant of AI activity where the relative potency order was **50a** (R^2 = F) > **50b** (R^1 = F) > **50d** (R^2 = SMe) > **50e** (R^1 = SMe). In contrast, the two regioisomers **50h** (R^1 = H, R^2 = SO_2Me) and **50i** (R^1 = SO_2Me, R^2 = H) were approximately equipotent AI agents. When two substituents (F, SMe), other than hydrogen, were present at the *para*-position of the phenyl rings, the regioisomer **50f** (R^2 = SMe) provided superior AI activity relative to the regioisomer **50g** (R^1 = SMe). These differences in potency for regioisomers are consistent with previous observations that *para*-phenyl substituents in regioisomeric compounds can

dramatically alter COX-2 selectivity and inhibitory potency as was shown in the isoxazole series [Khanna *et al.*, 1997; Carter *et al.*, 1999].

Although certain isoxazolines (**50a-b**) exhibited potent AI activity, no selectivity for inhibition of COX-2 was observed (Table **43**). In the tricyclic class of selective COX-2 inhibitors, as was shown in the isoxazole series, a central ring substituent may more favorably orient the ligand within the COX-2 binding site to enhance COX-2 selectivity. Therefore, the isoxazolines **50j** and **50k**, that possess an additional C-3 Me substituent were prepared to determine the effect of a C-3 Me substituent on COX-2 selectivity [Puig *et al.*, 2000]. Docking of isoxazolines **50h** having C-3 H substituent and **50k** having a C-3 Me substituent, on the binding site of the human COX-2 isozyme showed that the C-3 Me was essential for deep insertion of the $MeSO_2$ group in **50k** into the secondary COX-2 pocket to form a hydrogen bond with the Phe^{518} back bone as shown in Figure **14** in Section **3.2.16**. This latter observation is consistent with the potent inhibition of COX-2 (IC_{50} = 0.0042 μM) exhibited by **50k** and its high COX-2 selectivity index (SI = 61,454) relative to **50h**, which showed minimal or no inhibition of either COX-1 or COX-2 (IC_{50} > 100 μM) as shown in Table **43**.

Like **50k**, the C-3 Me analog **50j** also exhibited potent COX-2 inhibition (IC_{50} = 0.0316 μM) and selectivity (SI = 3162). The molecular volume of the selective COX-2 inhibitors **50j** (291.5 $Å^3$) and **50k** (287.5 $Å^3$), which is larger than that for isoxazolines **50a-i**, not possessing a C-3 Me substituent (230-271 $Å^3$ range), is similar to that of the selective COX-2 inhibitor, celecoxib (298.4 $Å^3$) but larger than that for ibuprofen (212.0 $Å^3$). A comparison of COX-2 isozyme inhibitory efficacies indicates that **50k** having a C-3 Me substituent attached to a sp^3 hybridized carbon on the less planar (more puckered)

4-isoxazoline central ring is a significantly more potent and selective inhibitor of COX-2 than the structurally related isoxazole analog **48a** having a C-3 Me substituent attached to an sp^2 hybridized carbon on the planar isoxazole ring. The distinct difference in COX-2 inhibitory potency and selectivity between **48a** and **50j** could be due to a number of factors that include differences in the conformation of the central heterocyclic ring, the orientation of the C-3 Me substituent and the smaller molecular volume of **48a** relative to **50j**. Furthermore, the C-3 Me compounds **50j** (ID_{50} = 41.5 mg/kg po dose) and **50k** (ID_{50} = 49.0 mg/kg po dose) also exhibited good AI activity, relative to the COX-2 selective inhibitor celecoxib (ID_{50} = 10.8 mg/kg po dose at 3 hours, or ID_{50} = 40.8 mg/kg po dose at 5 hours post drug administration).

The relative analgesic activity profile for isoxazolines **50a-k** generally followed a similar potency order to that observed for AI activity with the exception of isoxazolines **50e** and **50g** (R^1 = MeS), which exhibited significantly more potent analgesic activity.

In summary, the results of AI and analgesic activity and COX-2 selectivity data for isoxazolines **50a-k** showed that (i) incorporating a central ring C-3 Me substituent provided a useful drug design concept to orient the central isoxazoline ring in the primary COX-2 binding site such that the *para*-SO_2Me on the C-5 phenyl ring is suitably positioned for deep insertion into the COX-2 secondary pocket; (ii) a larger drug molecular volume ($Å^3$) closer to the volume of the larger COX-2 binding site (394 $Å^3$) enhanced COX-2 selectivity; and (iii) molecular modeling studies provided a complementary technique to optimize COX-2 selectivity.

Table 43. Antiinflammatory and Analgesic activities, *In Vitro* COX-1 and COX-2 Inhibition data, and Molecular Volumes of 4,5-Diarylisoxazolines **(50).**

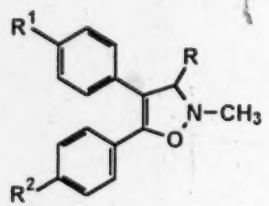

50

Cmpd	R	R^1	R^2	AI Activity[a] % Inhibit. at 3 hours	AI Activity[a] % Inhibit. at 5 hours	Analgesic Activity[b] % Inhibit. at 30 min.	Analgesic Activity[b] % Inhibit. at 60 min.	Volume ($Å^3$)[c]	IC_{50} (μM)[d] COX-1	IC_{50} (μM)[d] COX-2	Selectivity Index[e] (COX-1 /COX-2)
50a	H	H	F	86.2 ± 4.3	70.3 ± 3.5	72.4 ± 3.0	62.0 ± 2.3	230.0	2.64	4.96	0.53
50b	H	F	H	63.6 ± 6.5	51.2 ± 3.5	71.0 ± 13.5	88.6 ± 4.9	229.8	5.86	5.38	1.08
50c	H	F	F	71.0 ± 5.1	48.7 ± 3.3	69.0 ± 12.7	52.1 ± 2.0	233.8	—	—	—
50d	H	H	SMe	67.1 ± 1.9	40.5 ± 5.8	36.4 ± 8.5	48.4 ± 7.5	260.7	—	—	—
50e	H	SMe	H	-3.2 ± 6.2	15.0 ± 5.4	82.2 ± 4.3	92.4 ± 0.6	260.3	—	—	—
50f	H	F	SMe	53.0 ± 3.3	26.0 ± 19.4	53.0 ± 6.9	45.1 ± 6.4	264.9	—	—	—
50g	H	SMe	F	-1.5 ± 2.9	12.3 ± 3.3	75.4 ± 7.8	77.9 ± 6.6	264.5	—	—	—
50h	H	H	SO_2Me	7.5 ± 8.2	8.5 ± 7.8	57.9 ± 13.0	82.2 ± 0.9	271.7	>100	>100	—

(continued)

Cmpd	R	R^1	R^2	AI Activity[a]		Analgesic Activity[b]		Volume ($Å^3$)[c]	IC_{50} (μM)[d]		Selectivity Index[e]
				% Inhibit. at 3 hours	% Inhibit. at 5 hours	% Inhibit. at 30 min.	% Inhibit. at 60 min.		COX-1	COX-2	(COX-1 /COX-2)
50i	H	SO_2Me	H	9.9 ± 4.5	2.00 ± 9.0	35.7 ± 6.6	38.8 ± 2.0	271.9	5.86	5.38	1.089
50j	Me	F	SO_2Me	59.7 ± 3.0[f]	69.4 ± 8.9	59.8 ± 3.0	69.4 ± 8.9	291.5	>100	0.0316	3162
50k	Me	H	SO_2Me	50.3 ± 2.5[g]	48.1 ±1.5	84.1 ± 1.2	66.9 ± 7.6	287.7	258.11	0.0042	61, 454

[a]Inhibitory activity on carrageenan-induced rat paw edema; the result is the mean value ± SEM using four animals following a 50 mg/kg oral dose of the test compound. [b]Inhibitory activity in the rat 4% NaCl-induced abdominal constriction assay; the result is the mean value ± SEM using four animals following a 50 mg/kg intraparitoneal dose of the test compound. [c]The volume of the molecule, after minimization using the MM3 force field, was calculated using the Alchemy 2000 program. [d]The *in vitro* test compound concentration (μM) required to produce 50% inhibition of COX-1 or COX-2. The result is the mean of two determinations. Standard error was less than 10%. [e] Selectivity Index = IC_{50} for COX-1/ IC_{50} for COX-2. [f] ID_{50}= 41.50 mg/kg po dose. [g] ID_{50} = 44.0 mg/kg po dose.

3.3.3 Antiinflammatory and Analgesic Activity, and COX-2 Selective Inhibition by Celecoxib (53, 57) and Rofecoxib (61) Azido Analogues.

Celecoxib and rofecoxib analogues, having an azido group in place of the respective SO_2NH_2 and SO_2Me pharmacophores, were investigated to determine whether the azido substituent is a suitable bioisostere with respect to selective COX-2 inhibition, and AI and analgesic activities.

Structure-activity studies for the tricyclic class of selective COX-2 inhibitors have shown that a SO_2Me or SO_2NH_2 substituent at the *para*-position of one aryl ring usually confers optimal COX-2 inhibitory potency [Khanna *et al.*, 1997]. In the 1,2-diarylcyclopentene class of compounds, replacement of SO_2Me by SO_2CF_3, COMe, PO(OH)Me, CO_2H, or $PO(OH)_2$ abolished COX-2 inhibitory activity [Li *et al.*, 1995]. A similar replacement of SO_2Me by NO_2, which can dispose a pair of oxygen atoms like SO_2, in the 1,5-diarylpyrazole class also abolished COX-2 inhibitory activity [Penning *et al.*, 1997]. The azido group was expected to be a good choice for replacement of the SO_2 pharmacophore while retaining COX-2 inhibitory activity as discussed in Sections **3.1.5** and **3.2.1.7**.

The celecoxib azido analogue **(57)** showed selective inhibition of COX-2 (COX-1 $IC_{50} > 100$ μM; COX-2 $IC_{50} = 1.5$ μM; SI ≅ 64) whereas, the 1,3-regoisomer **(54)** showed a modest COX-2 selectivity (SI ≅ 4). These results are similar to those described by other studies utilizing compounds that do not have a 1,2-diarylstilbene-like structure [Penning *et al.*, 1997; Talley, 1999]. In a similar manner the azido analogue of rofecoxib **(61)** exhibited a potent and selective inhibition of COX-2 (COX-1 $IC_{50} = 159.7$ μM; COX-2 $IC_{50} = 0.196$ μM; SI ≅ 812) (Table **44**).

Table 44. Antiinflammatory and Analgesic Activities, *In Vitro* COX-1 and COX-2 Inhibition Data, and Molecular Volumes of 1-(4-Azidophenyl)-3-(4-methylphenyl)-5-trifluoromethylpyrazole (**54**), 1-(4-Azidophenyl)-5-(4-methylphenyl)-3-trifluoromethylpyrazole (**57**), and 4-(4-Azidophenyl)-3-phenyl-2(5*H*)-furanone (**61**).

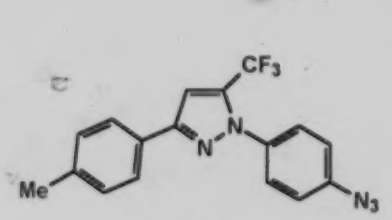

54

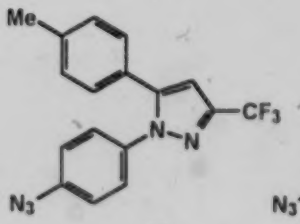

57

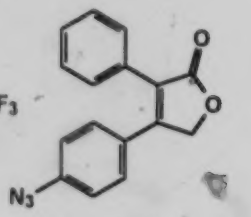

61

Compd	AI Activity [a]		Analgesic Activity [b]		Volume ($Å^3$) [c]	IC_{50}, μM [d]		Selectivity Index [e]
	% Inhibit. at 3 hours	% Inhibit. at 5 hours	% Inhibit. at 30 min	% Inhibit. at 60 min		COX-1	COX-2	(COX-1/COX-2)
54	———	———	———	———	278.3	9.88	2.63	3.74
57	46.6 ± 4.4	16.9 ± 2.7	60.9 ± 9.4	63.1 ± 1.2	279.4	> 100	1.55	64.55
61	42.9 ± 1.0	27.5 ± 4.6	46.7 ± 1.3	60.6 ± 1.6	242.1	159.72	0.196	812.4

[a]Inhibitory activity on carrageenan-induced rat paw edema; the result is the mean value ± SEM using four animals following a 50 mg/kg oral dose of the test compound. [b]Inhibitory activity in the rat 4% NaCl-induced abdominal constriction assay; the result is the mean value ± SEM using four animals following a 50 mg/kg intraperitoneal dose of the test compound. [c]The volume of the molecule, after minimization using the MM3 force field, was calculated using the Alchemy 2000 program. [d]The *in vitro* test compound concentration (μM) required to produce 50% inhibition of COX-1 or COX-2. The result (IC_{50}, μM) is the mean of two determinations. [e]Selectivity Index = IC_{50} for COX-1/ IC_{50} for COX-2.

The *in vitro* enzyme inhibition data was found to correlate well with the molecular modeling observations discussed in Section **3.2.1.7**. The azido analogues of celecoxib (**57**) and rofecoxib (**61**) exhibited good oral AI activity, inhibiting inflammation by 46.7% and 42.9 %, respectively at 3 hours post drug administration in a carrageenan induced rat paw edema assay. Compounds **57** and **61** also exhibited potent analgesic activities using a 50 mg/kg ip dose in the abdominal constriction model (Table **44**).

In summary, the AI, analgesic and COX-2 selectivity data for compounds **57** and **61** showed that (i) replacing the SO_2NH_2 and SO_2Me pharmacophore present in celecoxib and rofecoxib by an azido bioisostere retained COX-2 selective inhibition; (ii) molecular modeling studies provided a complementary technique to optimize COX-2 selectivity, and (iii) compounds **57** and **61** exhibited good oral AI and analgesic activities.

3.4 Quantitative Structure Activity Relationships (QSARs).

QSAR is a useful tool for optimizing the potency of a new lead compound. In the lead compound optimization phase of a synthetic project, various QSAR procedures with the aid of computer technology have been proposed. For example, the classical Hansch approach has been widely used in many successful studies that also include NSAIDs' AI and enzyme inhibition assays [Hadjpavlou-Litina, 2000]. The quantitative correlation of structure with AI activity of 2-arylindandiones was among the earliest QSAR studies for NSAIDs in the literature [Van de Berg *et al.*, 1975]. Before the isolation and characterization of COX isozymes, most QSAR studies for NSAIDs depended on 5-LO inhibition [Matsuda *et al.*, 1967], *in vivo* AI activity [Tanaka *et al.*, 1977] and the uncoupling of oxidative phosphorylation in hepatic and cardiac mitochondria [Terada *et*

al., 1974; Nakawa *et al.*, 1972]. Moreover, QSARs played an important role in the commercialization of Flobufen (**75**) [Fujita, 1997].

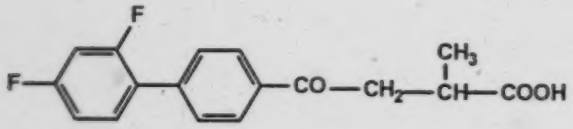

Flubofen (**75**)

In spite of the success of QSAR studies using *in vivo* data, this method is limited by the assumption that all NSAIDs in a data set have similar oral pharmacokinetic properties, which is not true in many cases.

It was therefore of interest, as part of our ongoing program to design and synthesize selective COX-2 inhibitors, to acquire quantitative structure activity correlations for isoxazoles **32b-c**, **32m-n**, **36**, **42**, **44**, and **48a-b** and isoxazolines **50a-b** and **50h-k**. QSAR studies mentioned in this section are based on the parameters listed in Table **45**.

Table **45**: Parameters used in QSAR studies.

Parameter	Description
$E_{intermol.}$	Intermolecular energy between ligand and receptor deduced from the docking experiments, as presented in Table **46**.
Log P	The logarithm (base 10) of the octanol-water partition coefficient, P.
Dipole	Dipole Moment.
MaxQ+	The largest positive charge over the atoms in a molecule.
MaxQ-	The largest negative charge over the atoms in a molecule.

(continued)

Parameter	Description
ABSQ	The sum of absolute values of the charges on each atom of the molecule, in electrons.
ABSQon	The sum of absolute values of the charges on the nitrogens and oxygens in the molecule, in electrons.
Mol. Weight	Molecular weight of a molecule.
Volume	The molecular volume of a molecule computed by the grid method of Boder [Boder *et al.*, 1989].
Polar	Molecular polarizability based on the additive approach given by Miller [Miller, 1990].
Sp. Pol.	Specific polarizability (Polar/Volume) of a molecule.
X1	First order molecular connectivity index [Kier & Hall, 1986; Katritzky *et al.*, 1993].
X3	Third order molecular connectivity index [Kier & Hall, 1986; Katritzky *et al.*, 1993].
XV0	Zero order valence connectivity index computed over all vertices (atoms) in the entire molecule [Kier & Hall, 1986; Katritzky *et al.*, 1993].
XV1	First order valence connectivity index over all edges (bonds) for the entire molecule.
Ka3	Kappa Alpha 3, a third order shape index for molecules.
Wien I.	Wiener Index, a topological parameter formulated by Wiener [Wiener, 1947].

Table 46. Enzyme inhibition (IC_{50}) and intermolecular energy ($E_{intermolecular}$) of isoxazoles **32b-c**, **32m-n**. **36**, **42**, **44** and **48a-b**, and isoxazolines **50a-b** and **50h-k**.

Compd	IC_{50} (COX-1)[a]	Log IC_{50} (COX-1)	$E_{intermol.}$ (COX-1)[b]	IC_{50} (COX-2)[a]	Log IC_{50} (COX-2)	$E_{intermol.}$ (COX-2)[b]
32b	2.1	0.3	-15.1	1.7	0.2	-39.1
32c	2.4	0.4	-14.3	2.3	0.4	-38.5
32m	2.7	0.4	-12.4	227.3	2.4	-39.1
32n	55.7	1.8	-5.1	26.3	1.4	-32.9
36	500	2.7	16.5	0.001	-3.0	-53.1
42	251	2.4	11.6	0.23	-0.6	-43.7
44	200	2.3	11.1	0.27	-0.6	-45.6
48a	100	2.0	1.8	100	2.0	-19.7
48b	100	2.0	1.8	100	2.0	-18.1
50a	2.64	0.4	-14.0	4.96	0.7	-36.7
50b	5.9	0.8	-13.1	5.38	0.7	-36.5
50h	100	2.0	2.8	100	2.0	-35.5
50i	5.86	0.8	-13.1	5.38	0.7	-37.1
50j	258	2.4	10.6	0.004	-2.4	-52.7
50k	100	2.0	2.0	0.032	-1.5	-49.2

[a] IC_{50} (μM) calculated from *in vitro* inhibition of COX-1 or COX-2. [b] Intermolecular energy (Kcal/mol) between the docked ligands and COX-1 or COX-2

The following statistical measures were used; n, the number of samples used to produce the regression equation; R^2, multiple correlation coefficient, which is a measure of the correlation between the experimentally measured property and the parameters introduced in the regression equation, the higher the R^2 value the greater the correlation; RMSD, root mean square deviation, a measure of the deviation of the regression equation derived value from the experimentally measured property, the lower the RMSD the better

the correlation and F-ratio, Fisher's statistics value, a measure of the statistical significance of the correlation, a higher F-ratio would indicate a more significant correlation.

3.4.1 QSARs of the Isoxazole Series as COX-1 and COX-2 Inhibitors.

Multiple regression analysis was conducted for the group of isoxazoles **32b-c**, **32m-n**, **36**, **42**, **44**, and **48a-b** for COX-1 inhibition using the SCIQSAR program. The regression equation obtained from this study is illustrated by equation **10.**

$$\text{Log } IC_{50} \text{ (COX-1)} = 1.06 + 0.065 * E_{intermol.} + 5.24 * 10^{-4} * \text{Wien I} \quad \text{(10)}$$

n = 9, RMSD = 0.24, R^2 = 0.93, F = 40.05.

The experimental *vs.* calculated log IC_{50} are shown in Table **47**.

Table **47**. Experimental *vs.* Calculated Log IC_{50} (COX-1) Values for the Isoxazole Series.

Compd.	Log IC_{50} exp.[a]	Log IC_{50} calc.[b]	$E_{intermol.}$[c]	Wien I.[d]
32b	0.32	0.43	-15.10	642
32c	0.38	0.31	-14.31	642
32m	0.43	0.57	-12.43	995
32n	1.75	1.54	-5.12	995
36	2.00	1.83	4.79	1249
42	2.00	1.83	1.82	1249
44	2.3	2.32	11.10	1037
48a	2.4	2.55	11.10	1475
48b	2.7	2.88	16.51	1431

[a] Experimental IC_{50} (μM). [b] Calculated IC_{50} (μM). [c] Intermolecular energy between the docked ligand and COX-1 or COX-2 (Kcal/mol). [d] Wiener index.

The parameters in equation **10** suggested that COX-1 inhibition is dependent on the intermolecular energy between the docked ligand and COX-1 and the Wiener index. The

$E_{intermolecular}$ parameter would indicate the importance of docking experiments in predicting enzyme inhibition activities. The high correlation between the Wiener index and enzyme inhibition is consistent with the earlier reports that *para*-phenyl substituents in regioisomeric compounds alter COX-2 inhibitory potency [Carter *et al.*, 1999]

Multiple regression analysis for the isoxazole series for COX-2 provided equation **11**.

$$\text{Log } IC_{50} \text{ (COX-2)} = 16.35 + 0.16 * E_{intermol.} - 2.76 * 10^{-3} * \text{Wien I} \quad \text{.....(11)}$$

$n = 9$, RMSD = 0.11, $R^2 = 0.90$, F = 14.83.

The experimental *vs.* calculated log IC_{50} values are shown in Table **48**.

Table **48**. Experimental *vs.* Calculated Log IC_{50} (COX-2) Values for the Isoxazole Series.

Compd.	Log IC_{50} exp.[a]	Log IC_{50}calc.[b]	$E_{intermol.}$[c]	Wien I.[d]
32b	-2.99	-2.79	-53.06	1431
32c	-0.64	-0.84	-43.66	1475
32m	-0.57	-0.64	-45.6	1037
32n	0.23	0.27	-39.13	642
36	0.36	0.34	-38.45	642
42	1.42	1.52	-32.86	995
44	2	2.01	-18.12	1249
42a	2	2.47	-19.68	1249
42b	2.35	1.97	-39.06	995

[a] Experimental IC_{50} (μM). [b] Calculated IC_{50} (μM). [c] Intermolecular energy between the docked ligand and COX-1 or COX-2 (Kcal/mol). [d] Wiener index.

In spite of the fact that both equations **10** and **11** suggested that COX-1 and COX-2 inhibition are highly correlated ($R^2 = 0.93$ and $R^2 = 0.90$, respectively) to both the intermolecular energy, between the docked ligands and COX-2, and the topological properties of the ligands, there are two distinct differences between equations **10** and **12**.

First, while COX-1 inhibition is directly proportional to the Wiener index, COX-2 inhibition is inversely proportional to the same parameter. Although this observation might not help to design new inhibitors for either COX-1 or COX-2, it proves that inhibition of either enzyme has different structural requirements as shown by isoxazoles **32m-n**. While isoxazole **32m** (5-(4-$MeSO_2Ph$)) inhibited COX-1 (IC_{50} = 2.7 μM), it was a 100-fold less potent inhibitor of COX-2 (IC_{50} = 227 μM). The other regioisomer **32n** (4-(4-$MeSO_2Ph$)) showed COX-2 inhibition (IC_{50} = 26.3 μM) at about half the concentration required for COX-1 inhibition (IC_{50} = 55.7 μM). Second, COX-2 inhibition is more affected (regression coefficient = 0.16) by the intermolecular energy than COX-1 (regression coefficient = 0.065). This observation would suggest that tight binding is the mode of inhibition of isoxazoles in that data set.

3.4.2 QSARs for the Isoxazoline Series as COX-1 and COX-2 Inhibitors.

In an attempt to determine which physicochemical parameters were determinants to COX-1 inhibition, isoxazolines **50a-b** and **50h-k** were subjected to multiple regression analysis. The result of this analysis provided equation **12**.

$$\text{Log } IC_{50}\text{ (COX-1)} = 1.71 + 0.0775 * E_{intermol.} \quad \text{.....(12)}$$

n = 6, RMSD = 0.12, R^2 = 0.97, F = 148.89.

The experimental *vs.* calculated log IC_{50} values are shown in Table **49**.

Equation **12** confirmed that the intermolecular energy between the docked isoxazolines and COX-1 is the most important predictor of COX-1 inhibition. Interestingly, the contribution of the intermolecular energy to the log IC_{50} (COX-1) for the isoxazoline series was found to be similar to that shown previously in equation **10** for isoxazoles.

Table 49. Experimental *vs.* Calculated Log IC_{50} (COX-1) Values for the Isoxazoline Series.

Cpd No.	$LogIC_{50}$ exp.[a]	$LogIC_{50}$ calc.[b]	$E_{intermol.}$[c]
50a	0.42	0.62	-14.08
50b	0.77	0.69	-13.12
50h	2.0	1.93	2.81
50i	0.77	0.69	-13.08
50j	2.40	2.54	10.58
50k	2.0	1.87	2.02

[a] Experimental IC_{50} (μM). [b] Calculated IC_{50} (μM). [c] Intermolecular energy between the docked ligand and COX-1 or COX-2 (Kcal/mol).

This similarity would indicate that COX-1 isozyme binding site residues undergoes minimal dynamic changes upon binding of a ligand, which is likely due to the limited space near the peptide chains surrounding the active site compared to COX-2 where the active site residues tend to relax in spaces occupied by peptide chains surrounding the active site [Bayly *et al.*, 1999].

A QSAR study for the isoxazoline series with respect to COX-2 inhibitory activity is represented by equation **13**.

$$\text{Log } IC_{50}\text{(COX-2)} = 50.07 - 9.88*X1 + 18.34*ABSQ \quad \textbf{(13)}$$

$n = 6$, RMSD = 0.30, $R^2 = 0.96$, $F = 36.45$.

The experimental *vs.* calculated log IC_{50} values are listed in Table **50**.

Equation **13** showed that isoxazolines **50a-b** and **50h-k** COX-2 inhibition is dependent on first order molecular connectivity index (X1), and the sum of the absolute value of charges on each atom of the molecule (ABSQ).

Table 50. Experimental *vs.* Calculated Log IC_{50} (COX-2) Values for the Isoxazoline Series.

Compd.	Log IC_{50} exp[a]	Log IC_{50} calc[b]	X1[c]	ABSQ[d]
50a	0.70	0.93	9.23	2.29
50b	0.73	0.46	9.23	2.27
50h	2.0	1.55	10.44	2.98
50i	0.73	1.16	10.44	2.96
50j	-2.40	-2.50	11.26	3.20
50k	-1.50	-1.36	10.87	3.05

[a] Experimental IC_{50} (μM). [b] Calculated IC_{50} (μM). [c] First order connectivity index. [d] Sum of the absolute value of charges on each atom of the molecule.

This equation implies the role of topological features, such as different substitution patterns on the central ring, and to a less extent the effect of charges on all atoms such as the isoxazole "*N*". The absence of an intermolecular energy parameter in equation **13** could be due to the importance of substitutions pattern and consequently the molecular volume as determinants of COX-2 inhibition by the isoxazoline series.

3.4.3 QSARs of the Combined Isoxazole and Isoxazoline Series of Compounds as COX-1 and COX-2 inhibitors.

When the data sets, for both the isoxazoles and isoxazolines were combined in one data set and analyzed using a multiple regression analysis for COX-1 inhibition equation **14** was generated.

$$\text{Log } IC_{50} \text{ (COX-1)} = 1.71 + 0.0775 * E_{intermol.} \quad \text{.....(14)}$$

$n = 15$, RMSD = 0.21, $R^2 = 0.94$, $F = 195.65$.

The experimental *vs.* calculated log IC_{50} values are shown in Table **51.**

Equation **14** showed as expected, that the most important determinant of COX-1 inhibition is the intermolecular energy between the docked ligand and COX-1. The contribution of intermolecular energy was almost identical to that observed previously for the isoxazole and isoxazoline series as shown by equations **10** and **12**, respectively.

Table **51**. Experimental *vs.* Calculated Log IC_{50} (COX-1) Values for Both the Isoxazole and Isoxazoline Series.

Compd.	Log IC_{50} exp.[a]	Log IC_{50} calc.[b]	$E_{intermol}$,[c]
32b	0.32	0.51	-15.10
32c	0.38	0.57	-14.31
32m	0.43	0.71	-12.43
32n	1.75	1.27	-5.12
36	2.7	2.92	16.51
42	2.4	2.50	11.10
44	2.3	2.50	11.10
48a	2.0	1.79	1.82
48b	2.0	1.79	1.79
50a	0.42	0.58	-14.08
50b	0.77	0.66	-13.13
50h	2.0	1.87	2.81
50i	0.77	0.66	-13.10
50j	2.39	2.46	10.58
50k	2.0	1.81	2.02

[a] Experimental IC_{50} (μM). [b] Calculated IC_{50} (μM). [c] Intermolecular energy between the docked ligand and COX-1 or COX-2 isozymes (Kcal/mol).

Regression analysis of the combined isoxazole and isoxazoline series of compounds provided equation **15** for COX-2.

$$\text{Log } IC_{50} \text{ (COX-2)} = 13.37 + 0.016 * E_{intermol} - 2.51 * \log P + 3.87 * 10^{-4} * \text{Wien I} \quad \text{.....(15)}$$

$n = 15$, RMSD = 0.58, $R^2 = 0.87$, $F = 23.63$.

The experimental *vs.* calculated log IC_{50} values are shown in Table **52.**

Table **52**. Experimental *vs.* Calculated Log IC_{50} (COX-2) Values for the Combined Isoxazole and Isoxazoline Series of Compounds.

Compd.	Log IC_{50} exp.[a]	Log IC_{50} calc.[b]	$E_{intermol.}$[c]	Log P[d]	Wien I.[e]
32b	0.23	1.05	-39.13	2.48	642
32c	0.36	0.72	-38.45	2.65	642
32m	2.35	1.19	-39.06	2.48	995
32n	1.42	0.91	-32.86	2.99	995
36	-3.0	-2.75	-53.06	3.22	1431
42	-0.64	-1.36	-43.66	3.28	1475
44	-0.57	-1.09	-45.60	2.98	1037
48a	2.0	2.54	-19.68	3.23	1249
48b	2	2.39	-18.12	3.39	1249
50a	0.7	0.77	-36.66	2.76	726
50b	0.73	0.42	-36.5	2.91	726
50h	2	1.68	-35.46	2.53	1106
50i	0.73	0.45	-37.1	2.92	1106
50j	-2.4	-1.45	-52.7	2.72	1374
50k	-1.5	-1.09	-49.26	2.77	1215

[a] Experimental IC_{50} (μM). [b] Calculated IC_{50} (μM). [c] Intermolecular energy between the docked ligand and COX-1 or COX-2 (Kcal/mol). [d] The logarithm (base 10) of the octanol-water partition coefficient. [e] Wiener index.

Equation **15** showed, similar to isoxazoles (equation **11**), that COX-2 inhibition is directly proportional to the intermolecular energy between the docked ligand and COX-2.

The Wiener index (a topological parameter, measuring the pattern of substitution) and log P (measuring the lipophilic character of compounds in the data set) were both contributors to COX-2 inhibition as reported earlier [Wilkerson *et al.*, 1995].

In summary, this QSAR study for isoxazoles **32b-c**, **32m-n**, **36**, **42**, **44**, and **48a-b**, and isoxazolines **50a-b** and **50h-k** showed that (i) the calculated intermolecular energy between the ligand and either COX-1 or COX-2, obtained from ligand docking studies, correlates very well to the enzyme inhibition data. Accordingly, molecular modeling experiments provides a good tool to design a lead compound and subsequent optimization of the lead compound; (ii) topological parameters such as Wiener index, which is a measure of regioisomeric substitution patterns was shown to be directly correlated to COX-1 and inversely correlated to COX-2 inhibition, and (iii) the tight binding mode resulting in COX-2 inhibition could be predicted, or is at least suggested from QSAR studies as shown from regression analysis of the isoxazole series.

4.0 Experimental.

Melting points (mp) were determined using a Thomas-Hoover capillary apparatus and are uncorrected. Infrared (IR) spectra were recorded using a Nicolet 550 Series II Magna FT-IR spectrometer. Nuclear magnetic resonance (^{1}H NMR, ^{13}C NMR, ^{19}F NMR) spectra were recorded on a Bruker AM-300 spectrometer. The assignment of all exchangeable protons (*O*H, *N*H) were confirmed by the addition of D_2O. NMR multiplicity data are denoted by s (singlet), d (doublet), t (triplet), q (quartet), m (multiplet), and br (broad). ^{13}C NMR spectra were acquired using the *J* modulated spin echo technique where methyl and methine carbons appear as positive peaks and methylene and quaternary carbon resonances appear as negative peaks. Microanalyses were within ±0.4% of theoretical values for all elements listed. Silica gel column chromatography was performed using Merck 7734 silica gel (70-230 mesh). Dichloromethane and toluene were dried with $CaCl_2$ just prior to distillation. Ethanol was dried with magnesium ethoxide. Ethanones **30a-b** [Teiicho, 1959], **30c** [Funasaka *et al.*, 1959], and **30d-h** [Talley *et al.*, 1996], isoxazole (**32a**), isoxazolium salt (**49a**), isoxazoline (**50a**) [Dominguez *et al.*, 1996], celecoxib (**17**) [Penning *et al.*, 1997], 3-aminoisoxazole (**43**) [Horsanyi et al., 1974] and 4-azidoacetophenone (**58**) [Kim *et al.*, 1993] were prepared according to the reported methods. All other reagents were purchased from Aldrich Chemical (Milwaukee, WI). Male Sprague-Dawley rats, used in the AI and analgesic screens, were supplied by Animal Health Services, University of Alberta. All experiments involving animals were carried out using protocols approved by the Animal Welfare Committee, University of Alberta.

4.1 Synthesis.

4.1.1 General Method for the Preparation of 3-Dimethylamino-1,2-diarylprop-2-ene-1-ones (31a-h).

Dimethylformamide dimethylacetal (DMFDMA) (4 ml, 30 mmol) was added dropwise to a stirred solution of the ethanones (**30a-h**, 25 mmol) in dry toluene under nitrogen at 25°C. After 12 h, DMFDMA (0.1 ml, 0.8 mmol) was added, and the mixture was heated at 50°C for 24 h. Then, over a period of three days, additional DMFDMA (0.1 ml, 0.8 mmol) was added and the reaction temperature was increased by about 15°C each day during the 5 day period. On the fifth day, when the reaction was completed (tlc monitoring), the solvent was removed in *vacuo*, and the residue was recrystallized from diethyl ether to afford the respective prop-2-ene-1-one **31a-h**. The IR and ^{1}H NMR spectral data for compounds **31a-h** are presented in Table **3**, ^{13}C spectral data are presented in Table **4**, and the physical data are presented in Table **5.**

4.1.2 General Method for the Preparation of 4,5-Diarylisoxazoles (32a-h).

Hydroxylamine hydrochloride (210 mg, 3.15 mmol) and Na_2CO_3 (170 mg, 1.6 mmol) were added to a solution of the respective prop-2-ene-1-one (**31a-h**, 2.86 mmol) in methanol (30 ml) and water (15 ml) with stirring, and this solution was maintained at 25°C for 1 h. This mixture was acidified to pH 4-5 using glacial acetic acid, and the reaction was allowed to proceed at reflux for 2 h. After cooling to 25°C, the pH of the reaction mixture was adjusted to pH 8 using aqueous NH_4OH. Extraction with CH_2Cl_2 (4 x 30 ml), drying the CH_2Cl_2 extracts (Na_2SO_4), and removal of the solvent in *vacuo* afforded a yellow oil, which was purified by silica gel column chromatography. Elution with CH_2Cl_2 afforded the respective 4,5-diarylisoxazoles (**32a-h**). The IR and ^{1}H NMR

spectral data for compounds **32a-h** are presented in Table **6**, ^{13}C and ^{19}F spectral data are presented in Table **7**, and the physical data are presented in Table **8.**

4.1.3 General Method for the Preparation of 4- or 5-(4-Methylsulfphinylphenyl)-4- or 5-(phenyl or 4-fluorophenyl)isoxazoles (32i-l).

A solution of *m*-chloroperbenzoic acid (50% w/w, 0.361 g, 2.2 mmol) in dry CH_2Cl_2 (30 ml) was added to a solution of the respective isoxazoles (**32e-h**, 1 mmol) in CH_2Cl_2 at 0°C with stirring under an argon atmosphere. The reaction mixture was allowed to warm to 25°C over 2-3 h, the reaction mixture was filtered, and the filtrate was washed with 5% w/v aqueous Na_2CO_3. The organic fraction was dried (Na_2SO_4), and the solvent was removed in *vacuo* to afford a yellow oil which was purified by silica gel column chromatography. Elution with CH_2Cl_2 yielded the respective isoxazoles (**32i-l**). The IR and ^1H NMR spectral data for compounds **32i-l** are presented in Table **6**, ^{13}C and ^{19}F spectral data are presented in Table **7**, and the physical data are presented in Table **8.**

4.1.4 General Method for the Preparation of 4- or 5-(4-Methylsulfphonyl-phenyl)-4- or 5-(phenyl or 4-fluorophenyl)isoxazoles (32m-p).

A solution of *m*-chloroperbenzoic acid (50% w/w, 2.90 g, 16.8 mmol) in dry CH_2Cl_2 (30 ml) was added to a solution of the respective isoxazoles (**32e-h**, 4 mmol) in CH_2Cl_2 at 0°C with stirring under an argon atmosphere. The reaction mixture was allowed to warm to 25°C over 2-3 h, the reaction mixture was filtered, and the filtrate was washed with 5% aqueous Na_2CO_3. The organic fraction was dried (Na_2SO_4), and the solvent was removed *in vacuo* to afford a yellow oil which was purified by silica gel column chromatography. Elution with CH_2Cl_2 yielded the respective isoxazoles **32m-p**. The IR and ^1H NMR

spectral data for compounds **32m-p** are presented in Table **6**, ^{13}C and ^{19}F spectral data are presented in Table **7**, and the physical data are presented in Table **8.**

4.1.5 Preparation of 3-(4-Methylsulphonylphenyl)-4-phenyl-5-trifluoromethyl-isoxazole (36).

4.1.5.1 Preparation of 4-(4-Methylthiophenyl)-3-phenyl-1,1,1-trifluoro-but-3-en-2-one (33).

A solution of 3-phenyl-1,1,1-trifluoropropan-2-one (1 g, 5.3 mmol), 4-methylthiobenzaldehyde (0.7 g, 5.3 mmol) and piperidine (20 mg) in benzene (40 ml) was heated at reflux for 24 h. The mixture was concentrated and the crude material was chromatographed on silica gel column chromatography using ethyl acetate: hexane (1:1) as eluent to give 1.17 g (69%) of the desired ketone **33**. The IR and ^{1}H NMR spectral data for compound **33** are presented in Table **9**, ^{13}C and ^{19}F spectral data are presented in Table **10**, and the physical data are presented in Table **11.**

4.1.5.2 Preparation of 4-Hydroxylamino-4-(4-methylthiophenyl)-3-phenyl-1,1,1-trifluorobutan-2-one (34).

A solution of the ketone **33** (1.0 g, 3.1 mmol), hydroxylamine hydrochloride (0.24 g, 3.5 mmol) and sodium acetate (290 mg, 3.5 mmol) in ethanol (30 ml) and water (3 ml) was heated at reflux for 90 minutes. The reaction was cooled to room temperature, water was added, and the crude product was filtered. Recrystallization from ethanol and water gave the ketone **34**. The IR and ^{1}H NMR spectral data for compound **34** are presented in Table **12**, ^{13}C and ^{19}F spectral data are presented in Table **13**, and the physical data are presented in Table **14.**

4.1.5.3 Preparation of 3-(4-Methylthiophenyl)-4-phenyl-5-trifluoromethyl-isoxazole (35).

A solution of KI (0.76 g, 12 mmol) and iodine (0.33 g, 1.3 mmol) in water (5 ml) was added to a solution of **34** (0.45 g, 1.3 mmol) and $NaHCO_3$ (0.45 g, 14 mmol) in THF (10 ml) and water (5 ml) in a reaction flask covered by aluminum foil. This reaction mixture was heated to reflux for 7 h, stirred at 25°C for 12 h, saturated aqueous sodium bisulfite solution (5 ml) was added, and the reaction mixture was extracted with EtOAc (4 x 50 ml). The combined organic extracts were dried (Na_2SO_4), the solvent was removed *in vacuo*, and the residue was purified by silica gel column chromatography using toluene as eluent to yield **35**. The IR and ^1H NMR spectral data for compound **35** are presented in Table **12**, ^{13}C and ^{19}F spectral data are presented in Table **13**, and the physical data are presented in Table **14.**

4.1.5.4 Preparation of 3-(4-Methylsulphonylphenyl)-4-phenyl-5-trifluoromethyl-isoxazole (36).

A solution of Oxone® (1.34 g) in H_2O (6 ml) and MeOH (4 ml) was added dropwise to a solution of **35** (0.45 g, 1.3 mmol) in THF (12 ml) at 25°C with stirring. The reaction was allowed to proceed for 2 h prior to addition of H_2O (10 ml) and filtration. Recrystallization of the product from EtOAc-hexane afforded **36.** The IR and ^1H NMR spectral data for compound **36** are presented in Table **12**, ^{13}C and ^{19}F spectral data are presented in Table **13**, and the physical data are presented in Table **14.**

4.1.6 Preparation of 4-(4-Methylsulphonylphenyl)-3-phenyl-5-trifluoromethyl-isoxazole (42).

4.1.6.1 Preparation of 2-(4-Methylthiophenyl)-3-phenyl-2-propenoic acid (37).

A solution of 4-methylthiophenylacetic acid (0.91 g, 5 mmol), benzaldehyde (0.53 g, 5 mmol) and Et_3N (0.5 g, 5 mmol) in Ac_2O (4 ml) was heated at reflux for 24 h. The reaction mixture was cooled to 110°C, H_2O (10 ml) was added, and the mixture was cooled to 25°C. The crystals obtained were filtered to afford **37**. The IR and ^1H NMR spectral data for compound **37** are presented in Table **9**, ^{13}C and ^{19}F spectral data are presented in Table **10**, and the physical data are presented in Table **11.**

4.1.6.2 Preparation of Methyl 2-(4-methylthiophenyl)-3-phenyl-2-propenoate (38).

A solution of **37** (1.0 g, 3.7 mmol) in MeOH (20 ml), containing concentrated H_2SO_4 (0.1 ml), was heated at reflux for 15 h. The reaction mixture was cooled to 25°C, neutralized with $NaHCO_3$, filtered, and the solvent was removed *in vacuo* to afford **38**. The IR and ^1H NMR spectral data for compound **38** are presented in Table **9**, ^{13}C and ^{19}F spectral data are presented in Table **10**, and the physical data are presented in Table **11.**

4.1.6.3 Preparation of 3-(4-Methylthiophenyl)-4-phenyl-1,1,1-trifluoro-but-3-en-2-one (39).

Trifluoromethyltrimethylsilane (4.1 ml, 2.5 mmol) was added to a mixture of **38** (0.57 g, 2 mmol) and CsF (93 mg, 0.02 mmol), and this mixture was stirred at 25°C for 3 h under a nitrogen atmosphere prior to addition of 4N HCl (4 ml), and stirring at 25°C for 3 h. Extraction with ether (3 x 30 ml), drying the combined ether extracts (Na_2SO_4), and removal of the solvent *in vacuo* gave a residue that was purified by silica gel column

chromatography using Et_2O-hexane (1:9, v/v) as eluent to yield **39**. The IR and ^1H NMR spectral data for compound **39** are presented in Table **9**, ^{13}C and ^{19}F spectral data are presented in Table **10**, and the physical data are presented in Table **11.**

4.1.6.4 Preparation of 4-Hydroxylamino-3-(4-methylthiophenyl)-4-phenyl-1,1,1-trifluorobutan-2-one (40).

A solution of **39** (1.0 g, 3.1 mmol), $HONH_2.HCl$ (0.24 g, 3.5 mmol) and NaOAc (0.29 g, 3.5 mmol) in EtOH (30 ml) and H_2O (3 ml) was heated at reflux for 90 min. The reaction mixture was cooled to 25°C, water (20 ml) was added, the crude product was removed by filtration, and then recrystallized from EtOH-H_2O to afford **40**. The IR and ^1H NMR spectral data for compound **40** are presented in Table **12**, ^{13}C and ^{19}F spectral data are presented in Table **13**, and the physical data are presented in Table **14.**

4.1.6.5 Preparation of 4-(4-Methylthiophenyl)-3-phenyl-5-trifluoromethyl-isoxazole (41).

A solution of KI (0.76 g, 12 mmol) and iodine (0.33 g, 1.3 mmol) in water (5 ml) was added to a solution of **40** (0.45 g, 1.3 mmol) and $NaHCO_3$ (0.45 g, 14 mmol) in THF (10 ml) and water (5 ml) in a reaction flask wrapped with aluminum foil. The reaction mixture was heated at reflux for 7 h, and then stirred at 25°C for 12 h. Saturated aqueous sodium bisulfite solution (5 ml) was added, and this mixture was extracted with EtOAc (3 x 50 ml), the combined EtOAc extracts were dried (Na_2SO_4), and the solvent was removed *in vacuo*. Purification of the residue obtained by silica gel column chromatography using toluene as eluent gave **41**. The IR and ^1H NMR spectral data for

compound **41** are presented in Table **12**, ^{13}C and ^{19}F spectral data are presented in Table **13**, and the physical data are presented in Table **14.**

4.1.6.6 Preparation of 4-(4-Methylsulphonylphenyl)-3-phenyl-5-trifluoromethyl-isoxazole (42).

A solution of Oxone® (1.34 g) in H_2O (6 ml) and MeOH (4 ml) was added dropwise to a solution of **41** (0.45 g, 1.3 mmol) in THF (12 ml), at 25°C with stirring. The reaction was allowed to proceed for 2 h at 25° prior to addition of water (3 ml). The crude product was removed by filtration, and recrystallized from EtOAc-hexane, to yield **42.** The IR and ^1H NMR spectral data for compound **42** are presented in Table **12**, ^{13}C and ^{19}F spectral data are presented in Table **13**, and the physical data are presented in Table **14.**

4.1.7 Preparation of 4,5-Diphenyl-3-methylsulphonamidoisoxazole (44).

Methanesulfonyl chloride (0.16 g, 2 mmol) was added to a solution of **43** (0.46 g, 2 mmol) in pyridine (10 ml) with stirring, the reaction was allowed to proceed at 25°C for 24 h, and then at 65°C for 1 h. The reaction mixture was poured onto ice-water (100 ml), the pH was adjusted to 12 by addition of 1% w/v aqueous NaOH, the precipitate removed by filtration was discarded, and the filtrate was acidified to pH 6 using acetic acid. The precipitate obtained upon acidification of the filtrate was collected and recrystallized from EtOH-H_2O to give **44.** The IR and ^1H NMR spectral data for compound **44** are presented in Table **15**, ^{13}C and ^{19}F spectral data are presented in Table **16**, and the physical data are presented in Table **17.**

4.1.8 General Method for the Preparation of 4-Aryl-3-methyl-5-(4-methylsulphonylphenyl)isoxazoles (48).

4.1.8.1 General Method for the Preparation of 3-Aryl-4-(4-methylthiophenyl)-3-buten-2-ones (45).

A solution of the 4-substituted-phenylacetone (10 mmol), 4-substituted-benzaldhyde (1.52 g, 10 mmol) and piperidine (35 mg, 0.4 mmol) in benzene (30 ml) was heated at reflux for 24 h. Removal of the solvent in *vacuo* gave a residue that was purified by silica gel column chromatography using ether-hexanes as eluent to give **45**. The IR and ^{1}H NMR spectral data for compound **45** are presented in Table **15**, ^{13}C and ^{19}F spectral data are presented in Table **16**, and the physical data are presented in Table **17**.

4.1.8.2 General Method for the Preparation of 3-Aryl-4-(4-methylthiophenyl)-3-buten-2-one oximes (46).

A solution of **45** (5.5 mmol) in EtOH (15 ml) was added to a solution of $NH_2OH.HCl$ (0.376 g, 5.5 mmol) and NaOAc (0.451 g, 5.5 mmol) in H_2O (7 ml) and the reaction mixture was heated at reflux for 5 h. The reaction mixture was cooled to 25C°, poured onto water (100 ml), and the crude product was filtered. Recrystallization from EtOH and H_2O gave **46**. The IR and ^{1}H NMR spectral data for compound **46** are presented in Table **15**, ^{13}C and ^{19}F spectral data are presented in Table **16**, and the physical data are presented in Table **17**.

4.1.8.3 General Method for the Preparation of 4-Aryl-3-methyl-5-(4-methylthiophenyl)isoxazoles (47).

A solution of KI (1.45 g, 8.75 mmol) and iodine (0.63 g, 2.5 mmol) in H_2O (5 ml)

was added to a solution of **46** (2.5 mmol) and $NaHCO_3$ (0.84 g, 10 mmol) in THF (20 ml) and water (5 ml) in a reaction flask covered by aluminium foil. The reaction mixture was heated at reflux for 7 h, saturated aqueous sodium bisulfite solution (5 ml) was added, and this reaction mixture was extracted with EtOAc (4 x 50 ml). The combined organic extracts were dried (Na_2SO_4), the solvent was removed *in vacuo*, and the residue was purified by silica gel column chromatography using toluene as eluent to yield **47.** The IR and ^1H NMR spectral data for compound **47** are presented in Table **15**, ^{13}C and ^{19}F spectral data are presented in Table **16**, and the physical data are presented in Table **17.**

4.1.8.4 General Method for the Preparation of 4-Aryl-3-methyl-5-(4-methylsulphonylphenyl)isoxazoles (48)

A solution of Oxone® (1.6 g) in H_2O (6 ml) and MeOH (4 ml) was added dropwise to a solution of **47** (1.53 mmol) in THF (10 ml) at 25°C with stirring. The reaction was allowed to proceed for 3 h prior to addition of H_2O (10 ml) and extraction with CH_2Cl_2 (4 x 30 ml). The organic layer was separated, dried (Na_2SO_4), and the solvent was removed *in vacuo*. The residue was purified by silica gel column chromatography using CH_2Cl_2 as eluent to yield **48.** The IR and ^1H NMR spectral data for compound **48** are presented in Table **15**, ^{13}C and ^{19}F spectral data are presented in Table **16**, and the physical data are presented in Table **17.**

4.1.9 General Method for the Preparation of 4,5-Diaryl-2-methylisoxazolium tetrafluoroborates (49).

A solution of the isoxazoles (**32b-n, 48a, 48c**) (2.2 mmol) in dry CH_2Cl_2 (20 ml) was added drop wise to a stirred suspension of trimethyloxonium tetrafluoroborate (0.5 g, 3.3

mmol) in CH_2Cl_2 (20 ml) under a nitrogen atmosphere, and the reaction was allowed to proceed at 25 °C for 15 h. Removal of the solvent *in vacuo* gave an oil that was triturated with dry Et_2O (2 ml) to yield a yellow powder that was filtered and recrystallized from CH_2Cl_2 to afford the respective salt (**49a-k**). The IR and ^1H NMR spectral data for compound **49** are presented in Table **18**, ^{13}C and ^{19}F spectral data are presented in Table **19**, and the physical data are presented in Table **20.**

4.1.10 General Method for the Preparation of 4,5-Diaryl-2-methyl-4-isoxazolines (50a-k).

A solution of the isoxazolium salt (**49a-k**) (0.33 mmol) in dry EtOH (5-10 ml) was added to a stirred suspension of $NaBH_4$ (110 mg, 2.9 mmol) in dry ethanol (15 ml) under an argon atmosphere at 25°C, and the reaction was allowed to proceed for 8-12 h. The reaction was quenched by addition of a saturated aqueous NH_4Cl solution (10 ml), and the mixture was extracted with dichloromethane (5 x 20 ml). The combined organic layers were washed with water (10 ml), dried (Na_2SO_4), and the solvent from the organic fraction was removed in *vacuo* to give brown oil that was purified by flash silica gel chromatography using CH_2Cl_2-hexane (1:1, v/v) as eluent to afford the respective isoxazolines **50a-k**. The IR and ^1H NMR spectral data for compounds (**50a-l**) are presented in Table **21**, ^{13}C and ^{19}F spectral data are presented in Table **22**, and the physical data are presented in Table **23.**

4.1.11 Preparation of 1-(4-Azidophenyl)-3-(4-methylphenyl)-5-trifluoromethyl-pyrazole (54).

4.1.11.1 Preparation of 4,5-Dihydro-5-hydroxy-3-(4-methylphenyl)-1-(4-nitro-phenyl)-5-trifluoromethylpyrazole (51).

4-Nitrophenylhydrazine (0.675, 4.4 ml) was added to a stirred solution of 1-(4-methylphenyl)-4,4,4-trifluorobutane-1,3-dione (0.92 g, 4.0 mmol) in EtOH (50 ml), and the mixture was heated at reflux with stirring for 20 h. After cooling to 25°C the solvent was removed *in vacuo*. The residue was dissolved into EtOAc (30 ml), washed with water (2 x 30 ml), and brine (2 x 30 ml) dried ($MgSO_4$), filtered, and the solvent was removed *in vacuo*. The solid obtained was chromatographed on a silica gel column using ether:hexanes (1:1, v/v) as an eluent to afford a white solid. The IR and ^1H NMR spectral data for compound **51** are presented in Table **24**, ^{13}C and ^{19}F spectral data are presented in Table **25**, and the physical data are presented in Table **26.**

4.1.11.2 Preparation of 3-(4-Methylphenyl)-1-(4-nitrophenyl)-5-trifluoromethyl-pyrazole (52).

A solution of **51** (0.5 g, 1.36 mmol) in HOAc (30 ml) was heated at reflux with stirring for 2 h. After cooling to 25°C, the reaction mixture was poured on cold water (100 ml), extracted with EtOAc (4 x 30 ml), washed with H_2O and then brine (2 x 30 ml), the organic fraction was dried ($MgSO_4$), filtered, and the solvent was removed *in vacuo*. The product was purified by silica gel column chromatography using ether:hexanes (1:1, v/v)) to afford **52** as a white solid. The IR and ^1H NMR spectral data for compound **52** are presented in Table **24**, ^{13}C and ^{19}F spectral data are presented in Table **25**, and the physical data are presented in Table **26.**

4.1.11.3 Preparation of 1-(4-Aminophenyl)-3-(4-methylphenyl)-5-trifluoromethyl-pyrazole (53).

10% Pd/C (10 mg) was added to a solution of **52** (0.347 g, 1 mmol) in 95% EtOH (20 ml). The suspension was warmed to 50°C with stirring. Hydrazine hydrate (0.21 ml) was added drop wise to the reaction mixture, which was subsequently heated at reflux for 45 min. After cooling to 25°C, the solvent was removed in *vacuo*, and the residue was purified by silica gel column chromatography using CH_2Cl_2:hexanes (1:1, v/v) as eluent to afford **53** as a pale yellow solid The IR and ^{1}H NMR spectral data for compound **53** are presented in Table **24**, ^{13}C and ^{19}F spectral data are presented in Table **25**, and the physical data are presented in Table **26.**

4.1.11.4 Preparation of 1-(4-Azidophenyl)-3-(4-methylphenyl)-5-trifluoromethyl-pyrazole (54).

A solution of $NaNO_2$ (60 mg, 0.87 mmol) in H_2O (7 ml), was added to an ice-cold solution of **53** (0.27 g, 0.85 mmol) in HCl (10 ml of 37% w/v) during 15 min, a solution of NaN_3 (0.55 g, 8.5 mmol) in H_2O (2 ml) was added dropwise with stirring at 0°C over 15 min, and the temperature of the reaction mixture was allowed to rise to 25°C. After stirring for another 15 min, the reaction mixture was extracted with CH_2Cl_2 (4 x 30 ml), the organic extract was dried (Na_2SO_4), the solvent was removed *in vacuo*, and the product was purified by silica gel column chromatography using ether:hexanes (1:3, v/v) as eluent to yield **54** as a white solid. The IR and ^{1}H NMR spectral data for compound **52** are presented in Table **24**, ^{13}C and ^{19}F spectral data are presented in Table **25**, and the physical data are presented in Table **26.**

4.1.12 Preparation of 1-(4-Azidophenyl)-5-(4-methylphenyl)-3-trifluoromethyl-pyrazole (57).

4.1.12.1 Preparation of 5-(4-Methylphenyl)-1-(4-nitrophenyl)-3-trifluoromethyl-pyrazole (55).

4-Nitrophenylhydrazine (0.5 g, 3.3 mmol) was added to a stirred solution of 1-(4-methylphenyl)-4,4,4-trifluorobutane-1,3-dione (0.75 g, 3.3 mmol) in EtOH (50 ml) and HCl (1 ml of 37% w/v). After heating at reflux for 20 h, the reaction mixture was cooled to 25°C, and the solvent was removed *in vacuo*. The residue was dissolved in EtOAc (30 ml), washed with water (2 x 30 ml), the organic fraction was dried ($MgSO_4$), filtered, and the solvent was removed in *vacuo*. The product was chromatographed on a silica gel column using ether:hexanes (1:1, v/v) as eluent to afford **55** as a white solid The IR and ^1H NMR spectral data for compound **55** are presented in Table **27**, ^{13}C and ^{19}F spectral data are presented in Table **28**, and the physical data are presented in Table **29.**

4.1.12.2 Preparation of 1-(4-Aminophenyl)-5-(4-methylphenyl)-3-trifluoromethyl-pyrazole (56).

10% Pd/C (10 mg) was added to a solution of pyrazole **55** (0.347 g, 1 mmol) in 95% EtOH (20 ml), and the suspension was warmed to 50°C with stirring. Hydrazine hydrate (0.21 ml) was added dropwise to the reaction mixture, which was subsequently heated at reflux for 1 h. After cooling to 25°C, the solvent was removed *in vacuo*, and the product was purified by silica gel column chromatography using ether:hexanes (1:1, v/v) as eluent to afford **56** as a pale yellow solid The IR and ^1H NMR spectral data for compound **56** are presented in Table **27**, ^{13}C and ^{19}F spectral data are presented in Table **28**, and the physical data are presented in Table **29.**

4.1.12.3 Preparation of 1-(4-Azidophenyl)-5-(4-methylphenyl)-3-trifluoromethyl-pyrazole (57).

A solution of $NaNO_2$ (60 mg, 0.87 mmol) in H_2O (7 ml), was added to an ice-cold solution of **56** (0.27 g, 0.85 mmol) in HCl (10 ml of 37% w/v) over 15 min. A solution of NaN_3 (0.55 g, 8.5 mmol) in H_2O (2 ml) was added drop wise with stirring at 0°C over 15 min, and the temperature of the reaction mixture was allowed to rise to 25°C. After stirring for another 15 min at 25°C, the reaction mixture was extracted with EtOAc (4 x 30 ml), the organic extract was dried (Na_2SO_4), the solvent was removed *in vacuo*, and the residue was purified by silica gel column chromatography using ether:hexanes (1:3, v/v) as eluent to yield **57** (0.29 g, 56%). The IR and ^1H NMR spectral data for compound **57** are presented in Table **27**, ^{13}C and ^{19}F spectral data are presented in Table **28**, and the physical data are presented in Table **29.**

4.1.13 Preparation of 4-(4-Azidophenyl)-3-phenyl-2(5H)-furanone (61).

4.1.13.1 Preparation of 4-Azidophenacyl bromide (59).

Bromine (0.22 ml, 4.4 mmol) was added dropwise to a solution of 4-azidoacetophenone (**58**) (0.6 g, 4 mmol) in CH_2Cl_2 (20 ml) during 10 min, and the reaction was allowed to proceed with stirring at 25°C for 2 h. The solvent was removed in *vacuo*, and the residue was purified by silica gel column chromatography to afford **59**. The IR and ^1H NMR spectral data for compound **59** are presented in Table **30**, ^{13}C and ^{19}F spectral data are presented in Table **31**, and the physical data are presented in Table **32.**

4.1.13.2 Preparation of 4-Azidophenacylphenyl acetate (60).

4-Azidophenacyl bromide **59** (0.24 g, 1 mmol) was added to a solution of phenylacetic acid (0.15 g, 1.1 mmol) in CH_3CN (10 ml) containing Et_3N (1 ml), and the reaction was allowed to proceed at 25°C for 1 h with stirring. The reaction mixture was extracted with CH_2Cl_2 (4 x 30 ml), washed successively with 2 N HCl (2 x 10 ml), 5% $NaHCO_3$ (2 x 10 ml), H_2O (2 x 30 ml), the organic fraction was dried (Na_2SO_4), and the solvent was removed *in vacuo* to afford **60.** The IR and ^1H NMR spectral data for compound **60** are presented in Table **30**, ^{13}C and ^{19}F spectral data are presented in Table **31**, and the physical data are presented in Table **32.**

4.1.13.3 Preparation of 4-(4-Azidophenyl)-3-phenyl-2(5H)-furanone (61).

A solution of **60** (0.15 g, 0.5 mmol) in MeCN (10 ml) containing Et_3N (1 ml) was heated at reflux for 6 h. The reaction mixture was extracted with CH_2Cl_2 (4 x 30 ml), washed successively with 2 N HCl (2 x 10 ml), 5% $NaHCO_3$ (2 x 10 ml), H_2O (2 x 30 ml), and the organic fraction was dried (Na_2SO_4). Removal of the solvent in *vacuo* yielded **61.** The IR and ^1H NMR spectral data for compound (**61**) are presented in Table **30**, ^{13}C and ^{19}F spectral data are presented in Table **31**, and the physical data are presented in Table **32.**

4.2 Antiinflammatory Activity Assay.

Antiinflammatory activity was measured using the carrageenan induced rat paw edema assay described in the literature [Winter *et al.*, 1962]. Four male Sprague-Dawley rats weighing 100-120 g were used in each group. Test compounds were orally administered as suspensions in water using gum acacia as suspending agent. One hour

later, the volume of the paw, to be injected with λ-carrageenan (purchased from Sigma-Cat. No. 3889), was measured with a mercury-displacement plethsysmograph, followed by a subplantar injection of λ-carrageenan (0.05 ml). The volume of the injected paw was measured repeatedly at 3 and 5 hours post injection of λ-carrageenan. The average of foot swelling in a group of drug treated animals was compared to that of a control group, where the test compound was replaced by the vehicle used. The percentage inhibition of edema is defined as 1 minus the difference in paw volume between the carrageenan-injected paw (V_d) and the preinjected paw (V_p) for the drug treated animal, divided by the increase in volume of the injected paw in the control (V_c) non-drug treated animal, less the volume of the preinjected paw. This term is multiplied by 100 to give the percentage of inhibition of edema.

$$\% \text{ Inhibition of edema formation} = (1 - V_d - V_p / V_c - V_p) \times 100.$$

The ED_{50} value was calculated using the test compound at three different doses.

4.3 Analgesic Activity Assay.

Analgesic activity was determined using the method described in the literature [Fukawa *et al.*, 1980]. Four male Sprague-Dawley rats, weighing between 120-150 g, were used for each test compound. The test compound was administered intraparitoneally, as a suspension in physiological saline using 10% (w/v) Tween 80 as suspending agent. After 30 and 60 min., the number of writhing responses, intermittent contractions of the abdomen, twisting and turning of the trunk and extension of the hind limbs, induced in each rat after ip injection of a 4% w/v NaCl solution, was counted during a 10 min. period.

The % inhibition of writhing responses, which is the measure of analgesic activity, was calculated using the following formula:

$$\% \text{ Inhibition} = W_1\text{-}W_2/W_1 \times 100$$

W_1 : number of control writhing responses

W_2 : number of writhing response at 30 and 60 minutes after injecting the test compound.

4.4 *In vitro* Enzyme Inhibition Assay.

The ability of the test compound to inhibit (IC_{50}, μM) the conversion of arachidonic acid (AA) to prostaglandin H_2 (PGH_2) by ram seminal vesicle cyclooxygenase-1 (oCOX-1) and sheep placental cyclooxygenase-2 (oCOX-2) was determined using a COX-1/COX-2 inhibitor screening assay kit (Kit No. 560101, Cayman Chemical, Ann Arbor, MI). Briefly, cyclooxygenase catalyzes the first step in the biosynthesis of AA to PGH_2. $PGF_{2\alpha}$, produced from PGH_2 by reduction with stannous chloride is measured by enzyme immunoassay (ACE™ competitive EIA). This assay is based on the competition between PGs and a PG-acetylcholinesterase conjugate (PG tracer) for a limited amount of PG antiserum. The amount of PG tracer that is able to bind to the PG antiserum is inversely proportional to the concentration of PGs in the wells since the concentration of the PG tracer is held constant while the concentration of PGs varies. This antibody-PG complex binds to a mouse anti-rabbit monoclonal antibody that has been previously attached to the well. The plate is washed to remove any unbound reagents and then Ellman's Reagent, which contains the substrate to acetylcholinesterase, is added to the well. The product of this enzymatic reaction produces a distinct yellow color that absorbs at 405 nm. The intensity of this color, determined spectrophotometrically, is proportional to the amount of PG tracer bound to the well, which is inversely proportional to the

amount of PGs present in the well during the incubation: Absorbance ∝ [Bound PG Tracer] ∝ 1/PGs. The percent inhibition was calculated by comparison of compound-treated to various control incubations. The concentration of the test compound causing 50% inhibition (IC_{50}, μM) was calculated from the concentration-inhibition response curve (duplicate determinations). The validity of this *in vitro* COX-1/COX-2 inhibition assay was demonstrated using celecoxib (**17**, Celebrex®) as a reference drug where it gave values (COX-1 IC_{50} = 22.9 μM; COX-2 IC_{50} = 0.0567 μM; SI = 404) close to those previously reported (COX-1 IC_{50} = 15 μM; COX-2 IC_{50} = 0.04 μM; SI = 375) (Penning et al., 1997).

4.5 Molecular Modeling Study.

4.5.1 Docking Study.

The coordinates from the X-ray crystal structure of COX-1 and COX-2 used in this simulation were obtained from the Protein Data Bank (PDB) (1CQE and 1CX2, respectively). The MM3 or PM3 optimized structures of ligands studied were subjected to molecular dynamics simulation using Alchemy 200 program at 300K over a 1 fs. *per* step for 1 ps. The lowest energy conformation was manually docked in the COX-1 or COX-2 active site using the Insight II program. In order to relieve any unfavorable side chain overlaps and non-bond energies introduced in the model structure, the measure/ bump command was used. Subsets of the enzyme were defined allowing residues within 10 Å to relax, whereas all other residues were fixed. The affinity command in the docking module was used to complete the docking experiment. Minimization of the ligand-active site assembly was performed to reach a convergence of 0.01 Kcal/mol using the steepest descent method followed by conjugate gradient to reach a final convergence

of 0.001 Kcal/mol. The CVFF force field was used in the docking experiment , except for the azido analogues of celecoxib **54** and **57** and rofecoxib **61**, where the ESFF force field was used. The intermolecular energy of the ligand-active site (assembly) was used to evaluate the quality of the docking.

4.5.2 Comparative Molecular Volume Study.

The molecular volume of compounds **32m** and **50h** calculated using the Insight II (Search and Compare module) were compared to the mean molecular volume of the training set shown in Table **41**, to deduce the difference required to enhance the selective COX-2 inhibition properties of either **32m** or **50h**.

4.5.3 Conformational Analysis.

Different conformations of compounds **36** and **48a-b** were studied by changing the dihedral angles between the aryl rings in the *cis*-stilbene like structure and the isoxazole ring using 100 steps with 3.6° each step. The energy of each conformation calculated using the MM3 force field in Cache (v. 4.4) from Fujitsu (Beaverton, OR) was plotted against the dihedral angles in a rigid map.

4.5.4 Quantitative structure Activity Relationship (QSAR).

The test compounds structures were geometrically optimized in Alchemy 2000 using MM3 set to RMS gradient = 1 Kcal/Å mol and a delta of energy = 0.001 1 Kcal/Å mol. The optimized structures were then used to calculate the regression equation for QSAR using SCIQSAR program version 3 (developed by SciVision Inc.) and Cache (v. 4.4) from Fujitsu (Beaverton, OR).

5.0 Conclusions.

The results of this thesis research has led to the structure-based design of novel selective COX-2 inhibitors, which are orally active AI and analgesic agents.

The potency and selectivity exhibited by compounds **36**, **42**, **44**, **50j-k**, **57** and **61** were dependent upon a number of factors.

First, although a $MeSO_2$ pharmacophore is essential for both potent and selective COX-2 inhibition, it was not the only requirement, since isoxazoles **32m-p** contained the $MeSO_2$ pharmacophore, but showed no selectivity towards the COX-2 isozyme (SI = 0.012-2.1).

Second, the nature and size of the central ring substituent were found to play a crucial role in enhancing selective COX-2 inhibition. A central ring CF_3 substituent that is present in isoxazole **36** undergoes *H*-bonding with residues lining the primary channel, particularly Arg^{120}. This phenomenon was not observed with isoxazoles **48a-b**, which have a central ring methyl substituent.

Third, the $MeSO_2$ pharmacophore and the CF_3 central ring substituent acted cooperatively to properly orient the position of the inhibitor in the COX-2 active site. Although compounds **36** and **42** each contain a $MeSO_2$ pharmacophore and CF_3 central ring substituent, the isoxazole **36** was greater than 200 times more potent and more than 400 times more selective (COX-2 IC_{50} = <0.001 μM, SI = 500,000) than its regioisomer **42** (COX-2 IC_{50} = 0.233 μM, SI = 1,122). These differences are attributed to the relative position of the 4-$MeSO_2$Ph ring relative to the CF_3 group.

Four, the volume of the inhibitor played an unambiguous role in inducing selectivity. This was attributed to the larger volume of the COX-2 active site compared to that of

COX-1. This volume effect was clearly manifested by the higher inhibitory potency for isoxazolines **50j-k** (volume 291.5 and 287.7 $Å^3$, COX-2 IC_{50} = 0.031 and 0.004 μM, respectively) towards COX-2 compared to their isoxazole precursors **48a** and **48c** (volume 270.1 and 287.7 $Å^3$, COX-2 IC_{50} >100, respectively).

Five, replacement of the H_2NSO_2 and $MeSO_2$ pharmacophores in celecoxib and rofecoxib, respectively (COX-2 IC_{50} = 0.059 μM and SI = 404, COX-2 IC_{50} = 0.34 μM and SI = 76.5, respectively) with the dipolar azido group as in compounds **57** and **61** (COX-2 IC_{50} = 1.55 μM and SI = 64.55, COX-2 IC_{50} = 0.19 μM and SI = 812.4, respectively) was found to preserve both the inhibitory potency and selectivity towards COX-2. The efficacy of this new azido pharmacophore is attributed to its electrostatic interaction with residues lining the secondary pocket of COX-2, particularly Arg^{513}.

Six, a QSAR study showed that the theoretical (computer-calculated) binding energies calculated for COX-2 inhibitors correlate well with experimental enzyme inhibition data. Accordingly, molecular modeling experiments provided useful methodologies to design and optimize COX-2 inhibitory potency and selectivity.

6.0 References.

Abdulla R, Fuhr K (**1978**). An efficient conversion of ketones to α,β-unsaturated ketones. *J. Org. Chem.* 43: 4248-4250.

Ajay, Murcko MA (**1995**). Computational methods to predict binding free energy in ligand receptor complexes. *J. Med. Chem.* 38: 4953-4967.

Almansa C, De Arriba AF, Caval Canti FL, Gómez LA, Miraalles A, Merlos M, Garcia-Rafanell J, Forn J (**2001**). Synthesis and SAR of new series of COX-2 selective inhibitors: Pyrazolo[1,5-*a*]pyrimidines. *J. Med. Chem.* 44: 350-361.

Amin AR, Vyas P, Attur M, Leszczynska-Piziak J, Patel IR, Weissmann G, Abramson SB (**1995**). The mode of action of aspirin-like drugs: Effect on inducible nitric oxide synthase. *Proc. Natl. Acad. Sci. USA* 92: 7926-7930.

Anderson GD, Hauser SD, Bremer ME, McGarity KL, Isakson PC, Gregory SA (**1996**). Selective inhibition of cyclooxygenase-2 reverses inflammation and expression of COX-2 and IL-6 in rat adjuvant arthritis. *J. Clin. Invest.* 97: 2672-2679.

Andrews PR, Tintelnat M (**1990**). Intermolecular forces and molecular binding. In *Comprehensive Medicinal Chemistry*; Hansch C, Sammes PG, and Taylor JB (Eds.); Pergamon Press, Oxford, Vol. 4, pp 321-348.

Appleby SB, Ristimaki A, Neilson K, Narko K, Hla T (**1994**). Structure of the human cyclooxygenase-2 gene. *Biochem. J.* 302: 723-727.

Arthritis Society of Canada. www.arthritis.ca/can/

Balsinde J, Balboa MA, Insel PA, Dennis EA (**1999**). Regulation and inhibition of phospholipase A_2. *Ann. Rev. Pharmacol. Toxicol.* 39: 175-189.

Barta TE, Stealey MA, Collins PW, Weier RM (**1998**). Antiinflammatory 4,5-diarylimidozoles as selective cyclooxygenase inhibitors. *Biorg. Med. Chem. Lett.* **8**: 3443-3448.

Batt DG, Pint DJP, Orwat MJ, Petraitis JY (**1996**). Novel prostaglandin synthase inhibitors. *World Patent* **WO 96 10012**.

Bauer MK, Lieb K, Schulze-Osthoff, Berger M, Gebicke-Haerter PJ, Bauer J, Fiebich BL (**1997**). Expression and regulation of cyclooxygenase-2 in rat microglia. *Eur. J. Biochem.* 243: 726-731.

Bayly CI, Black C, Leger S, Ouimet N, Ouellet M, Percival MD (**1999**). Structure-based design of COX-2 selectivity into flurbiprofen. *Biorg. Med. Chem. Lett.* 9:307-312.

Benhamou CL (**1990**). Large-scale open trials with etodolac (Lodine^{R}) in France: An assessment of safety. *Rheumatol. Int.* 10 (Suppl): 29-34 (Abstract).

Bensen WG, Fiechtner JJ, McMillen JI, Zhau WW, Yu SS, Woods EM, Hubbard RC, Isakson PC, Verburg KM, Geis GS (**1999**). Treatment of osteoarthritis with celecoxib, a cyclooxygenase-2 inhibitor, a randomized controlled trial. *Mayo Clin. Proc.* 74: 1095-1105.

Boder NS, Gabanyi Z, Wong C-K (**1989**). A new method for the estimation of partition coefficient. *J. Am. Chem. Soc.* 111: 3783-3786.

Bresnihan B, Alvaro-Garcia JM, Cobby M, Doherty M, Domljan Z, Emery P, Nuki G, Pavelka K, Rau R, Rozman B, Watt I, Williams B, Aitchison R, McCabe D, Musikic P (**1998**). Treatment of rheumatoid arthritis with recombinant human interleukin-1 receptor antagonist. *Arth. Rheum.* 41: 2196-2204.

Beswick PJ, Campbell IB, Naylor A **(1996)**. Imidazo[1,2-a]pyridine derivatives. *World Patent* **WO 96 31509**.

Blain H, Jouzeau JY, Blain A, Terlain B, Trechot P, Touchon J, Netter P, Jeandel C **(2000)**. Nonsteroidal antiinflammatory drugs with selectivity for cyclooxygenase-2 in Alzheimer's disease. Rationale & Perspectives. *Press Medical* 29: 267-73 (Abstract).

Borne RF **(1995)**. Nonsteroidal antiinflammatory drugs. In *Principles of Medicinal Chemistry*, 4th ed.; Foye WO, Lemke TL, and Williams DA (Eds.); Williams and Wilkins, Baltimore, pp 570-574.

Bottomley KM, Johnson WH, Walter DS **(1998)**. Matrix metalloproteinase inhibitors in arthritis. *J. Enzyme Inhibit.* 13: 79-101.

Brideau C, Kargman S, Liu S, Dallob AL, Ehrich EW, Rodger IW, Chan CC **(1996)**. A human whole blood assay for clinical evaluation of biochemical efficacy of cyclooxygenase inhibitors. *Inflamm. Res.* 45: 68-74.

Brooks BR, Bruccoleri RE, Olafson BD, States DJ, Swaminathan S, Karplus M **(1983)**. CHARMM: a program of macromolecular energy minimization, and dynamics calculations. *J. Comput. Chem.* 4: 187-217.

Buolamwini JK, Knaus EE **(1990)**. Synthesis and antinociceptive activity of 4-pyridyl and –dihydropyridyl analogues of meperidine and ketobemidone. *Drug Design Del.* 7: 19-31.

Burkert U, Allinger NL **(1982)**. Molecular Mechanics; American Chemical Society; Washington D.C., pp 1-75.

Burton G, Clarke GJ, Douglas JD, Eglington AJ, Frydrych CH, Hinks JD, Hird NW, Hunt E, Mass SF, Naylor A, Nicholson NH, Pearson MJ **(1996)**. Novel C-2

substituted carbapenem derivatives. Part II. Synthesis and structure activity relationships of isoxazoline-2-yl, isoxazolidine-2-yl and pyrazolin-2-yl carbapenems generated using 1,3-dipolarcycloaddition chemistry. *J. Antibiot.* 49: 1266-1274 (Abs.).

Carter JS, Rogier DJ, Graneto MJ, Seibert K, Koboldt CM, Zhang Y, Talley JJ **(1999)**. Design and synthesis of sulfonyl-substituted 4,5-diarylthiazoles as selective cyclooxygenase-2 inhibitors. *Biorg. Med. Chem. Lett.* 9: 1167-1170.

Chaki H, Kuroda H, Makino S, Mitta J, Tanaka K, Inaba T (1996). 2,3-substituted pyridines for the treatment of inflammation. *World Patent* **WO 96 24584**.

Chan CC, Boyce S, Brideau C, Charleson S, Cromlish W, Ethier D, Evans J, Ford-Hutchinson AW, Forrest MJ, Gauthier JY, Gordon R, Gresser M, Guay J, Kargman S, Kennedy B, Leblanc Y, Leger S, Mancini J, O'Neill GP, Ouellet M, Patrick D, Percival MD, Perrier H, Prasit P, Rodger I et al. **(1999)**. Rofecoxib [Vioxx, MK-0966; 4-(4′-methylsulfonylphenyl)-3-phenyl-2-(5H)-furanone]: A potent and orally active cyclooxygenase-2 inhibitor. Pharmacological and biochemical profiles. *J. Pharm. Exp. Therap.* 290: 551-560.

Charifson PS, Corkey JJ, Murcko MA, Walters WP **(1999)**. Consensus scoring: A method for obtaining improved hit rates from docking databases of 3-D structures into proteins. *J. Med. Chem.* 42: 5100-5109.

Chiara JL, Gomez-Sánchez A **(1994)**. NMR spectra. In *The Chemistry of Enamines*; Rappoport Z (ed.); John Wiley and Sons, Chichester, pp 325-365.

Clark T **(1985)**. A Handbook of Computational Chemistry, Wiley-Interscience, New York, pp 1-332.

Clark RD, Leonard JM, Stzizhev A (**2000**). Pharmacophore modes and comparative molecular field analysis (CoMFA). In *Pharmacophore, Perception, Development and Use in Drug Design*; Güner OF (Ed.); International University Line, La Jolla, pp. 151-170.

Cohn J (**1994**). Zileuton (A-64077): A 5-Lipoxygenase Inhibitor. In *Nonsteroidal Anti-Inflammatory Drugs*; Lewis AJ, and Furst DE (Eds.); Marcel-Dekker, NewYork; pp 367-390

Copeland RA, Williams JM, Giannaras J, Nurnberg S, Covington M, Pinto D, Pick S, Trzaskos JM (**1994**). Mechanism of selective inhibition of the inducible isoform of prostaglandin G/H synthase. *Proc. Natl. Acad. Sci. (U.S.A.)* 91: 11202-11206.

Cramer RD 3rd, Snader KM, Willis CR, Chakrin LW, Thomas J, Sutton BM (**1979**). Application of quantitative structure-activity relationships in the development of the antiallergic pyranenamines. *J. Med. Chem.* 22: 714-25.

Cramer RD, Patterson DE, Bunce JD (**1988**). Comparative molecular field analysis (CoMFA). Effect of shape on binding of steroids to carrier proteins. *J. Am. Chem. Soc.* 110: 5959-5967.

Crankshaw DJ, Dyal R (**1994**). Effects of some naturally occurring prostanoids and some cyclooxygenase inhibitors on the contractillity of the human uterine segment *in vitro*. *Can. J. Physiol. Pharmacol.* 72: 870-874.

Cryer B, Feldman M (**1998**). Cyclooxygenase-1 and cyclooxygenase-2 selectivity of widely used nonsteroidal antiinflammatory drugs. *Am. J. Med.* 104: 413-421.

Dabrowski J, Kamienska-Trela K, Kozeishi L (**1974**). Conformation studies by nuclear magnetic resonance. VII- The direct observation of rotational isomers in some

enamino carbonyl compounds and their derivatives by carbon magnetic resonance. *Org. Mag. Res.* 6: 499-502.

Davis R, Brogden RN **(1994)**. Nimesulide: An update on its pharmacodynamic and pharmacokinetic properties, and therapeutic efficacy. *Drugs* 48: 431-454.

Dawson W, Willoughby DA **(1985)**. Inflammation mechanisms and mediators. In *Nonsteroidal Antiinflammatory Drugs*; Lombardino JG (Ed.); John Wiley & Sons, New York, pp 1-75.

Day R, Morrison B, Luza A, Castaneda O, Strusberg A, Nahir M, Helgetveit KB, Kress B, Daniels B, Bolognese J, Krupa D, Seidenberg B, Ehrich E **(2000)**. A randomized trial of the efficacy and tolerability of the COX-2 inhibitor rofecoxib and ibuprofen in patients with osteoarthritis. Rofecoxib/Ibuprofen comparator study group. *Arch. Intern. Med.* 160: 1781-1787.

Diaz-Gonzalez F, Sanchez-Madrid F **(1998)**. Inhibition of leukocyte adhesion: An alternative mechanism of action for antiinflammatory drugs. *Immunology Today* 19:169-172.

Dietz R, Nastainczyk W, Ruf HH **(1988)**. Higher oxidation states of prostaglandin H synthase. Rapid electronic spectroscopy detected two spectral intermediates during the peroxidase reaction with prostaglandin G2. *Eur. J. Biochem.* 171: 321-8.

Dingle JT **(1991)**. Cartilage maintenance in osteoarthritis: Interaction of cytokines, NSAIDs, and prostaglandins in particular cartilage damage and repair. *J. Rheumatol.* 18 (suppl. 28): 30-37.

Dinur U, Haglar AT **(1991)**. New approaches to empirical force fields. In *Reviews in Computational Chem.*; Lipkowitz KB, and Boyd DB (Eds.); Weinchaim, Hanover, Vol. 2, pp 1-76.

Dominguez E, Martinez de Marigorta E, San Martin R, Olivera P **(1995)**. A short and efficient synthesis of 4,5-diarylpyrimidines. *Synlett* 955-956.

Dominguez E, Ibeas E, Martinez de Marigorta M, Palacious JK, SanMartin R **(1996)**. A convenient one-pot preparative method for 4,5-diarylisoxazoles involving amine exchange reactions. *J. Org. Chem.* 61: 5435-5439.

DuBois RN **(1995)**. Nonsteroidal antiinflammatory drug use and sporadic colorectal adenomas. *Gastroentrology* 108: 1310-1314.

Ducharme Y, Gauthier JY, Prasit P, Leblanc Y, Wang Z, Leger S, Thirien M **(1995)**. Phenyl heterocycles as cyclooxygenase-2 inhibitors. *World Patent* **WO 95/00501**.

Eberhart CE, Coffey RJ, Radhika A, Giardiello FM, Ferrenbach S, DuBois RN **(1994)**. Up regulation of cyclooxygenase-2 gene expression in human colorectal adenomas and adenocarcinomas. *Gastroentrology* 107: 1183-1188.

Emery P, Zeidler H, Kvien TK, Guslandi M, Naudin R, Stead H, Verburg KM, Isakson PC, Hubbard RC, Geis GS **(1999)**. Celecoxib versus diclofenac in long-term management of RA: Randomized double blend comparison. *Lancet* 354: 2106-2111.

Ewing JA, Kuntz ID **(1997)**. Critical evaluation of search algorithms for automated molecular docking and data base algorithms. *J. Comput. Chem.* 18: 1175-1189.

Filizolá M, Pérez JJ, Palomer A, Mauleon D **(1997)**. Comparative molecular modeling study of the three dimensional structures of prostaglandin endoperoxide H2 synthase 1 and 2 (COX-2 & COX-2). *J. Mol. Graph.* 15: 290-300.

Fletcher BS, Kubuju DA, Perrin DM, Herschman HR **(1992)**. Structure of the mitogen-inducible TIS10 gene and demonstration that the TIS10-encoded protein is a functional prostaglandin G/H synthase. *J. Biol. Chem.* 267: 4338-4344.

Friesen RW, Dube D, Fortin R, Frenette R, Prescott S, Cromlish W, Greig GM, Kargman S, Wong E, Chan CC, Gordon R, Xu LJ, Riendeau D **(1998)**. Novel 1,2-diaryl cyclobutenes. Selective and orally active COX-2 inhibitors. *Biorg. Med. Chem. Lett.* 6: 2677-2682.

Fujita T **(1997)**. Recent success stories leading to commercializable bioactive compounds with the aid of traditional QSAR procedures. *Quant. Struct. Act. Relat.* 16: 107-112.

Fukawa K, Kawano O, Hibi M, Misaka N, Ohba S, Hatanaka A **(1980)**. Method for evaluating analgesic agents in rats. *J. Pharmacol. Methods* 4: 251-259.

Funasaka W, Ando T **(1959)**. Organic fluorine compounds. I. Tris-(*p*-fluorophenyl)ethylene and tris-(*m*-fluoro-*p*-methoxyphenyl)ethylene. *Yuki Gosei Kagaku Kuokaishi* 17: 334-338; (Chem. Abstr. 53: 17970d).

Futaki N, Yoshikawa K, Hamasaka Y, Arai I, Higuchi S, Iizuka H, Otomo S **(1993)**. NS-398, a novel nonsteroidal antiinflammatory drug with potent analgesic and antipyretic effects which causes minimal stomach lesions. *Gen. Pharmacol.* 24: 105-110.

Gans KR, Galbraith W, Roman RJ, Haber SB, Kerr JS, Schmidt W, Smith C, Hewes WE, Ackerman NR **(1990)**. Antiinflammatory and safety profile of DuP 697, a novel orally effective prostaglandin synthesis inhibitor. *J. Pharmacol. Exp. Ther.* 254: 180-187

Garavito RM **(1996)**. The cyclooxygenase-2 structure. New Drugs for an old target. *Nature Str. Biol.* 3: 897-901.

Garavito RM, DeWitt DL (**1999**). The cyclooxygenase isoforms: Structural insights into the conversion of arachidonic acid to prostaglandins. *Biochem. Biophys. Acta* 1441: 278-287.

Garcia-Rodriguez LA, Cattaruzzi, Troncon MG, Agostinis L (**1998**). Risk of hospitalization for upper gastrointestinal tract bleeding associated with Ketorolac, other nonsteroidal antiinflammatory drugs, calcium antagonists and other anti-hypertension drugs. *Arch. Intern. Med.* 158: 33-39.

Gawronski J (**1989**). Spectral properties of enones. In *The Chemistry of Enones*; Patai S, Rappoport Z (Eds); John Wiley and Sons, Chichester, pp 61-65.

Gierse JK, Hauser SD, Creely DP, Koboldt C, Rangwala SH, Isakson PC, Seibert K (**1995**). Expression and selective inhibition of the constitutive and inducible forms of human cyclooxygenase. *Biochem. J.* 305: 479-84.

Gierse JK, McDonald JJ, Hauser SD, Rangwala S, Koboldt CM, Seibert K (**1996**). A single amino acid difference between cyclooxygenase-1 (COX-1) and -2 (COX-2) reverses the selectivity of COX-2 specific inhibitors. *J. Biol. Chem.* 271: 15810-15814.

Goda H, Sato M, Ihara H, Hirayama C (**1992**). Facile synthesis of 5-substituted 2-acetylthiophenes. *Synthesis* 849-851.

Goldstein JL, Silverstein FE, Agrawal NM, Hubbard RC, Kaiser J, Maurath CJ, Verburg KM, Geis GS (**2000**). Reduced risk of upper gastrointestinal ulcer complications with celecoxib, a novel COX-2 inhibitor. *Am. J. Gastro.* 95: 1681-1690.

Good AC, So SS, Richards WG (**1993**). Structure-activity relationships from molecular similarity matrices. *J. Med. Chem.* 36: 433-438.

Graham DY, Smith JL, Holmes GI, Davies RO **(1985)**. Nonsteroidal antiinflammatory effect of sulindac sulfoxide and sulfide on gastric mucosa. *Clin. Pharmacol. Ther.* 38: 65-70.

Greenhill JV **(1977)**. Enaminones. *Chem. Soc. Rev.* 6: 277- 294.

Grünanger P, Vita-Finzi P **(1991)**. Isoxazoles-Part 1. In *The Chemistry of Heterocyclic Compounds*; Taylor EC (Ed.); John Wiley and Sons, New York, pp 126-182.

Grünanger P, Vita-Finzi P **(1991a)**. Isoxazolines (dihydroisoxazoles). In *Isoxazoles*-Part 1; Taylor EC (Ed.); John Wiley and Sons, New York, pp 638-640.

Grünanger P, Vita-Finzi P **(1991b)**. Isoxazolines (dihydroisoxazoles). In *Isoxazoles*-Part 1; Taylor EC (Ed.); John Wiley and Sons, New York, pp 265-273.

Habib A, Creminon C, Frobert Y, Grassi J, Prodelles P, Maclouf J **(1993)**. Demonstration of an inducible cyclooxygenase in human endothelial cells using antibodies raised against the carboxyl terminal region of the cyclooxygenase-2. *J. Biol. Chem.* 268, 23448-23454.

Hadjipavlou-Litina D **(2000)**. Quantitative structure-activity relationship (QSAR) studies on nonsteroidal antiinflammatory drugs (NSAIDs). *Curr. Med. Chem.* 7: 375-388.

Hahn M, Rogers D **(1995)**. Receptors surface models 2. Applications to quantitative structure-activity relationships studies. *J. Med. Chem.* 38: 2091-2102.

Hall IH, Izydore RA, Zhou X, Daniels DL, Woodward T, Debnath ML, Tse E, Muhammad RA **(1997)**. Synthesis and cytotoxic action of 3,5-isoxazolidinediones and 2-isoxazolin-5-ones in murine and human tissues. *Arch. Pharm.* 330: 67-73 (Abs.).

Hansch C **(1971)**. Quantitative structure activity relationships in Drug Design; Ariens EJ (Ed.); Academic Press, New York, Vol. 1, pp 271-342.

Hansch C, Leo A, Unger SH, Kim KH, Nkaitani D, Lien EJ **(1973)**. Aromatic substituent constants for structure activity correlations. *J. Med. Chem.* 16:1207-1216.

Hansch C **(1977)**. Quantitative structure activity relationships. In *Biological Activity and Chemical Structure*; Keverling B (Ed.); Elsevier, Amsterdam, pp 47-50.

Hansch C, Fujita T **(1964)**. P-σ-π-Analysis. A method for the correlation of biological activity and chemical structure. *J. Am. Chem. Soc.* 80: 1616-1620.

Hargreaves K, Dubner R, Brown F, Flores C, Joris J **(1988)**. A new and sensitive method for measuring thermal nociception in cutaneous hyperalgesia. *Pain* 32: 77-88.

Harris RC, McKanna JA, Akai Y, Jacobson HR, Dubois RN, Breyer MD **(1994)**. Cyclooxygenase-2 is associated with the macula densa of rat kidneys and increases with salt restriction. *J. Clin. Invest.* 94: 2504-2510.

Haruta J, Hashimoto H, Mitsushita M **(1996)**. Oxazole derivatives and use thereof. WO 96 19462.

Hawkey CJ **(1999)**. COX-2 Inhibitor. *Lancet* 353: 307-314.

Hayashi Y, Yano T, Yamamoto S **(1981)**. Enzyme immunoassay of $PGF_{2\alpha}$. *Biochem. Biophys. Acta* 663: 661-668.

Hayashi Y, Ueda N, Yakota K, Kawamura S, Ogushi F, Yamamoto Y, Yamamoto S, Nakamura K, Yamashita K, Miyazoki H, Kato K, Terao S **(1983)**. Enzyme immunoassay of thromboxane B_2. *Biochem. Biophys. Acta* 75: 322-329.

Hemler ME, Lands WE **(1980)**. Evidence for a peroxide-initiated free radical mechanism of prostoglandin biosynthesis. *J. Biol. Chem.* 255: 6253-6261.

Henkel JG, Billings EM (**1995**). Molecular modeling. In. *Principles of Medicinal Chemistry;* Foye WO, Lemke TL, and Williams DA (Eds.); Williams & Wilkings, Baltimore; pp 58-74.

Herschman HR (**1996**). Prostaglandin Synthase 2. *Biochem. Biophys. Acta* 1299: 125-40.

Hiroshima O, Hayoshi H, Ito S, Hayaishi O (**1986**). Basal level of prostaglandin D_2 in rat brain by a solid phase enzyme immunoassay. *Prostaglandins* 32: 63-80.

Hoftiezer JW, Silvoso GR, Burks M, Ivey KJ (**1980**). Comparison of the effects of regular and enteric-coated aspirin on gastroduodenal mucosa of man. *Lancet* 2(8195 part 1): 609-612 (Abstract).

Horsanyi K, Takacs K, Horvath K (**1974**). Dehydrierung eines β-hydroxylamino-amidoxims mit azodicarbonsäureester. *Chem. Ber.* 107: 2569-2577.

Huang HC, Chamberlain TS, Seibert K, Koboldt CM, Isakson PC, Reitz DB (**1995**). Diarylindenes and benzofurans: Novel classes of potent and selective COX-2 inhibitors. *Biorg. Med. Chem. Lett.* 5: 2377-2380.

Hüll M, Fiebich BL, Schumann G, Lieb K, Bauer J (**1999**). Antiinflammatory substances a new therapeutic option in Alzheimer's disease. *Drug Discovery Today* 4: 275-282.

Jackson DY, Quan C, Artis DR, Rawson T, Blackburn B, Struble M, Fitzgerald G, Chan K, Mullins S, Burnier JP, Fairbrother WJ, Clark K, Berisini M, Chui H, Renz M, Jones S, Feng S (**1997**). Potent α4B1 peptide antagonists as potential anti-inflammatory agents. *J. Med. Chem.* 40:3359-3368.

Jain AN, Koila K, Chapman D (**1994**). Compass: predicting biological activities from molecular surface properties. Performance comparisons on a steroid benchmark. *J. Med. Chem.* 37: 2315-2327.

Jenner PN **(1990)**. A 12 month post marketing surveillance study of nabumetone. A preliminary report. *Drugs* 40 (Suppl 5): 80-86 (Abstract).

Jones G, Willet P, Glen RC **(1995)**. Molecular recognition of a receptor site using a genetic algorithm with a description of desolvation. *J. Mol. Biol.* 245:43-53.

Jones G, Willet P, Glen RC, Leach AR, Taylor R **(1997)**. Development and validation of a genetic algorithm for flexible docking. *J. Mol. Biol.* 267: 727-748.

Jouzeau JY, Terlain B, Abid A, Nedelec E, Netter P **(1997)**. Cyclooxygenase isoenzymes. How recent findings affect thinking about nonsteroidal antiinflammatory drugs. *Drugs* 53: 563-582.

Kalgutkar AS, Kozak KR, Crews BC, Hochgesang GP, Marnett LJ **(1998)**. Covalent modification of cyclooxygenase-2 (COX-2) by acetoxyphenyl alkyl sulfides, a new class of selective COX-2 inactivators. *J. Med. Chem.* 41: 4800-4818.

Kalgutkar AS, Crews BC, Rowlinson SW, Marnett AB, Kozak KR, Remmel RP, Marnett LJ **(2000)**. Biochemical based design of cyclooxygenase-2 (COX-2) inhibitors: Facile conversion of nonsteroidal antiinflammatory drugs to potent and highly selective COX-2 inhibitors. *Proc. Natl. Acad. Sci. U.S.A.* 97: 925-930.

Katritzky AR, Gordeeva EV **(1993)**. Traditional topological indices vs. electron, geometrical and combined molecular descriptors in QSAR/QSPR research. *J. Chem. Inf. Comput. Sci.* 33: 835-857.

Kawamori T, Rao CV, Seibert K, Reddy BS **(1998)**. Chemopreventive activity of celecoxib, a specific cyclooxygenase-2 inhibitor, against colon carcinogenesis. *Cancer Res.* 58: 409-412.

Khanna IK, Weier RM, Yu Y, Collins PW, Miyashiro JM, Koboldt CM, Veenhuizen AW, Currie JL, Seibert K, Isakson PC (**1997**). 1,2-Diarylpyrroles as potent and selective inhibitors of cyclooxygenase-2. *J. Med. Chem.* 40: 1619-1633.

Kier LB, Hall LH (**1986**). *Molecular Connectivity in Structure Activity Analysis, Chemometrics Series*; Research Studies Press Ltd., Wiley, New York, Vol. 9, pp 1-150.

Kim PR, Carlson KE, Katzenellenbogen JA (**1993**). Progestin 16 alpha, 17 alpha-dioxolane ketals as molecular probes for the progesterone receptor: Synthesis, binding affinity, and photochemical evaluation. *J. Med. Chem.* 36:1111-1119.

Klebe G, Abraham U, Mietzner T (**1994**). Molecular similarity indices in a comparative analysis (CoMSIA) of drug molecules to correlate and predict their biological activity. *J. Med. Chem.* 37: 4130-4146.

Klein T, Nusing RM, Pfeilschifter J, Ullrich V (**1994**). Selective inhibition of cyclooxygenase 2. *Biochem. Pharmacol.* 48: 1605-1610.

Kothekar V, Sahi S, Srinivasan M (**1999**). Computer simulation of the interaction of non-steroidal antiinflammatory drugs: Indoprofen and NS-398 with cyclooxygenase. *J. Biomol. Struct. Dyn.* 16: 901-915.

Kraemer SA, Meade EA, DeWitt DL (**1992**). Prostaglandin endoperoxide synthase gene structure: Identification of the transcriptional start site end 5'-flanking regulatory sequences. *Arch. Biochem. Biophys.* 293: 391-400.

Kuchar M, Maturova E, Brunova B, Grimova J, Timkova H, Holubek KJ (**1988**). Quantitative relations between structure and antiinflammatory activity of aryloxoalkanoic acids. *Coll. Czech. Chem. Comm.* 53: 1862-1872.

Kulmacz RJ, Lands WE (**1985**). Stoichiometry and kinetics of the interaction of prostaglandin H synthase. *J. Biol. Chem.* 260: 12572-1578.

Kuntz ID, Meng EC, Shoichet BK (**1994**). Structure based molecular design. *Acc. Chem. Res.* 27: 117-123.

Kurose I, Wolfe R, Miyasaka M, Anderson DC, Granger DN (**1996**). Microvascular dysfunction induced by nonsteroidal antiinflammatory drugs: Role of leukocytes. *Am. J. Physiol.* 270: G363-369 (abstract).

Kurumbail RG, Stevens AM, Gierse JK, McDonald JJ, Stegeman RA, Pak JY, Gildehaus D, Miyashiro JM, Penning TD, Seibert K, Isakson PC, Stallings WC (**1996**). Structural basis for selective inhibition of cyclooxygenase-2 by antiinflammatory agents. *Nature* 384: 644-648.

Laneuville O, Breuer DK, Xu N, Huang ZH, Gage DA, Watson JT, Lagarde M, DeWitt DL, Smith WL (**1995**). Fatty acid substrate specificities 12-hydroxy-(9Z, 13E/Z, 15Z)-octadecatrienoic acids from alpha-linolenic acid. *J. Biol. Chem.* 270: 19330-6.

Langenbach R, Morham SG, Tiano HF, Loftin CD, Ghanayem BI, Chulada PC, Mahler JF, Lee CA, Goulding EH, Kluckman KD, Ledford A, Lee CA et al., (**1995**). Prostaglandin synthase 2 gene disruption causes severe renal pathology in the mouse. *Cell* 83: 473-482.

Langman MJ, Jensen DM, Watson DJ, Harper SE, Zhao PL, Quan H, Bolognese JA, Simon TJ (**1999**). Adverse upper gastrointestinal effects of Rofecoxib compared with NSAIDs. *JAMA* 282: 1929-1933.

Lanza FL, Rack MF, Callison DA, Hubbard RC, Yu SS, Talwalker S, Geis GS (**1997**). A pilot endoscopic study of the gastroduodenal effects of SC 58635, a novel COX-2 selective inhibitor. *Dig. Dis. Week* (May 10-16, 1997 Washington DC) Abstract 400.

Lau CK, Black WC, Bayly C, Belley M, Chan C, Charleson S, Denis D, Gauthier JY, Gordon R, Guay D, Hamel P, Kargman S, Leblanc Y, Mancini J, Ouellet M, Percival D, Prasit P Roy P, Skorey K, Tagarey R, Vickers P, Wong E (**1996**). From indomethacin to a selective COX-2 inhibitor: Development of indolalkanoic acid as potent and selective COX-2 inhibitors. *Biorg. Med. Chem. Lett.* 6: 725-730.

Leach AR (**1994**). Ligand docking to proteins with discrete side chain flexibility. *J. Mol. Biol.* 235: 345-356.

Leblanc Y, Gauthier JY, Ethier D, Guay J, Mancini J, Riendeau D, Tagari P, Vickers P, Wong E, Prasit P (**1995**). Synthesis and biological evaluation of 2,3-diarylthiophenes as selective COX-2 and COX-1 inhibitors. *Biorg. Med. Chem. Lett.* 5: 2123-2128.

Leblanc Y, Black WC, Chan CC, Charleson S, Delorme D, Denis D, Gauthier JY, Grimm EL, Gordon R, Guay P, Hamel P, Kargman S, Lau CK, Mancini J, Ouellet M, Percival D, Roy D, Skorey K, Tagari P, Vickers E, Wong E, Xu L, Prasit P (**1996**). Synthesis and biological evaluation of both enantiomers of L-761,000 as inhibitors of cyclooxygenase-1 and 2. *Biorg. Med. Chem. Lett.* 6: 731-736.

LeComte M, Laneuville O, Ji C, DeWitt DL, Smith WL (**1994**). Acetylation of human prostaglandin endoperoxide synthase-2 (COX-2) by aspirin. *J. Biol. Chem.* 269: 13207-15.

Levitt M (**1983**). Molecular dynamics of native protein. II. Analysis and nature of motion. *J. Mol. Biol.* 168: 621-657.

Lewis AJ, Manning AM **(1999)**. New targets for antiinflammatory drugs. *Curr. Opin. Chem. Biol.* 3: 489-494.

Li JJ, Anderson GD, Burton EG, Cogburn JN, Collins JT, Garland DJ, Gregory SA, Huang HC, Isakson PC, Koboldt CM, Logusch EW, Norton DB **(1995)**. 1,2-Diarylcyclopentenes as selective cyclooxygenase-2 inhibitors and orally active anti-inflammatory agents. *J. Med. Chem.* 38: 4570-4578.

Li JJ, Norton MB, Reinhard EJ, Anderson GD, Gregory SA, Isakson PC, Koboldt CM, Masferrer JL, Perkins WE, Seibert K, Zhang Y, Zweifel BS, Reitz DB **(1996)**. Novel terphenyls as selective cyclooxygenase-2 inhibitors and orally active anti-inflammatory agents. *J. Med. Chem.* 39: 1846-1856.

Lii JH, Allinger NL **(1989)**. Molecular mechanics. The MM3 force field for hydrocarbon. 3. The van der Waals' potentials and the crystal data for aliphatic and aromatic hydrocarbons. *J. Am. Chem. Soc.* 111: 65-76.

Livingston R, Ramachandra Rao C **(1960).** An electron diffraction investigation of the molecular structure of methyl azide. *J. Phys. Chem.* 64: 756-759.

Llorens O, Perez JL, Palomer A, Mauleon D **(1999)**. Structural basis for dynamic mechanism of ligand binding to COX. *Biorg. Med. Chem. Lett.* 9: 2779-2784.

Luong C, Miller A, Barnett J, Chow J, Ramesha C, Browner MF **(1996)**. Flexibility of the NSAID binding site in the structure of human cyclooxygenase-2. *Nature Structural Biology* 3: 927-933.

Lipsky LP, Abramson SB, Crofford L, DuBois RN, Simon LS, van de Putte LB **(1998)**. The classification of cyclooxygenase inhibitors. *J. Rheumat.* 25: 2298-2303.

Lombardino JG **(1985)**. Medicinal chemistry of acidic NSAIDs. In *Nonsteroidal Anti-inflammatory drugs*; Lombadino JG (Ed.); John Wiley and Sons. New York, pp 387-390.

Mangold U, Dax CI, Soar K, Schwab W, Kirschbaum B, Mullner S **(1999)**. Identification and characterization of potential new therapeutic targets in inflammatory and autoimmune diseases. *Eur. J. Biochem.* 266: 1184-1191.

Mankin HJ **(1985)**. Normal articular cartilage and the alterations in osteoarthritis. In *Nonsteroidal Antiinflammatory Drugs*; Lombardino JG (Ed.); John Wiley & Sons, New York, pp 1-74.

Marshall GR **(1993)**. Binding-site modeling of unknown receptors. In *3D QSAR in Drug Design*; Kubinyi H; Leiden, The Netherlands, pp 80-116.

Martin YC, Holland JB, Jarboe CH, Plotnikoff N **(1974)**. Discriminant analysis of the relationship between physical properties and the inhibition of monoamine oxidase by aminotetralins and aminoindans. *J. Med. Chem.* 17: 409-413.

McAdam BF, Catella-Lawson F, Mardini IA, Kapoor S, Lawson JA, FitzGerald GA **(1999)**. Systemic biosynthesis of prostacyclin by cyclooxygenase (COX)-2: The human pharmacology of a selective inhibitor of COX-2. *Proc. Natl. Acad. Sci. U.S.A* 96: 272-277.

Meng EC, Shoichet BK, Kuntz ID **(1992)**. Automated docking with grid-based energy evaluation. *J. Comput. Chem.* 13: 505-524.

Miller DK, Sadowski S, DeSousa D, Maycock AL, Lombardo DL, Young RN, Hayes EC, **(1985)**. Development of enzyme-linked immunosorbent assays for measurement of leukotriene and prostaglandin. *J. Immunol. Methods* 81: 169-185.

Miller KJ (**1990**). Additivity methods in molecular polarizability. *J. Am. Chem. Soc.* 112: 8533-8542.

Miller MD, Keasley SK, Underwood DJ, Sheridan RP (**1995**). FLOG: a system to select quasi-flexible ligands complementary to a receptor of known three dimensional structure. *J. Comp. Aided Molec. Design* 8:153-524.

Mitsuda H, Yasumoto K, Yamamoto A (**1967**). Inhibition of lipoxygenase by saturated monohydric alcohols through hydrophobic bondings. *Arch. Biochem. Biophys.* 118: 664-669.

Miyamoto T, Ogino N, Yamamoto S, Hayaishi O (**1976**). Purification of prostaglandin endoperoxide synthase from bovine vesicular gland microsomes. *J. Biol. Chem.* 251: 2629-2636.

Mizuno K, Yamamoto S, Lands WE (**1982**). Effect of nonsteroidal antiinflammatory drugs on fatty acid cyclooxygenase and prostaglandin hydroperoxidase activities. *Prostaglandins* 23: 743-757.

Moreland LW, Baumgartner SW, Schiff MH, Tindall EA, Fleischmann RM, Weaver AL, Ettlinger RE, Cohen S, Koopman WJ, Mohler K, Widmer MB, Blosch CM (**1997**). Treatment of rheumatoid arthritis with a recombinant human tumor necrosis factor receptor (p-75)-F_c fusion protein. *New Engl. J. Med.* 337:141-147.

Morris GM, Goodsell DS, Huey R, Olson AJ (**1996**). Disturbed automated docking of flexible ligands to proteins: Parallel applications of Auto Dock 2.4. *J. Comput. Aided Mol. Design* 10: 293-304 (Abstract).

Murphy RC, Harper TW (**1985**). Mass spectrometry and icosanoid analysis. In: *Biochemistry of Arachidonic Acid Metabolism*; Martinus JJ and Nijhoft AI (Eds.); Kroeger Publishing, Boston, pp 417-434.

Murzin AG, Brenner SE, Hubbard T, Chothia C **(1995)**. SCOP: A structural classification of protein databases for the investigation of sequences and structures. *J. of Molecular Biology* 247: 536-540.

Nakaue HS, Caldwell RS, Buhler DR **(1972)**. Bisphenols: Uncouplers of phosphorylating respiration. *Biochem. Pharmacol.* 21: 2273-2277.

Noble S, Balfour JA **(1996)**. Meloxicam. *Drugs* 51: 424-432.

Newton RC, Decicco CD **(1999)**. Therapeutic potential and strategies for inhibiting tumor necrosis factor-α. *J. Med. Chem.* 42: 2295-2314.

O'Banion MK, Chang JW, Coleman PD **(1997)**. Decreased expression of prostaglandin G/H synthase-2 (PGHS-2) in Alzheimer's disease brain. *Adv. Exp. Med. Biol.* 407: 171-177 (Abstract).

Ogino N, Ohki S, Yamamoto S, Hayaishi O **(1978)**. Prostaglandin endoperoxide synthetase from bovine vesicular gland microsomes. Inactivation and activation by heme and other metallaporphyrins. *J. Biol. Chem.* 253: 5061-5068.

O'Neill GP, Mancini JA, Kargman S, Yergey J, Kwan MY, Falgueyret JP, Abramovitz M, Kennedy BP, Ouellet M, Cremlish W, et al. **(1994)**. Over expression of human prostaglandin G/H synthase-1 and-2 by recombinant vaccine virus: Inhibition by nonsteroidal antiinflammatory drugs and biosynthesis of 15-hydroxy eicosatetraenoic acid. *Mol. Pharmacol.* 45: 245-54 (Abstract).

O'Sullivan MG, Chilton FH, Huggins EM Jr., McCall CE **(1992)**. Lipopolysacharide priming of alveolar macrophages for enhanced synthesis of prostanoids involves induction of a novel prostaglandin H synthase. *J. Biol. Chem.* 267: 14547-14550.

Oschiro CM, Kuntz ID, Dixon JS **(1995)**. Flexible ligand docking using a genetic algorithm. *J. Comp. Aided Molec. Design.* 9:113-130.

Otto JC, DeWitt DL, Smith WL **(1993)**. N-glycosylation of prostaglandin endoperoxide synthases-1 and-2 and their orientations in the endoplasmic reticulum. *J. Biol. Chem.* 268: 18234-18242.

Otterness IG, and Bliven ML **(1985).** Laboratory models for testing nonsteroidal antiinflammatory drugs. In *Nonsteroidal Antiinflammatory Drugs*; Lambardino JG (Ed.); John Wiley & Sons, New York, pp 116-232.

Pairet M, Van Ryn J, Mauz A **(1997)**. Differential inhibition of COX-1 and COX-2 by NSAIDs: A summary of results obtained using various test systems. In *Selective COX-2 Inhibitors Pharmacology, Clinical effects and Therapeutic Potential*; Vane J, Botting J (Eds); Kluwer Academic Publishers, Dordrecht, pp 27-46.

Pairet M, Van Ryn J, Mauz A, Schierok H, Diederen W, Turck D, Engelhardt PG **(1998)**. Differential inhibition of COX-1 and COX-2 by NSAIDs: A summary of results obtained using various test systems. In *Selective Cyclooxygenase-2 Inhibitors: Pharmacology, Clinical Effects and Therapeutic Potential;* Vane J, Botting J (Eds.); Kluwer Academic, Dordrecht, pp 27-46.

Palmoski MJ, Brandt KD **(1983)**. Benoxaprofen stimulates proteoglycan synthesis in normal canine knee cartilage in vitro. *Arth. Rheum.* 26: 771-774.

Parnham MJ **(1996)**. Inflammation: Mechanisms and therapeutics. *Drug News Perspect* 9: 631-639.

Pathak D, Jindal DP **(1998)**. Synthesis and anti-inflammatory activity of steroidal isoxazoles. *Asian J. Chem.* 10: 813-817 (Abs.).

Patoia I, Santucci I, Furno P, Dionisi MS, Dell' Orso S, Romagnoli M, Sattarinia A, Marini MG (**1996**). A four week, double-blind, parallel-group study to compare the gastrointestinal effects of meloxicam 7.5 mg, meloxicam 15 mg, piroxicam 20 mg and placebo by means of focal blood loss, endoscopy and symptoms evaluation in healthy volunteer. *Br. J. Rheumatol.* 35: 61-67.

Pauling L, (**1960**). *The Nature of the Chemical Bond*, 3rd Ed., Cornell University Press, Ithaca, New York.

Penning TD, Talley JJ, Bertenshaw SR, Carter JS, Collins PW, Docter S, Graneto MJ, Lee LF, Malecha JW, Miyahiro JM, Rogers RS, Rogier DT, Yu SS, Anderson GD, Burton EG, Cogburn JN, Gregory SA, Koboldt CM, Perkins WE, Seibert K, Veenhuizen AW, Zhang YY, Isakson PC (**1997**). Synthesis and biological evaluation of the 1,5-diarylpyrazole class of cyclooxygenase-2 inhibitors: Identification of 4-[5-(4-methylphenyl)-3-(trifluoromethyl)-1*H*-pyrazol-1-yl)]benzenesulfonamide (SC58635, celecoxib). *J. Med. Chem.* 40: 1347-1365

Picot D, Loll PJ, Garavito RM (**1994**). The x-ray crystal structure of the membrane protein prostaglandin H_2-synthase-1. *Nature* 367: 243-249.

Prasit P, Wang Z, Brideau C, Chan CC, Charleson S, Cromlish W, Ethier D, Evans JF, Ford-Hutchiason AW, Gauthier JY, Gordon R, Guay J, Gresser M, Kargman S, Kennedy B, Leblanc Y, Leger S, Mancini J, O'Neill GP, Ouellet M, Percival MD, Perrier H, Riendeau D, Rodger J, Togari P, Therien M, Vickers P, Wong E, Xu LJ, Young RN, Zamboni R, Boyce S, Rupniak N, Forrest M, Visco D, Patrick D (**1999**). The discovery of refocoxib, [MK-966, Vioxx®, 4-(4'-methylsulfonylphenyl)-3-

phenyl-2(5H)-furanone], an orally active cyclooxygenase-2 inhibitor. *Biorg. Med. Chem. Letts.* 9: 1773-1778.

Puig C, Crspo MI, Godessart N, Feixas J, Ibarzo J, Jiménez JM, Soca L, Cardeliús I, Heredia A, Miralpeix M, Puig J, Beleta J, Huerta JM, Lopez M, Segarra V, Ryder H, Palacios JM (2000). Synthesis and biological evaluation of 3,4-diarylisoxazolones: A new class of orally active cyclooxygenase-2 inhibitors. *J. Med. Chem.* 43: 214-223.

Rarey M, Kramer B, Lengauer T (1997). Multiple automatic base selection: Protein-ligand docking based on incremental construction without manual intervention. *J. Comput. Aided Mol. Design* 11: 369-384.

Reitz DB, Li JJ, Norton MB, Reinhard EJ, Collins JT, Anderson GD, Gregory SA, Koboldt CM, Perkins WE, Seibert K, Isakson PC (1994). Selective cyclooxygenase inhibitors: Novel 1,2-diarylcyclopentenes are selective orally active COX-2 inhibitors. *J. Med. Chem.* 37: 3878-3881.

Reitz DB, Seibert K (1995). Selective cyclooxygenase inhibitors. *Ann. Rept. Med. Chem.* 30: 179-188.

Reitz DB, Huang HC, Li JL, Garland DJ, Manning RE, Anderson GD, Gregory SA, Koboldt CM, Perkins WE, Seibert K, Isakson PC (1995). Selective cyclooxygenase inhibitors: Novel 4-spiro-1,2-diarylcyclopentenes are potent and orally active COX-2 inhibitors. *Biorg. Med. Chem. Lett.* 5: 867-872.

Rome LH, Lands WE (1975). Structural requirements for time-dependent inhibition of prostaglandin biosynthesis by antiinflammatory drugs. *Proc. Natl. Acad. Sci. (U.S.A).* 72: 4863-4865.

Rufer C, Bahnlmann F, Schroder E, Bottcher I **(1982)**. Nictsteroidale Entziindungshemmer. 8. Entziingshemmerde methansulfonamide III (Non-steroidal antiinflammatory agents 8. Methansulfonamide III). *Eur. J. Med. Chem.* 17: 173-189.

Sahi, S.; Srinivasan, M.; Kothekar, V. **(2000).** 530 ps molecular dynamics simulation of indoprofen and NS-398 with COX-1 and COX-2. Study of perturbative changes in the complexes. *J. Mol. Struct. (Theochem)* 498: 133-148.

San Martin R, Martinez de Margiorta E, Dominguez E **(1994)**. A convenient alternative route to β-aminoketones. *Tetrahedron* 50: 2255-2264.

Singh RP, Cao G, Kirchmeier RL, Shreeve JM **(1999)**. Cesium fluoride catalysed trifluoromethylation of esters, aldehydes and ketones with (trifluoromethyl)trimethylsilane. *J. Org. Chem.* 64: 2873-2876.

Sano H, Hla T, Maier JA, Crofford LJ, Case JP, Maciag T, Wilder RL **(1992)**. *In vivo* cyclooxygenase expression in synovial tissues of patients with rheumatoid arthritis and osteoarthritis and rats with adjuvant and streptococcal arthritis. *J. Clin. Invest.* 89: 97-108.

Schmassmann A, Peskar BM, Stettler C, Netzer P, Stroff T, Flogerzi B, Halter F **(1998)**. Effects of inhibition of prostaglandin endoperoxide syntha · 2 in chronic gastrointestinal ulcer models in rats. *Brit. J. Pharmacol.* 123: 795-804.

Schneider C, Brash AR **(2000)**. Stereospecificity of hydrogen abstraction in the conversion of arachidonic acid to 15R-HETE by aspirin-treated cyclooxygenase-2. Implications for the alignment of substrate in the active site. *J. Biol. Chem.* 275: 4743-4746.

Schuna AA, Megeff C **(2000)**. New drugs for the treatment of rheumatoid arthritis. *Am. J. Health Sys. Pharm.* 57:225-34

Scott LJ, Lamb HM **(1999)**. Rofecoxib. *Drugs* 58: 499-505.

Schwab JH, Anderele SK, Brown RR, Dalldarf FG, Thompson RC **(1991)**. Pro- and antiinflammatory roles of interleukin-1 in recurrence of bacterial cell wall-induced arthritis. *Infect. Immunol.* 59: 4436-4442 (Abstract).

Seibel GL, Kollman PA **(1990)**. Molecular mechanics and the modeling of drug structures. In *Comprehensive Medicinal Chemistry*; Hansch C, Sammes PG, and Taylor JB (Eds.); Pergamon Press, Oxford, Vol. 4, pp 125-138.

Shimokawa T, Smith WL **(1991)**. Essential histidine of prostaglandin synthase. His-309 is involved in heme binding. *J. Biol. Chem.* 266: 6168-6173.

Shoichet BK, Bodian DL, Kuntz ID **(1992)**. Molecular docking using shape descriptors. *J. Comput. Chem.* 13: 380-397.

Siegle I, Klein T, Backman JT, Saal JG, Nusing RM, Fritz P **(1998)**. Expression of cyclooxygenase-1 and cyclooxygenase-2 in human synovial tissue. *Arthritis & Rheum.* 41: 122-129.

Silverstein FE, Faich G, Goldstein JL, Simor LS, Pincus T, Whelten S, Makuch R, Eisen G, Agrawal NM, Stenson WF, Burr AM, Zhao WW, Kent JD, Lefkowith JB, Verburg KM, Geis GS **(2000)**. Gastrointestinal toxicity with celecoxib vs nonsteroidal anti-inflammatory drugs for osteoarthritis and rheumatoid arthritis: the CLASS study: A randomized controlled trial. Celecoxib Long-term Arthritis Safety Study *JAMA* 284: 1247-1255.

Simon LS, Lanza FL, Lipsky PE, Hubbard RC, Talwalker S, Shwartz BD, Isakson PC, Geis GS **(1998)**. Preliminary study of the safety and efficacy of SC-58635, a novel cyclooxygenase-2 inhibitor. *Arth. & Rheum.* 41: 1591-1602.

Simon LS, Weaver AL, Graham DY, Kivitz AJ, Lipsky PE, Hubbard RC, Isakson PC, Verburg KM, Yu SS, Zhao WW, Geis GS **(1999)**. Antiinflammatory and upper gastrointestinal effects of celecoxib in rheumatoid arthritis: A randomized controlled trial. *JAMA* 282: 1921-8.

Smith WL, Marnett LJ **(1991)**. Prostaglandin endoperoxide synthase: Structure and catalysis. *Biochem. Biophys. Acta* 1083: 1-17.

Smith WL, Eling TE, Kulmacz RJ, Marnett LJ, Tsai A **(1992)**. Tyrosyl radicals and their role in hydroperoxide-dependent activation and inactivation of prostaglandin endoperoxide synthase. *Biochemistry* 31: 3-7.

Smith WL, DeWitt DL **(1995)**. Biochemistry of prostaglandin endoperoxide H synthase-1 and synthase-2 and their differential susceptibility to nonsteroidal antiinflammatory drugs. *Seminars in Nephrology* 15: 179-94.

Smith WL, Garavito RM, DeWitt DL **(1996)**. Prostaglandin endoperoxide H synthases (cyclooxygenases)-1 & -2. *J. Biol. Chem.* 271: 33157-33160.

Smith CJ, Zhang Y, Koboldt CM, Muhammad J, Zweifel BS, Shaffer A, Talley JJ, Masferrer JL, Seibert K, Isokson PC **(1998)**. Pharmacological analysis of cyclooxygenase-1 in inflammation. *Proc. Natl. Acad. Sic. U.S.A.* 95: 13313-13318.

Somasundaram S, Hayllar H, Rafi S, Wrigglesworth JM, Macpherson AJ, Bjarnason I **(1995)**. The biochemical basis of non-steroidal antiinflammatory drugs induced

damage to the gastrointestinal tract: A review and hypothesis. *Scand. J. Gastroentrol.* 30: 289-299.

So OY, Scarafia LE, Mak AY, Callan OH, Swinney DC **(1998)**. Dynamics of prostaglandin H synthases-studies with prostaglandin H synthase 2 Y355F unmask mechanism of time dependent inhibition and allosteric activation. *J. Biol. Chem.* 273: 5801-5807.

Song Y, Connor DT, Doubleday R, Sorenson RJ, Sercel AD, Unangst PC, Roth BD, Gilbertsen RB, Chan K, Schrier DJ, Guglietta A, Bornemeier DA, Dyer RD **(1999)**. Synthesis, structural-activity relationships, and *in vivo* evaluation of substituted di-tert-butylphenols as a novel class of potent, selective, and orally active cyclooxygenase-2 inhibitors. 1. Thiazolone and oxazolone series. *J. Med. Chem.* 42: 1151-1160.

Stern RS, Wintraub BU **(1989)**. Adverse cutaneous reactions to nonsteroidal antiinflammatory drugs. In *Nonsteroidal Antiinflammatory Drugs*; Lowe NJ and Hensby CN (Eds.); Korger, Basil, pp 148-157.

Steinbach G, Lynch PM, Phillips RK, Wallace MH, Hawk E, Gordon GB, Wakabayashi N, Saunders B, Shen Y, Fujimura T, Su LK, Levin B **(2000)**. The effect of celecoxib, a cyclooxygenase-2 inhibitor, in familial adenomatous polyposis. *New Eng. J. Med.* 342: 1946-1952 (Abstract).

Steinhilber D **(1999)**. 5-Lipoxygenase: A target for antiinflammatory drugs revisited. *Curr. Med. Chem.* 6: 71-85.

Suzuki M, Nozaki DL, Hosoya T, Suzuki T, Basaki Y, Kozima M **(1994)**. Styrene derivatives and salts thereof. *World Patent* **WO 94/10157**.

Takahashi Y, Roman C, Chemtob S, Tse MM, Lin E, Heymann MA, Clyman RI **(2000)**. Cyclooxygenase-2 inhibitors constrict the fetal lamb ducts arteriosus both *in vitro* and *in vivo*. *Am. J. Physiol. Regulat. Integrat. & Comparat. Physiol.* 278: R1496-1505 (Abstract).

Talanian RV, Brady KD, Cryns VL **(2000)**. Caspases as targets for antiinflammatory and anti-apoptotic drug discovery. *J. Med. Chem.* 43: 3351-3371.

Talley JJ, Brown DL, Nagarajian S, Carter JS, Weier RM, Stealey MA, Collins PW, Rogers RS **(1995)**. Substituted isoxazoles for the treatment of inflammation. USP 5, 633, 272.

Talley J, Brown D, Nagarajan S, Carter J, Stealey M, Collins P, Seibert K, Graneto M, Xu X, Partis R. **(1996)** Substituted isoxazoles for the treatment of inflammation. *World Patent* **WO 96/25405.**

Talley JJ **(1999)**. Selective inhibitors of cyclooxygenase-2 (COX-2). *Prog. Med. Chem.* 36: 201-234.

Tavares IA, Bishai PM, Bennett A **(1995)**. Activity of nimesulide on constitutive and inducible cycloxygenases. *Arzneimittel-Forschung* 45: 1093-1095.

Teiichi A **(1959)**. Reaction of α-halocarbonyl compounds with Grignard reagents. II. Reactions of α-chloroacetophenones. *Yuki Gosei Kagaku Kuokaishi* 17: 777-782 (Chem. Abstr. 54: 4492c).

Terada H, Muraoka S, Fujita T **(1974)**. Structure-activity relationships of fenamic acids. *J. Med. Chem.* 17: 330-334.

Therien M, Brideau C, Chan CC, Cromlish W, Gauthier JY, Gordon R, Greig G, Kargman S, Lau CK, Leblanc Y, Li CS, O'Neill GP, Riendeau D, Roy P, Wang Z,

Xu L, Prasit P **(1997)**. Synthesis and biological evaluation of 5,6-diarylimidazo[2,1-b]thiazole as selective COX-2 inhibitors: 5,6-Diarylthiazolo[3,2-b][1,2,4]triazole. *Biorg. Med. Chem. Lett.* 7: 57-62.

Topliss JG, Costello JR **(1972)**. Chance correlations in structure-activity studies using multiple regression analysis. *J. Med. Chem.* 15: 1066-1068.

Tsai AL, Wu G, Kulmacz RJ **(1997)**. Stoichiometry of the interaction of prostaglandin H synthase with substrates. *Biochem.* 36, 13085-13094.

Tsujii M, DuBois RN **(1995)**. Alterations in cellular adhesion and apoptosis in epithelial cells over expressing prostaglandin endoperoxide synthase 2. *Cell* 83: 493-501.

Tsuji K, Konishi N, Spears GW, Ogino T, Nakamura K, Tojo T, Ochi T, Shimajo F, Senoh H, Matsuo M **(1997)**. Studies on antiinflammatory Agents. V. Synthesis and pharmacological properties of 3-difluoromethyl-1-(4-methoxyphenyl)-5-(4-methylsulphonylphenyl)pyrazole and related compounds. *Chem. Pharm. Bull.* 45: 1475-1481.

Tute MS **(1990)**. History and objectives of quantitative drug design. In *Comprehensive Medicinal Chemistry*; Hansch C, Sammes PG, and Taylor JB (Eds.); Pergamon Press, Oxford, Vol. 4, pp 1-32.

Van den Berg G, Bultsma T, Nauta WT **(1975)**. Inhibition of prostaglandin biosynthesis by 2-aryl-1,3-indandiones. *Bioch. Pharmacol.* 24: 1115-1119.

Vane JR **(1971)**. Inhibition of prostaglandin synthesis as a mechanism of action for aspirin-like drugs. *Nature* 23:232-235.

Wagener M, Sodowski J, Gasteiger J **(1995)**. Autocorrelation of molecular surface properties for modeling corticosteroid binding globulin and cytosolic Ah receptor activity by neural networks. *J. Am. Chem. Soc.* 117: 7769-7775.

Wallace JL, Reuter B, Cicala C, McKnight W, Grisham M, Cirino G **(1994)**. A diclofenac derivative without ulcerogenic properties. *Eur. J. Pharmacol.* 257: 249-255.

Wallace JL, Bak A, McKnight W, Asfaha S, Sharkey KA, MacNaughton WK **(1998)**. Cyclooxygenase-1 contributes to inflammatory responses in rats and mice: Implications for gastrointestinal toxicity. *Gastroentrol.* 115: 101-109.

Wiener H **(1947)**. Structural determination of paraffin boiling points. *J. Am. Chem. Soc.* 69: 17-20.

Weiner SJ, Kollman PA, Nguyen DT, Case DA **(1986)**. An all atom force field for simulations of proteins and nucleic acids. *J. Comput. Chem.* 7: 230-252.

Wiesenberg-Boettcher I, Schweizer A, Mueller K, Maerki F, Pfeilschifter J **(1989)**. The pharmacological profile of CGP 28238, a highly potent antiinflammatory compound. *Drugs Under Experimental & Clinical Research. 15:501-509* (Abstract).

Wilkerson WW, Copeland RA, Covington M, Trzakos JM **(1995)**. Antiinflammatory 4,5-diarylpyrroles. 2. Activity as a function of cyclooxygenase-2 inhibition. *J. Med. Chem.* 38: 3895-3901.

Willson TM, Brown PJ, Sternbach DD, Henke BR **(2000)**. The PPARs: From orphan receptors to drug discovery. *J. Med. Chem.* 43: 527-550.

Wong PC, Quan ML, Crain EJ, Watson CA, Wexler RR, Knabb RM **(2000)**. Nonpeptide factor Xa inhibitors: I. Studies with SF303 and SK549, a new class of potent antithrombotics. *J. Pharmacol. Exper. Ther.* 292: 351-7 (Abs.).

Xu X, Williams JW, Gong H, Finnegan A, Chong AS **(1996)**. Two activities of the immunosuppressive metabolite of leflunamide. A77 1726: Inhibition of pyrimidine nucleotide synthesis and protein tyrosine phosphorylation. *Biochem. Pharmacol.* 52: 527-534.

Yamagata K, Andreasson KI, Kaufmann WE, Barnes CA, Worley PF **(1993)**. Expression of a mitogen-inducible cyclooxygenase in brain neurons. Regulation by synaptic activity and glucocorticoids. *Neuron.* 11: 371-386 (Abstract).

Zeng J, Fenna RE **(1992)**. X-ray crystal structure of canine myeloperoxidase at 3Å resolution. *J. Mol. Biol.* 226: 185-207.

Zhao SZ, McMillen JI, Markenson JA, Dedhiya SD, Zhao WW, Osterhaus JT, Yu SS **(1999)**. Evaluation of the functional aspects of health-related quality of life of patients with osteoarthritis treated with celecoxib. *Pharmacother.* 19: 1269-1278.

Zimmerman HJ **(1994)**. Hepatic injury associated with nonsteroidal antiinflammatory drugs. In *Nonsteroidal Antiinflammatory Drugs*; Lewis AJ and Furst DE (Eds.); Marcel-Dekker, New York, pp 171-194.